NMR Studies of Protein and Peptide Structure and Dynamics

by

Michael Piazza

A thesis

presented to the University of Waterloo

in fulfillment of the

thesis requirement for the degree of

Doctor of Philosophy

in

Chemistry

Waterloo, Ontario, Canada, 2016

AUTHOR'S DECLARATION

I hereby declare that I am the sole author of this thesis. This is a true copy of the thesis, including any required final revisions, as accepted by my examiners.

I understand that my thesis may be made electronically available to the public.

Michael Piazza

Abstract

Calmodulin (CaM) is a small, acidic cytosolic calcium binding protein that responds to increases in intracellular Ca^{2+} concentrations. It is proposed to be involved in binding to and regulating over 300 functionally and structurally diverse proteins. It is comprised of an N- and C- terminal lobe separated by a highly flexible central linker region. Each of these lobes contains two EF hand motifs that are each capable of binding to one Ca^{2+}-ion. CaM is found to exist primarily in two states: the Ca^{2+}-replete form, holoCaM, or the Ca^{2+}-deplete form, apoCaM. Both forms of CaM are able to bind to target proteins. CaM also undergoes post translational modifications that play a role in its regulation of target proteins.

An important target of CaM are the nitric oxide synthase (NOS) enzymes. NOS catalyzes the conversion of L-arginine to L-citrulline and nitric oxide (·NO). Three isoforms of NOS are found in mammalian cells: endothelial (eNOS); neuronal (nNOS); and inducible (iNOS). All three isoforms of NOS are homodimeric and comprised of an N-terminal heme domain, containing the active site, and a C-terminal flavin-binding domain containing FAD-, FMN-, and NADPH- binding sites, linked together by a CaM-binding region. The nNOS and eNOS isoforms are constitutively expressed and are Ca^{2+}-CaM-dependent. In contrast, iNOS is regulated at the transcriptional level and is Ca^{2+}-independent. NOS is also found to be regulated through the phosphorylation and de-phosphorylation of key residues, specifically Thr 495, which is found in the CaM-binding domain. The exact mechanism of how CaM activates NOS is not fully understood. Studies have shown CaM to act like a switch that causes a conformational change in NOS to allow for the electron transfer between the reductase and oxygenase domains through a process that is thought to be highly dynamic. This thesis

is focused on the structure and dynamics of CaM and CaM mutant constructs bound to the target peptides of the NOS CaM-binding domain at saturating and physiological concentrations of Ca^{2+}.

To investigate the structural and functional effects that the phosphorylation of Thr495 of eNOS may have on eNOS activation by CaM, the solution structure of CaM bound to the peptide comprising the eNOS CaM-binding domain phosphorylated at Thr495 was determined. To investigate the Ca^{2+}-dependency of CaM binding NOS, nuclear magnetic resonance (NMR) studies were performed at various free Ca^{2+} concentrations to determine the structure and dynamics of NOS and CaM interactions at physiological Ca^{2+} concentrations. The results illustrate that structures of CaM-NOS complexes determined at saturating Ca^{2+} concentrations cannot provide a complete picture because the differences in intramolecular dynamics become visible only at physiological Ca^{2+} levels.

Numerous studies use CaM mutants incapable of binding Ca^{2+} in either the N- or C-lobe to mimic apoCaM, with some of these studies reporting functional differences when comparing the mutant and apo forms of CaM. We investigated the structural consequences of these mutations by determining the residue-specific chemical shift perturbations induced by these mutations. This was accomplished by determining the full backbone chemical shift assignments of three Ca^{2+}-deficient CaM mutants in the absence and presence of Ca^{2+}, and investigating their interaction with the iNOS enzyme through determination of the solution structure of a Ca^{2+}-deficient CaM mutant with iNOS. The use of NMR spectroscopy allowed for the determination of high resolution structures of these complexes. ^{15}N relaxation and H/D exchange experiments also allowed for the analysis of the structural dynamics occurring in these complexes. NMR spectroscopy is an efficient method for studying the dynamics and structures of protein-protein and protein-peptide complexes.

Acknowledgements

I would like to thank my supervisors Dr. Thorsten Dieckmann and Dr. Guy Guillemette for all their guidance, support and encouragement during my studies at UW. I am grateful for the leadership and knowledge they provided me and for the experience to be able to work with them. I especially enjoyed our long conversations spent discussing politics and sports.

I would also like to thank my advisory committee members: Dr. Elizabeth Meiering and Dr. Michael Palmer; and my external examiners: Dr. Todd Holyoak and Dr. Logan Donaldson for reading and reviewing my thesis, and for their valuable suggestions and comments.

Many thanks go to my lab mates in the Dieckmann and Guillemette labs: Dr. Jason Da Costa, Dr. Valentina Taiakina, and Erica Lee for making the lab a fun and enjoyable place to work. And thank you to my friends in the department, who have supported me through my studies and helped make this an amazing experience.

Special thanks go to my family and friends, who have been very supportive of me throughout my studies. Even though you guys would always regret asking me how my research was going, I appreciate you trying to understand what I have been doing. And especially to Kailey, for supporting me throughout all of this, and having the patience to deal with all my late nights spent in the lab and sometimes endless discussions of my research.

Dedication

To my family,

for your love and support throughout my studies

Table of Contents

List of Figures

List of Tables

List of Abbreviations

AI loop	Autoinhibitory loop
apoCaM	Ca^{2+}-deplete CaM
BMRB	Biological Magnetic Resonance Bank
CaM	Calmodulin
CaM_{12}	N-terminal Ca^{2+}-deficient CaM (D20A and D56A)
CaM_{1234}	Ca^{2+}-deficient CaM (D20A, D56A, D93A and D129A)
CaM_{34}	C-terminal Ca^{2+}-deficient CaM (D93A and D129A)
CaM-eNOS	CaM-eNOS CaM binding domain peptide complex
CaM-iNOS	CaM-iNOS CaM binding domain peptide complex
CaMKI	CaM-dependent protein kinase I
CaMKII	CaM-dependent protein kinase II
CARA	Computer Aided Resonance Assignment
CaV	Voltage-dependent Ca^{2+} channels
cCaM	C-terminal EF hand pair and central linker of CaM (residues 76-148)
CD	Circular dichroism
CKII	Casein kinase II
cNOS	Constitutive nitric oxide synthase
CNS	Crystallography and NMR system
Dansyl chloride	5-dimethylaminonaphthalene-1-sulfonyl chloride
Dansyl CaM	Dansyl chloride labeled wild-type CaM
DAPK	Death-associated protein kinase
DHPC	1,2-dihexanoyl-sn-glycero-3-phosphocholine
DMPC	1,2-dimyristoyl-sn-glycero-3-phosphocholine
DMPG	1,2-dimyristoyl-sn-glycero-3-phospho-rac-(1'-glycerol)
DOPG	1,2-dioleoyl-*sn*-glycero-3-phospho-(1'-*rac*-glycerol)
DTT	Dithiothreitol
E. coli	*Escherichia coli*
EDTA	Ethylenediaminetetraacetic acid
EF	Edema factor
EGTA	Ethylene glycol-bis(β-aminoethyl ether)-N,N,N',N'-tetraacetic acid
EM	Electron microscopy
eNOS	Endothelial nitric oxide synthase
ESI-MS	Electrospray ionization-mass spectrometry
FAD	Flavin adenine dinucleotide
FMN	Flavin mononucleotide
FRET	Fluorescence resonance energy transfer
H_4B	(6*R*)-5,6,7,8-tetrahydrobiopterin
Heme	Iron protoporphyrin IX
holoCaM	Ca^{2+}-replete calmodulin
HSQC	^{1}H-^{15}N-heteronuclear single quantum correlation
iNOS	Inducible nitric oxide synthase
IPTG	Isopropyl-*β*-D-thiogalactopyranoside

ITC	Isothermal titration calorimetry
LTA	Lipoteichoic acid
MLCK	Myosin light chain kinase
mRNA	Messenger RNA
$Na_v1.5$	Voltage-gated sodium channels
$NADP^+$	Oxidized nicotinamide adenine dinucleotide phosphate
NADPH	Reduced nicotinamide adenine dinucleotide phosphate
nCaM	N-terminal EF hand pair (residues 1-75)
NH H/D exchange	amide proton hydrogen/deuterium exchange
NMR	Nuclear magnetic resonance
nNOS	Neuronal nitric oxide synthase
•NO	Nitric oxide
NOE	Nuclear Overhauser enhancement
NOESY	Nuclear Overhauser Effect SpectroscopY
NOS	Nitric oxide synthase
NRPS	Non-ribosomal peptide synthetases
PDB	Protein Data Bank
PMCA	Plasma-membrane Ca^{2+}-ATPases
PMSF	Phenylmethylsulphonylfluoride
POPE	1-palmitoyl-2-oleoyl-*sn*-glycero-3-phosphoethanolamine
RF	Radiofrequency
RMSD	Root-mean-square distance
SDS-PAGE	Sodium dodecyl sulphate polyacrylamide gel electrophoresis
SK K^+ channel	Small conductance Ca^{2+}-activated K^+ channel
SPR	Surface plasmon resonance
TOCSY	TOtal Correlation SpectroscopY
TPK-III	Tyrosine protein kinase III
T1 relaxation	Longitudinal relaxation
T2 ralaxation	Transverse relaxation
TFE	Trifluoroethanol
TOCL	Tetraoleyl-cardiolipin
TROSY	Transverse Relaxation-Optimized SpectroscopY

Chapter 1

Literature Review

1.1 Calmodulin

1.1.1 Calcium Signaling.

Calcium (Ca^{2+}) ions are important intracellular secondary messengers that relay information within cells to regulate their activity. Intracellular Ca^{2+} concentrations regulate multiple cellular processes such as cell-cell interactions, cell proliferation, fertilization, muscle contraction, neuron transmission, and cell death (Berridge et al., 1998; Evenäs et al., 1998). The intracellular Ca^{2+} concentration ranges from a resting state of 50-100 nM up to 1-10 μM in an activated cell (Carafoli, 1987; Evenäs et al., 1998; Islam, 2012). Intracellular Ca^{2+} can be derived from internal sources by being released from Ca^{2+} stores in the endoplasmic or sarcoplasmic reticulum, or from external sources outside by passing through various channels spanning the plasma membrane (Berridge et al., 1998; Evenäs et al., 1998; Islam, 2012). The functional response to increased calcium levels is regulated by a group of Ca^{2+}-binding proteins that respond to these increases in intracellular Ca^{2+} concentration. Many of these Ca^{2+}-binding proteins contain a Ca^{2+}-binding motif, called an EF hand (Figure 1.1).

The EF hand motif consists of a helix-loop-helix structure with Ca^{2+} binding occurring in the loop region. It is normally paired with another EF hand, with the loop region of each interacting through an antiparallel β sheet (Babu et al., 1988; Strynadka and James, 1989). An important Ca^{2+}-binding protein that contains an EF hand motif is calmodulin (CaM), which contains two pairs. Each EF hand motif of CaM consists of 12 amino acids, rich in aspartate and glutamate residues (Figure 1.1B), which adopt a coil structure between positions 1-6, a short β strand between 7-9, and an α-

helix between 10-12. Ca^{2+} is coordinated through 7 oxygen ligands from six residues in the 1-3-5-7-9-12 positions (Figure 1.1). This results in a pentagonal bipyramidal co-ordination of Ca^{2+} (Babu et al., 1988). The destabilizing repulsion caused by the close proximity of the negatively-charged carboxylate sidechains involved in coordinating the Ca^{2+} ion is offset by the hydrogen-bonding network in the loop. In the absence of Ca^{2+} the EF hands pack with their central core consisting of hydrophobic residues and their solvent-exposed faces consisting of charged, hydrophilic residues, in a "closed" conformation (Strynadka and James, 1989). Once a Ca^{2+} ion binds, the helices rearrange, into a more "open" conformation, causing the exposure of the hydrophobic residues that are then able to bind to target proteins (Strynadka and James, 1989).

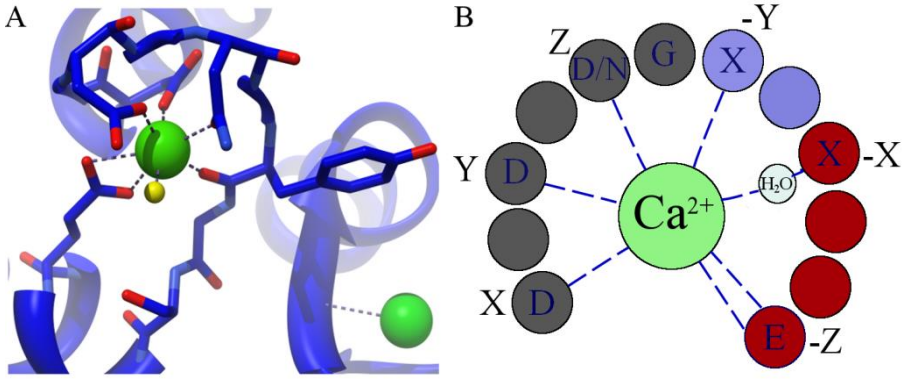

Figure 1.1: Ca^{2+}-binding EF hand motif showing Ca^{2+} co-ordination.

(A) Stick representation of Ca^{2+} co-ordination by the EF hand III of CaM. The pentagonal bipyramidal co-ordination of the Ca^{2+} ion and oxygen atoms used to stabilize the ligand co-ordination of Ca^{2+} are represented by dashed lines. The oxygen atoms, Ca^{2+} ion, and coordinating water are shown in red, green and yellow, respectively. Figure derived from PDB 3CLN (Babu et al., 1988). (B) Consensus Ca^{2+}-binding loop for CaM's 4 EF hand motifs. This shows the 1-3-5-7-9-12 position pattern of the coordinating amino acids, *X*, *Y*, *Z*, -X, -Y and -Z, in the pentagonal bipyramidal co-ordination binding of Ca^{2+} (Gifford et al., 2007). Secondary structure elements are colored gray for coil, blue for β strand and red for α-helix.

1.1.2 Overview of Calmodulin.

CaM is a ubiquitous, multifunctional protein, consisting of 148 amino acids and having a molecular weight of 16.7 kDa. It is a highly conserved protein that functions as a cytosolic Ca^{2+} receptor in

response to varied intracellular signals in almost all eukaryotic cells (Ikura and Ames, 2006). CaM is found to have 100% sequence homology in vertebrates, although it is coded for by three genes, CaM I, CaM II, and CaM III (Chien and Dawid, 1984; Ikura and Ames, 2006). CaM is transcribed into eight mRNAs that are targeted to different cellular domains, where local protein synthesis occurs. This indicates that mRNA translocation, and not the CaM protein, is responsible for local CaM pools in the different intracellular compartments (Palfi et al., 2002; Kortvely and Gulya, 2004). CaM is also found to be highly conserved in other organisms such as plants, fungi and protozoa (Friedberg, 1990).

1.1.3 Structure of CaM.

CaM is a small, highly acidic protein (pI approximately 3.9 to 4.3), consisting of N- and C-terminal globular domains connected by a flexible central linker (Liu, Y. P.Cheung, 1976; Crouch and Klee, 1980). Each domain contains an EF hand motif pair, giving CaM the ability to bind a total of four Ca^{2+} ions (Crouch and Klee, 1980; Perret et al., 1988). The EF hands of the C-terminal domain (K_d~10^{-6}M) have a 10-fold higher affinity for Ca^{2+} than the EF hands of the N-terminal domain (K_d~10^{-5}M), with cooperative binding within each domain (Crouch and Klee, 1980; Martin et al., 1985). It has been shown that Ca^{2+}-binds to CaM in the order of EF hand III, EF hand IV, EF hand I, then EF hand II, with Ca^{2+} ion dissociating in the reverse order (Kilhoffer et al., 1992). Even though CaM could potentially exist in various Ca^{2+} bound states, it is primarily found in two states: fully Ca^{2+}-deplete, apoCaM; and fully Ca^{2+}-bound, holoCaM (Figure 1.2).

The N-terminal domain of CaM is comprised of residues 1-75 and the C-terminal domain is comprised of residues 82-148, with residues 76-81 corresponding to the flexible central linker. The secondary structure of CaM is essentially the same in the apo and holo-forms; however, there are differences in helix packing. The structure of apoCaM is more compact than holoCaM, with each

domain consisting of four tightly packed antiparallel α-helices. Although these helices are packed tighter in the apo form compared to the holo form of CaM, they have been found to be much more mobile, with Ca^{2+} binding dramatically reducing their flexibility (Zhang et al., 1995a). Also apoCaM's C-terminal domain is much more dynamic than its N-terminal domain as observed in the solution structures determined by Kuboniwa et al. (1995)(Figure 1.2A).

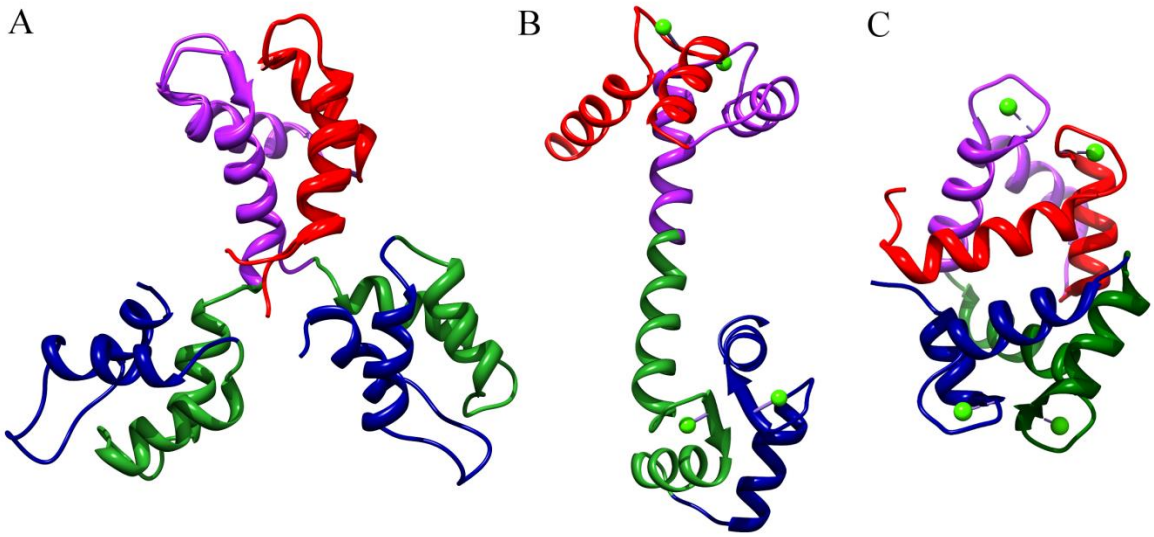

Figure 1.2: Structure comparison of apo and holo CaM.

(A) ApoCaM from PDB 1CFC (Kuboniwa et al., 1995), showing highly mobile C-terminal domain, (B) holoCaM from PDB 3CLN (Babu et al., 1988), and (C) holoCaM from PDB 1PRW in a compact conformation (Fallon and Quiocho, 2003). Residues 1−40 of CaM (EF hand I) are colored red, residues 41−79 (EF hand II) purple, residues 80−114 (EF hand III) green, and residues 115−148 (EF hand IV) blue. Ca^{2+} ions are shown in green.

Upon Ca^{2+} binding, the EF hands undergo a structural rearrangement, consisting of the antiparallel packing of the α-helices shifting to a perpendicular packing. This allows the negatively charged side chains to coordinate the Ca^{2+} ion, resulting in a hydrophobic pocket being present on the surface of each domain that is not present in the apo-CaM conformation (Kuboniwa et al., 1995; Zhang et al., 1995a). This causes the two globular domains of CaM to rotate outwards, increasing the distance between them, and changing the more compact shape of apoCaM to the more extended

dumbbell shape of holoCaM (Yamniuk and Vogel, 2004). The structures of holoCaM can be in an extended state or a compact form (Figure 1.2B and C), illustrating the wide range of conformations CaM can adopt because of its highly flexible linker region (Babu et al., 1988; Chattopadhyaya et al., 1992; Fallon and Quiocho, 2003).

The large hydrophobic patches exposed in holoCaM are rich in methionine residues, with four in each domain and one in the central linker, contributing 46% of the total hydrophobic surface area (Zhang *et al.*, 1995a). These 9 methionine residues comprise 6% of the total amino acid content of CaM, which is much greater than the 1% methionine content average in known proteomes (Ikura and Ames, 2006). This high abundance of methionine residues is thought to play an important role in CaM's target recognition due to the high polarizability of the methionine sulfur atom and the ability of the long flexible side chains to allow them to be highly conformationally adaptable (Gellman, 1991). The central linker region of holoCaM, was originally thought to be a long rigid α-helix from the crystal structures, however, it is found to be highly flexible, with the ability to be bent. This allows for the orientation of the N- and C-terminal domains to change independently of each other to accommodate the binding of different target proteins (Persechini and Kretsinger, 1988).

1.1.4 CaM binding to Target Proteins.

Through the use of protein databases recognizing CaM binding motifs, it has been proposed that CaM is able to bind to over 300 target proteins (Yap et al., 2000; Shen et al., 2005; Ikura and Ames, 2006). This analysis involves the evaluation of a sequence on the basis of its electronic and hydrophobic properties and secondary-structure tendency to identify putative basic amphiphilic α-helical motifs (Yap et al., 2000; Shen et al., 2005). Currently over 80 unique CaM complexes have been deposited in the PDB, along with the characterization of the binding affinity of many more CaM-binding

proteins (Shen et al., 2005; Tidow and Nissen, 2013; Mruk et al., 2014). As mentioned earlier CaM could potentially exist in various Ca^{2+}-bound states, specifically the Ca^{2+}-replete, or holo state, and the Ca^{2+}-deplete, or apo state. Each of these Ca^{2+}-saturated states of CaM has been found to bind to target proteins. When CaM interacts and binds in the apo form it is referred to as Ca^{2+}-independent activation, and in the holo form as Ca^{2+}-dependent (Rhoads and Friedberg, 1997; Vetter and Leclerc, 2003).

A defined consensus sequence doesn't exist for CaM-binding sites, however, target proteins that bind to CaM generally have a small binding domain of approximately 20 amino acids. These domains contain a hydrophobic face in contact with CaM and a basic face in contact with solvent and the negatively charged amino acids of CaM's linker region (O'Neil and DeGrado, 1990). This basic face also has important electrostatic interactions that may form salt bridges with aspartate and glutamate residues in CaM's central linker and C-terminal domain (Crivici and Ikura, 1995). The binding domains have a tendency to form basic, amphiphilic α-helices, containing bulky hydrophobic amino acids (O'Neil and DeGrado, 1990). These conserved bulky hydrophobic amino acids are typically arranged in a 1-5-8-14 (which also contains the 1-8-14 motif), 1-5-10 or IQ motif. The 1-5-8-14 motif is composed of (FILVW)XXX(FAILVW)XX(FAILVW)XXXXX(FILVW) and the 1-5-10 motif is composed of (FILVW)XXX(FILV)XXXX(FILVW). The underlined amino acids occupy sites 1-5-8-14 or 1-5-10 and represent anchoring residues, whereas X can be any amino acid (Rhoads and Friedberg, 1997). They are termed anchoring residues because they interact with the hydrophobic patches in the terminal domains of CaM, allowing the basic residues between them to interact with the linker region (Afshar et al., 1994). Some target proteins are also able to bind to CaM in a Ca^{2+}-independent manner. These target proteins include those that are only bound to apoCaM, and those that are tightly bound to CaM in the presence and absence of Ca^{2+} (Rhoads and Friedberg, 1997).

These proteins contain the consensus IQ motif that has the general sequence IQXXXRGXXXR, where X can be any amino acid (Rhoads and Friedberg, 1997). However, this consensus sequence is also found in some Ca^{2+}-dependent proteins (Jurado et al., 1999). Some examples of well characterized CaM binding proteins and their binding modes are summarized in Table 1.1.

Table 1.1: Overview of some CaM-target proteins.

Group	Target enzyme or protein	Number of Ca^{2+}
CaM binding with canonical binding mode		
Protein kinases	CaM-dependent protein kinase I (CAMKI)	4
	CaM-dependent protein kinase II (CAMKII)	4
	Myosin light chain kinase (MLCK)	4
	Death-associated protein kinase (DAPK)	4
Phosphatases	Calcineurin	4
Second messenger	Nitric Oxide Synthase (NOS)	4
	Inducible NOS	0
	Plasma-membrane Ca^{2+}-ATPases (PMCA)	4
	Voltage-dependent Ca^{2+} channels (CaV1.1)	4
	CaV2.1	4
	Ryanodine receptor RYR1	4
	Type I adenylate cyclase	4
Cytoskeletal and membrane proteins	Neuromodulin	0
	PEP-19	0
CaM binding in elongated binding mode		
	Bacillus anthracis edema factor (EF)	2
Ion Channels	Small-conductance Ca^{2+}-activated K^+ channels (SK2)	2
	Voltage-gated sodium channels ($Na_v1.5$)	4
	$Na_v1.5$	0
2 CaM bind 1 target protein		
	Myosin-5A	0
1 CaM binds 2 target proteins		
Enzyme	Glutamate decarboxylase	4

Table made with information from Jurado et al. (1999); Tidow and Nissen (2013); Mruk et al. (2014).

Through the structure determination of CaM bound to target peptides or proteins by X-ray crystallography and NMR spectroscopy it has been shown that CaM is able to bind in a variety of conformations (Table 1.1 and Figure 1.3). The most common binding conformation for canonical CaM-recognition motifs consists of the unwinding of the central linker and the N- and C-terminal

domains of CaM wrapping around the target protein. This binding can be in a parallel or anti-parallel conformation: parallel indicates that the N-terminal lobe of CaM binds towards the N-terminal lobe of the target protein and the C-terminal lobe of CaM binds towards the C-terminal lobe of the target protein; antiparallel indicates that the terminal lobes of CaM bind to the opposite terminal lobes of the target protein (Yamniuk and Vogel, 2004). The electrostatic interactions described above play a big role in the orientation of the target protein with respect to the lobes of CaM (Afshar et al., 1994). Other unique conformations of CaM binding to target proteins can involve a conformation where: CaM itself is wrapped by the target protein and one lobe of CaM is Ca^{2+}-saturated (Drum et al., 2002); more than one CaM subunit is required for target binding (Houdusse et al., 2006); one CaM subunit can bind multiple targets (Yap et al., 2003); and only one lobe of CaM is involved in binding (Elshorst et al., 1999).

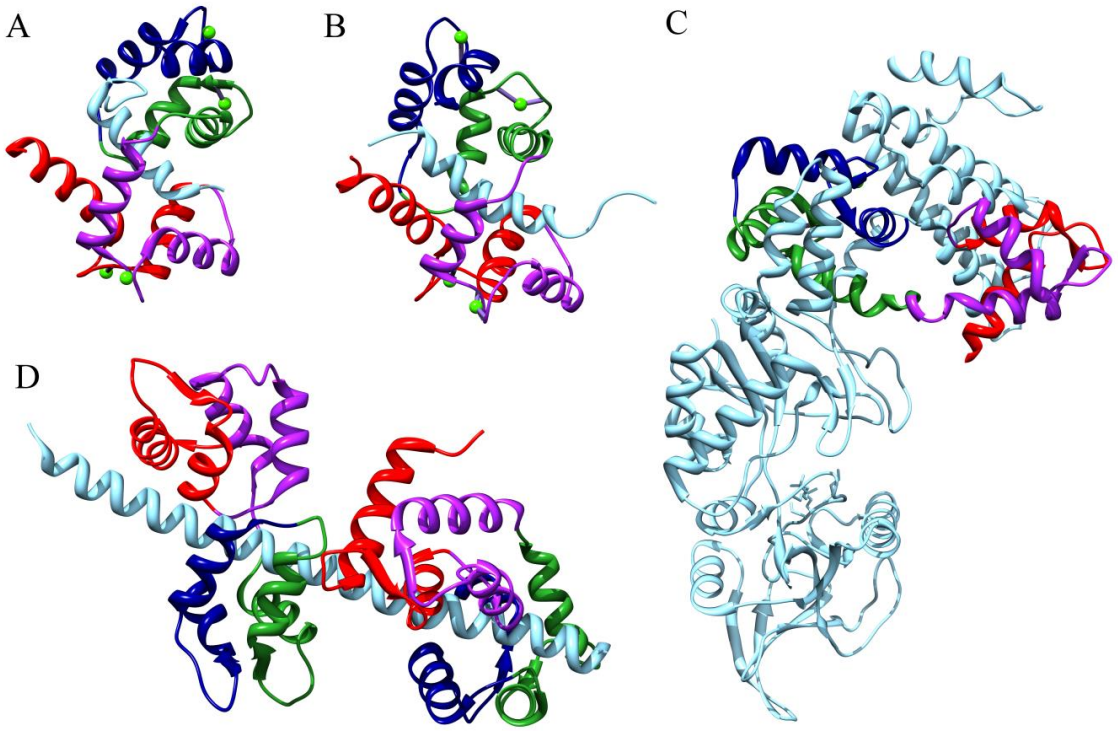

Figure 1.3: Structures of CaM bound to various target proteins in various conformations.

(A) CaM bound to CaM-dependent kinase kinase (CaMKK) in a parallel conformation from PDB 1IQ5 (Kurokawa et al., 2001). (B) CaM bound to myosin light chain kinase (MLCK) in an anti-parallel conformation from PDB 2BBN (Ikura et al., 1992). (C) CaM in complex with the edema factor of adenylyl cyclase of *B. anthracis* from PDB 1K93 (Drum et al., 2002). (D) Two apoCaMs bound to an unconventional myosin V IQ domain from PDB 2IX7 (Houdusse et al., 2006). CaM has the same color scheme as Figure 1.2.The target peptide or enzyme is rendered in light blue.

1.1.5 Post-Translational Modifications of CaM.

CaM is found to undergo post-translational modifications that have been suggested to play a role in regulating its activity with target proteins. The modifications CaM is found to undergo *in vivo* include acetylation, trimethylation, carboxylmethylation, proteolytic cleavage, and phosphorylation (Benaim and Villalobo, 2002). The effect of these CaM modifications on the binding and activation of different target proteins still remains unclear (Ikura and Ames, 2006).

CaM has 18 putative sites that could be phosphorylated, including 4 serine, 12 threonine and 2 tyrosine, with 8 sites (Figure 1.4) being shown to be phosphorylated *in vitro* (Benaim and Villalobo, 2002). Furthermore, three of these sites, Thr79, Ser81, and Ser101, have been found to be phosphorylated *in vivo* in rat liver, by protein-serine/threonine kinases, (i.e. casein kinase II and myosin light-chain kinase) and protein-tyrosine kinases, (i.e. the insulin receptor and the epidermal growth factor receptor) (Quadroni et al., 1994; Benaim and Villalobo, 2002).

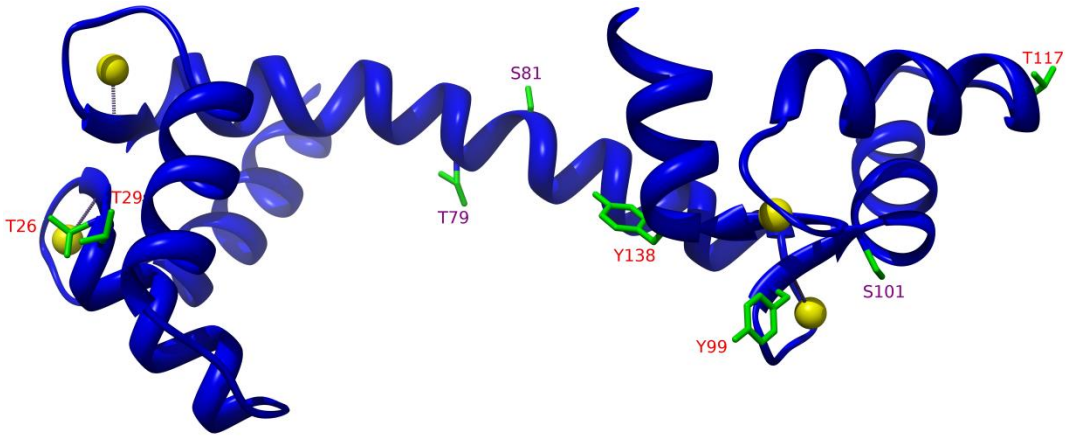

Figure 1.4: Structural representation of known phosphorylation sites in CaM.
The 8 amino acid sites in CaM know to be phosphorylated are labeled in red and purple. Residues labeled in purple have been found to be phosphorylated *in vivo*.

The effect of phosphorylated CaM on target proteins has been investigated. A study by Quadroni *et al.* (1998) found that CaM phosphorylated *in vitro* by casein kinase II (CKII) increased the V_{max} of neuronal nitric oxide synthase (nNOS) 2.6-fold and its activity 2-fold. This group previously showed CKII is able to phosphorylate CaM at residues Thr79, Ser81and Ser101, but did not determine which one was important for the increase in nNOS activity (Quadroni et al., 1994, 1998). Another study involving the *in vitro* phosphorylation of CaM at Tyr99 by tyrosine protein kinase III (TPK-III) determined that Tyr99-phosphorylated CaM increased the V_{max} of nNOS 3.45-fold and its activity 2.16-fold (Corti et al., 1999). Mishra *et al.* (2010) hypothesized that hypoxia-

induced CaM phosphorylated at Tyr99 by TPK-III has a higher affinity for nNOS than non-phosphorylated CaM, leading to increased activation of nNOS and increased production of nitric oxide (·NO). The increased tyrosine phosphorylation of CaM at Tyr99 in the cerebral cortex of newborn piglets resulting from hypoxia is mediated by the ·NO derived from nNOS (Mishra et al., 2010).

1.2 Nitric Oxide Synthase (NOS)

One of the many target enzymes that CaM has been found to bind and regulate is nitric oxide synthase (NOS). NOS catalyzes the conversion of L-arginine to L-citrulline and nitric oxide (·NO) through two monooxygenase reactions. This reaction (Figure 1.5) uses reduced nicotinamide adenine dinucleotide phosphate (NADPH) as the electron donor in the presence of oxygen. ·NO is a short-lived, highly reactive diatomic free radical that can be induced in a variety of cell types and is essential in many biological functions (Nahrevanian and Amini, 2009). ·NO has been found to be associated with neurotransmission, cellular signaling, vasodilation and the immune response (Alderton et al., 2001; Nahrevanian and Amini, 2009).

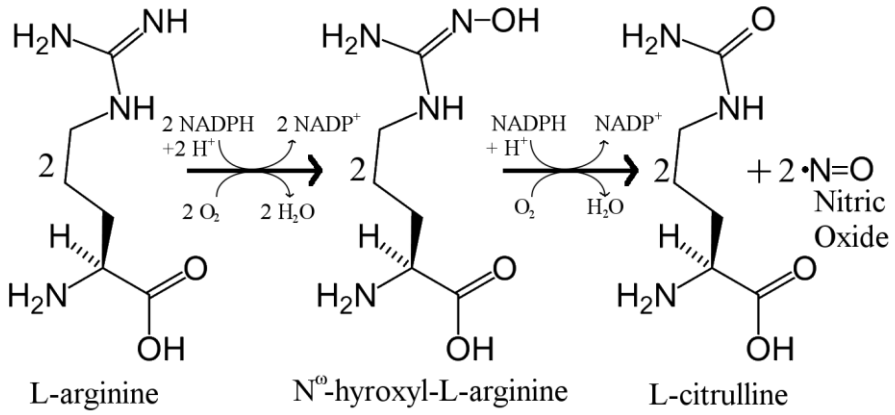

Figure 1.5: Reaction scheme of NOS-catalyzed conversion of L-arginine to L-citrulline and ·NO.

1.2.1 Isoforms of mammalian NOS.

Three isoforms of NOS exist in mammals, all of which have different localization and cellular function. The three isoforms are neuronal NOS (nNOS, NOS I), inducible NOS (iNOS, NOS II), and endothelial NOS (eNOS, NOS III). These isoforms have 51-57% sequence homology in humans and differ in size from one another, with nNOS, eNOS and iNOS having a molecular weight of 165, 133 and 130 kDa, respectively (Alderton et al., 2001; Zhang et al., 2001). The eNOS and nNOS enzymes have been found to be constitutively expressed and are thus referred to as the constitutive NOS (cNOS) isoforms. They are found to be activated by increased cellular Ca^{2+} through binding to holoCaM and are thus Ca^{2+}-dependent (Roman et al., 2002). In contrast, iNOS is regulated at the transcriptional level *in vivo* by cytokines in macrophages and tightly binds CaM at basal levels of Ca^{2+}. Since iNOS binds to CaM regardless of Ca^{2+} concentration it is classified as Ca^{2+}-independent (Cho et al., 1992; Roman et al., 2002).

The NOS enzymes are homo-dimeric proteins, with each monomer containing an N-terminal oxygenase domain and a multi-subdomain C-terminal reductase domain (Figure 1.6). The oxygenase domain contains binding sites for iron protoporphyrin IX (heme), (6*R*)-5,6,7,8-tetrahydrobiopterin (H_4B), and the substrates L-arginine and molecular oxygen (Alderton et al., 2001). The reductase domain contains binding sites for flavin mononucleotide (FMN), flavin adenine dinucleotide (FAD), NADPH and in the cNOS isoforms an autoinhibitory region (Alderton et al., 2001). The reductase and oxygenase domains are connected by a linker containing a CaM binding domain.

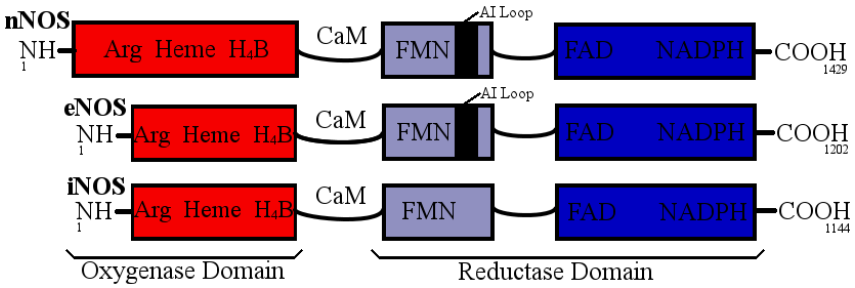

Figure 1.6: Domain structure of NOS isozymes.

The oxygenase and reductase domains are shown in red and pink, respectively. A CaM-binding domain separates the oxygenase and reductase domains. Numbers represent the amino acid residue at the start and end of the oxygenase, FMN, and FAD/NADPH domains (Alderton et al., 2001).

Currently there are no structures of any of the full isoforms available, due to their large size and dynamic nature which makes X-ray crystallography and NMR spectroscopy not feasible. However, crystal structures of the individual domains have been determined, along with an electron microscopy study modelling the eNOS, nNOS and iNOS holoenzymes in the absence (only nNOS and eNOS) and presence of holoCaM (Figures 1.7 and 1.8). These include: the oxygenase domain of all three isoforms (Fischmann et al., 1999; Li et al., 2001, 2014; Matter et al., 2005, PDBs 4NOS, 1FOP, 1ZVL, 4D1N and 4D1O); the reductase domain of nNOS (Zhang et al., 2001; Garcin et al., 2004, PDBs 1TLL and 1F20; CaM bound to the CaM-binding region of eNOS (Aoyagi et al., 2003, PDB 1NIW) and nNOS (Valentine *et al*., 2006, PDB 2O60); CaM bound to the CaM-binding region of iNOS (Ng *et al.*, 2009, PDB 3GOF) and CaM bound to the FMN domain with the CaM-binding region of iNOS (Xia et al., 2009, PDB 3HR4).

Figure 1.7: Crystal structures of NOS oxygenase domains and NOS CaM-binding regions in complex with holo-CaM.

The crystal structure of (A) bovine eNOS oxygenase domain dimer (from PDB 1FOP Li et al., 2001), (B) human eNOS oxygenase domain dimer (from PDB 4D1O Li et al., 2014), (C) CaM bound to CaM-binding region peptide of eNOS (from PDB 1NIW Aoyagi et al., 2003) (D) rat nNOS oxygenase domain dimer (from PDB 1ZVL Matter et *a*l., 2005), (E) human nNOS oxygenase domain dimer (from PDB 4D1N Li et al., 2014), (F) CaM bound to CaM-binding region peptide of nNOS (from PDB 2O60 Valentine *et al*., 2006), (G)human iNOS oxygenase domain dimer (from PDB 4NOS Fischmann et al., 1999), (H) CaM bound to CaM-binding region peptide with FMN domain (from PDB 3HR4 Xia *et al.*, 2009), (I) CaM bound to CaM-binding region peptide of iNOS (from PDB 3GOF Ng *et al.*, to be published), (J) rat nNOS reductase domain dimer (from PDB 1TLL Garcin et al., 2004) and (K) rat nNOS reductase (from PDB 1F20 Zhang et al., 2001).

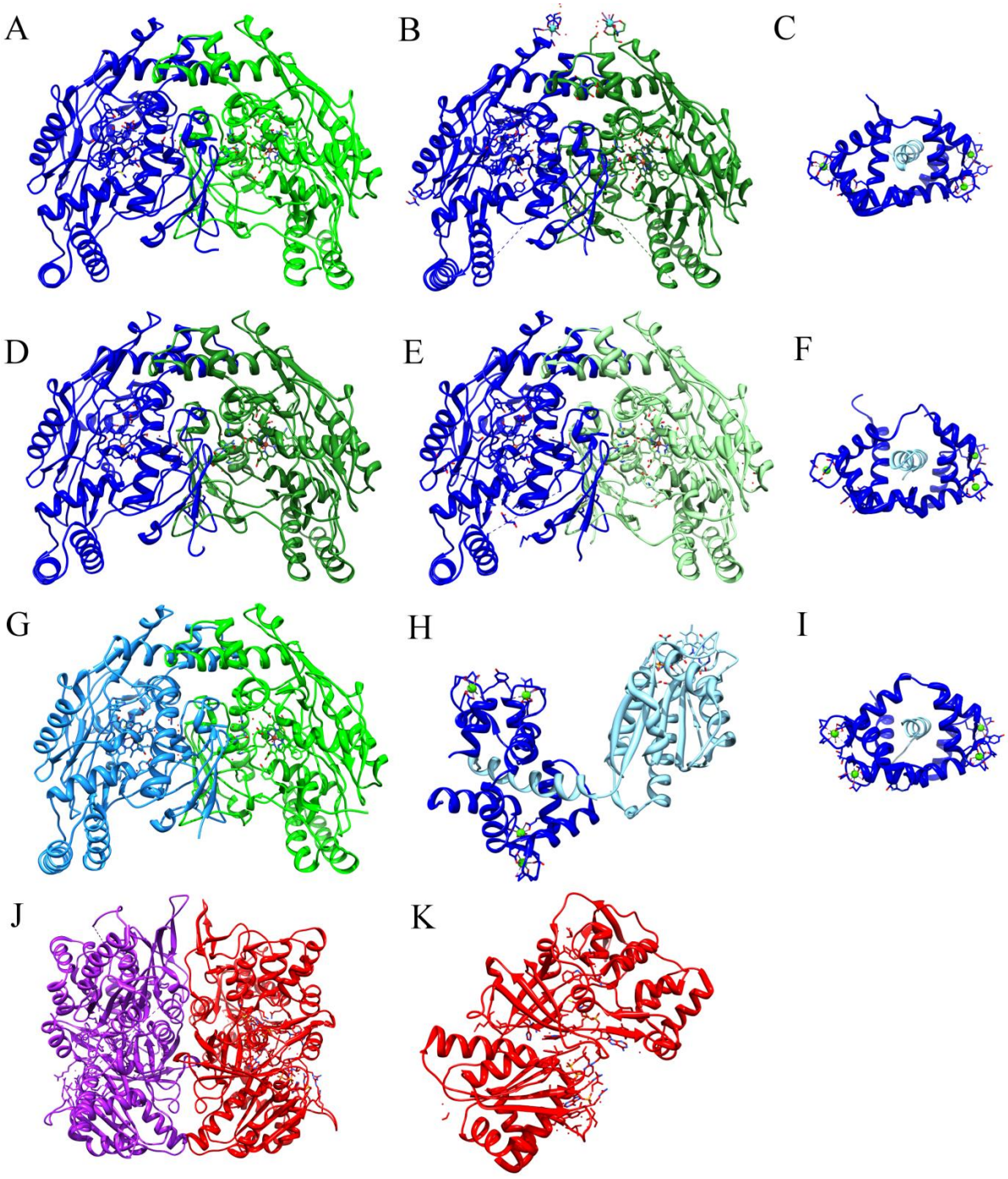
A
B
C
D
E
F
G
H
I
J
K

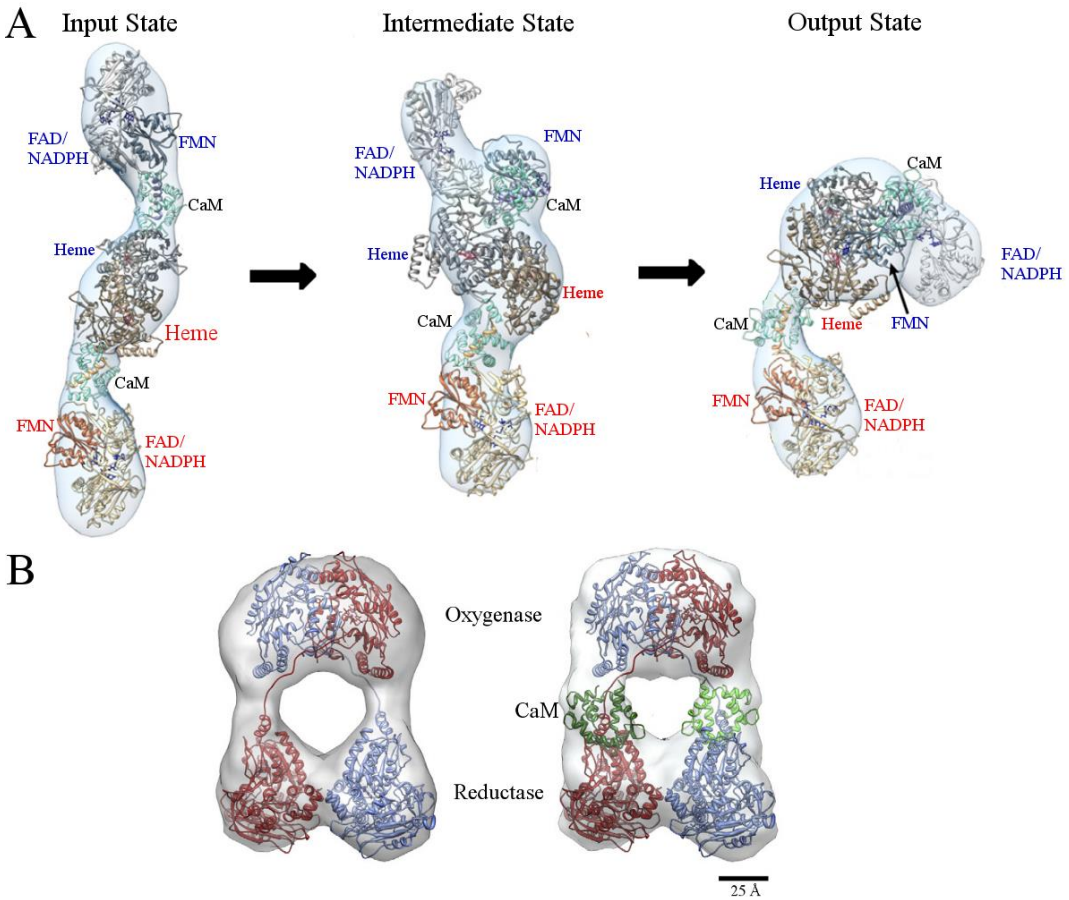

Figure 1.8: Model Structure of iNOS and eNOS architecture based on EM data

A. The iNOS homology model was generated based on fitting the nNOS reductase crystal structure (PDB 1TLL), iNOS FMN/CaM binding domain structure (PDB 3HR4) and the iNOS oxygenase dimer (PDB 4NOS). They were fit into a reconstruction of the EM map from the input, the intermediate, and the output states of iNOS. Reprinted from Proc. Natl. Acad. Sci. U. S. A, 111 (35), Campbell, M. G.; Smith, B. C.; Potter, C. S.; Carragher, B.; Marletta, M., Molecular Architecture of Mammalian Nitric Oxide Synthases, E3614–E3623, 2014 with permission from PNAS. B. The eNOS homology model was generated based on fitting the nNOS reductase crystal structure (PDN 1TLL), iNOS FMN/CaM binding domain structure (PDB 3HR4) and the eNOS oxygenase dimer (PDB 1FOP). The final model fit of the eNOS homodimer into the reconstruction of eNOS cryo-EM maps in the absence of CaM on the left and presence of CaM on the right. One monomer is shown in red, the other in blue. Reprinted from Journal of Structural Biology, 188 (1), Volkmann, N.; Martasek, P.; Roman, L. J.; Xu, X. P.; Page, C.; Swift, M.; Hanein, D.; Masters, B. S., Holoenzyme structures of endothelial nitric oxide synthase - An allosteric role for calmodulin in pivoting the FMN domain for electron transfer, 46-54, 2014, with permission from Elsevier. Data in B was acquired in the absence of $NADP^+$, suggesting a "closed" state, whereas an "open" state would occur when both CaM and $NADP^+$ are bound, as observed in the input state in A with data from Campbell et al. The structures in A would more accurately describe NOS.

The crystal structures of the oxygenase domains show that all three isoforms have a similar fold and that the dimer interface contains the heme and a structural zinc ion coordinated by four conserved cysteine residues, two from each monomer, which are involved in dimer stability (Roman et al., 2002). These structures have also shown the reductase domains of eNOS and nNOS form dimers, stabilized by salt bridges and hydrogen bonding in the interface, which has been disputed (Roman et al., 2002; Campbell et al., 2014). The iNOS reductase domain has not been observed to form a dimer (Roman et al., 2002; Garcin et al., 2004).

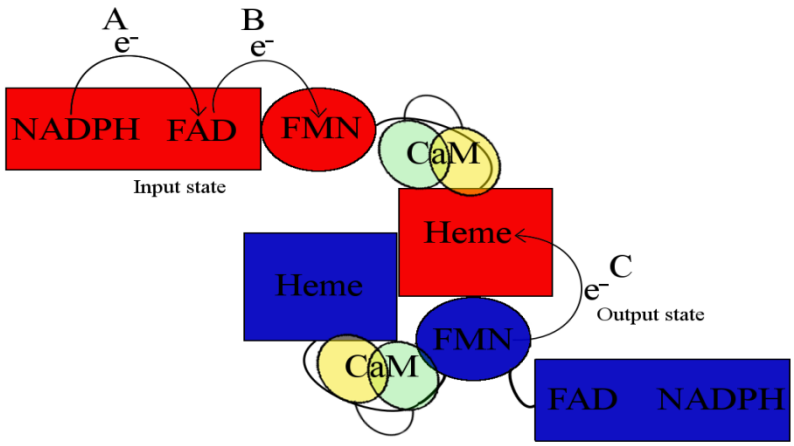

Figure 1.9: Electron transfer within NOS dimer.

The two NOS monomers are shown in blue and red. Electrons are transferred from (A) NADPH to FAD (B) to the FMN subdomain of the reductase domain of one monomer. Then (C) to the heme in the oxygenase domain of the opposite monomer (Alderton et al., 2001; Campbell et al., 2014).

1.2.2 NOS mechanism.

The mechanism of the electron transfer in NOS is still not fully understood, but possible mechanisms have been proposed. However, CaM binding to the CaM-recognition linker of the NOS enzymes is required to initiate the electron transfer reaction. This mechanism begins with the transfer of electrons from NADPH to FAD (Figure 1.9A), then from FAD to FMN in the reductase domain, which is known as the input state (Figure 1.9B). This is followed by transition to the output state (Figure

1.9C), that involves the electron transfer from the FMN subdomain to the heme of the oxygenase domain of the opposite monomer (Alderton et al., 2001; Campbell et al., 2014). This electron transfer from FMN to the heme of the opposite oxygenase domain cannot proceed without a subunit realignment and occurrence of conformational changes because the distance between them is 70 Å (Garcin et al., 2004). It was previously thought that CaM binding to the CaM-binding domain of NOS causes a dynamic process where the FMN subdomain is allowed to swing back and forth between the FAD and heme, shown in Figure 1.10 (Garcin et al., 2004; Daff, 2010).

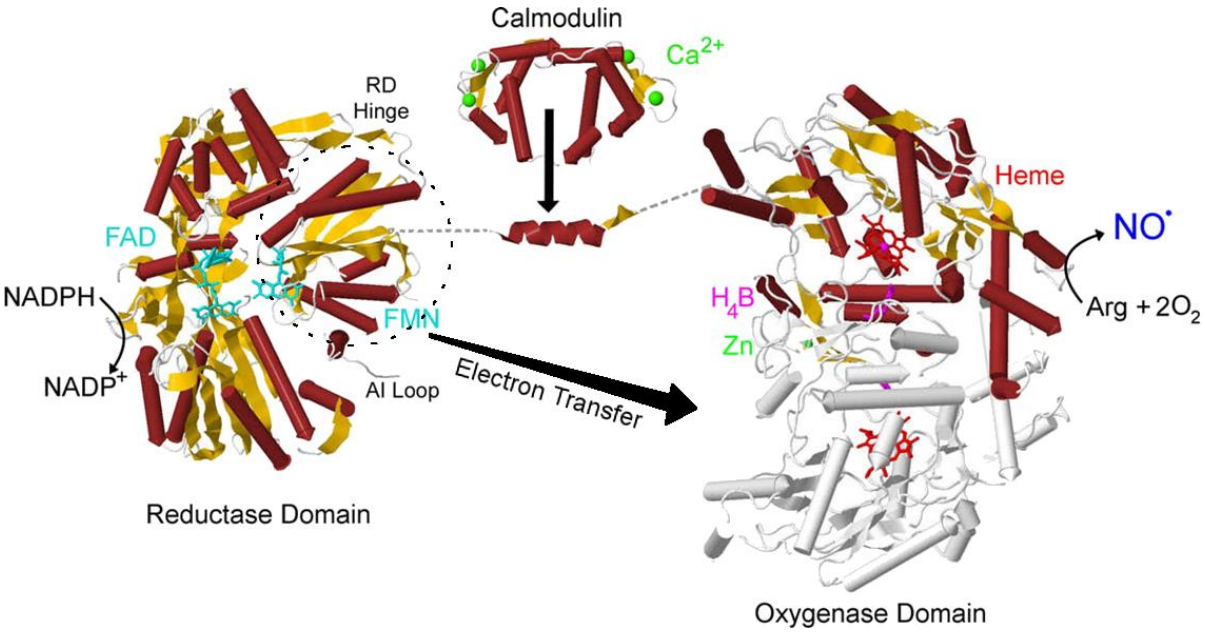

Figure 1.10: Structures of the domains of NOS aligned by amino acid sequence.

Shown is the reductase domain of nNOS (PDB 1TLL), CaM-binding region of eNOS bound with CaM (PDB 1NIW) and the dimeric oxygenase domain of nNOS (PDB 1ZVL). The FMN domain proposed to "swing" between the FAD and heme is circled in black. Reprinted from Nitric Oxide, 23 (10), Daff, S., NO Synthase: Structures and Mechanisms, 1-11, 2010, with permission from Elsevier.

More recent studies using cryo-electron microscopy, and biophysical techniques, such as pulsed-electron paramagnetic resonance, have given better insight into the CaM activated NOS mechanism (Campbell et al., 2014; Leferink et al., 2014; Volkmann et al., 2014). Although crystal

structures of individual domains of NOS have been reported, no NOS holoenzyme structure had been determined. Electron-microscopy studies were used to obtained a higher order domain architecture of inducible, endothelial, and neuronal NOS with and without CaM bound. The structures are similar, consisting of a dimerized oxidase domain, which acts as the anchoring dimeric structure for the entire enzyme molecule. It is flanked by two separated reductase domains, which exist in an equilibrium of conformations that alternate between FAD-FMN electron transfer and FMN–heme electron transfer with CaM binding inducing a shift in the conformational equilibrium to allow efficient electron transfer in NOS enzymes (Campbell et al., 2014; Volkmann et al., 2014). The conformations in Figure 1.8 represent snapshots of the continuous electron transfer pathway from the reductase domain in one monomer to the oxidase domain in the opposite monomer, which reveal that only a single reductase domain participates in electron transfer at a time. CaM activates NOS through the stabilization of structural intermediates and precise positioning of the pivot for the FMN domain tethered shuttling motion to accommodate efficient and rapid electron transfer in NOS (Campbell et al., 2014; Leferink et al., 2014; Sobolewska-Stawiarz et al., 2014; Volkmann et al., 2014).

All this information leads to a refined mechanism of NOS activity that suggests NOS exists in an equilibrium of conformations (Figure 1.11). In the resting state, both reductase domains adopt mostly open or ‘extended’ conformations, which shift towards a more ‘closed’ conformation upon binding of NADPH (Sobolewska-Stawiarz et al., 2014). Upon CaM binding, NOS adopts a variety of conformations compatible with both inter-flavin electron transfer, “input” state, and FMN to heme electron transfer, “output” state (Campbell et al., 2014; Volkmann et al., 2014).

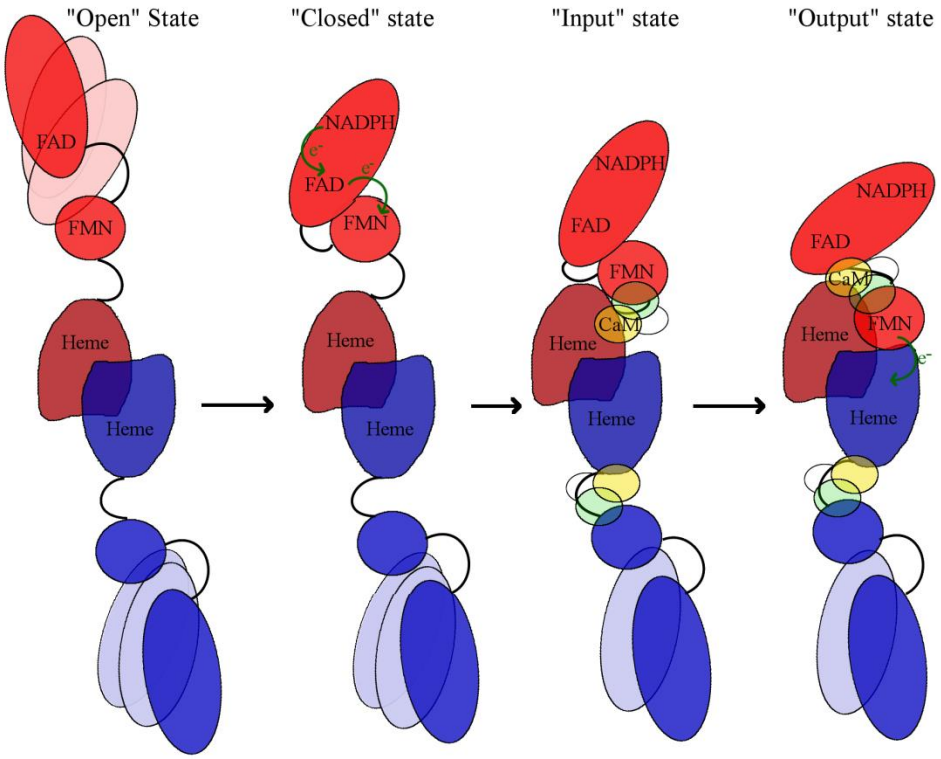

Figure 1.11: Current proposed mechanism for electron transfer:

In the open state (resting state), both reductase domains adopt mostly open or 'extended' conformations, which are very flexible. This shift towards a more 'closed' conformations upon binding of NADPH. Upon CaM binding, NOS adopts a variety of conformations compatible with both inter-flavin electron transfer, "input" state, and FMN to heme electron transfer, "output" state, indicated by the yellow arrow. Only one FMN domain participates in electron transfer at a time (Campbell et al., 2014; Leferink et al., 2014).

1.2.3 CaM binding to NOS enzymes.

CaM binds to NOS with a 1-5-8-14 CaM-binding motif, as shown in Figure 1.12, with the binding region consisting of residues 491-512 of eNOS, 731-752 of nNOS and 510-531 of iNOS (Aoyagi et al., 2003).

1 5 8 14

eNOS TRKKT FKEVA NAVKI SASLM GT (491-512)

nNOS RRAIG FKKLA EAVKF SAKLM GQ (731-752)

iNOS RREIP LKVLV KAVLF ACMLM RK (510-531)

Figure 1.12: Sequence of CaM-binding domains of NOS.

Residues corresponding to the 1-5-8-14 CaM-binding motif are shown. The sequences are for human iNOS, rat nNOS and bovine eNOS. Acidic and basic residues are shown in red and blue, respectively.

A previous crystal structure and a solution structure from our lab show that the CaM binding region of iNOS forms an α-helix that CaM wraps around, as shown in Figure 1.7 H and I (Xia et al., 2009; Piazza et al., 2012). Although iNOS displays Ca^{2+}-independent binding, it contains a 1-5-8-14 consensus binding motif of Ca^{2+}-dependent proteins, similar to cNOS, instead of containing the consensus IQ binding motif characteristic of Ca^{2+}-independent proteins, as described in section 1.1.3. However, its sequence differs from nNOS and eNOS by 42% and 30%, respectively, and has a much larger patch of hydrophobic residues in its α-helical conformation that binds with higher affinity to CaM (Aoyagi et al., 2003). Spratt *et al.* (2007) had previously shown that an iNOS peptide containing the CaM binding region binds to CaM in an antiparallel orientation, which was confirmed by the determined structures of the CaM-iNOS complex.

The rate constants for the binding of CaM to the NOS target peptides have been determined using several methods and show that CaM binds to the iNOS peptide with a higher affinity than the cNOS peptides (Table 1.2). The methods used include: fluorescence measurements with dansylated CaM (Vorherr et al., 1993; Anagli et al., 1995; Matsubara et al., 1997); surface plasmon resonance (SPR, Zoche et al., 1996); competition assays (Zhang and Vogel, 1994; Venema et al., 1996; Yuan et al., 1998); and FRET and stopped-flow spectroscopy (Wu et al., 2011).

These results showed that the cNOS peptides reversibly bind to CaM with nanomolar affinities and no binding was observed in the absence of Ca^{2+}, suggesting that the regulation of

cellular Ca^{2+} concentrations modulates this dynamic interaction. CaM binding to the iNOS peptide was found to be irreversible, Ca^{2+}-independent and to occur with a higher affinity. Ca^{2+} removal did not remove CaM from the iNOS peptide. However, Wu et al. found that the Ca^{2+}-depleted N- and C-lobes of CaM slowly separated from each other likely due to the conformational rearrangement of apo CaM.

Table 1.2: Binding kinetics of CaM binding to NOS peptides.

	k_a ($M^{-1}s^{-1}$)	k_d (s^{-1})	K_d (nM)
eNOS	2.9 x 10^{8}[i]	4.5[i]	1.6[i], 2.9[g], 4.0[f]
nNOS	1.58 x 10^{5}[e], 6.6 x 10^{8}[i]	7.87 x 10^{-4}[e], 3.7[i]	1.0[c], 1.8[a], 2.2[b], 5.0[e], 5.6[i]
iNOS	3 x 10^{4}[e], 6.1 x 10^{8}[i]	<10^{-5}[e], 0.063[i]	<0.1[d,e], 0.1[f], 0.3[h], 1.5[f], 3.3[i]

[a] (Vorherr et al., 1993)
[b] (Zhang and Vogel, 1994)
[c] (Sheta et al., 1994)
[d] (Anagli et al., 1995)
[e] (Zoche et al., 1996)
[f] (Venema et al., 1996)
[g] (Matsubara et al., 1997)
[h] (Yuan et al., 1998)
[i] (Wu et al., 2011)

A study by Weissman et al. (2002) showed four steps are required for CaM binding and activation of nNOS. First Ca^{2+} binds to the C-lobe of CaM, followed by this now Ca^{2+}-replete lobe binding to nNOS. When the intracellular Ca^{2+} concentration is increased the N-lobe binds Ca^{2+}, then this Ca^{2+}-replete lobe binds to nNOS. This model also suggests the reverse order of these steps occurs for deactivation of nNOS when the intracellular Ca^{2+} concentration decreases (Weissman et al., 2002).

1.2.4 Regulation of NOS.

The cNOS isoforms contain an autoinhibitory (AI) loop and all NOS isoforms contain extended C-terminal tails that act in conjunction with CaM as elements to regulate NOS's activity. The AI loop

found in the cNOS enzymes is positioned adjacent to the CaM-binding region and is thought to lock the FMN domain in its electron accepting position when Ca^{2+} concentrations are low. Upon the increase of the Ca^{2+} concentration the AI loop is only displaced upon Ca^{2+}-replete CaM binding (Salerno et al., 1997; Garcin et al., 2004). Another study showed that when this AI loop was removed from the cNOS isoforms, Ca^{2+}-dependent CaM activation was reduced and enzymatic activity increased by a factor of two compared to wild-type, and when it was inserted in the iNOS reductase domain, activity decreased by one third of wild-type (Montgomery et al., 2000; Knudsen et al., 2003). This implicates the AI loop in playing a role in the Ca^{2+} dependency of the cNOS isoforms perhaps by the direct interaction with CaM or the CaM binding site (Jones et al., 2004).

The C-terminal domain is thought to play a role in the electron transfer between the flavins, as well as protecting the NOS enzymes from becoming fully oxidized (Roman et al., 2002). All three isoforms have a C-terminal tail, ranging from 21 to 42 amino acids, with nNOS being the longest and iNOS the shortest. Removal of this tail from the NOS isoforms resulted in a large increase in electron flow between the flavins; however, these truncated NOS enzymes became fully oxidized without exhibiting the one-electron semiquinone form of the wild-type enzyme (Roman et al., 2002).

These regulatory elements are responsible for the control of the Ca^{2+} dependency of the NOS isoforms, and the control of electron flow, as well as providing a protective function for NOS. The binding of CaM to cNOS displaces these regulatory elements; however, the absence of this AI loop and the shorter C-terminal tail in iNOS along with the Ca^{2+}-independence of iNOS require further study.

1.2.5 Post-Translational Modifications of NOS.

The binding of CaM and the transfer of electrons from the reductase to the oxygenase domain of the cNOS enzymes, particularly eNOS, is dependent on protein phosphorylation and dephosphorylation (Fleming and Busse, 2003). Phosphorylation of eNOS can occur on serine, tyrosine and threonine residues and eNOS contains many potential phosphorylation sites that can play a role in regulating its activity (Fleming et al., 1998; Harris et al., 2001; Michell et al., 2001; Kou et al., 2002). Phosphorylation of Ser 1177, which is located in the C-terminal tail extension, in the reductase domain has been found to result in the activation of eNOS, whereas the phosphorylation of Thr 495 within the CaM-binding domain has been found to reduce eNOS activity (Fleming et al., 2001; Matsubara, 2003; Tran et al., 2008). Phosphorylation of Ser 633, found in the AI loop, has also been shown to increase eNOS activity (Michell et al., 2002) Perturbations of eNOS phosphorylation have been reported in a number of diseases (Kolluru et al., 2010). Phosphorylation of Thr495 acts as a negative regulatory site and has been reported to interfere with the binding of CaM to the CaM-binding domain affecting activation of the enzyme (Fleming et al., 2001; Fleming and Busse, 2003).

1.3 NMR Spectroscopy

One of the main methods to determine the 3D structure of a protein is through the use of NMR spectroscopy. NMR can be used to determine high resolution 3D structures, comparable to X-ray crystallography, and to monitor protein-ligand interactions and internal dynamics of a protein (Wüthrich, 1986). NMR is also used to determine structures of proteins and molecules that cannot be crystallized due to their high flexibility and mobility. The determination of large protein structures becomes a limitation of NMR because of chemical shift overlap and lower sensitivity. Also, proteins require the incorporation of isotopes such as ^{15}N and ^{13}C, which are costly (Wüthrich, 1986;

Cavanagh et al., 2007). For NMR studies of complexes, both partner proteins must be available in stable isotopically (^{13}C, ^{15}N) labeled forms. The most common technique for isotopically labeling proteins is to clone and over express them in bacteria, most frequently using *E. coli*.

The NMR experiment consists of placing a solution of the protein of interest inside a static magnetic field and detecting the unique resonance frequencies of the NMR active nuclei when they are exposed to radiofrequency (RF) radiation (Wüthrich, 1986; Ernst, Richard et al., 1987). The first step in this structure determination is to completely assign the ^{1}H spectrum of the protein, then assign as many nuclear Overhauser enhancement (NOE) interactions as possible (James and Oppenheimer, 1994; Neuhaus and Williamson, 2000).The principal information necessary for determining the 3D structure of a protein is derived from NOE measurements, which provide a set of internuclear proton distance constraints (James and Oppenheimer, 1994). NOEs are due to the dipolar coupling, through-space, between nuclei, in which the local field at one nucleus is influenced by the presence of the other (Neuhaus and Williamson, 2000). The larger the number of NOE restraints, the higher the accuracy of the structure.

The problem with the assignment of larger proteins is overlapping of resonances and increased line widths, due to the increasing rotational correlation time. The solutions to these problems are the isotopic labelling of the sample and the use of 2D and 3D heteronuclear NMR (Ernst, Richard et al., 1987; Evans, 1995). 2D experiments are used to measure the correlation of two nuclei resonance frequencies through-bond or through-space (Wüthrich, 1986). The use of 3D and 4D experiments have aided in overcoming the problem of overlapping peaks by expanding the 2D spectrum into additional dimensions, allowing these overlapping areas to be separated into layers.

One of the key spectra used in structure determination is the ^{1}H-^{15}N-heteronuclear single quantum correlation (HSQC) experiment (Bodenhausen and Ruben, 1980). This experiment

correlates each proton attached to a nitrogen atom in the protein, which include the backbone amides except proline, and the side chain amides. This spectrum provides the "finger print" of the protein, typically giving rise to one peak for each amino acid in the protein. Assignment of these peaks to specific residues in the protein cannot be done using the ^{1}H-^{15}N-HSQC alone, and other 3D experiments must be performed. These experiments were used to assign the ^{1}H, ^{13}C, and ^{15}N chemical shifts for the protein and are shown in Figure 1.13. Once all of the ^{1}H, ^{13}C, ^{15}N resonance assignments have been determined, the through-space nuclear Overhauser effect spectroscopy (NOESY) experiment can be used to determine distance constraints. The NOESY shows NOE cross-peaks of nuclei that are close (within ~5Å) in the folded protein but may be far away in the primary sequence (Wüthrich, 1986).

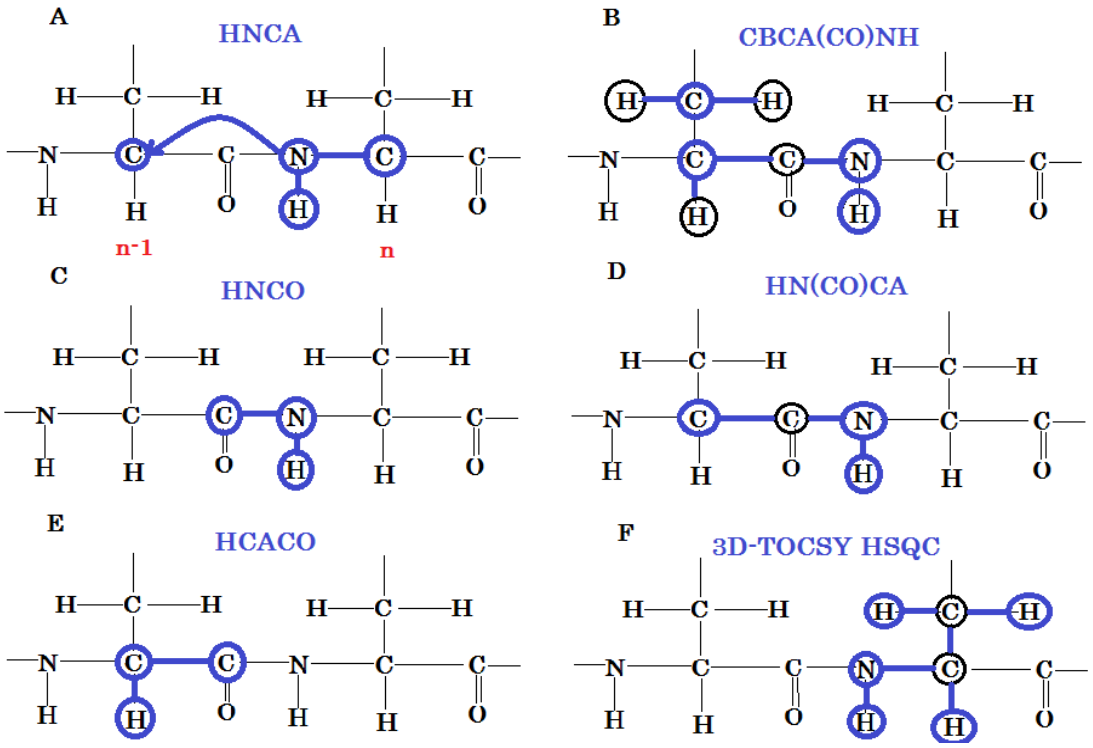

Figure 1.13: Heteronuclear multidimensional NMR experiments used for resonance assignments of proteins.

NMR experiments used to make resonance assignments for ^{1}H, ^{13}C and ^{15}N nuclei in a protein (Cavanagh et al., 2007). This is done by the transfer of magnetization through bonds, shown by blue lines, to different nuclei, shown by blue circles. (A) HNCA-3D experiment which correlates the ^{15}N and NH chemical shifts with the intraresidue and preceding residue Cα shift (Kay et al., 1990). (B) CBCA(CO)NH-3D experiment which correlates the ^{15}N and NH chemical shifts with the preceding residue Cα and Cβ shift (Grzesiek and Bax, 1992b). (C) HNCO-3D experiment which correlates the ^{15}N and NH chemical shifts with the preceding residue carbonyl shift (Kay et al., 1990). (D) HN(CO)CA-3D experiment which correlates the ^{15}N and NH chemical shifts with the preceding residue Cα shift (Bax and Ikura, 1991). (E) HCACO which correlate the carbonyl shift the intraresidue Cα and Hα shifts (Kay et al., 1990). (F) 3D-TOCSY (TOtal Correlation SpectroscopY) HSQC-3D experiment which correlates the ^{15}N and NH chemical shifts with the side chain ^{1}H shifts (Bax et al., 1990).

1.3.1 Strategy for NMR spectra assignment.

The NMR spectra were visualized and assignments made using the Computer Aided Resonance Assignment (CARA) version 1.8.4 (Keller, 2005). The assignment of the protein starts with the ^{1}H-^{15}N-HSQC spectrum. After arbitrarily assigning system numbers to each peak in the ^{1}H-^{15}N-HSQC spectrum, HNCA, HN(CO)CA and CBCA(CO)NH spectra are used to correlate the HN of amino acid "i" on the ^{15}N-HSQC to a Cα of amino acid "i" and "i-1", and Cβ of "i-1".

After all possible peaks are assigned to HN, $C\alpha_i$, $C\alpha_{i-1}$ and $C\beta_{i-1}$, the HNCA is used to start the backbone assignment. The residues are connected by finding the best matches of the $C\alpha_i$ chemical shift from one system with the $C\alpha_{i-1}$ chemical shift of a different system. This is done by viewing the HNCA spectrum as a strip for each amide peak system and aligning all best possible carbon chemical shifts for the preceding and subsequent amide system. Residues chosen as starting points for the backbone assignment are those that have unique carbon chemical shifts, such as threonine, alanine and glycine. The backbone is connected by confirming that the chemical shifts of the adjacent amino acids are in the correct range for the required amino acid in the sequence.

After a tentative backbone assignment is made using the HNCA spectrum, the ^{15}N-NOESY-HSQC spectrum is used to aid in confirming the assignment. In the H_{NOE} plane of each NH in the ^{15}N-NOESY, cross peaks of the NH_{i-1} and NH_{i+1} should be present, which, if the backbone assignment is correct, will correspond to the NH of the adjacent amino acids in the sequence. Next, the intraresidue side chain carbon and proton peaks are assigned using various TOCSY experiments obtained. The side chain carbon assignments are made using the hCCH-$TOCSY_{ali}$ experiment, whereas, the side chain proton assignments are made using the HCcH-$TOCSY_{ali}$, ^{15}N-TOCSY-HSQC and HcccoNH experiments. After all possible spins are assigned to each amino acid, NOE cross peaks can be

assigned by analyzing the various NOESY experiments obtained. The ^{15}N-NOESY HSQC and $^{13}C_{ali}$-NOESY HSQC spectra are viewed and all cross peaks not assigned to intraresidue protons are assigned to interresidue protons.

1.3.2 NMR methods for studying protein dynamics.

In addition to 3D structures, NMR spectroscopy can also provide quantitative information on molecular dynamics of protein systems at a residue specific level. These studies provide direct evidence of structural changes and intramolecular dynamics associated with functions that are central to understanding the role of dynamics in protein function (Kay, 1998, 2005; Ishima and Torchia, 2000; Wand, 2001; Kempf and Loria, 2003; Kwan et al., 2011). By tracking chemical shift changes, NMR spectroscopy is able to characterize very weak interactions between proteins and ligands at atomic (or residue) levels (Pochapsky et al., 2010; Sikic et al., 2010). NMR spectroscopy can also provide information about conformational dynamics and exchange processes of biomolecules at timescales ranging from picoseconds to seconds, and is very efficient in determining ligand binding and mapping interaction surfaces of protein/ligand complexes as shown in Figure 1.14 (Kay, 1998; Ishima and Torchia, 2000).

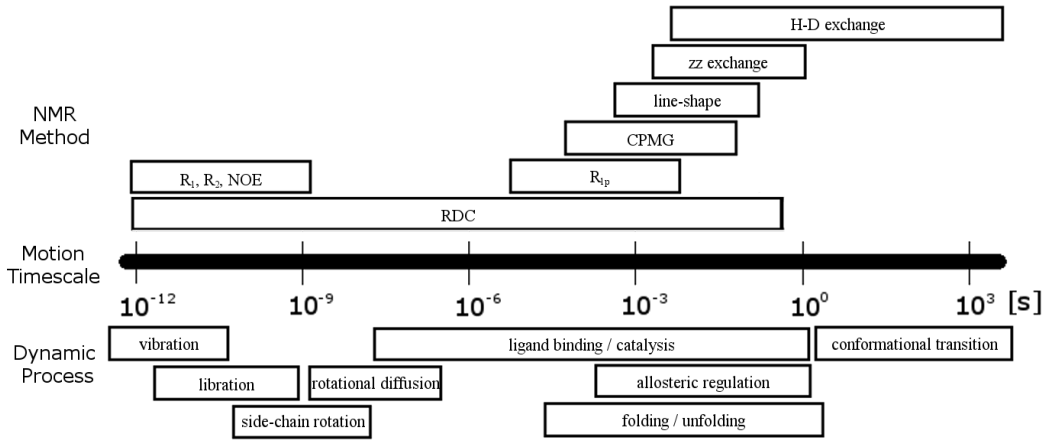

Figure 1.14: Time scales of various dynamic processes found in proteins and NMR method used to determine them (Kay, 1998, 2005; Ishima and Torchia, 2000).

1.3.2.1 Amide exchange experiments.

Detailed information about fluctuations in protein structures and site-specific information on the stability of secondary structural elements can also be obtained from the measurement of amide proton (NH) hydrogen/deuterium exchange (H/D) rates using NMR spectroscopy (Andrec et al., 1995; Polshakov et al., 2006; Ma and Nussinov, 2011). These fluctuations expose some of the NH to the D_2O solvent, thus facilitating the NH/ND exchange process while other amide protons remain protected from exchange. The exchange rate of NHs in proteins is determined by a combination of their intrinsic exchange rate in the absence of secondary structure and the presence of secondary structure and solvent inaccessibility that protect from exchange (Englander and Kallenbach, 1983; Englander and Mayne, 1992). H/D exchange experiments are also useful for accessing the stability of specific structure elements within a protein or protein complex (Williams et al., 2003, 2004).

1.3.2.2 ^{15}N relaxation experiments.

Information about residue specific internal dynamics on the fast, picosecond to nanosecond, timescale is determined primarily from model-free analyses (Lipari and Szabo, 1982a; Kay, 1998). This is

accomplished through the analysis of longitudinal (T_1) and transverse (T_2) relaxation, as well as heteronuclear NOEs (Kay et al., 1989). This allows internal motions such as bond vibrations and librations to be interpreted through the determination of order parameters (S^2) and internal effective correlation times (τ_e) by the "model free" approach (Lipari and Szabo, 1982a). These parameters quantitatively describe the magnitude and time scale of local, intramolecular motions and thus allow one to correlate molecular dynamics with biological function. The model-free approach characterizes backbone mobility using an order parameter S^2, which may be interpreted as the amplitude of the motion, and a correlation time, τ_i, which is the characteristic time constant of this motion (Kay, 2005, 2015; Kay and Frydman, 2014).

1.4 Research Objectives

The purpose of this thesis was to further characterize the structural and dynamic interaction of CaM with the NOS enzymes. This was to be accomplished by:

1. Determining the solution structure of CaM bound to the peptide of the eNOS CaM-binding domain phosphorylated at Thr495.
2. Elucidating the chemical shift perturbations induced by residue specific mutations of CaM interacting with NOS peptides and determining the structure of a Ca^{2+}-deficient CaM mutant with eNOS.
3. Determine the structure and dynamics of NOS and CaM interactions at physiological Ca^{2+} concentrations.
4. Investigate the structural changes induced by Ca^{2+}-binding disabling mutations to CaM.

Chapter 2

Solution structure of calmodulin bound to the target peptide of endothelial nitric oxide synthase phosphorylated at Thr495*

2.1 Introduction

CaM is a ubiquitous cytosolic Ca^{2+}-binding protein that consists of two globular domains joined by a flexible central linker region. CaM binds and activates the Ca^{2+}- dependent cNOS enzymes at elevated intracellular cellular Ca^{2+} concentrations, whereas, CaM binds and activates iNOS in a Ca^{2+}-independent manner. A large conformational change that CaM induces in the reductase domain of the NOS enzymes allows for the FMN domain to interact with the FAD to accept electrons and pass the electrons on to the heme during catalysis (Welland and Daff, 2010). Clearly, these conformational changes caused by CaM are important in stimulating efficient electron transfer within the NOS enzymes.

---

* **The results presented in this chapter have been published:**

Piazza, M., Taiakina, V., Guillemette, S. R., Guillemette, J. G., Dieckmann, T., (2014) Solution Structure of Calmodulin bound to the target peptide of Endothelial Nitric Oxide Synthase phosphorylated at Thr495, *Biochemistry*, 53 1241-1249.

Unless otherwise stated, all of the work reported in this chapter was performed and analyzed by the candidate. The experiment depicted in Figure 2.5 was performed by S. R. Guillemette. The experiment depicted in Figure 2.13 was performed by V. Taiakina.

The activity of eNOS is regulated by multiple mechanisms, including posttranslational modifications such as protein phosphorylation (Fleming and Busse, 2003; Piazza et al., 2012). The binding of CaM and the transfer of electrons from the reductase to the oxygenase domain of eNOS is dependent on protein phosphorylation and dephosphorylation (Fleming and Busse, 2003). The eNOS enzyme can be phosphorylated on serine, tyrosine and threonine residues and contains many potential phosphorylation sites that can play a role in regulating its activity (Fleming et al., 1998; Harris et al., 2001; Michell et al., 2001; Kou et al., 2002). Phosphorylation of Ser1177 in the reductase domain has been found to result in the activation of eNOS, whereas the phosphorylation of Thr495 within the CaM-binding domain has been found to reduce eNOS activity (Fleming et al., 2001; Matsubara, 2003; Tran et al., 2008). Perturbations of eNOS phosphorylation have been reported in a number of diseases (Kolluru et al., 2010). Phosphorylation of Thr495 acts as a negative regulatory site and has been reported to interfere with the binding of CaM to the CaM-binding domain affecting activation of the enzyme (Fleming et al., 2001; Fleming and Busse, 2003).

There is considerable interest in understanding the structural and functional effects that the phosphorylation of Thr495 in eNOS has on the calcium dependent CaM binding and activation of the enzyme. In the present study the structural and functional effects that the phosphorylation of eNOS has on binding to CaM were investigated. Steady-state fluorescence and isothermal titration calorimetry (ITC) were used to monitor the binding of CaM to the wild type eNOS CaM-binding domain peptide and the eNOS CaM-binding domain peptide phosphorylated at Thr495 at various free Ca^{2+} concentrations. The structural effects of Thr495 phosphorylation on CaM binding to eNOS were investigated by the determination of the solution structure of CaM bound to the eNOS CaM-binding domain peptide phosphorylated at Thr495. This investigation provides a better understanding of the

interaction of CaM with the phosphorylated or nonphosphorylated CaM-binding domain of eNOS at Thr495.

2.2 Methods and experiments

2.2.1 CaM protein expression.

The vector pET9d (NOVAGEN) used to express the rat calmodulin was made by Newman (2003) by cloning in the CaM sequence using restriction enzyme sites, *NcoI* and *BaMHI*. An overnight culture of transformed *E. coli* BL21 (DE3) with pET9dCaM was used to inoculate 1 L of LB media in 4 L flasks supplemented with 30 μg/ml of kanamycin. Protein expression was induced after an OD_{600nm} of 0.6 - 0.8 was reached with 500 μM isopropyl-*β*-D-thiogalactopyranoside (IPTG) and the cells were harvested after 4 h by centrifugation at 6000 x g at 4°C for 5 minutes.

2.2.2 CaM purification.

Cells were resuspended in 4 volumes of 50 mM MOPS, 100 mM KCl, 1 mM EDTA, 1 mM DTT, pH 7.5 and lysed by homogenization using an Avestin EmulsiFlex-C5 homogenizer (Ottawa, ON). The lysate was then clarified by centrifugation at 48,000 x g for 30 minutes at 4°C. To the clarified supernatant, $CaCl_2$ was added to a concentration of 5 mM in order to saturate CaM with Ca^{2+} and induce the exposure of hydrophobic patches in the N- and C-domains of CaM to allow CaM to interact with the resin. This Ca^{2+}-saturated supernatant was then loaded onto phenyl sepharose 6 fast flow highly-substituted resin (GE Healthcare Bio-Sciences, Baie d'Urfe, PQ) in a 1 cm x 10 cm column connected to the Äkta design system (GE Healthcare Bio-Sciences, Baie d'Urfe, PQ) equilibrated with 50 mM Tris-HCl, 1 mM $CaCl_2$, pH 7.5 @ 4°C. After the Ca^{2+}-saturated solution was loaded; the resin was washed with 5 column volumes of the above buffer. The resin was

subsequently washed with 3 column volumes of 50 mM Tris-HCl, 500 mM NaCl, 1 mM $CaCl_2$, pH 7.5 @ 4°C to remove any non-specific proteins that were interacting with the resin. The resin was finally washed with 3 column volumes of 50 mM Tris-HCl, 1 mM $CaCl_2$, pH 7.5 to remove NaCl from the resin. CaM was then eluted from the phenyl sepharose resin with 10 mM Tris-HCl, 10 mM EDTA, pH 7.5 @ 4°C and 2 mL fractions were collected. Fractions were then scanned from 325 to 250 nm on a Varian Cary UV–visible Spectrophotometer (Varian, Mississauga, ON). Fractions displaying the characteristic absorbance peaks of CaM at 277 nm (for tyrosine residues) and 269, 265, 259, and 253 nm (for phenylalanine residues) were pooled and concentrated to 2 mL sample sizes. The samples were then run through a HiLoad 16/600 Superdex 75 column (GE Healthcare Bio-Sciences, Baie d'Urfe, PQ) connected to the Äkta design system using buffer consisting of 50 mM Tris-HCl, 0.5 mM EDTA, pH 7.5. Fractions eluted at the characteristic time point for proteins of CaM's size were collected. Isolation and purity of the CaM proteins (148 residues) were confirmed by ESI-MS and SDS-PAGE.

2.2.3 NOS CaM-binding domain peptides.

The human eNOS (TRKKTFKEVANAVKISASLMGT, 22 residues corresponding to residues 491-512 from the full length eNOS protein) peptide was custom synthesized by Sigma-Aldrich Inc. The Thr495 phosphorylated human eNOS (TRKKpTFKEVANAVKISASLM, 20 residues corresponding to residues 491-510 from the full length eNOS protein) peptide was custom synthesized by GenScript. The phosphorylation was confirmed by ESI-MS.

2.2.4 NMR experiments.

2.2.4.1 Sample preparation for NMR investigation.

An overnight culture of transformed *E. coli* BL21 (DE3) with pET9dCaM was used to inoculate 1 L of M9 media (11.03 g/L $Na_2HPO_4 \cdot 7H_2O$, 3.0 g/L KH_2PO_4, 0.5 g/L NaCl, 2 mM $MgSO_4$, 0.1 mM $CaCl_2$, 3 μM $(NH_4)_6(MO_7)_{24}$, 400 μM H_3BO_3, 30 μM $CoCl_2$, 10 μM $CuSO_4$, 80 μM $MnCl_2 \cdot 4H_2O$, 10 μM $ZnCl_2$, 10 mM $FeSO_4$, 100 μg/mL kanamycin) containing 2 g/L ^{13}C-glucose and 1 g/L $^{15}NH_4Cl$. ^{13}C-^{15}N CaM was purified as described in section 2.2.2. The samples were prepared for NMR experiments via a buffer exchange into NMR solution (100 mM KCl, 10 mM $CaCl_2$, 0.2 mM NaN_3, 90% H_2O/10% ^2H_2O) at pH 6.0 using a YM10 centrifugal filter device (Millipore Corp., Billerica, USA). All NMR samples contained at least 1 mM CaM in a total volume of 500 μL. The samples were transferred into 5 mm NMR sample tubes and stored at 4^{o}C until required for NMR experiments.

The expression and purification of the various isotopically labeled CaM constructs produced peptide-free holoCaM. To obtain the complex, CaM samples were titrated with eNOSpT495 peptide to saturation in a 1:1 CaM:peptide ratio.. The synthetic eNOSpT495 peptide was prepared by dissolving the powdered peptide in water to produce a concentration of 1 mM, aliquot into 200 μL and 100 μL fractions in 0.5 mL Eppendorf tubes and then lyophilized. Complex formation was monitored after each addition by acquisition of a ^1H-^{15}N heteronuclear single-quantum coherence (HSQC) spectrum.

2.2.4.2 NMR spectroscopy and data analysis.

NMR spectra were recorded at 25^{o}C on a Bruker 600 MHz DRX spectrometer equipped with XYZ-gradients triple-resonance HCN probe (Bruker, Billerica, MA, USA). Spectra were analyzed using the program CARA (Keller, 2005).

Specific assignments of the CaM backbone resonances were achieved using a combination of 3D triple resonance experiments including HNCA, HN(CO)CA, CBCA(CO)NH, and HNCO (Grzesiek and Bax, 1992b; Muhandiram and Kay, 1994). Side-chain resonances were assigned using the TOCSY type experiments HC(C)H-TOCSY, (H)CCH-TOCSY and H(CCO)NH (Bax et al., 1990). Specific assignments of the eNOSpThr495 peptide were obtained from ^{15}N-double-filtered NOESY experiments (Ikura and Bax, 1992).

2.2.4.3 Structure calculation.

The ^{1}H, ^{13}C and ^{15}N resonance assignments were utilized to identify constraints for the structure calculations. Distance constraints for the solution structure of CaM-eNOSpThr495 were obtained from ^{15}N-NOESY-HSQC, ^{13}C- NOESY-HSQC and ^{15}N-double-filtered NOESY spectra acquired on samples containing labeled CaM and unlabeled peptide (Fesik and Zuiderweg, 1990; Clore and Gronenborn, 1991; Ikura and Bax, 1992). In addition, dihedral angle restraints were derived from chemical shift analysis with TALOS+ (Shen et al., 2009). CNSsolve version 1.2 (Brunger et al., 1998) was used to perform the structure calculations. The calculation was initiated with an extended conformation file and run through several iterations of a standard simulated annealing protocol to minimize the energies. The final 20 lowest energy structures were selected.

2.2.4.4 Accession Numbers.

The coordinates and NMR parameters for the ‘Solution Structure of Calmodulin bound to the target peptide of Endothelial Nitrogen Oxide Synthase phosphorylated at Thr495' have been deposited in the PDB and BMRB and have been assigned RCSB ID code rcsb103588, Protein Data Bank (PDB) ID code 2mg5 and BMRB accession number 19586.

2.2.5 Delphi calculation of the CaM structures.

Delphi electrostatic potentials of the structure was calculated using the DelPhiController interface of UCSF Chimera 1.5.3, build 33475 (Pettersen et al., 2004). The parseRes atomic radii file and atomic charge file were used as the input files in the calculation. The electrostatic potential surface was visualized in Chimera.

2.2.6 Dansylation of CaM.

Dansyl-CaM was prepared as previously described (Kincaid et al., 1982). CaM (1 mg/ml) was buffer exchanged into 10 mM $NaHCO_3$, 1 mM EDTA, pH 10.0, at 4°C. 30 µl of 6 mM dansyl-chloride (5-dimethylaminonapthalene-1-sulfonyl chloride) in DMSO (1.5 mol/mol of CaM) was added to 2 ml of CaM, with stirring. After incubation for 12 hr at 4°C, the mixture was first exhaustively dialyzed against 500 volumes of 150 mM NaCl, 1 mM EDTA, 20 mM Tris-HCl, pH 7.5, at 4°C, and then exhaustively dialyzed against 500 volumes of water. Labeling yields were determined from absorbance spectra using the ε_{320} of 3,400 $M^{-1}cm^{-1}$ and were compared to actual protein concentrations determined using the Bradford method with wild-type CaM used as the protein standard (Chen, 1968). ESI-MS was used to confirm successful dansyl-labeling of each CaM protein. The concentration of dansyl-CaM in all experiments was 2 µM.

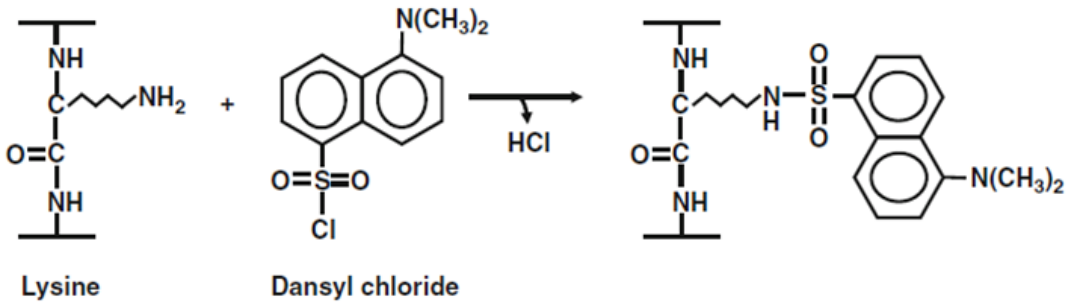

Figure 2.1: Mechanism of dansyl chloride labelling of wild-type CaM.

2.2.7 Steady state fluorescence.

Fluorescence emission spectra were obtained using a PTI QuantaMaster spectrofluorimeter (London,ON). Fluorescence measurements were made on 50 μL samples consisting of dansyl-CaM (2 μM) alone or with eNOS or eNOSpThr495 peptide in 30 mM MOPS, 100 mM KCl, 10 mM EGTA, pH 7.2 with an increasing concentration of free Ca^{2+}. Free Ca^{2+} concentration was controlled using the suggested protocol from the calcium calibration buffer kit from Invitrogen. The excitation wavelength for all of the dansyl-CaMs was set at 340 nm and emission was monitored between 400 and 600 nm. Slit widths were set at 2 nm for excitation and 1 nm for emission. Relative fluorescence was calculated by the following equation: relative fluorescence = $(F - F_0)/(F_{max} - F_0)$, where F is the measured intensity, F_{max} is the maximum intensity, and F_0 is the intensity without added Ca^{2+}.

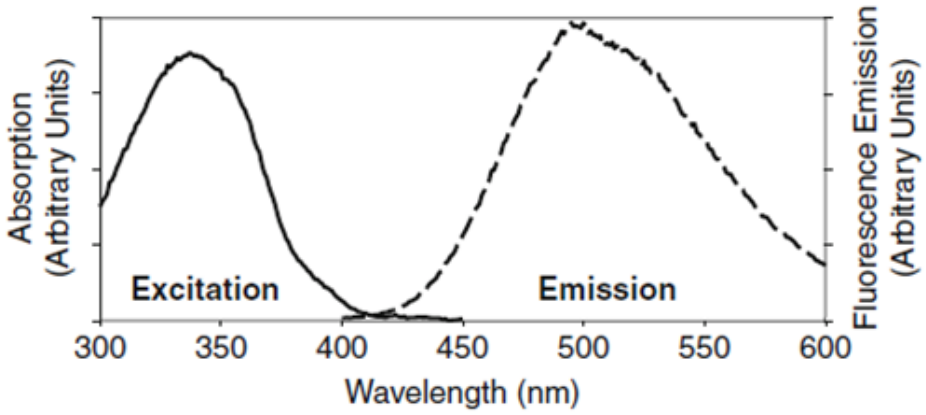

Figure 2.2: Fluorescence emission spectrum of D-CaM (solid line, excitation at 340 nm) and excitation spectrum (dotted line, emission max at 500 nm).

2.2.8 Isothermal titration calorimetry.

All ITC recordings were performed on a Microcal ITC200 from Microcal (Northampton, MA) at 25°C, 1000 rpm stir speed, and reference power set to 5 µcal/s. In the experiments at saturating Ca^{2+} concentrations the buffer used was 30 mM MOPS, 100 mM KCl, pH 7.2 and 1 mM $CaCl_2$ and was identical between cell and syringe. In the experiments at 225 nM free Ca^{2+} the calcium calibration buffer kit from Invitrogen was used and the buffer consisted of 30 mM MOPS, 100 mM KCl, pH 7.2 10 mM EGTA and 6.0 mM CaEGTA and was identical between cell and syringe. Buffer into buffer, peptide into buffer and buffer into CaM controls showed no significant baseline decay or drift and relatively low, consistent heats of injection, indicating sufficiently matched cell and syringe buffer conditions. 39 µL of each peptide was titrated into 200 µL of CaM at varying concentrations (optimal starting conditions were determined empirically), typically from 100 µM peptide into 10 µM CaM to 500 µM peptide into 50 µM CaM, over the course of 20–30 injections at 2–3 min intervals. Data analysis was performed using Origin ITC200 Origin70 module with pre-loaded fitting equations for one- and two-sites models. The one-set-of-sites model was found to be applicable to all experiments.

2.2.9 Circular dichroism (spectropolarimetry).

CD was performed using a Jasco J-715 CD spectropolarimeter and analyzed using J-715 software (Jasco Inc., Easton, MD, USA) as previously described (Fernando et al., 2002) with some modifications. Samples were measured in a 1 mm quartz cuvette (Hellma, Concord, ON) and kept at 25°C using a Peltier type constant-temperature cell holder (model PFD 3505, Jasco, Easton, MD). Samples consisted of 10 μM of synthetic eNOS or eNOSpThr495 CaM-binding domain peptides. Samples were in 10 mM Tris-HCl buffer (pH 7.5), 150 mM NaCl, and 200 μM $CaCl_2$. Spectra were recorded over a 190-250 nm range with a 1.0 nm band width, 0.2 nm resolution, 100 mdeg sensitivity at a 0.125 s response and a rate of 100 nm/min with a total of 25 accumulations. Data is expressed as the mean residue ellipticity ($\boldsymbol{\theta}$) in degree cm^2dmol^{-1}.

2.3 Results and discussion

2.3.1 NMR spectroscopy and CD.

NMR spectroscopy was used to assess changes to the CaM-eNOS complex due to the phosphorylation of Thr495. However, as mentioned above in section 2.2.4.1, the eNOSpThr495 peptide had to be titrated into the ^{13}C-^{15}N CaM solution to achieve the 1:1 binding of CaM to the eNOSpT495 peptide. This was done by acquiring a ^{15}N-HSQC spectrum after each titration of eNOSpT495 and monitoring the shift changes of the CaM amide peaks (shown in Figure 2.3). The titration of CaM with eNOSpT495 exhibited a slow exchange, where, as the titration proceeded, one could see that the intensity of the amide peak of the unbound CaM decreased as the intensity of the amide peak of the eNOSpT495 bound CaM increased. The sample was considered to be fully bound

to the eNOSpT495 peptide when the peak of free CaM disappeared and only the peak of bound CaM was visible. This saturated sample was used for all other NMR experiments.

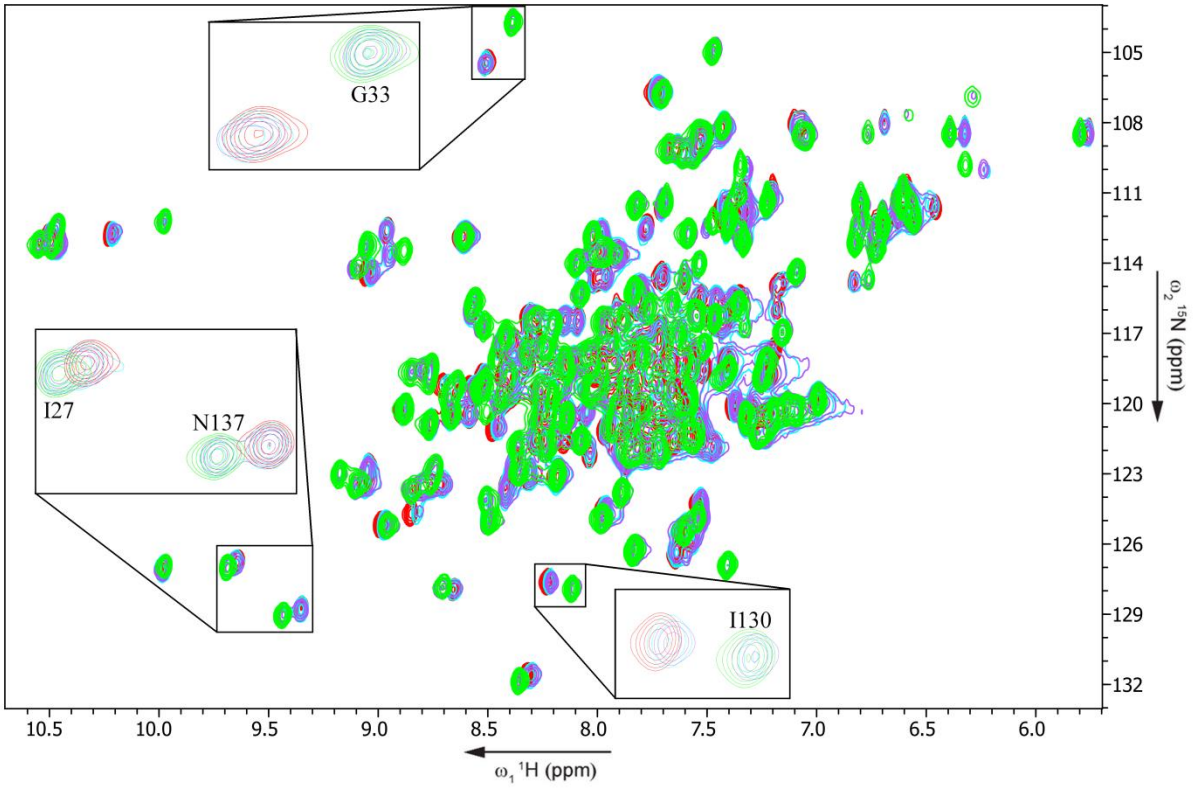

Figure 2.3: Overlay of ^{1}H-^{15}N HSQC spectra of CaM being titrated with eNOSpThr495 peptide. The initial ^{15}N-HSQC spectrum of CaM (red) was overlaid with the spectra of different ratios of eNOSpT495 peptide to Ca^{2+}-CaM. The ratios are 1:3 ratio (blue), 2:3 ratio (purple) and 1:1 ratio (green). The HSQC spectra show amino acid residue assignments determined for the peptide-bound CaM.

The ^{15}N-HSQC spectrum of CaM-eNOSpThr495 was compared to that of CaM with the wild type eNOS peptide. Figure 2.4 shows the overlay of the ^{15}N-HSQC spectra of CaM-eNOS with that of CaM-eNOSpThr495. Cross peaks for the majority of amides in the CaM-eNOSpThr495 complex overlap with those of CaM-eNOS complex. However, amides in the *C*-domain, specifically the amides of residues in EF hand IV, do not overlap with those of CaM-eNOS due to differences in chemical shifts. Also not seen in Figure 2.4 is the chemical shift difference of E7, which is located in

the heavily overlapped central portion of the spectra. This data suggests that the structures of the CaM-eNOS complex and the CaM-eNOSpThr495 complex are quite similar. This provides further evidence that this phosphorylation affects residues E7 and E127, which are in close proximity to the phosphorylated Thr495 in the structure. This has been previously postulated by Aoyagi et al. when they suggested that the addition of a negatively charged phosphate group would cause electrostatic repulsion between E7 and E127 (Aoyagi et al., 2003).

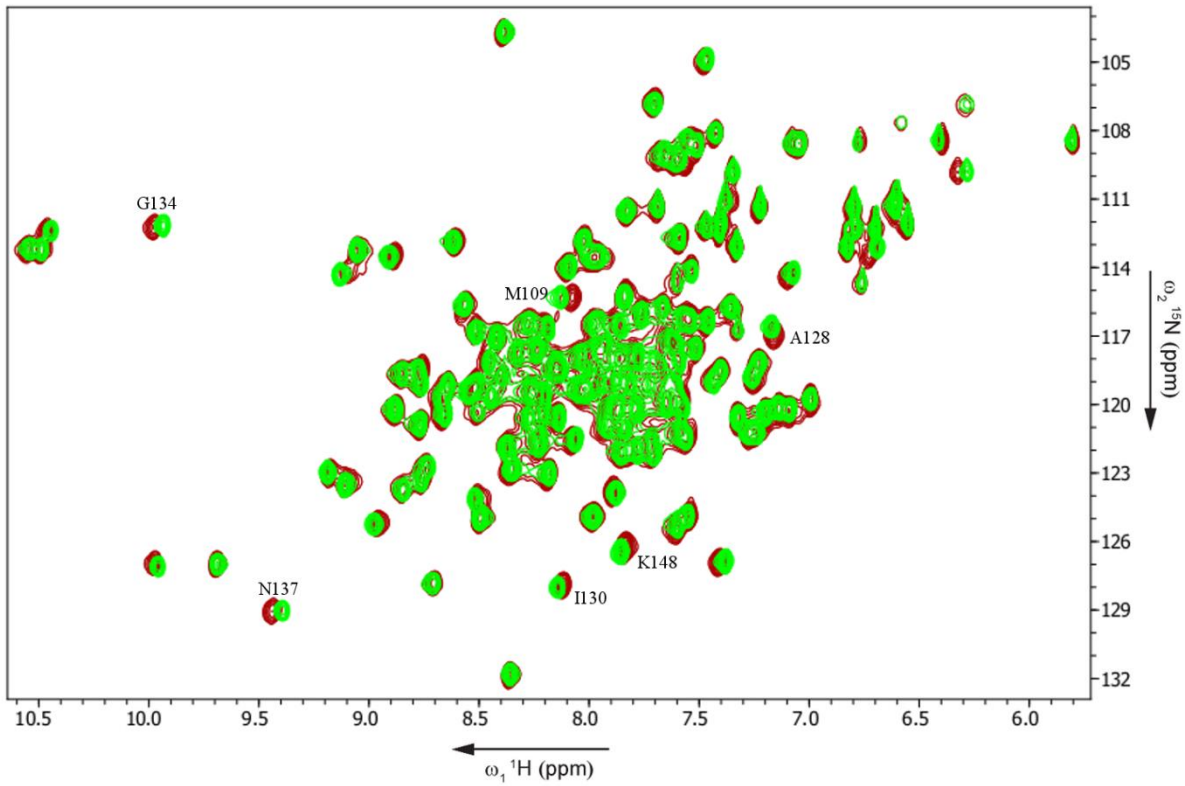

Figure 2.4: Overlay of ^{1}H-^{15}N HSQC spectra of the CaM−eNOS peptide complex (green) and the CaM−eNOSpThr495 peptide complex (red).

The effect of phosphorylation on the secondary structure of the peptide was investigated using trifluoroethanol (TFE) monitored by circular dichroism spectroscopy. The TFE is used to mimic hydrophobic environments and is known to induce α-helical conformation in peptides that

have a propensity to form this secondary structure. Both eNOS peptides showed no apparent structure in the buffer solution with 0% TFE. A comparison of the tendency of each peptide to form an α-helix was then performed by recording spectra after the addition of increasing concentrations of TFE. The formation of an α-helix is generally accompanied by the appearance of negative ellipticity at 208 and 222 nm. Both peptides showed increased amounts of secondary structure as more TFE was added. In both cases, there was an increase in apparent α-helical structure with increasing TFE concentration. With increasing concentrations of TFE, the negative ellipticity at 222 nm of both peptides plateau at TFE concentrations above 30% (see Figure 2.5). While this result indicates that the increase in helical structure does not appreciably change above 30% TFE, the phosphorylated peptide did not show as large an α-helical content as the nonphosphorylated peptide (Figure 2.5). The structural effects of the phosphorylation leading to the diminished helical structure of the peptide can be due to the charged and bulky nature of the phosphate, destabilization of electrostatics that can result in nonproductive interaction with neighboring residues or the high desolvation penalty of the side chain (Broncel et al., 2010). Specifically, it has been previously proposed that phosphorylation at Thr495 OG1 would disrupt its hydrogen bond with the Glu498 backbone amide, possibly affecting the α-helical secondary structure of the peptide (Aoyagi et al., 2003). In addition, the Thr495 is next to one of the anchoring residues in the classical '1-5-8-14' CaM binding sequence motif. A negatively charged phosphorylated Thr495 next to the first residue of the motif will likely disrupt the helical structure of the region.

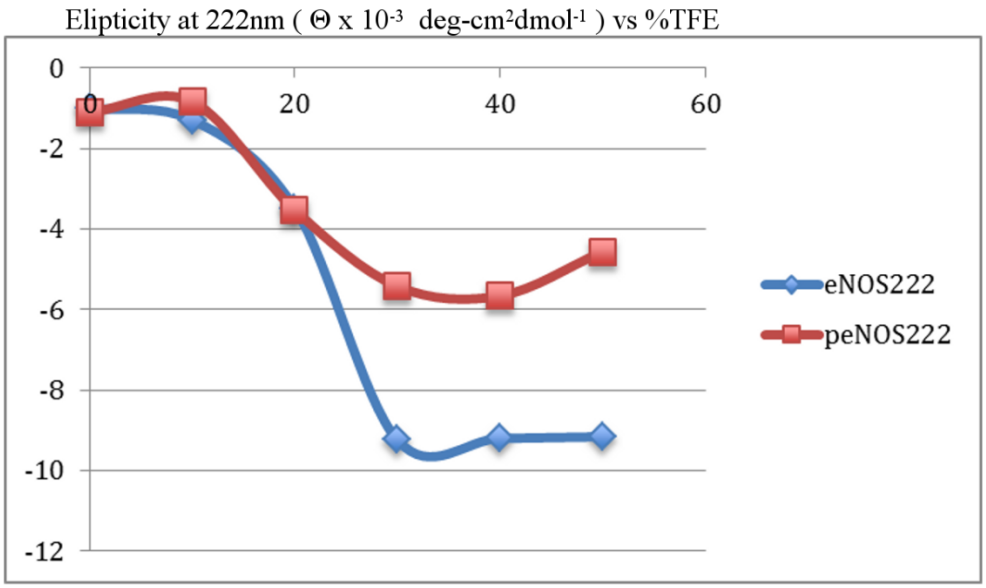

Figure 2.5: Comparison of UV−CD spectra between wild-type eNOS and eNOSpThr495 CaM-binding peptides in buffers with varying TFE concentrations.

The ellipticiy at 222 nm is shown as a function of TFE concentration.

While the propensity of the phosphorylated eNOS CaM binding domain to form an α-helix appears to be diminished, the final structure of the peptide bound to CaM is very similar to that of the nonphosphorylated form of the peptide. The diminished α-helical propensity could account for the reduced activity of the enzymes associated with the phosphorylated form.

2.3.2 Structure of CaM-eNOSpThr495 CaM binding domain peptide complex.

The NMR analysis of CaM with the eNOSpThr495 peptide (Figure 2.6A) followed routine procedures with the backbone resonance assignment based primarily on 3D triple resonance techniques, using the previously assigned chemical shifts of CaM with wild type eNOS peptide as a starting point. The HNCA experiment (Figure 2.6B) was supported by CBCA(CO)NH and HN(CO)CA experiments. This combination of techniques resulted in complete backbone assignments for CaM, with the exception of the prolines and the first two N-terminal amino acids (Appendix B).

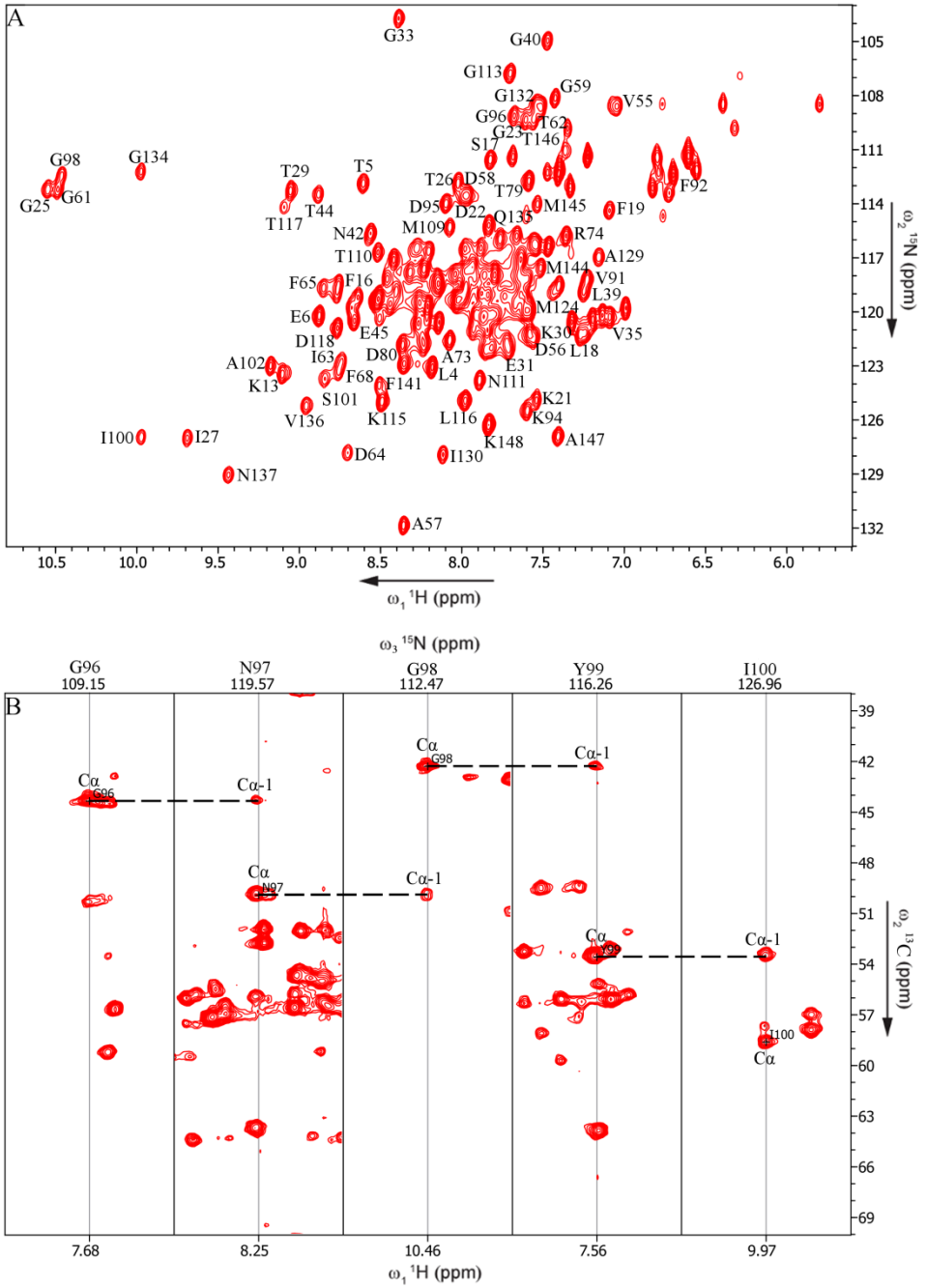

Figure 2.6: Composite figure of NMR structural data.

(A) ^{1}H-^{15}N HSQC spectrum of the eNOSpThr495 CaM-binding domain peptide. (B) 3D HNCA strips of sequential amino acids Gly96 to Ile100 of CaM. The connection between the alpha carbon of the previous and successor residue are shown.

Subsequently, sidechain resonances for CaM were assigned using HC(C)H-TOCSY, (H)CCH-TOCSY and H(CCO)NH experiments and for the eNOSpThr495 peptide using the ^{15}N-^{13}C-double-filtered NOESY experiment (Figure 2.7).

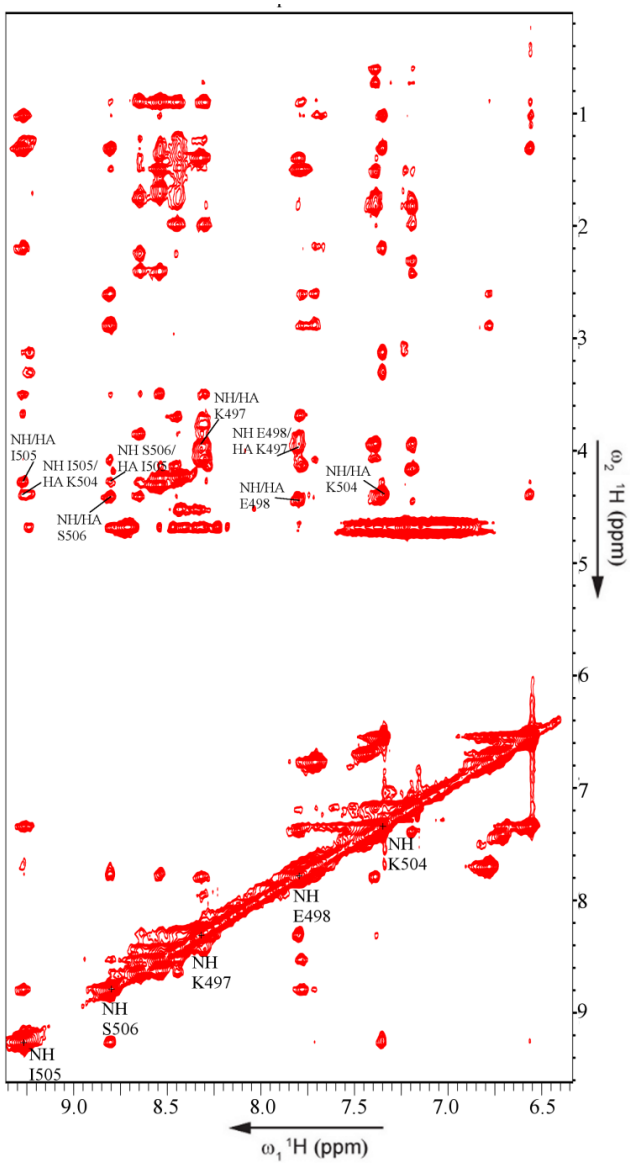

Figure 2.7: ^{15}N-^{13}C-double filtered NOESY spectrum of eNOSpThr495 of the CaM-eNOSpThr495 complex.

Some of the NH, NH/HA and NOE cross peaks are labeled in the spectrum. The peaks are numbered as per the residue number from the full length eNOS enzyme.

NOEs for structure determination of the eNOSpThr495 peptide bound to CaM were extracted from ^{15}N-^{13}C-edited NOESY, $^{13}C_{ali}$-NOESY and ^{15}N-double-filtered NOESY experiments. The three dimensional solution structure of CaM bound to the human eNOS CaM binding domain peptide phosphorylated at Thr495 (CaM-eNOSpThr495) was calculated using the CNSsolve software program. The structure of the complex is based on a large number of experimental constraints and is well defined. Structure and input data statistics are summarized in Table 2.1.

Table 2.1: Statistics for the CaM-eNOSpThr495 peptide structural ensemble

	CaM-eNOSphos Complex		
NMR-derived distance and dihedral angle restraints			
	Calmodulin	eNOSphos peptide	CaM-eNOSphos complex
NOE constraints	1513	119	62
Dihedral angles from TALOS+	288	N/A	N/A
Total number of restraints		1982	
Structure statistics for the 20 lowest energy structures			
Mean deviation from ideal covalent geometry			
Bond lengths (Å)		0.010	
Bond angles (deg.)		1.3	
Average pairwise RMSD (Å) for all heavy atoms of the 20 lowest energy structures	All Residues	Ordered Residues[a]	Selected Residues[b]
Backbone Atoms	1.3	0.9	0.9
Heavy Atoms	1.7	1.4	1.4
Ramachandran statistics (%)			
Residues in most favored region		86.0	
Residues in additional allowed regions		13.5	
Residues in generously allowed region		0.4	
Residues in disallowed region		0.0	

[a] Ordered residue ranges: 6A-8A,10A-36A,39A-77A,79A-148A,495B-508B
[b] Selected residue ranges: 6A-8A,10A-36A,39A-77A,79A-148A,495B-508B

The family of 20 final structures is shown in Figure 2.8A. The average structure showing the location of the phosphorylation of Thr495 of the eNOS peptide, which is found near the N-terminal end of the peptide is shown in Figure 2.8B. Residues 1-4 (corresponding to 491-494 of eNOS) at the *N*-terminus of the eNOSpThr495 CaM binding region peptide were not included in the structure calculation because they could not be unambiguously assigned. This could be due to the addition of the phosphate group which has been theorized to destabilize the helical propensity of the peptide (Aoyagi et al., 2003). Based on the comparison of the ^{15}N-double filtered NOESY experiments for CaM with eNOS peptide and CaM with eNOSpThr495 peptide there was little change in the chemical shifts observed for pThr495 and Thr495.

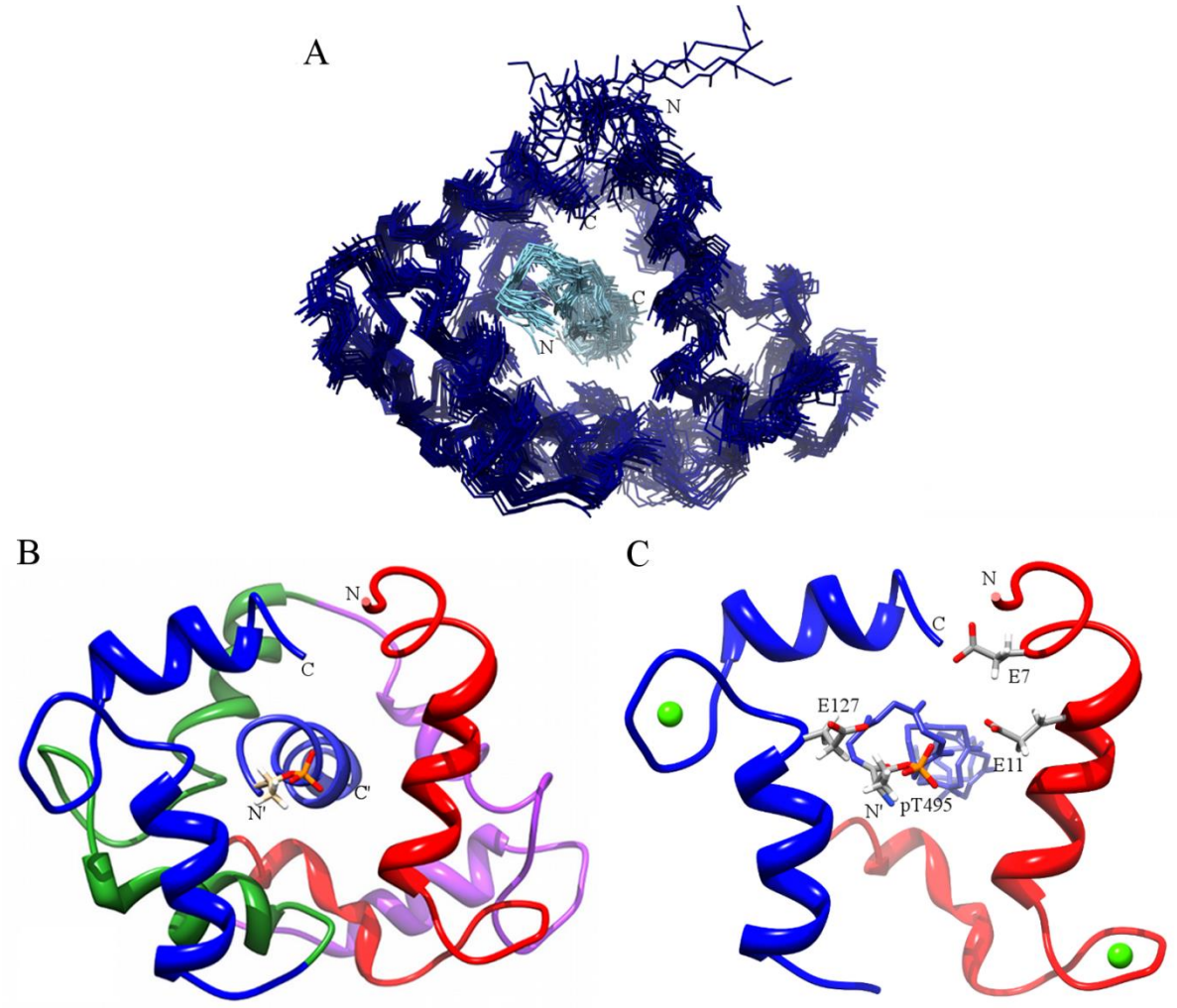

Figure 2.8: Solution structure of CaM bound to eNOSpThr495 CaM binding domain peptide.

(A) Superposition of the ensemble of the 20 lowest energy structures of CaM bound to the eNOSpThr495 peptide. Backbone atom traces of CaM are shown in dark blue and the eNOSpThr495eNOS peptide are shown in light blue. (B) Cartoon ribbon view of the average solution structure of CaM-eNOSpThr495 complex. (C) Cartoon ribbon view showing residues in close proximity to the phosphorylated Thr495 of the eNOS peptide. Ca^{2+} ions are shown as green dots and are modeled in their known locations. Residues 1-40 of CaM (EF Hand I) are colored red, 41-79 (EF Hand II) are purple, 80-114 (EF Hand III) are green, and 115-148 (EF Hand IV) are blue. The peptide is colored in a lighter blue and the N and C terminus are labeled N' and C', respectively. The phosphorylated Threonine is shown as stick model.

2.3.3 Comparison of the CaM-eNOS vs CaM-eNOSpThr495 complexes.

When the solution structure of CaM-eNOS is superimposed onto that of the CaM-eNOSpThr495 structure, the two structures are shown to be quite similar, however, a few local differences are seen (Figure 2.9). When aligned with respect to the backbone atoms of the peptide, a difference is shown in the orientation of helix A of CaM between the two structures, with helix A of CaM-eNOSpThr495 pushed away from the N-terminus of the peptide (where the phosphorylated Thr495 is located). EF hand IV (colored blue) is also shifted farther away from the peptide in the CaM-eNOSpThr495 structure. The rest of the CaM-eNOSpThr495 structure superimposes quite well on the CaM-eNOS structure. This, along with the ^{1}H-^{15}N-HSQC spectra overlay, confirms that the phosphorylation of Thr495 doesn't have an effect on the structure of CaM away from the site of the phosphorylation.

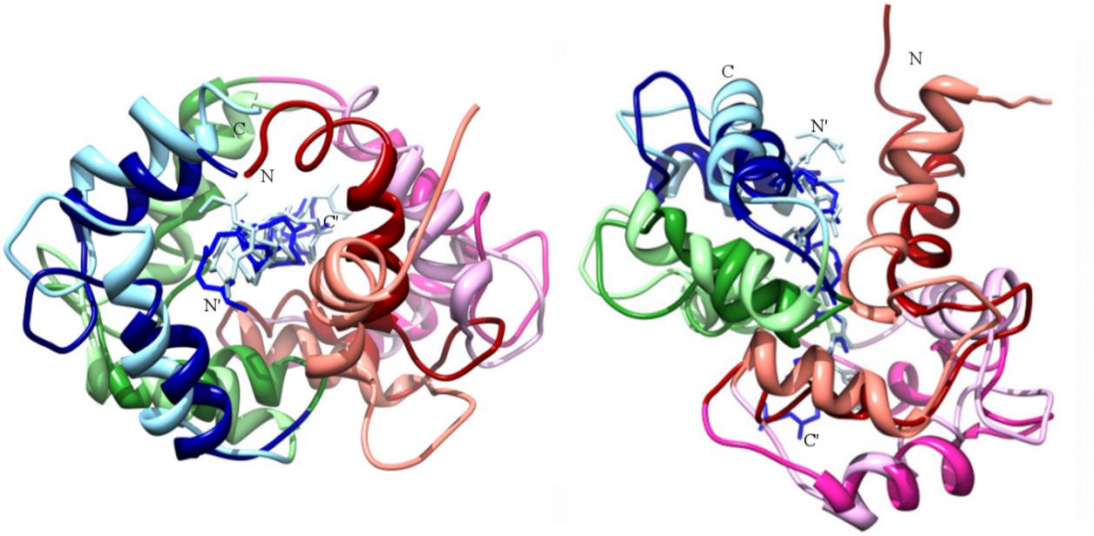

Figure 2.9: Superpositions of the CaM-eNOS peptide solution structure and the CaM-eNOSpThr495 peptide solution structure.

Comparison of solution structures of CaM-eNOSpThr495 peptide (dark colors) with CaM-eNOS peptide (light colors) by superimposing the two structures and viewing it along the bound peptide from its N-terminus (N') to its C-terminus (C') on the left (front view), and rotated 90° around the horizontal axis with the N-terminus of the bound peptide on the top on the right (bottom view). The two structures are aligned by superimposing backbone atoms of the bound peptides. The color scheme is the same as figure 2.8.

2.3.4 Electrostatic effects of the phosphorylation of Thr495.

The addition of the phosphate group to Thr495 of the eNOS peptide shows structural effects on EF hands I and IV. This is first illustrated by the ^{1}H-^{15}N-HSQC spectra overlay of the CaM-eNOS and CaM-eNOSpThr495 complexes (Figure 2.4) and is clearly shown by the structure overlay of the two structures (Figure 2.9). The analysis of the CaM-eNOSpThr495 structure with DelPhi illustrates that this modification to the peptide creates a more negative potential on the N-terminal region of the peptide, which is located in a negatively charged region of CaM (Figure 2.10C, D). This negative charge is not present in the CaM-eNOS complex (figure 2.10B) and thus would not cause any electrostatic repulsion. This phosphate group is in close proximity to E7, which is found in helix A of EF hand I, and E127, found in helix G of EF hand IV. The electrostatic repulsion between the phosphate group and helix A of EF hand I gives an explanation as to why helix A is pushed further from the peptide in the CaM-eNOSpThr495 complex, as shown in Figure 2.9. This also explains why helix G and EF hand IV are shifted further away from the eNOSpThr495 peptide. This electrostatic repulsion could be affecting CaM's ability to coordinate Ca^{2+} by interfering with the EF hands I and IV, which would help explain why CaM has diminished ability to bind eNOS phosphorylated at Thr495 at physiological Ca^{2+} levels.

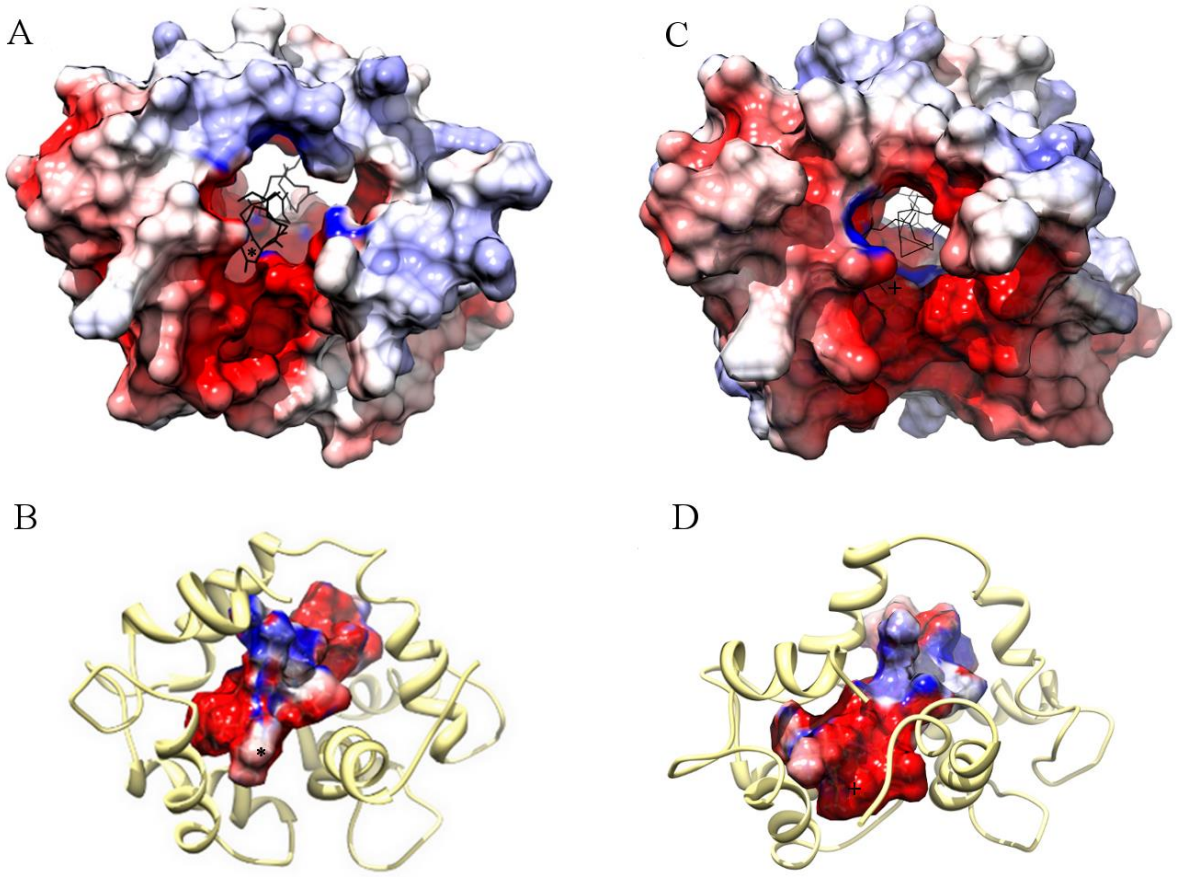

Figure 2.10: Delphi-calculated electrostatic potential maps.

The Delphi-calculated electrostatic potential maps are projected on the surface of the CaM-eNOS peptide complex (A, B) and the CaM-eNOSpThr495 peptide complex (C, D). Thr495 and pThr495 are displayed on the peptide by an * and +. The Delphi-calculated electrostatic potential maps are colored with a chimera color key ranging from (-15) red to (0) blue.

2.3.5 Fluorescence spectroscopy suggests increased Ca^{2+} sensitivity of CaM with the eNOS peptide.

Binding of the eNOS and eNOSpThr495 peptides with CaM was further studied using dansylated CaM (dansyl-CaM). Dansyl-CaM is a useful tool to detect conformational changes in CaM as a result of interactions with Ca^{2+}, peptides or other proteins because the intensity of the fluorescence spectrum is enhanced and shifted when the dansyl moiety becomes embedded in a hydrophobic environment

(Kincaid et al., 1982; Johnson and Wittenauer, 1983). Without Ca^{2+} present there was no blue shift or enhancement of dansyl fluorescence spectrum observed when eNOS peptide or eNOSpThr495 peptide were added. In the presence of Ca^{2+}, this shift and enhancement of the fluorescence spectrum was observed. To analyze the Ca^{2+} dependency of the two complexes we performed Ca^{2+} titration fluorescence experiments in triplicate (Figure 2.11).

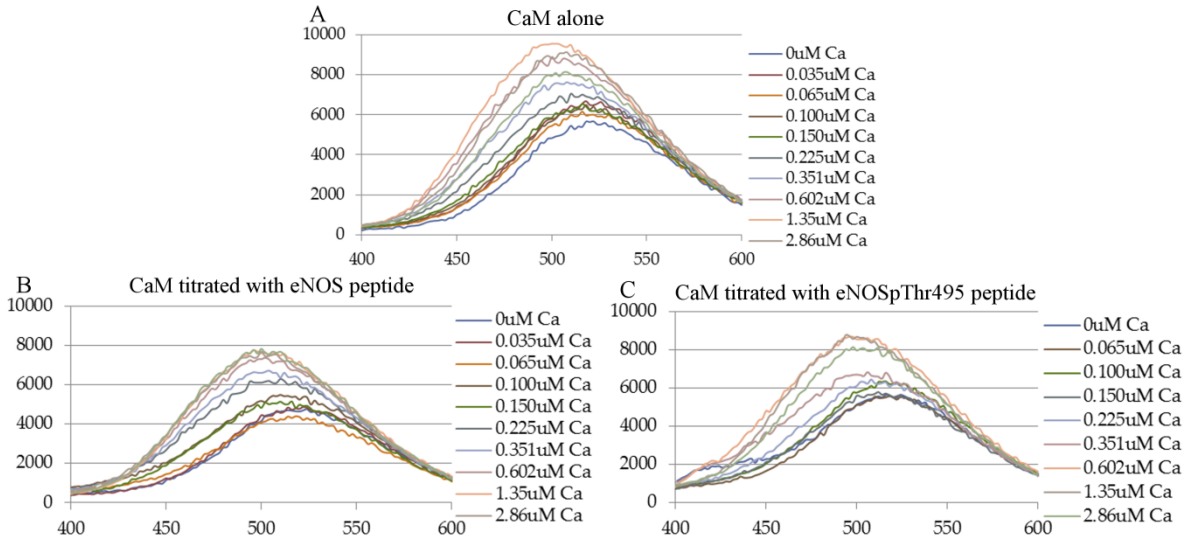

Figure 2.11: Fluorescence emission spectra of dansyl-CaM in the presence of eNOS and eNOSpThr495 peptides.

Fluorescence measurements were made on 50 µL samples consisting of dansyl-CaM (2 µM) alone or with eNOS or eNOSpThr495 peptide in 30 mM MOPS, 100 mM KCl, 10 mM EGTA, 10 mM CaEGTA, pH 7.2 with an increasing concentration of free Ca^{2+}. The excitation wavelength for all of the dansyl-CaMs was set at 340 nm and emission was monitored between 400 and 600 nm. Slit widths were set at 2 nm for excitation and 1 nm for emission.

The relative fluorescence was calculated for CaM and for CaM with either eNOS or eNOSpThr495 peptide (Figure 2.12). Without peptides, dansyl-CaM exhibited fluorescence changes in a Ca^{2+} concentration range of 0.35-2.8 µM. The fluorescence changes of the dansyl-CaM-eNOS complex occurred in a much lower Ca^{2+} concentration range, which may correspond to a physiological Ca^{2+} concentration. The dansyl-CaM-eNOSpThr495 complex showed no difference in

Ca^{2+} dependency when compared to CaM alone. These Ca^{2+} titration experiments provide information about the conformational transitions of CaM with the peptides and Ca^{2+}.

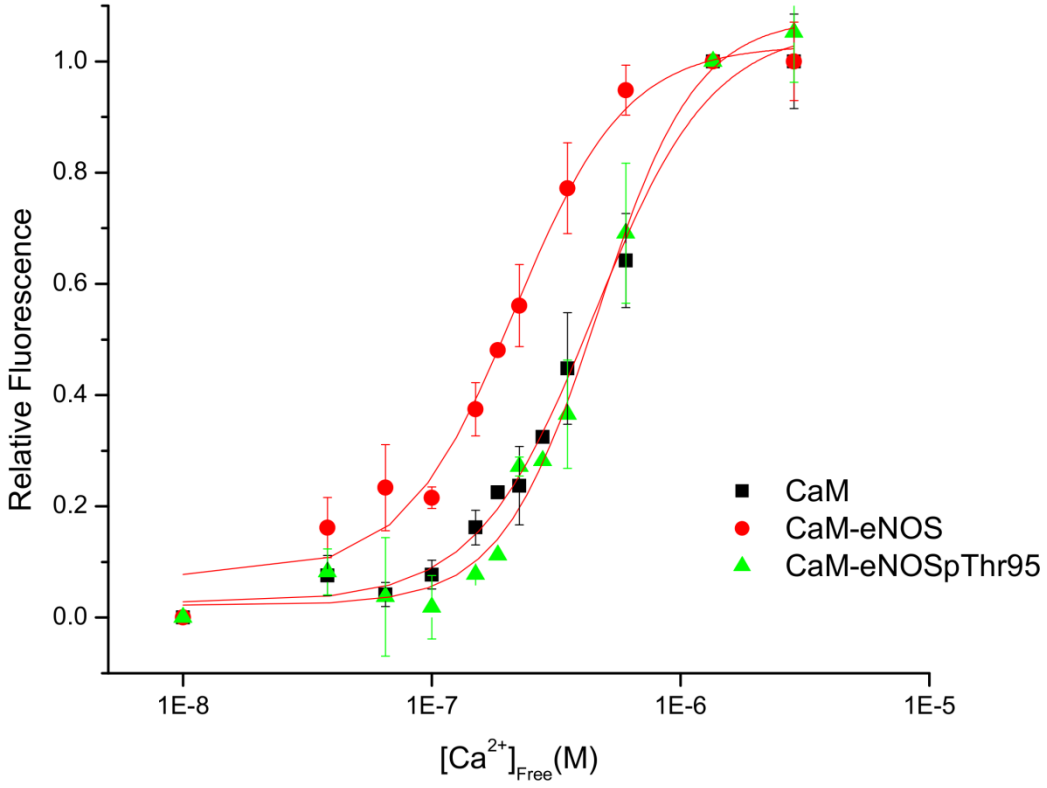

Figure 2.12: Ca^{2+} dependency of dansyl-CaM fluorescence with or without eNOS and eNOSpThr495 peptides.

Normalized fluorescence is shown for CaM, CaM-eNOS complex, and CaM-eNOSpThr495 under assay conditions described in section 2.2.7.

The result of the CaM-eNOS complex binding with Ca^{2+} at lower Ca^{2+} concentrations than CaM alone indicate that the Ca^{2+} affinity of CaM is enhanced with peptide binding to CaM. This is not seen in interaction of CaM with eNOSpThr495 peptide. This increased Ca^{2+} sensitivity of CaM have also been seen with other peptides interacting with CaM (Mori et al., 2000). This suggests that binding of eNOS peptide to CaM increases the Ca^{2+} sensitivity of CaM in the physiological Ca^{2+} range, whereas eNOSpThr495 does not.

2.3.6 Isothermal titration calorimetry.

Isothermal titration calorimetry (ITC) was used to examine the thermodynamic profiles associated with the binding CaM to the two target peptides. Since the values obtained for binding constants show slight variations when performed using different methods and conditions (Vorherr et al., 1993; Censarek et al., 2002), all of our experiments were performed by ITC using exactly the same conditions. Representative titrations for each are shown in figure 2.13.

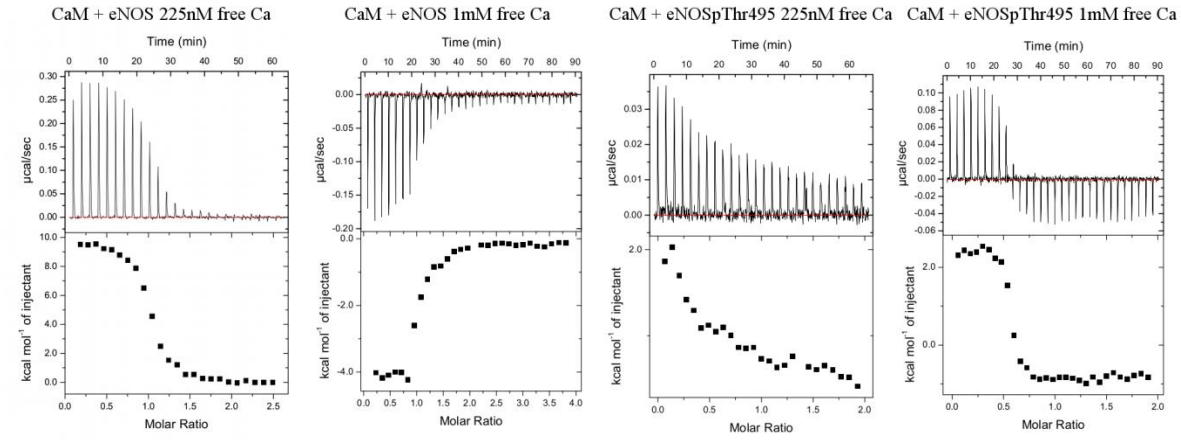

Figure 2.13: Isothermal titration calorimetry (ITC) data for CaM with eNOS and eNOS pThr495 at saturated and 225 nM free Ca^{2+}.

ITC analysis indicates binding of the eNOS peptide and no binding of eNOSpThr495 peptide to CaM at physiological Ca^{2+} levels**.** Representative raw sample data for several CaM-peptide titrations.

Table 2.2: Thermodynamics of CaM-peptide interactions measured by ITC.

	N (sites)	K_d (µM)	ΔH (kcal/mol)	ΔS (cal/mol/K)
CaM-eNOS with 225 nM free Ca^{2+}	1.00 ± 0.01	0.2 ± 0.03	9.39 ± 0.13	62.0
CaM-eNOS with 1mM free Ca^{2+}	1.02 ± 0.02	0.7 ± 0.2	-4.48 ± 0.16	13.3
CaM-eNOSpThr495 with 225 nM free Ca^{2+}	0.0096 ± 0.86*	>50	41.07 ± 369.9*	140*
CaM-eNOSpThr495 with 1 mM free Ca^{2+}	1.11 ± 0.01	0.3 ± 0.08	1.74 ± 0.03	35.5

*These results cannot be fit reliably by the ITC software and are indicative of poor or no binding between CaM and the eNOSpThr495 peptide.

In the presence of excess calcium (1mM) wild type eNOS peptide binds to CaM by an exothermic interaction. As previously reported for the binding of the nNOS peptide, (Yamniuk and Vogel, 2005) eNOS binding proceeds with a negative enthalpy (ΔH), a positive entropy (ΔS) and modest affinity (K_d = 0.7μM) (Table 2.2). This indicates that the interaction is driven by favorable enthalpy and entropy. In contrast, the binding of the eNOSpThr495 peptide under the same conditions is weakly endothermic, with a comparable affinity to that of wild type (K_d = 0.3μM). A similar endothermic interaction has been reported for apoCaM titrated with mutant peptides corresponding to the CaM binding domain of iNOS, an isoform that is known to bind to CaM in the absence of Ca^{2+} (Censarek et al., 2004). The eNOSpThr495 binding interaction proceeds with positive ΔH and ΔS. The interaction is therefore driven by the increase in entropy. Both peptides showed a 1:1 stoichiometry with CaM as expected.

Because our fluorescence studies showed an apparent difference in binding at low calcium concentrations, we attempted to thermodynamically characterize the interactions under these conditions. Intriguingly, at low $[Ca^{2+}]_{free}$, the binding of wild type eNOS peptide to CaM becomes highly endothermic, the entropy gain increases over fourfold, and its affinity for CaM increases slightly (K_d = 0.2μM). A similar result showing a switch from an exothermic to an endothermic interaction has been reported for the binding of the nNOS CaM target domain to CaM by simply changing the experimental conditions going from a higher to a lower temperature (Yamniuk and Vogel, 2005). The ΔH under low 225nM calcium conditions is now positive and unfavorable for binding. The change in enthalpy is compensated by a positive ΔS much larger than that observed for the wild type peptide binding in excess calcium. In contrast, the binding of eNOSpThr495 to CaM in these low $[Ca^{2+}]_{free}$ conditions becomes negligible (Figure 2.13). This is consistent with our fluorescent experiments showing no apparent binding under these conditions. In essence, these results

indicate that non-phosphorylated eNOS is more sensitive to ambient cellular Ca^{2+}, and phosphorylation serves as an attenuator of Ca^{2+}-CaM regulation of eNOS.

2.4 Conclusions

We set out to understand how phosphorylation of a single residue in the CaM target domain results in diminished NOS enzyme activity. Previous studies had shown that an eNOS enzyme carrying a phosphomimetic T495D mutation binds very weakly to CaM. In contrast, the control mutant T495A showed strong binding to CaM (Fleming et al., 2001). Enzyme studies also showed that only phosphorylation of T495 or the mutation T495D resulted in the loss of eNOS enzyme activity. It had been postulated that phosphorylation of T495 reduces output by hindering the association of CaM with its binding site (Aoyagi et al., 2003). Until the present study, there had not been a structural study using a phosphorylated T495 residue. Our solution structure shows that in the presence of excess calcium, phosphorylation does not prevent the binding of CaM to the phosphorylated peptide. While the exact mechanism of how phosphorylation of Thr495 in eNOS adversely affects the activation of the enzyme is still unknown, a careful look at the complex does provide some idea of the reported cause for the reduced enzyme activity. A comparison of the two structures in figures 2.4 and 2.8 show that the most significant changes in the pThr495 solution structure involved two CaM amino acids E7 and E127. In addition both E11 and M124 are found to be in close proximity to the pThr495 phosphate group. The previously reported crystal structure of CaM bound to the human eNOS peptide shows that the side chains of these amino acids are in contact with a number of amino acids in the eNOS peptide (Aoyagi et al., 2003). Both E7 and E11 are part of helix A of the EF hand 1 in CaM. The E7 side chain is in contact with eNOS residues K497 and E498 and has ionic interactions with R492. The E11 side chain is in contact with eNOS residues E498, A502 and I505 and has a hydrogen

bond with N501. Our results shown in Figure 2.9 indicate that helix A is pushed away from the peptide likely due to electrostatic repulsion.

The M124 and E127 residues are both in helix G of EF hand 4 in CaM. The side chain of M124 is in contact with eNOS residues T495, F496 and V499. Residue E127 of CaM has contact with T495 and K497. In addition E127 has ionic interactions with K493 and the backbone of T496. Electrostatic repulsion could again account for the displacement of helix G of EF hand 4 away from the peptide (Figure 2.9). Looking closely at the Delphi image with the phosphate present, the phosphorylation of Thr495 adds a negative charge that is close to helix G (Figure 2.10). The displacement of helix A and G may not be significant under conditions with 1 mM calcium, but under physiological low calcium concentration conditions, a more significant displacement of these helices may have a detrimental effect on enzyme binding and activation. This comes from our dansyl-CaM experiments showing that the pThr495 peptide required significantly higher concentrations of calcium to bind to CaM. Our calorimetric study also showed a lack of binding of CaM to the phosphorylated peptide in the presence of 225nM free calcium. We used TFE to induce α-helical formation and used spectropolarimetry to monitor the changes in the secondary structure of the two eNOS peptides. The secondary structure of both peptides plateaus in 30% TFE but phosphorylation appears to result in a reduction in the degree of α-helical structure in the peptide. In the presence of high concentrations of Ca^{2+}, the solution structure shows that both peptides form an α-helical structure when bound to CaM.

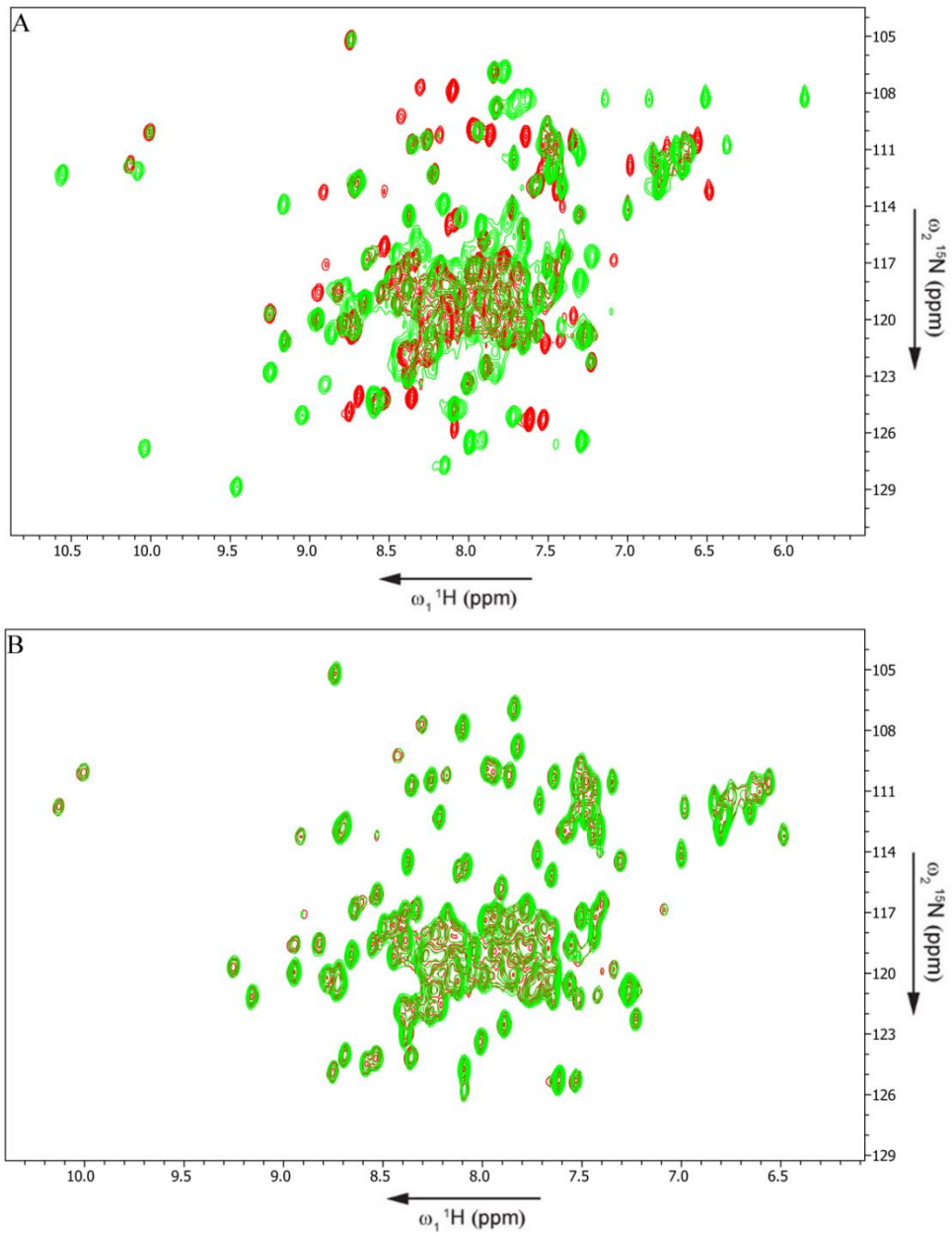

Figure 2.14: ^{1}H-^{15}N HSQC spectra of CaM, CaM-eNOS and CaM-eNOSpThr495 peptide complexes.

(A) Overlay of ^{1}H-^{15}N HSQC spectra of CaM (red) and CaM-eNOS peptide complex (green) at 225nM free Ca^{2+}. (B) Overlay of ^{1}H-^{15}N HSQC spectra of CaM (red) and CaM-eNOSpThr495 peptide complex (green) at 225nM free Ca^{2+}. This indicates binding of the eNOS peptide to CaM, as seen by the difference of the two HSQC spectra but no binding of the eNOSpThr495 peptide at 225nM free Ca^{2+}.

In summary, the interactions of CaM with the peptides based on the eNOS CaM binding domain or the eNOS CAM binding domain phosphorylated at Thr495 are very similar at saturating Ca^{2+} concentrations. This is confirmed by our NMR spectroscopy, fluorescence and ITC results. At the lower Ca^{2+} concentration of 225nM, near physiological Ca^{2+} levels, no significant binding of CaM to eNOSpThr495 is observed by either method (Figure 2.14), whereas CaM is binding to nonphosphoryated eNOS. When Thr495 is phosphorylated, our results indicate there is a diminished propensity for the formation of an α-helix by the peptide in combination with electrostatic repulsion that may account for the diminished CaM-dependent activation of the eNOS enzyme under low physiological calcium concentrations.

Chapter 3

Chemical shift perturbations induced by residue specific mutations of CaM interacting with NOS peptides*

3.1 Introduction

CaM consists of two globular domains joined by a flexible central linker region. Each one of these domains contains two EF hand pairs capable of binding to Ca^{2+}. Each EF hand consists of a helix-loop-helix structural element, with the 12 residue long loop being rich in aspartates and glutamates. Upon Ca^{2+} binding to CaM's EF hands, CaM undergoes a conformational change that exposes hydrophobic patches on each domain thereby allowing CaM to associate with its intracellular target proteins. The central linker's flexibility allows it to adapt its conformation to optimally associate with its intracellular targets (Persechini and Kretsinger, 1988). CaM is able to bind to target proteins in the

* The results presented in this chapter have been published as part of:

Piazza, M., Guillemette, J. G., Dieckmann, T., (2015) Chemical Shift perturbations induced by residue specific mutations of CaM interacting with NOS peptides, *Biomolecular NMR Assignments*, 9, 299-302.

Piazza, M., Guillemette, J. G., Dieckmann, T., (2016) Chemical Shift Assignments of Calmodulin constructs with EF hand mutations, *Biomolecular NMR Assignments*, 10, 193-198.

Unless otherwise stated, all of the work reported in this chapter was performed and analyzed by the candidate.

Ca^{2+}-replete and Ca^{2+}-deplete forms. There is considerable interest in obtaining a better understanding of the structural basis for CaM's ability to bind and recognize its numerous target proteins.

NOS enzymes are one of the target proteins bound and regulated by CaM. At elevated Ca^{2+} concentrations, CaM binds to and activates eNOS making it a Ca^{2+}-dependent NOS enzyme. In contrast, iNOS is transcriptionally regulated *in vivo* by cytokines and binds to CaM at basal levels of Ca^{2+}. The Ca^{2+}-deficient mutant CaM proteins can be used to allow for a specific structural investigation of Ca^{2+}-dependent/independent activation and binding of CaM to iNOS. To study the Ca^{2+}-dependent/independent properties of binding and activation of target proteins by CaM, numerous studies use a series of CaM mutants that involves conversion of Asp to Ala at position 1 of each EF hand (Geiser et al., 1991; Xia et al., 1998; Xiong et al., 2010). Changing the aspartate residue at position 1 of the EF hand loop of CaM inactivates the EF hand toward Ca^{2+} binding. These CaM proteins are defective in Ca^{2+} binding in either the N-terminal lobe EF hands (CaM_{12}; CaM D20A and D56A mutations), the C-terminal lobe EF hands (CaM_{34}; CaM D93A and D129A), or all four of its Ca^{2+}-binding EF hands (CaM_{1234}; mutations at D20A, D56A, D93A and D129A inclusive). A recent study by Xiong et al. (2010) has shown that although conversion of D93 and D129 to Ala effectively inhibits Ca^{2+} binding to EF hands III and IV, the mutations may cause some structural perturbations in the C-domain. This suggests that the Ca^{2+}-deficient CaM mutants may adapt a different structure compared to that of the apo N- and C-domains of CaM.

The interaction of CaM with NOS is also regulated by a number of post-translation modifications including phosphorylation at Tyrosine 99 (Corti et al., 1999; Jang et al., 2007; Mishra et al., 2010). Studies of central nervous tissue hypoxia in newborn piglets indicated that phosphorylation of Y99 of CaM affect the activity of NOS in vivo (Mishra et al., 2009, 2010). The helix 2-helix 6 region (latch domain) of CaM is also an important interaction site between CaM and

NOS and plays a critical role in NOS activation (Su et al., 1995). Amino acid mutations in this site have been shown to impair activation of the NOS enzymes also (Su et al., 1995). To allow the structural studies to be performed, a phosphomimetic form of CaM, CaM Y99E, and CaM Y99E containing a N111D latch domain mutation were used in the investigation.

Here we present the NMR resonance assignments of C-lobe Ca^{2+}-replete and deplete CaM_{12}, N-lobe Ca^{2+}-replete and deplete CaM_{34}, CaM_{1234} in the absence of Ca^{2+}, N-lobe Ca^{2+}-replete CaM_{34} with the iNOS peptide, CaM Y99E with the eNOS peptide and CaM Y99E N111D with the iNOS peptide. Prior to this study the solution structures of apoCaM, holoCaM and holoCaM with the iNOS and eNOS CaM-binding domain peptide have been determined (Kuboniwa et al., 1995; Piazza et al., 2012). By comparing to the wild type complexes we clearly show that the phosphomimetic CaM and mutation of a latch domain residue cause slight perturbations of resonance frequencies for residues near the mutation sites and involved in the C-terminal Ca^{2+} binding sites, whereas the N-terminal and linker region residues appear unaffected. These assignments can also be used to solve the solution structures of these Ca^{2+}-deficient CaM mutants and compare them to known structures of apoCaM. Furthermore, this method allows for quick structural characterization of other CaM or CaM mutants interacting with various NOS peptides and provides the basis for a detailed study of CaM-NOS interaction dynamics using ^{15}N relaxation methods.

3.2 Methods and experiments

3.2.1 Expression of CaM mutant proteins: CaM Y99E; CaM Y99E N111D; CaM_{1234}; CaM_{12}; and CaM_{34}.

The QuikChange site-directed mutagenesis procedure was used to produce vectors coding for CaM Y99E and CaM Y99E N111D. These plasmids were subcloned into the kanamycin resistant pET9dCaM plasmid. Plasmids coding for CaM_{12}, CaM_{34} and CaM_{1234} were a generous gift from Dr. John Adelman (Oregon Health & Sciences University, Portland, OR, USA) (Lee et al., 2003). These plasmids were subcloned into the kanamycin resistant vector pET9dCaM. CaM Y99E, CaM Y99E N111D, CaM_{12}, CaM_{34} and CaM_{1234} were expressed in *E. coli* BL21DE3 competent cells and grown in M9 media 1 L of M9 media (11.03 g/L $Na_2HPO_4 \cdot 7H_2O$, 3.0 g/L KH_2PO_4, 0.5 g/L NaCl, 2 mM $MgSO_4$, 0.1 mM $CaCl_2$, 3 μM $(NH_4)_6(MO_7)_{24}$, 400 μM H_3BO_3, 30 μM $CoCl_2$, 10 μM $CuSO_4$, 80 μM $MnCl_2 \cdot 4H_2O$, 10 μM $ZnCl_2$, 10 mM $FeSO_4$, 100 μg/mL kanamycin) containing 2 g/L glucose and 1 g/L $^{15}NH_4Cl$ at 37°C. Protein expression was induced at an OD_{600nm} of 0.6 with 500 μM isopropyl-*β*-D-thiogalactopyranoside (IPTG) and harvested after 4 h by centrifugation at 6000 x g at 4°C for 5 minutes.

3.2.2 Purification of CaM mutant proteins.

Cells were resuspended in 4 volumes of 50 mM MOPS, 100 mM KCl, 1 mM EDTA, 1 mM DTT, pH 7.5 and lysed by homogenization using an Avestin EmulsiFlex-C5 homogenizer (Ottawa, ON). The lysate was then clarified by centrifugation at 48,000 x g for 30 minutes at 4°C. To the clarified supernatant, $CaCl_2$ was added to a concentration of 5 mM in order to saturate CaM with Ca^{2+} and induce the exposure of hydrophobic patches in the N- and C-lobes of CaM to allow CaM to interact

with the resin. This Ca^{2+}-saturated supernatant was then loaded onto 20 mL of phenyl sepharose 6 fast flow highly-substituted resin (GE Healthcare Bio-Sciences, Baie d'Urfe, PQ) in a 1 cm x 30 cm Econo-column (Bio-Rad Laboratories, Mississauga, ON) equilibrated with 50 mM Tris-HCl, 1 mM $CaCl_2$, pH 7.5 @ 4°C. After the Ca^{2+}-saturated solution was loaded; the resin was washed with 100 mL of the above. The resin was subsequently washed with 80 mL of 50 mM Tris-HCl, 500 mM NaCl, 1 mM $CaCl_2$, pH 7.5 @ 4°C to remove any non-specific proteins that were interacting with the resin. The resin was finally washed with 50 mL of 50 mM Tris-HCl, 1 mM $CaCl_2$, pH 7.5 to remove NaCl from the resin. CaM was then eluted from the phenyl sepharose resin with approximately 30 mL of 10 mM Tris-HCl, 10 mM EDTA, pH 7.5 @ 4°C and 2 mL fractions were collected. Fractions were then scanned from 325 to 250 nm on a Varian Cary UV–visible Spectrophotometer (Varian, Mississauga, ON). Fractions displaying the characteristic absorbance peaks of CaM at 277 nm (for tyrosine residues) and 269, 265, 259, and 253 nm (for phenylalanine residues) were pooled and concentrated to 2 mL sample sizes. The samples were then run through a HiLoad 16/600 Superdex 75 column (GE Healthcare Bio-Sciences, Baie d'Urfe, PQ) connected to the Äkta design system (GE Healthcare Bio-Sciences, Baie d'Urfe, PQ) using buffer consisting of 50 mM Tris-HCl, 0.5 mM EDTA, pH 7.5. Fractions eluted at the characteristic time point for proteins of CaM's size were collected. Isolation and purity of the CaM proteins (148 residues) were confirmed by ESI-MS and SDS-PAGE.

3.2.3 NOS CaM-binding domain peptides.

The human iNOS (RREIPLKVLVKAVLFACMLMRK, 22 residues corresponding to residues 510-531 from the full length iNOS protein) and eNOS (TRKKTFKEVANAVKISASLMGT, 22 residues

corresponding to residues 491-512 from the full length eNOS protein) peptides were synthesized and purchased from Sigma.

3.2.4 NMR spectroscopy.

3.2.4.1 Sample preparation for NMR investigation.

The CaM Y99E or CaM Y99E N111D samples were prepared for NMR experiments via a buffer exchange into 100 mM KCl, 10 mM $CaCl_2$, 0.2 mM NaN_3, 90% H_2O/10% ^2H_2O at pH 6.0 using a YM10 centrifugal filter device (Millipore Corp., Billerica, USA). The Ca^{2+} saturated CaM_{12} and CaM_{34} samples were prepared for NMR experiments via a buffer exchange into 100 mM KCl, 10 mM $CaCl_2$, 0.2 mM NaN_3, 90% H_2O/10% ^2H_2O at pH 6.0 using a YM10 centrifugal filter device (Millipore Corp., Billerica, USA). The Ca^{2+} free CaM_{12} and CaM_{34} samples were prepared for NMR experiments via a buffer exchange into 100 mM KCl, 0.5 mM EDTA, 0.2 mM NaN_3, 90% H_2O/10% ^2H_2O at pH 6.0 using a YM10 centrifugal filter device. All NMR samples contained at least 1 mM CaM Y99E, CaM Y99E N111D, CaM_{12}, CaM_{34} or CaM_{1234} in a total volume of 500 μL. The samples were transferred into 5 mm NMR sample tubes and stored at 4^oC until required for NMR experiments. NMR experiments on the complexes were conducted on samples titrated with either iNOS or eNOS peptide to saturation in a 1:1 CaM:peptide ratio. Complex formation was monitored after each addition by acquisition of a ^1H-^{15}N heteronuclear single-quantum coherence (HSQC) spectrum.

3.2.4.2 NMR spectroscopy and data analysis.

NMR spectra were recorded at 298K on Bruker 600 MHz DRX spectrometers equipped with XYZ-gradients triple-resonance HCN probe (Bruker, Billerica, MA, USA). Specific NMR resonance

assignments were achieved using ^{1}H-^{15}N HSQC, HNCA, CBCA(CO)NH, (H)CCH-TOCSY, HC(C)H-TOCSY, 15N-TOCSY-HSQC, ^{13}C-NOESY-HSQC and ^{15}N-NOESY-HSQC experiments, while using the NMR resonance assignments of the previous wild type CaM or CaM-complexes as a starting point. Spectra were analyzed using the program CARA (Keller, 2005).

3.3 Results

3.3.1 Assignments and data deposition for CaM Y99E with eNOS peptide.

Figure 3.1 shows the superposition of the ^{1}H-^{15}N HSQC spectra of the CaM Y99E bound to the eNOS CaM binding domain peptide versus wild type CaM bound to the eNOS CaM binding domain peptide. Chemical shift changes (Figure 3.2) induced by the phosphomimetic mutant appear for the amides in the C-lobe, specifically the amides of residues 96-101 and 130-138. Almost all of these residues participate in coordinating the Ca^{2+} ion in EF hands III and IV. The rest of the amide resonances overlay quite well with each other suggesting a similar structure of the N-domain for both complexes.

Almost complete amide resonance assignment for CaM Y99E bound to the eNOS CaM binding domain peptide was achieved (Appendix C). Overall 97.9% of all $^{1}H^{N}$, ^{15}N resonances were assigned with the exception of the first A1 residue, D129, E140 and the two Proline residues. The chemical shift assignment of CaM Y99E with eNOS was deposited in the BMRB database under accession number 25257.

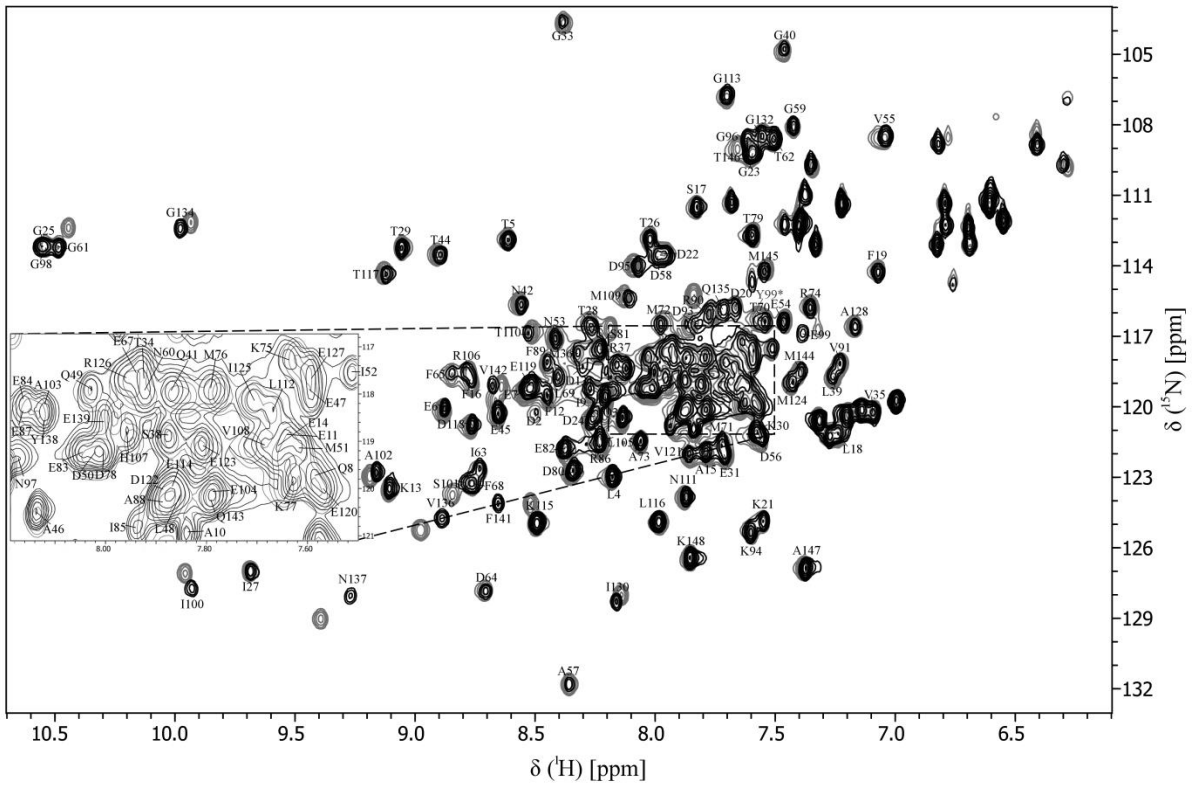

Figure 3.1: Superposition of ^{1}H-^{15}N HSQC spectra of CaM Y99E-eNOS peptide (black) and wild type CaM-eNOS peptide (grey).

Each backbone amide resonance is labeled with the amino acid type and position in the sequence.

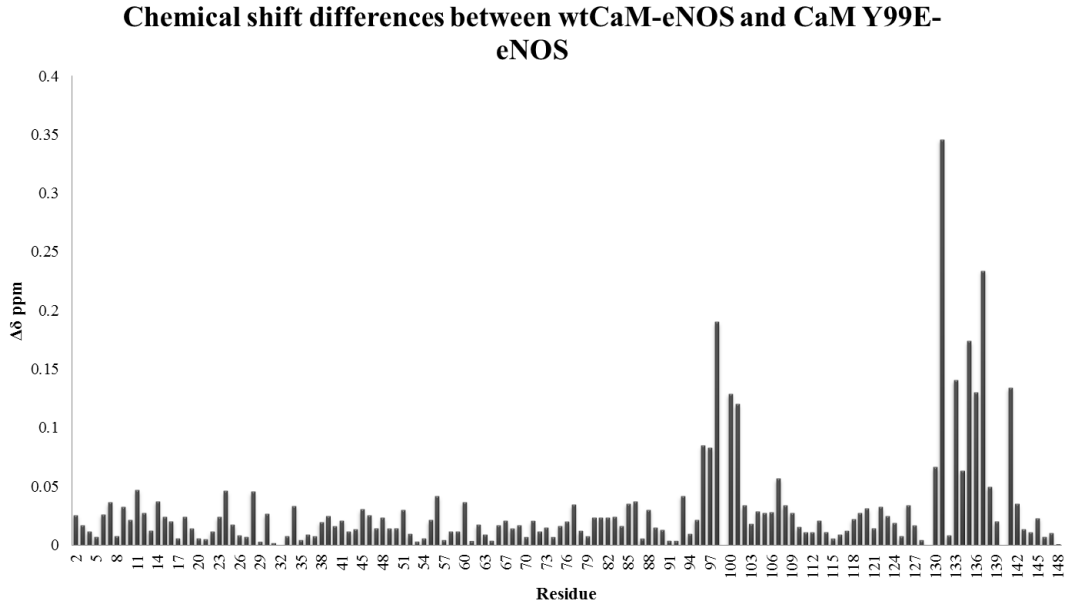

Figure 3.2: Chemical shift differences between wtCaM-eNOS and CaM Y99E-eNOS.

The contribution of ^{1}HN and ^{15}N chemical shift changes for each residue was calculated as $\Delta\delta = \sqrt{[(\Delta\delta^{1}HN)^2 + (\Delta\delta^{15}N/5)^2]}$, where $\Delta\delta^{1}$HN and $\Delta\delta^{15}$N are the differences in ^{1}HN and ^{15}N chemical shifts between the indicated protein.

3.3.2 Assignments and data deposition for CaM Y99E N111D with iNOS peptide.

Figure 3.3 shows the superposition of the ^{1}H-^{15}N HSQC spectra recorded at 298 K on the CaM Y99E N111D bound to the iNOS CaM binding domain peptide versus wild type CaM bound to the iNOS CaM binding domain peptide. Chemical shift changes (Figure 3.4) induced by the phosphomimetic and latch domain mutant appear for the amides in the C-lobe, specifically the amides of residues 96-103, 110-115 and 130-138. These residues participate in coordinating the Ca^{2+} ion in EF hands III and IV and are part of helix 6 of the latch domain. Surprisingly the rest of the amide resonances overlay quite well with each other suggesting a similar structure of the N-lobe for both complexes, including the residues of helix 2 which are part of the helix 2-helix 6 latch domain.

Almost complete amide resonance assignment for CaM Y99E N111D bound to the iNOS CaM binding domain peptide was achieved (Appendix D). Overall 98.6% of all $^{1}H^{N}$, ^{15}N resonances were assigned with the exception of the first A1 residue, E120 and the two Proline residues. The chemical shift assignment of CaM Y99E N111D with iNOS was deposited in the BMRB database under accession number 25253.

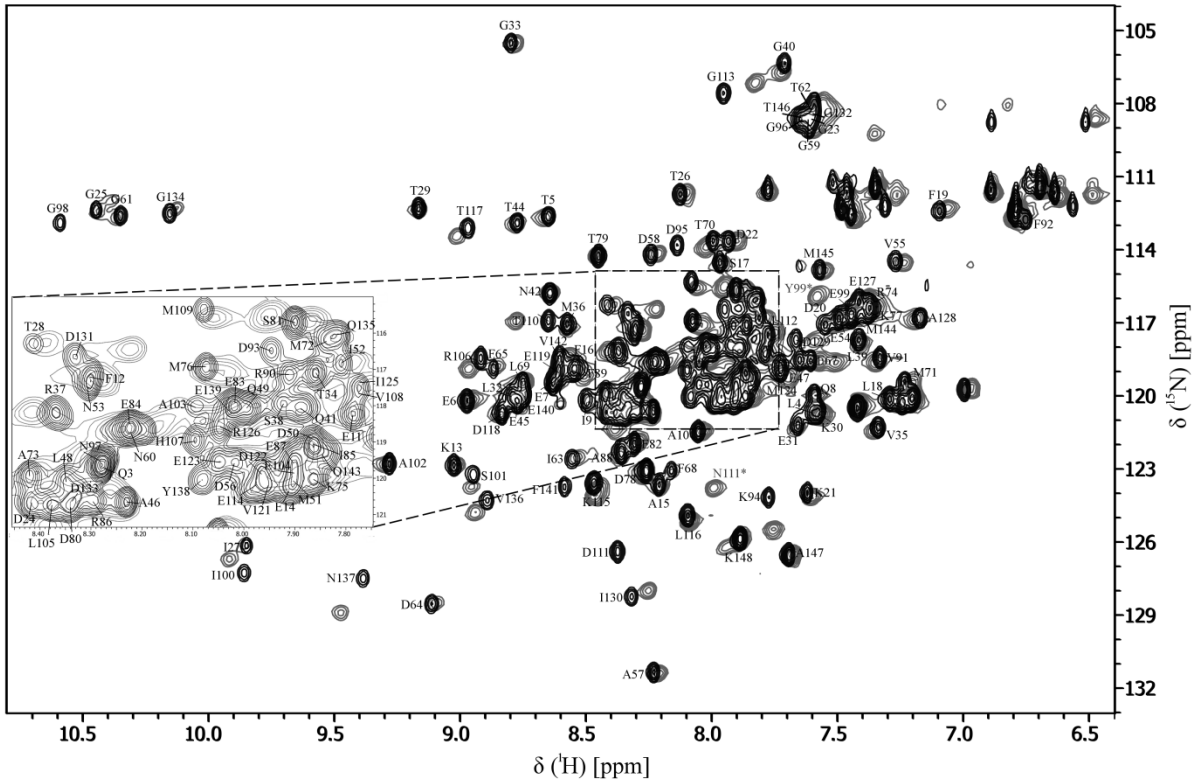

Figure 3.3: Superposition of ^{1}H-^{15}N HSQC spectra of CaM Y99E N111D-iNOS peptide (black) and wild type CaM-iNOS peptide (grey).

Each backbone amide resonance is labeled with the amino acid type and position in the sequence.

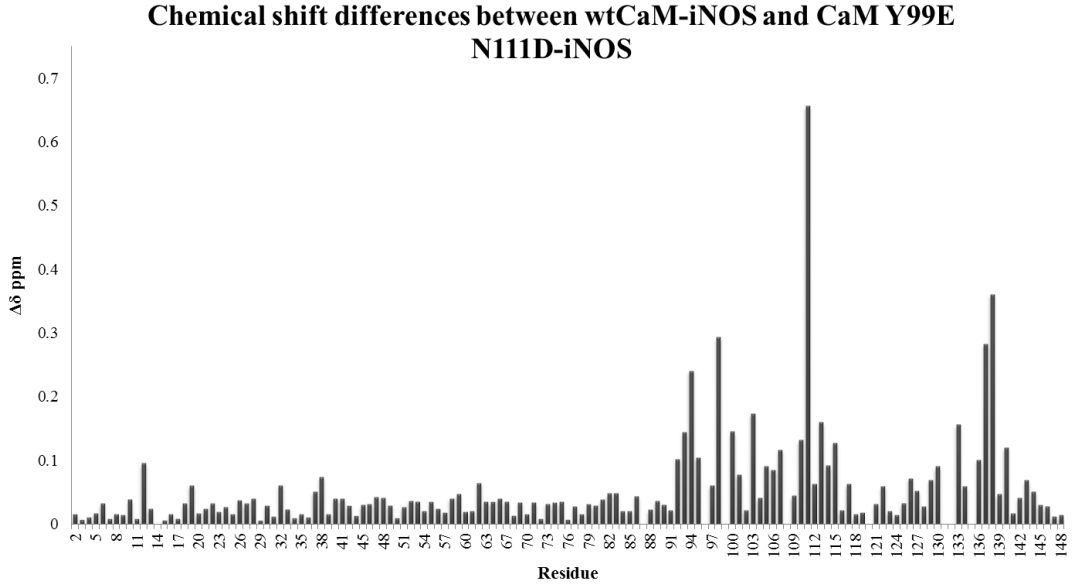

Figure 3.4: Chemical shift differences between wtCaM-iNOS and CaM Y99E N111D-iNOS.

The contribution of ^{1}HN and ^{15}N chemical shift changes for each residue was calculated as $\Delta\delta = \sqrt{[(\Delta\delta^{1}HN)^2 + (\Delta\delta^{15}N/5)^2]}$, where $\Delta\delta^{1}$HN and $\Delta\delta^{15}$N are the differences in ^{1}HN and ^{15}N chemical shifts between the indicated protein.

3.3.3 Assignments and data deposition for Ca^{2+} deplete and Ca^{2+} replete CaM_{12} and CaM_{34}.

Table 3.1 shows the list of Ca^{2+}-deficient CaM mutants used in this study, the completion of their chemical shift assignments and their BMRB accession identification codes. For apoCaM_{12} almost all non-proline backbone resonances were assigned (97.9%) with the exception of A1, D2 and F92 (Appendix F). The chemical shift assignment of apoCaM_{12} was deposited in the BMRB database under accession number 26682. ApoCaM_{34} had most non-proline backbone resonances assigned (94.5%) with the exception of residues A1, D2, R90, V91, F92, I100, V136 and E140 (Appendix G). The chemical shift assignment of apoCaM_{34} was deposited in the BMRB database under accession number 26683. For the Ca^{2+}-CaM_{12} construct 97.9% of non-proline backbone resonances were assigned excluding A1, D2 and A57. The chemical shift assignment of Ca^{2+}-CaM_{12} was deposited in

the BMRB database under accession number 26685. Ca^{2+}-CaM_{34} all non-proline backbone resonances were assigned (91.8%) with the exception of A1, D2, E67, M72, R86, R90, V91, F92, A93, I100, V136 and E140. The chemical shift assignment of Ca^{2+}-CaM_{34} was deposited in the BMRB database under accession number 26686.

Table 3.1: Ca^{2+}-deficient CaM mutants used in this study and completion of chemical shift assignments.

CaM mutant	Nuclei assigned	% Backbone assigned	% Sidechain assigned	Residues missing[a]	BMRB #
$ApoCaM_{12}$	H, NH	97.9	N/A[b]	A1, D2, F92	26682
$ApoCaM_{34}$	H, NH	94.5	N/A[b]	A1, D2, R90, V91, F92, I100, V136, E140	26683
Ca^{2+}-CaM_{12}	H, NH	97.9	N/A[b]	A1, D2, A57	26685
Ca^{2+}-CaM_{34}	H, NH	91.8	N/A[b]	A1, D2, E67, M72, R86, R90, V91, F92, A93, I100, V136, E140	26686
$ApoCaM_{1234}$	H, NH, Cα, Cβ, Hα, Hβ, Hγ, Hδ	97.2	96.6 Cα, 90.5 Cβ, 84.0 sidechain H, 96.6 Hα, 91.9 Hβ	A1, D2, R90, I100	26681
Ca^{2+}-CaM_{34}-iNOS	H, NH, Cα, Cβ, Cγ ,Cδ , Hα, Hβ, Hγ, Hδ	98.6	97.3 Cα, 96.4 Cβ, 89.4 sidechain H, 97.3 Hα, 96.4 Hβ	A1, I100	26687

[a]Chemical shifts were not assigned for P43 or P66.
[b]Experiments to assign sidechain nuclei were not acquired.

The chemical shift changes induced by Ca^{2+} binding to $apoCaM_{12}$ occur for residues only in the C-lobe. This lobe contains the EF hands not affected by mutation and thus still able to undergo the conformational change associated with binding Ca^{2+}. The N-lobe residues show little chemical shift differences indicating a similar structure for the N-lobe in both proteins (Figure 3.5A). A similar result is found with Ca^{2+} binding to $apoCaM_{34}$, however, in the opposite lobes (Figure 3.5B). Tiny chemical shift differences are seen for the C-lobe and large chemical shift differences are seen for the N-lobe.

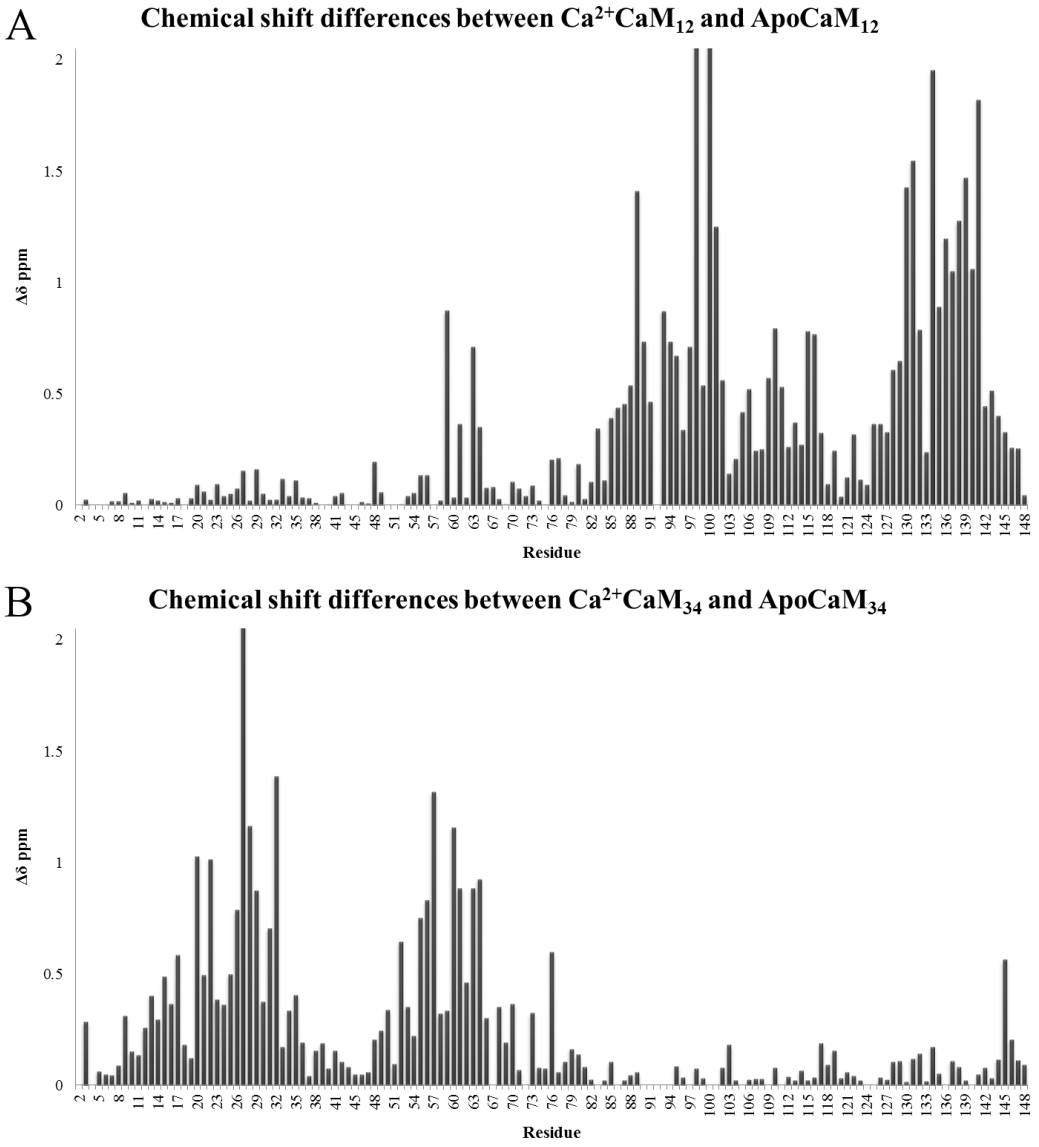

Figure 3.5: Chemical shift differences between (A) Apo and $Ca^{2+}CaM_{12}$, and (B) Apo and $Ca^{2+}CaM_{34}$.

The contribution of ^{1}HN and ^{15}N chemical shift changes for each residue was calculated as $\Delta\delta = \sqrt{[(\Delta\delta^{1}HN)^2 + (\Delta\delta^{15}N/5)^2]}$, where $\Delta\delta^{1}HN$ and $\Delta\delta^{15}N$ are the differences in ^{1}HN and ^{15}N chemical shifts between the indicated protein. The greatest differences are localized to Ca^{2+} binding loops where each mutation is present.

3.3.4 Assignments and data deposition for CaM_{1234}.

Figure 3.6 shows the ^{1}H-^{15}N HSQC spectrum of the CaM_{1234}. Almost complete amide resonance assignment for apoCaM_{1234} was achieved (Appendix E). Overall 97.2% of all $^{1}H^{N}$, ^{15}N resonances were assigned with the exception of the first residue A1, and D2, R90, I100 and the two Proline residues. Among the backbone resonances, 96.6% of Cα, 90.5% of Cβ, and 96.6% of Hα were assigned. In total, 84.0% of sidechain ^{1}H resonances, with 91.9% of Hβ resonances were assigned. Overall, the ^{1}H-^{15}N HSQC spectrum exhibits good resolution and well dispersed signals, indicating a uniform and folded protein structure. Chemical shift changes induced by the 4 EF hand mutations appear for the amides throughout all 4 of the Ca^{2+}-binding EF hands, with the greatest differences occurring for the amides in the center of the Ca^{2+}-binding loop (Figure 3.7). The amide resonances of the loop region between EF hands I and II and the linker region between EF hands II and III show little chemical shift differences with each other suggesting a similar structure for both proteins. The chemical shift assignment of apoCaM_{1234} was deposited in the BMRB database under accession number 26681.

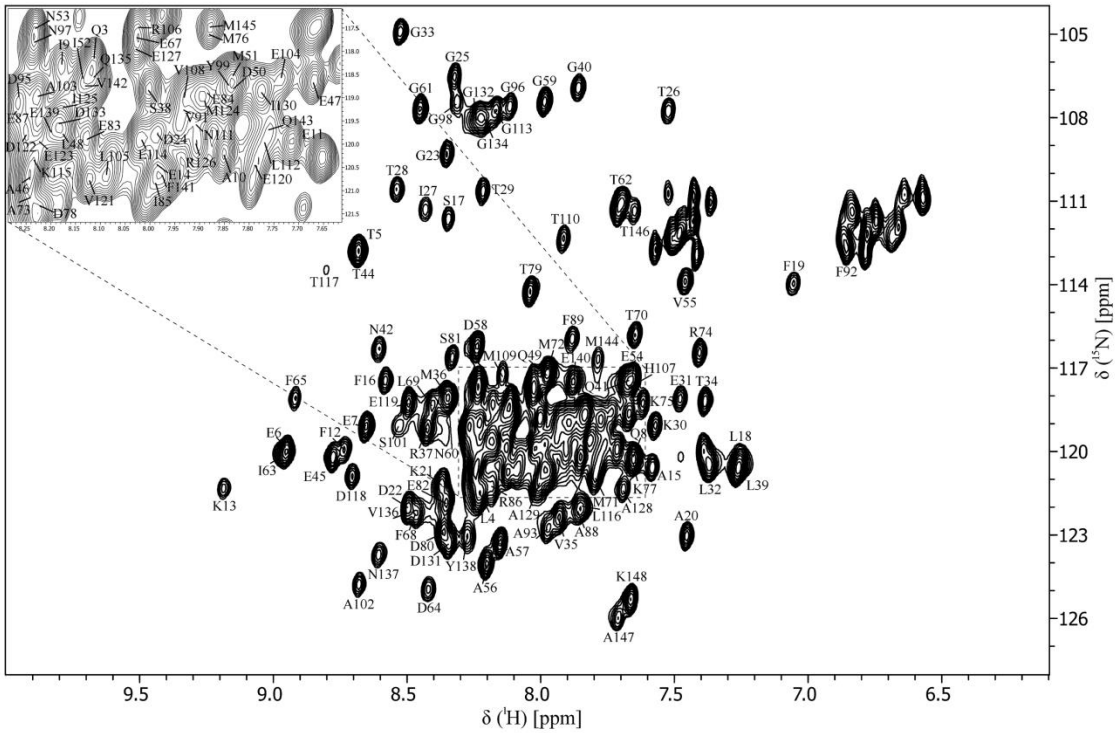

Figure 3.6: ^{1}H-^{15}N HSQC spectrum of CaM$_{1234}$.

Each backbone amide resonance is labeled with the amino acid type and position in the sequence.

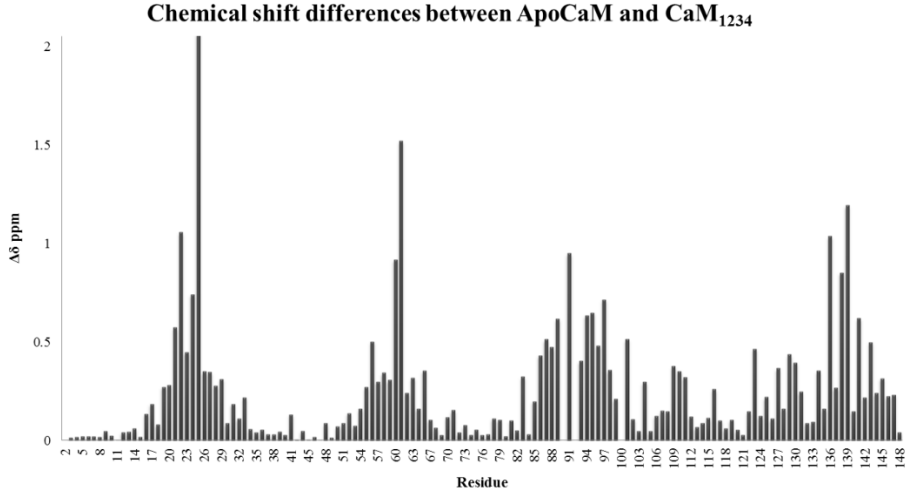

Figure 3.7: Chemical shift differences between ApoCaM and CaM$_{1234}$.

The contribution of ^{1}HN and ^{15}N chemical shift changes for each residue was calculated as $\Delta\delta = \sqrt{[(\Delta\delta^{1}\mathrm{HN})^2 + (\Delta\delta^{15}\mathrm{N}/5)^2]}$, where $\Delta\delta^{1}$HN and $\Delta\delta^{15}$N are the differences in ^{1}HN and ^{15}N chemical shifts between the indicated protein. The greatest differences are localized to Ca^{2+} binding loops where each mutation is present.

3.3.5 Assignments and data deposition for CaM_{34} with iNOS peptide.

Figure 3.8 shows the ^{1}H-^{15}N HSQC spectrum of Ca^{2+}-CaM_{34} bound to the iNOS CaM binding domain peptide (Appendix I). Almost complete amide resonance assignment was achieved. Overall 98.6% of all $^{1}H^{N}$, ^{15}N resonances were assigned with the exception of the first A1 residue, I100 and the two Proline residues. Among the backbone resonances, 97.3% of Cα, 96.4% of Cβ, and 97.3% of Hα were assigned. In total 89.4% of sidechain ^{1}H resonances, with 96.4% of Hβ of resonances were assigned. Overall, the ^{1}H- ^{15}N HSQC spectrum exhibits good resolution and well dispersed signals, indicating a uniform and folded protein structure. Chemical shift changes induced by the C-lobe EF hand mutations appear for the amides in the C-domain, specifically the amides of residues that participate in coordinating the Ca^{2+} ion in EF hands III and IV, with the greatest differences occurring for the amides in the center of the Ca^{2+}-binding loop (Figure 3.9). The amide resonances of the N-lobe show little chemical shift differences suggesting a similar structure of the N-lobe bound to iNOS for both complexes. The chemical shift assignment of CaM_{34} with iNOS was deposited in the BMRB database under accession number 26687.

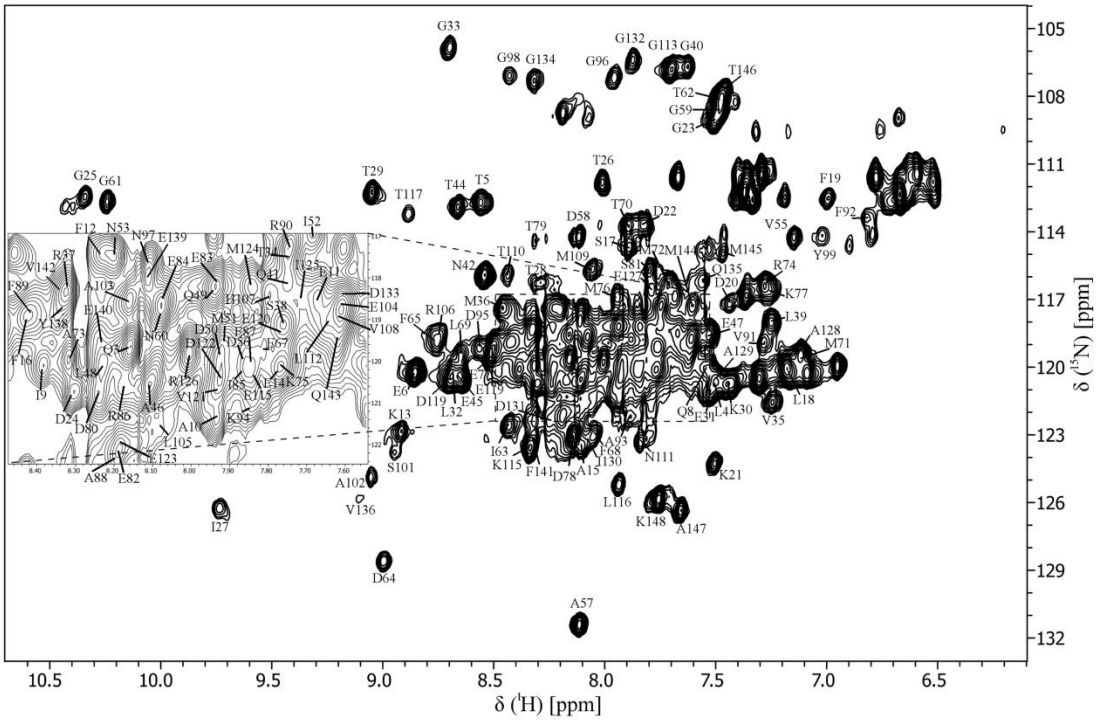

Figure 3.8: ^{1}H-^{15}N HSQC spectrum of CaM$_{34}$-iNOS.

Each backbone amide resonance is labeled with the amino acid type and position in the sequence.

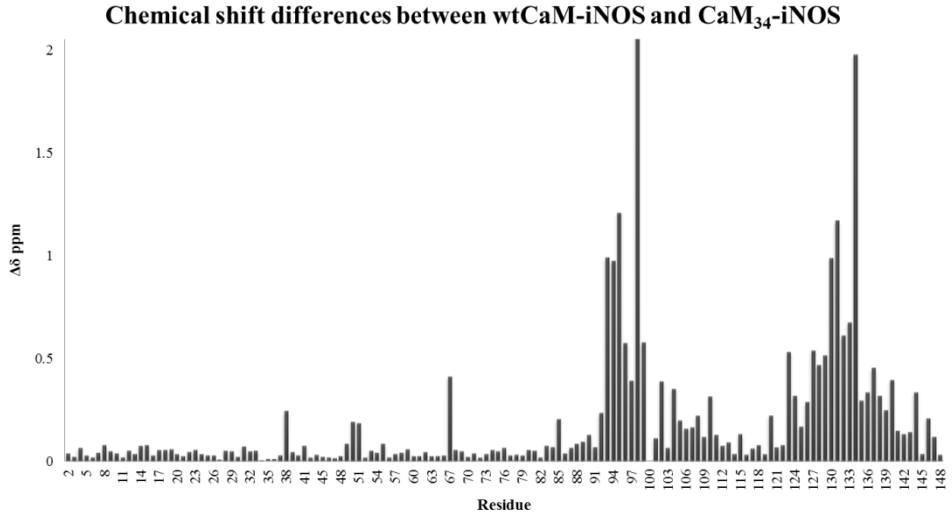

Figure 3.9: Chemical shift differences between wtCaM-iNOS and CaM$_{34}$-iNOS.

The contribution of ^{1}HN and ^{15}N chemical shift changes for each residue was calculated as $\Delta\delta = \sqrt{[(\Delta\delta^{1}HN)^2 + (\Delta\delta^{15}N/5)^2]}$, where $\Delta\delta^{1}$HN and $\Delta\delta^{15}$N are the differences in ^{1}HN and ^{15}N chemical shifts between the indicated protein. The greatest differences are localized to Ca^{2+} binding loops where each mutation is present.

Chapter 4

Dynamics of nitric oxide synthase calmodulin interactions at physiological calcium concentrations*

4.1 Introduction

CaM is a small cytosolic Ca^{2+}-binding protein that is found in all eukaryotic cells. It is able to bind and regulate hundreds of different intracellular proteins (Ikura and Ames, 2006). CaM consists of two globular domains connected by a flexible central linker region. Each globular domain contains two EF hand pairs that are capable of binding to Ca^{2+}. Binding of Ca^{2+} to CaM causes conformational changes that expose hydrophobic patches that allow it to bind and activate its intracellular target proteins. The flexibility of CaM's central linker separating the N- and C-domains allows it to adapt its conformation to optimally associate with its intracellular targets (Persechini and Kretsinger, 1988).

NOS enzymes are one of CaM's target enzymes. The CaM binding domains of NOS contain the classical 1-5-8-14 CaM-binding motif. CaM binds and activates the Ca^{2+}- dependent eNOS enzyme at elevated cellular Ca^{2+} concentrations (Busse and Mulsch, 1990). In contrast, iNOS is

* The results presented in this chapter have been published as part of:

Piazza, M., Guillemette, J. G., Dieckmann, T., (2015) Dynamics of Nitric Oxide Synthase Calmodulin - Interactions at Physiological Calcium Concentrations, *Biochemistry*, 54, 1989–2000. *Unless otherwise stated, all of the work reported in this chapter was performed and analyzed by the candidate.*

controlled at the transcriptional level *in vivo* by cytokines and binds to CaM in a Ca^{2+}-independent manner (Balligand et al., 1994). A large conformational change that CaM induces in the reductase domain of the NOS enzymes allows for the FMN domain to interact with both the FAD and the heme to accept and pass on the electrons during catalysis (Ghosh and Salerno, 2003; Welland and Daff, 2010).

Understanding the structural basis of CaM's target protein interactions and diverse regulatory functions is crucial for rationalizing the regulation pathways and for developing strategies for controlling them for medical purposes. It is well established that CaM is able to interact with its target enzymes in many different conformations. CaM's interactions with the various NOS isozymes have previously been studied by NMR (Zhang and Vogel, 1994; Zhang et al., 1995b; Matsubara et al., 1997; Piazza et al., 2012, 2014). In addition to 3D structures, NMR spectroscopy can also provide quantitative information on molecular dynamics of protein systems at a residue specific level. These studies provide direct evidence of structural changes and intramolecular dynamics associated with functions that are central to understanding the role of dynamics in protein function (Kay, 1998; Ishima and Torchia, 2000; Wand, 2001; Kempf and Loria, 2003; Kwan et al., 2011). By tracking chemical shift changes, NMR spectroscopy is able to characterize very weak interactions between proteins and ligands at atomic (or residue) levels (Pochapsky et al., 2010; Sikic et al., 2010).

Detailed information about fluctuations in protein structures and site-specific information on the stability of secondary structural elements can also be obtained from the measurement of amide proton (NH) hydrogen/deuterium exchange (H/D) rates using NMR spectroscopy (Andrec et al., 1995; Polshakov et al., 2006; Ma and Nussinov, 2011). These fluctuations expose some of the NH to the D_2O solvent, thus facilitating the NH/ND exchange process while other amide protons remain protected from exchange. The exchange rate of NHs in proteins is determined by a combination of

their intrinsic exchange rate in the absence of secondary structure and the presence of secondary structure and solvent inaccessibility that protect from exchange (Englander and Kallenbach, 1983; Englander and Mayne, 1992). NH H/D exchange experiments are also useful for accessing the stability of specific structure elements within a protein or protein complex (Williams et al., 2003, 2004).

Most structural and dynamics studies on CaM-NOS interactions have been performed at non-physiological conditions using either apo (Ca^{2+} free with EDTA present) or Ca^{2+} saturated (greater than 1mM Ca^{2+}) conditions. Here we present NMR structural and dynamics data of the CaM-NOS complexes at free Ca^{2+} concentrations that are in the resting intracellular Ca^{2+} concentration range of less than 100 nM (Carafoli, 1987; Islam, 2012), and at elevated intracellular Ca^{2+} concentrations of 225 nM as well as under saturation conditions (1mM). Our data highlights remarkable differences in the dynamic properties of CaM-NOS complexes at high millimolar Ca^{2+} concentrations when compared to nanomolar physiological Ca^{2+} concentrations in a residue specific manner. Although the CaM-NOS complexes have similar structures at these Ca^{2+} concentrations, our studies show that the complexes behave more dynamic at lower (physiological) concentrations.

4.2 Methods and experiments

4.2.1 CaM Protein Expression and Purification.

Wild-type CaM protein was expressed and purified using phenyl sepharose chromatography, as previously described in section 2.2.1 and 2.2.2. Isolation of the CaM protein (148 residues) was confirmed by ESI-MS and purity was judged to be > 95% by SDS-PAGE. The human iNOS (RREIPLKVLVKAVLFACMLMRK, 22 residues corresponding to residues 510-531 from the full

length iNOS protein) and eNOS (TRKKTFKEVANAVKISASLMGT, 22 residues corresponding to residues 491-512 from the full length eNOS protein) peptides were synthesized and purchased from Sigma.

4.2.2 Dansylation of CaM.

Dansyl-CaM was prepared as previously described in section 2.2.6. CaM (1 mg/ml) was buffer exchanged into 10 mM $NaHCO_3$, 1 mM EDTA, pH 10.0, at 4°C. 30 µl of 6 mM dansyl-chloride (1.5 mol/mol of CaM) in DMSO was added to 2 ml of CaM, with stirring. After incubation for 12 hr at 4°C, the mixture was first exhaustively dialyzed against 500 volumes of 150 mM NaCl, 1 mM EDTA, 20 mM Tris-HCl, pH 7.5, at 4°C, and then exhaustively dialyzed against 500 volumes of water. Labeling yields were determined from absorbance spectra using the ε_{320} of 3,400 $M^{-1}cm^{-1}$ and were compared to actual protein concentrations determined using the Bradford method with wild-type CaM used as the protein standard. ESI-MS was used to confirm successful dansyl-labeling of each CaM protein. The concentration of dansyl-CaM in all experiments was 2 µM.

4.2.3 Steady State Fluorescence.

Fluorescence emission spectra were obtained using a PTI QuantaMaster spectrofluorimeter (London,ON). Fluorescence measurements were made on 50 µL samples consisting of dansyl-CaM (2 µM) alone or with eNOS or iNOS peptide in 30 mM MOPS, 100 mM KCl, 10 mM EGTA, pH 7.2 with an increasing concentration of free Ca^{2+}. Free Ca^{2+} concentration was controlled using the suggested protocol from the calcium calibration buffer kit from Invitrogen. The excitation wavelength for all of the dansyl-CaMs was set at 340 nm and emission was monitored between 400 and 600nm. Slit widths were set at 2 nm for excitation and 1 nm for emission. Relative fluorescence was

calculated by the following equation: relative fluorescence = $(F - F_0)/(F_{max} - F_0)$, where F is the measured intensity, F_{max} is the maximum intensity, and F_0 is the intensity without added Ca^{2+}.

4.2.4 Sample Preparation for NMR Investigation.

CaM for NMR experiments was expressed in E. coli in 1 L of M9 media (11.03 g/L $Na_2HPO_4 \cdot 7H_2O$, 3.0 g/L KH_2PO_4, 0.5 g/L NaCl, 2 mM $MgSO_4$, 0.1 mM $CaCl_2$, 3 μM $(NH_4)_6(MO_7)_{24}$, 400 μM H_3BO_3, 30 μM $CoCl_2$, 10 μM $CuSO_4$, 80 μM $MnCl_2 \cdot 4H_2O$, 10 μM $ZnCl_2$, 10 mM $FeSO_4$, 100 μg/mL kanamycin) containing 2 g/L ^{13}C-glucose and 1 g/L $^{15}NH_4Cl$. ^{13}C-^{15}N-CaM was purified as described in section 2.2.2. The Ca^{2+} saturated ^{13}C-^{15}N-CaM samples were prepared for NMR experiments via a buffer exchange into 100 mM KCl, 10 mM $CaCl_2$, 0.2 mM NaN_3, 90% H_2O/10% ^2H_2O at pH 6.5 using a YM10 centrifugal filter device (Millipore Corp., Billerica, USA) and had a final concentration of 1 mM in a total volume of 500 μL. The 17 nM, 100 nM and 225 nM free [Ca^{2+}] ^{13}C-^{15}N-CaM samples were prepared via a buffer exchange into 30 mM MOPS, 100 mM KCl, 90% H_2O/10% ^2H_2O, pH 7.2, and combinations of 10 mM EGTA and 10mM CaEGTA to obtain 17 nM, 100 nM and 225 nM concentrations of free Ca^{2+}. These samples had a final ^{13}C-^{15}N-CaM concentration of 200 μM in a total volume of 500 μL. The 225 nM free [Ca^{2+}] ^{13}C-^{15}N-CaM samples used for the H/D exchange and ^{15}N relaxation experiments had a final ^{13}C-^{15}N-CaM concentration of 1 mM in a total volume of 500 μL. The samples were transferred into 5 mm NMR sample tubes and stored at 4^{o}C until required for NMR experiments. NMR experiments on the complexes were conducted on samples titrated with either iNOS or eNOS peptide to saturation in a 1:1 CaM:peptide ratio. Complex formation was monitored after each addition by acquisition of a ^{1}H-^{15}N heteronuclear single-quantum coherence (HSQC) spectrum. For the proton-deuterium exchange studies, the CaM-peptide complex samples

were lyophilized overnight. The samples were then resuspended in ~100% D_2O to the same volume and immediately placed into the previously tuned and calibrated NMR spectrometer.

4.2.5 NMR Spectroscopy and Data Analysis.

NMR spectra were recorded at 25°C on Bruker 600 MHz DRX spectrometers equipped with XYZ-gradients triple-resonance probes (Bruker, Billerica, MA, USA). Spectra were analyzed using the program CARA (Keller, 2005). The amide resonances were assigned by using the previously obtained amide chemical shifts of Ca^{2+} saturated CaM with iNOS or eNOS peptide as reference (Piazza et al., 2012). H/D exchange data was obtained by successive acquisition of ^{1}H-^{15}N HSQC spectra of each sample immediately after they were resuspended in D_2O. Each ^{1}H-^{15}N HSQC experiment was acquired with 32 scans and 128 increments for a total acquisition time of 100 minutes. ^{15}N T_1 measurements were acquired for eight different durations of the T_1 relaxation delay, T= 5, 100, 200, 300, 400, 500, 600, and 800ms. ^{15}N T_2 measurements were acquired for eight different durations of the T_2 relaxation delay, T= 16.6, 33.2, 49.8, 66.4, 99.6, 116.2, 132.8, and 149.4ms. ^{1}H-^{15}N NOE measurements were recorded with two spectra, one with the NOE effect and one without. The standard model free approach (Lipari and Szabo, 1982b) was used to determine order parameters (S^2) for each of the CaM-peptide complexes. The order parameters were calculated using the TENSOR program version 2.0 (Dosset et al., 2000; Tsan et al., 2000).

4.2.6 Model of CaM-eNOS Peptide at 225 nM [Ca^{2+}].

In order to visualize the dynamics data a model of CaM-eNOS peptide at 225 nM Ca^{2+} was prepared using CNSsolve version 1.2 (Brunger et al., 1998). The calculation used the structural constraints for the C-terminal residues from the solution structure of CaM with eNOS at saturated Ca^{2+} along with

the inter-residue constraints of the C-terminal residues to the eNOS peptide. All N-terminal intra and inter-residue constraints were deleted and replaced with constraints for the N-terminal residues from the apoCaM structure deposited in the PDB (1CFC). The structure calculation was initiated with an extended conformation file. The calculation was run through several iterations of a standard simulated annealing protocol to minimize the energies. The average of the final 20 lowest energy structures was selected for the visualization model.

4.3 Results

4.3.1 Fluorescence Spectroscopy of Dansyl-CaM Binding to NOS Peptides.

The Ca^{2+} dependent binding properties of the CaM binding domains used in our study were first investigated using dansyl-labeled CaM proteins (Figure 4.1). Dansyl-CaM is a useful tool to detect conformational changes in CaM as a result of interactions with Ca^{2+}, peptides or other proteins because the intensity of the fluorescence spectrum is enhanced and shifted when the dansyl moiety becomes embedded in a hydrophobic environment (Kincaid et al., 1982; Johnson and Wittenauer, 1983). Without peptides or Ca^{2+} present, dansyl-CaM exhibited a fluorescence maximum at 510nm (Figure 4.1A). When Ca^{2+} was titrated into the sample a blue shift (to 490nm) and enhancement of dansyl fluorescence spectrum were observed in a Ca^{2+} concentration range of 0.65-2.86 μM (Figure 4.1B).

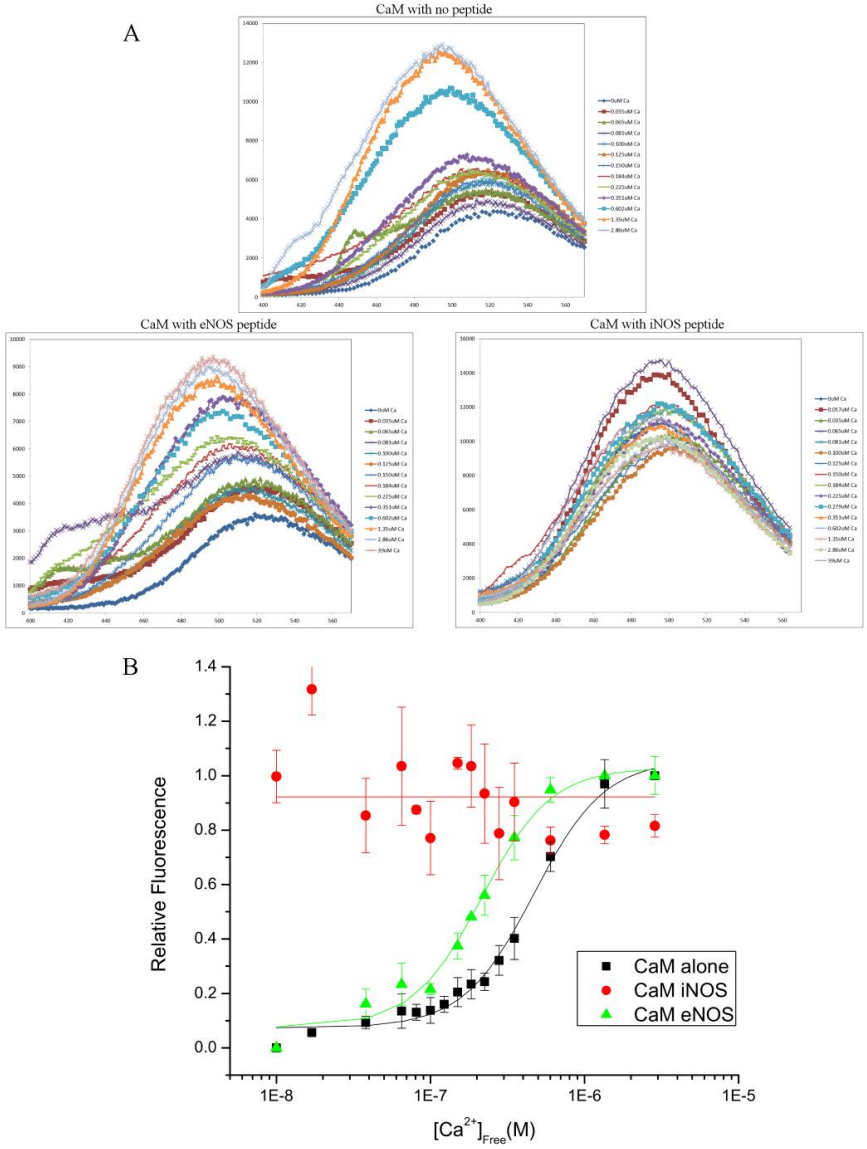

Figure 4.1: Ca^{2+} dependency of dansyl-CaM fluorescence with or without eNOS and iNOS peptides.

(A) Fluorescence emission spectra of dansyl-CaM in the absence or presence of iNOS and eNOS peptides. Fluorescence measurements were made on 50 µL samples consisting of dansyl-CaM (2 µM) alone or with iNOS or eNOS peptide in 30 mM MOPS, 100 mM KCl, 10 mM EGTA, 10 mM CaEGTA, pH 7.2 with an increasing concentration of free Ca^{2+}. The excitation wavelength for all of the dansyl-CaMs was set at 340 nm and emission was monitored between 400 and 600 nm. Slit widths were set at 2 nm for excitation and 1 nm for emission. (B) Normalized fluorescence is shown for CaM, CaM-eNOS complex, and CaM-eNOSpThr495 under assay conditions described in section 4.2.3.

When iNOS peptide was added in the absence of Ca^{2+} the same blue shift and enhancement of dansyl fluorescence spectrum observed with addition of Ca^{2+} to CaM alone was seen, but not when eNOS peptide was added to the dansyl-CaM (Figure 4.1A). The dansyl-CaM-iNOS complex showed no Ca^{2+} dependency when Ca^{2+} was titrated into the sample, as indicated by the lack of fluorescence change (Figure 4.1A) and little relative fluorescence difference over the whole range of free Ca^{2+} concentration additions (Figure 4.1B). With the addition of Ca^{2+}, this blue shift and enhancement of the fluorescence spectrum seen with CaM alone was then also observed with the eNOS peptide. However, the fluorescence changes of the dansyl-CaM-eNOS complex occurred at a much lower Ca^{2+} concentration range, beginning at 225 nM. This is consistent with previous studies of eNOS that show the enzyme requires 200-300 nM concentrations of free Ca^{2+} to achieve half maximal activity (Sessas et al., 1992; Ruan et al., 1996). Hence a concentration of 225 nM free Ca^{2+} was used for the NMR studies, corresponding to physiological Ca^{2+} concentrations above basal levels.

4.3.2 NMR Spectroscopy at Physiological Ca^{2+} Concentrations.

NMR experiments were performed at physiological free Ca^{2+} concentrations to provide further insights into the structural differences between the two CaM-NOS complexes. ^{1}H-^{15}N HSQC spectra show that the CaM-eNOS complex at a physiological free Ca^{2+} concentration of 225 nM has a C-terminal lobe that is structurally similar to the Ca^{2+}-replete CaM-eNOS complex (Figure 4.2), and an N-terminal lobe structurally similar to unbound, Ca^{2+} free apoCaM (Figure 4.3). This can be visualized by overlaying the ^{15}N-HSQC spectra of CaM-eNOS at 225 nM free [Ca^{2+}] with either Ca^{2+}-replete CaM-eNOS or apoCaM. Cross peaks for amides in the C-domain of CaM-eNOS at 225 nM [Ca^{2+}] overlap with those of Ca^{2+}-replete CaM-eNOS, but amides in the N-domain do not (Figure

4.2). And vice versa, cross peaks for amides in the N-domain of CaM-eNOS at 225 nM [Ca^{2+}] overlap with those of apoCaM, but amides in the C-domain do not (Figure 4.3).

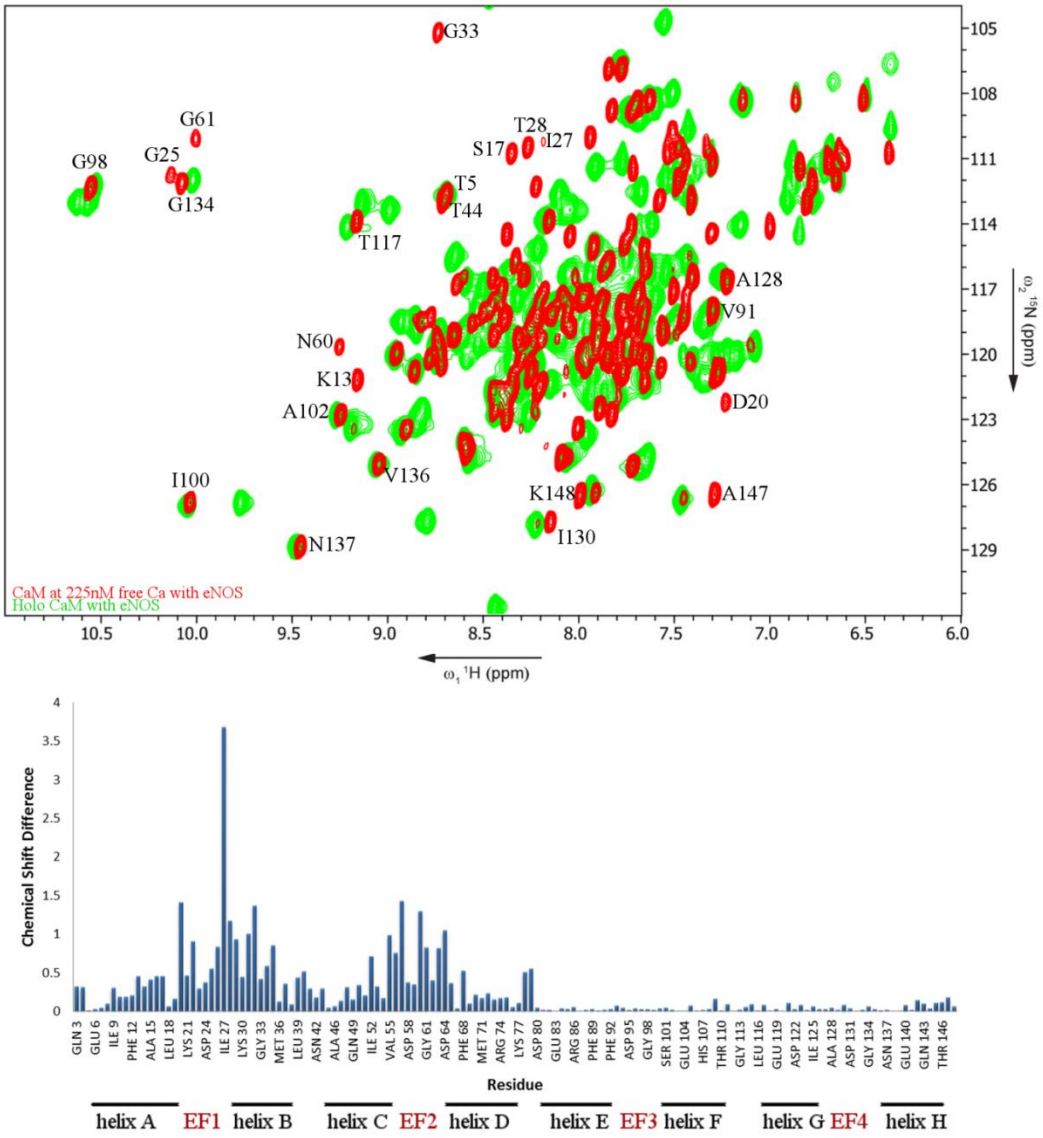

Figure 4.2: Overlay of ^{1}H-^{15}N HSQC spectra of CaM-eNOS peptide complex at 10 mM $CaCl_2$ (green) and 225 nM free [Ca^{2+}] (red).

Chemical shift differences between CaM-eNOS peptide complex at 10mM $CaCl_2$ and 225 nM free [Ca^{2+}]. The contribution of ^{1}HN and ^{15}N chemical shift changes for each residue was calculated as $\Delta\delta = \sqrt{[(\Delta\delta^{1}HN)^2 + (\Delta\delta^{15}N/5)^2]}$, where $\Delta\delta^{1}HN$ and $\Delta\delta^{15}N$ are the differences in ^{1}HN and ^{15}N chemical shifts between the indicated protein.

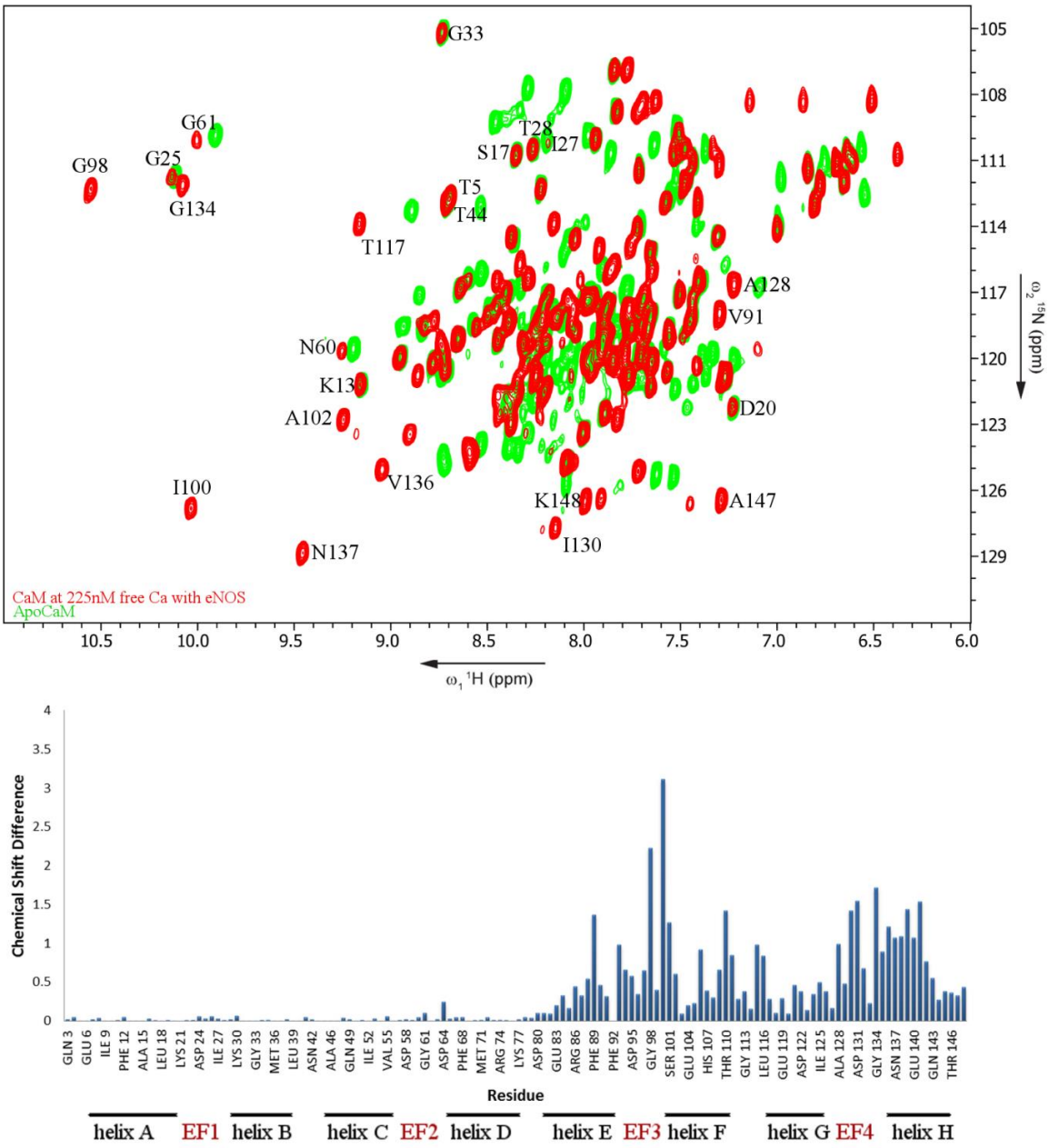

Figure 4.3: Overlay of ^{1}H-^{15}N HSQC spectra of apoCaM (green) and CaM-eNOS peptide complex at 225 nM free [Ca^{2+}] (red).

Chemical shift differences between apoCaM and CaM-eNOS peptide complex at 225nM free [Ca^{2+}]. The contribution of ^{1}HN and ^{15}N chemical shift changes for each residue was calculated as $\Delta\delta = \sqrt{[(\Delta\delta^{1}HN)^2 + (\Delta\delta^{15}N/5)^2]}$, where $\Delta\delta^{1}HN$ and $\Delta\delta^{15}N$ are the differences in ^{1}HN and ^{15}N chemical shifts between the indicated protein.

More specifically the cross peaks assigned to G25 (EF1), G61 (EF2), I27, I63 (the short antiparallel β-sheets between EF1 and EF2), G98 (EF3), G134 (EF4) and I100 and V136 (the short antiparallel β-sheets between EF3 and EF4) have specific chemical shifts characteristic of Ca^{2+} binding to each EF hand and the conformation of the EF hand pairs. The cross peaks assigned to G98, G134, I100 and V136 for CaM-eNOS at 255 nM Ca^{2+} have very similar chemical shifts to those assigned for Ca^{2+}-replete CaM-eNOS, indicating that the C-lobe of CaM at 225 nM [Ca^{2+}] is Ca^{2+} replete and bound to the eNOS peptide. On the other hand, the cross peaks assigned to G25, G61, I27 and I63 have very similar chemical shifts to those assigned for apoCaM, indicating that the N-lobe of CaM at 225 nM [Ca^{2+}] is Ca^{2+} deplete and not bound to the eNOS peptide.

This behavior is clearly shown by calculating the chemical shift difference between each set of amides. In the overlay of CaM-eNOS at 225 nM free [Ca^{2+}] and Ca^{2+}-replete CaM-eNOS the amide chemical shifts show a difference for all the residues of the N-domain, whereas the amide chemical shifts of the C-domain have very small differences (Figure 4.2). In the overlay of CaM-eNOS at 225 nM [Ca^{2+}] and apoCaM the amide chemical shifts show a difference for all the residues of the C-domain, whereas the amide chemical shifts of the N-domain have very small differences (Figure 4.3). Comparison of the ^{1}H-^{15}N HSQC spectrum of the eNOS-CaM complex under Ca^{2+} replete versus that at a Ca^{2+} concentration of 225nM clearly shows that the C-lobe of CaM is the first to bind to Ca^{2+} and the eNOS peptide. This is further supported by comparing the ^{1}H-^{15}N HSQC spectra in the presence of 225nM [Ca^{2+}] and the apo form of the CaM. These results are consistent with the known Ca^{2+} binding properties of the N and C lobes of free CaM in solution (Linse et al., 1991; Pedigo and Shea, 1995).

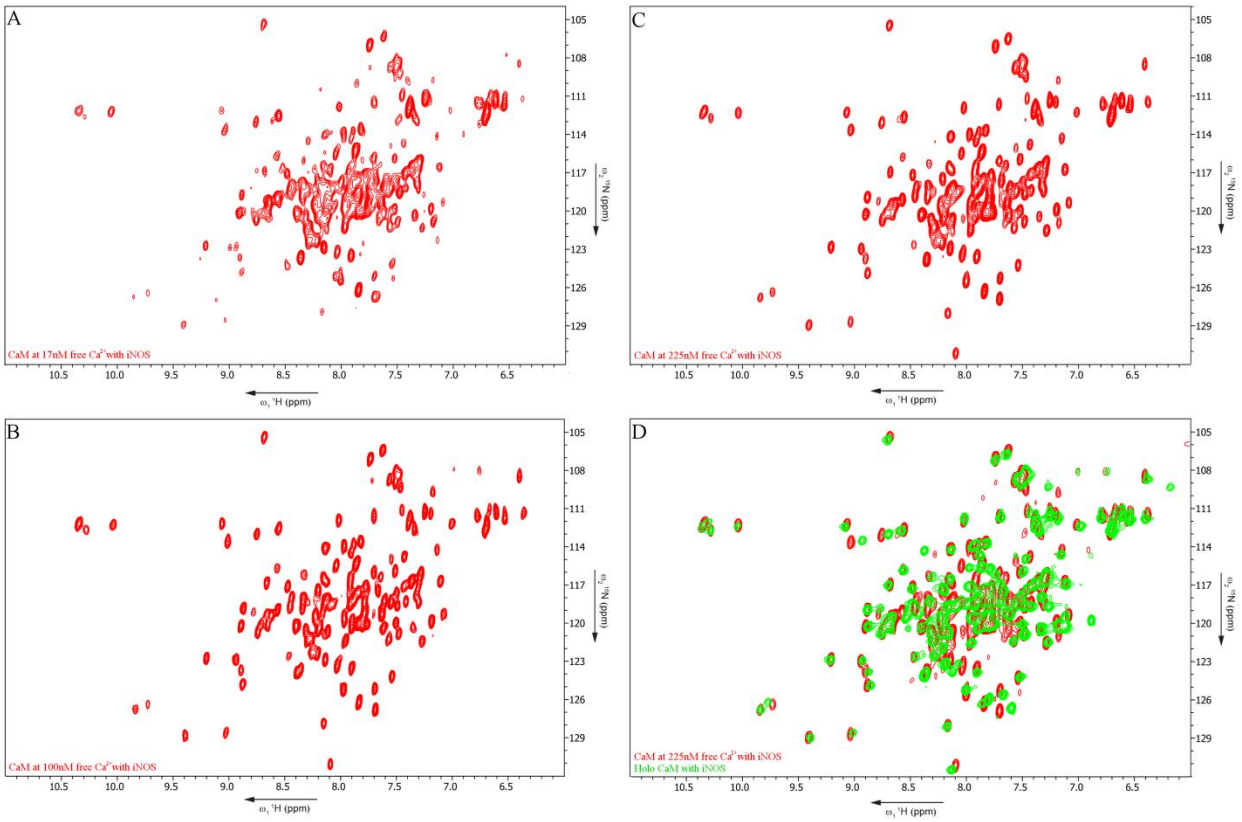

Figure 4.4: ^{1}H-^{15}N HSQC spectra of CaM-iNOS peptide complex at (A) 17 nM, (B) 100 nM and (C) 225 nM free [Ca^{2+}].

The spectra at all 3 of these low [Ca^{2+}] levels show the same amide chemical shift patterns. (D) Overlay of ^{1}H-^{15}N HSQC spectra of CaM-iNOS peptide complex at 10 mM $CaCl_2$ (green) and 225nM free [Ca^{2+}] (red). The ^{1}H-^{15}N HSQC spectra indicate that CaM-iNOS peptide complex maintains structural integrity at all Ca^{2+} levels.

When a similar comparison is made using the CaM-iNOS complex, ^{1}H-^{15}N HSQC spectra indicate that the CaM-iNOS complex maintains structural integrity at all Ca^{2+} levels (Figure 4.4). This observation makes sense because CaM interacts with iNOS in a Ca^{2+}-independent manner. Figure 4.4 shows ^{1}H-^{15}N HSQC spectra of CaM-iNOS at 17 nM, 100 nM and 225 nM free [Ca^{2+}]. The spectra at all 3 of these low Ca^{2+} levels show the same chemical shift patterns for the amides (Figure 3A-C), indicating that the structure of this complex doesn't change going from free Ca^{2+} levels representative of resting intracellular Ca^{2+} levels (17 and 100 nM Ca^{2+}) to elevated Ca^{2+} levels (225 nM Ca^{2+}). When

these spectra are compared to the ^{1}H-^{15}N HSQC spectrum of CaM-iNOS complex at saturated [Ca^{2+}] (10 mM Ca^{2+}) we see that the spectra all overlay quite well. The few amide cross peaks that are slightly shifted are likely due to the different buffer and pH used for the low Ca^{2+} sample (pH 7.2) and saturated Ca^{2+} samples (pH 6.5). A comparison of the specific cross peaks characteristic of Ca^{2+} binding to each EF hand and the conformation of the EF hand pairs as done with CaM-eNOS for all the CaM-iNOS samples illustrates that the structure of CaM bound to the iNOS peptide is very similar at low and high free Ca^{2+} concentrations. This suggests that the CaM-iNOS complex binds Ca^{2+} at this low basal Ca^{2+} level. NMR data could not be collected for the iNOS peptide interacting with apoCaM or CaM_{1234} (CaM that contains a mutation in each EF hand that disables Ca^{2+} binding) due to precipitation of the protein upon addition of the peptide. This behavior has also been seen in other studies at higher concentrations of CaM and iNOS peptide (Anagli et al., 1995; Censarek et al., 2004). This suggests that in the Ca^{2+} deplete form CaM-iNOS adopts a different conformation which may expose hydrophobic regions that leads to this aggregation, or that a larger portion of the iNOS enzyme is required for binding in apo conditions, as previously suggested (Ruan et al., 1996).

4.3.3 Amide Exchange and Internal Protein Dynamics for CaM-eNOS Complexes at Low and Saturating Ca^{2+} Concentrations.

H/D exchange patterns of amides were classified into three categories based on the length of time for which the amide peaks were observable in the spectra after D_2O exposure: fast exchange (amide peaks disappear before first experiment); intermediate exchange (amide peaks disappear between 3 min and 100 min); and slow exchange (amide peaks remained longer than 200 min). The criteria for slow exchange were based on the observation that little change occurs in the spectrum when additional ^{1}H-^{15}N HSQC spectra were obtained after 200 min (data not shown). An intermediate

exchange lower limit of 3 min was determined by the amount of time elapsed prior to the acquisition of the first NMR spectrum.

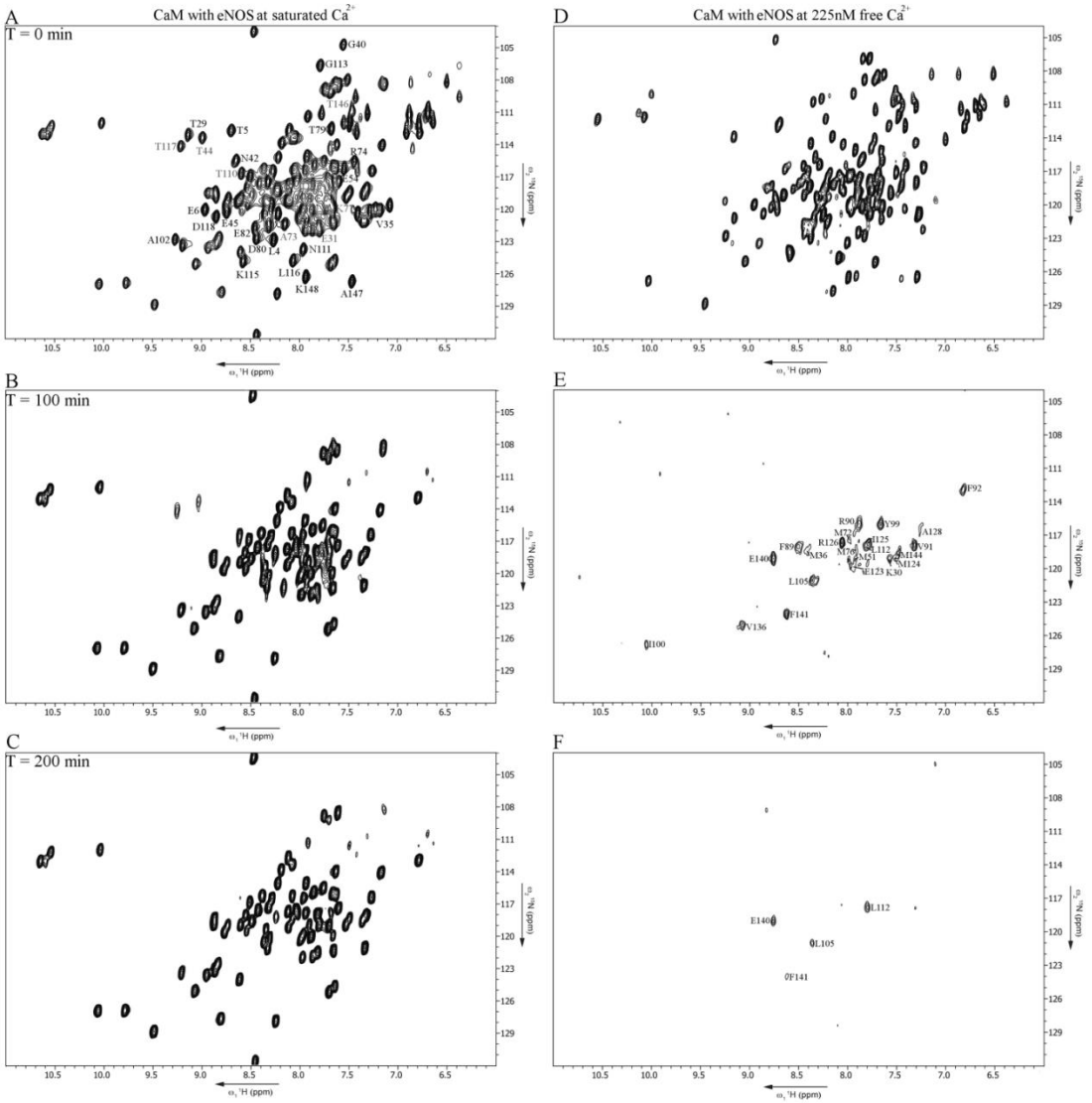

Figure 4.5: Selected spectra from the amide H2O/D2O exchange time-course for CaM-eNOS.

(A) ^{1}H-^{15}N HSQC spectrum of CaM-eNOS peptide complex at 10 mM $CaCl_2$ obtained in H_2O. The amide peaks labeled in black indicate amides that have undergone fast exchange with D_2O, amide peaks labeled grey indicate amides that have undergone intermediate exchange. (B,C) Spectra obtained 100 and 200 min after addition of D_2O. (D) ^{1}H-^{15}N HSQC spectrum of CaM-eNOS peptide complex at 225nM free [Ca^{2+}] obtained in H_2O. (E,F) Spectra obtained 100 and 200 min after addition of D_2O.

The amide exchange investigation of the CaM-eNOS complex under Ca^{2+} saturated conditions showed very little change over the period investigated (Figure 4.5A-C). Relatively few residues have undergone exchange with the D_2O as evidenced by the lack of signal disappearance in the ^{1}H-^{15}N HSQC spectra. The few residues that have undergone exchange are found to be at the N and C termini, in the loop regions between the two EF hands in each lobe of CaM and in the linker region. These are residues that are exposed to the solvent and are not well protected by secondary structure elements, such as H-bonding in α-helices, or by binding to the eNOS peptide. Figure 4.7 shows the H/D exchange data projected onto the previously determined structure of the Ca^{2+} replete CaM-eNOS complex (Aoyagi et al., 2003; Piazza et al., 2012). Residues that have undergone fast exchange were colored red, while residues that exhibit intermediate exchange have been colored light blue and residues exhibiting slow exchange colored blue.

When the same set of experiments were performed at 225 nM [Ca^{2+}], after 100 min most amide protons exchanged with the D_2O as shown by the lack of amide cross peaks in the ^{1}H-^{15}N HSQC spectrum. After 200 min only a very few amide resonances remained (Figure 4.5D-F). The amides that exhibited fast H/D exchange were mostly found to be from residues in the N-lobe of CaM, while those that were protected from exchange, and most of those exhibiting intermediate exchange, belonged to residues in the C-lobe of CaM. This amide H/D data was projected onto a model representative of the NMR data for the CaM-eNOS complex at 225 nM [Ca^{2+}], using the same color scheme as above (Figure 4.7). Note that this model has been prepared to better visualize the differences between the structure of the CaM-eNOS complex at the 225 nM Ca^{2+} concentration compared to the structure at saturating Ca^{2+} concentrations. It does not represent a 3D solution structure of the complex under these conditions.

As was described above, the ^{1}H-^{15}N HSQC data suggest that only the C-lobe of CaM is Ca^{2+}-replete and bound to the eNOS peptide, while the N-lobe would be Ca^{2+} free and not bound to the peptide. Since the N-lobe is not bound to the peptide it would be more exposed to the solvent, which could explain why almost all of the N-lobe residues undergo fast exchange. There are a few residues of the N-lobe that exhibit intermediate exchange, such as K30, M36, M51, M72 and M76. These residues are all part of α-helices and are found to directly interact with L509, one of the anchoring residues of eNOS, in the crystal and solution structures of the complex (Table 4.1) (Aoyagi et al., 2003; Xia et al., 2009; Piazza et al., 2012). This suggests that even though this lobe is Ca^{2+} free and not tightly bound to the peptide it is still maintaining its structural integrity and might also maintain some transient interactions with the peptide. The amides of the C-lobe residues that show intermediate or slow exchange have been previously shown to interact with the 1-5-8-14 anchoring residues of the eNOS peptide (Aoyagi et al., 2003; Piazza et al., 2012). The four slow exchanging amides correspond to residues L105, L112, E140 and F141 which interact with the anchoring residues F496, A500 and V503 of the eNOS peptide in the structure of the Ca^{2+}-replete CaM-eNOS complex. The amides that show intermediate exchange are found to either interact with these anchoring residues of the eNOS peptide or be a part of α-helices in this lobe.

The internal dynamics of the CaM complexes at 225 nM [Ca^{2+}] and saturating [Ca^{2+}] were further investigated by measuring the relaxation properties of the backbone ^{15}N nuclei in CaM. T_1, T_2, and ^{1}H-^{15}N NOE values were measured (Figure 4.6). The standard model free approach was used to determine order parameters (S^2) and internal correlation times (τ_i) for each of the CaM-peptide complexes. The comparison of the internal dynamics between the CaM-eNOS complex at 225 nM [Ca^{2+}] and saturating [Ca^{2+}] agrees well with the results found for the H/D exchange experiments. For the CaM-eNOS complex at saturating Ca^{2+} concentration low S^2 and high τ_i values were found for the

residues of the linker region and also in the loop regions between the EF hand pairs. The high degree of mobility observed in these regions agrees very nicely with the H/D exchange data, which is shown in figure 4.7 by the correlation between worm radius and structure color. S^2 values for the rest of CaM were between 0.8 and 1.0, indicating very little mobility, and agreeing very well with the high degree of exchange protection observed in the H/D exchange data.

Table 4.1: Residues of CaM shown to be within 4 Å of the NOS peptides.

	Alignment of NOS Cam-binding domains		CaM sidechains in contact with peptides		
Motif 1-5-8-14	Human eNOS	Human iNOS	N-terminal Domain	C-terminal Domain	Central Linker
	R492	R511	E6, E7, A10		
	K493	E512		E120, E123, E127	
	K494	I513	E14		
	T495	P514		M124, E127	
1	F496	L515		L105, M124, E127, A128, V136, F141, M144	
	K497	K516	E7	E127, M144, A147	
	E498	V517	E7, A10, E11, E14		
	V499	L518	E14	M109, E114, M124	
5	A500	V519		F92, F141, M144, M145	
	N501	K520	E11	M145	
	A502	A521	E11, E14, A15, L18		
8	V503	V522		V91, F92, L112	
	K504	L523		S81, E84, I85, A88, M145	
	I505	F524	E11, E14, A15, M72		M76
	S506	A525	A15, L18, F19, L39		
	A507	C526	L39	E87	
	S508	M527	M72, K75	E87	M76
14	L509	L528	F19, M36, M51, M71, M72, K75		
	M510	M529	L39, Q41, K75	E87	

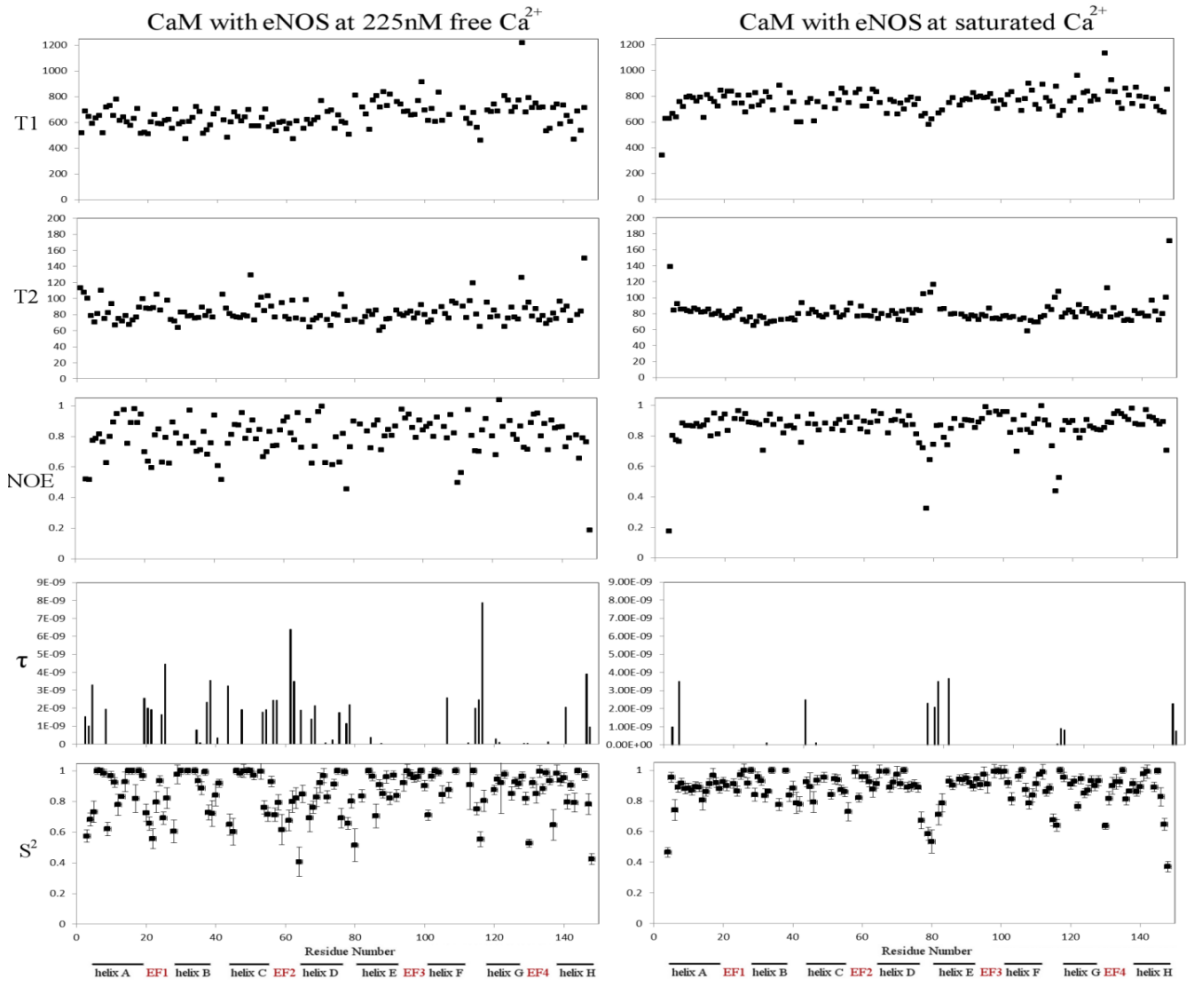

Figure 4.6: ^{15}N Relaxation data and model free order parameters for the CaM-eNOS complex at 225nM Ca^{2+} and saturating Ca2+ conditions.

Plots as a function of residue number of the measured T1 and T2 values, the ^{1}H-^{15}N NOE, τ_i, internal correlation times, and the order parameter, S^2, with associated uncertainty are shown. Only residues for which the ^{15}N-^{1}H cross peaks were sufficiently well resolved to permit accurate measurement of its intensity are included.

Table 4.2: Average S^2 order parameter for each structure element of the CaM-eNOS complex.

	S^2														
	A	EF1	B	Loop	C	EF2	D	Link	E	EF3	F	Loop	G	EF4	H
CaM-eNOS 225nM Ca^{2+a}	0.92 ± 0.11	0.75 ± 0.14	0.91 ± 0.11	0.80 ± 0.14	0.90 ± 0.15	0.72 ± 0.16	0.86 ± 0.10	0.73 ± 0.18	0.88 ± 0.09	0.93 ± 0.04	0.91 ± 0.10	0.80 ± 0.17	0.92 ± 0.05	0.87 ± 0.14	0.90 ± 0.08
CaM-eNOS sat Ca^{2+b}	0.88 ± 0.05	0.92 ± 0.06	0.90 ± 0.08	0.84 ± 0.07	0.89 ± 0.06	0.89 ± 0.08	0.93 ± 0.05	0.67 ± 0.15	0.88 ± 0.08	0.96 ± 0.04	0.91 ± 0.08	0.86 ± 0.15	0.88 ± 0.06	0.87 ± 0.10	0.93 ± 0.06

[a]Residues comprising each segment: A 6-19; EF1 20-26, 28-29; B 30, 32, 34-39; Loop 40, 41, 44; C 45-51, 53-55; EF2 56-59, 61-64; D 65, 67-72, 74-75; Link 76-80; E 82, 84-92; EF3 94-100; F 101-105, 106-107, 109; Loop 113-117; G 120-123, 125-126; EF4 127-138; H 139-144.
[b]Residues comprising each segment: A 6-19; EF1 20-21, 23-29; B 30-34,36, 38-39; Loop 40-42, 44; C 45-47, 49, 51-55; EF2 56, 58-64; D 65, 67-75; Link 76-77, 79-80; E 82-83, 85-86, 88-92; EF3 93-96, 98-100; F 101-103, 105-111; Loop 112-118; G 120-126; EF4 127-128, 130-138; H 139-142, 144.

When the internal dynamics were analyzed for the CaM-eNOS complex at 225 nM [Ca^{2+}], a significant increase of internal dynamics is found, especially in the N-lobe. The linker region shows the same high degree of mobility as observed at saturating [Ca^{2+}]. However, an increase of mobility is observed for the loop regions between the EF hand pairs, which can be seen by comparing figure 4.7. The average order parameter values for each structural element of the C-lobe are very similar at 225 nM and saturating [Ca^{2+}] (Table 4.2), however, the CaM-eNOS complex at 225 nM [Ca^{2+}] displays greater fluctuation in its S^2 values, and also contains a greater number of residues that show an increased internal correlation time, τ_i (Figure 4.6). In contrast, the N-lobe of CaM with eNOS at 225 nM [Ca^{2+}] displays an increased internal mobility across the whole domain compared to CaM-eNOS at saturated Ca^{2+}. More specifically, EF hands 1 and 2 have average order parameter values of 0.75 and 0.72, respectively, compared to 0.92 and 0.89 for CaM-eNOS at saturating [Ca^{2+}] (Table 4.2). The N-terminal residues, EF hands and loop region between the EF hand pairs also show an increased τ_i compared to CaM-eNOS at saturating [Ca^{2+}], indicating faster internal motions for these regions at 225 nM [Ca^{2+}]. The observed increased mobility, shown by the lower S^2 and increased τ_i, for the N-

lobe of CaM indicates a more dynamic and less rigid structure for this lobe, which correlates well with the H/D exchange data.

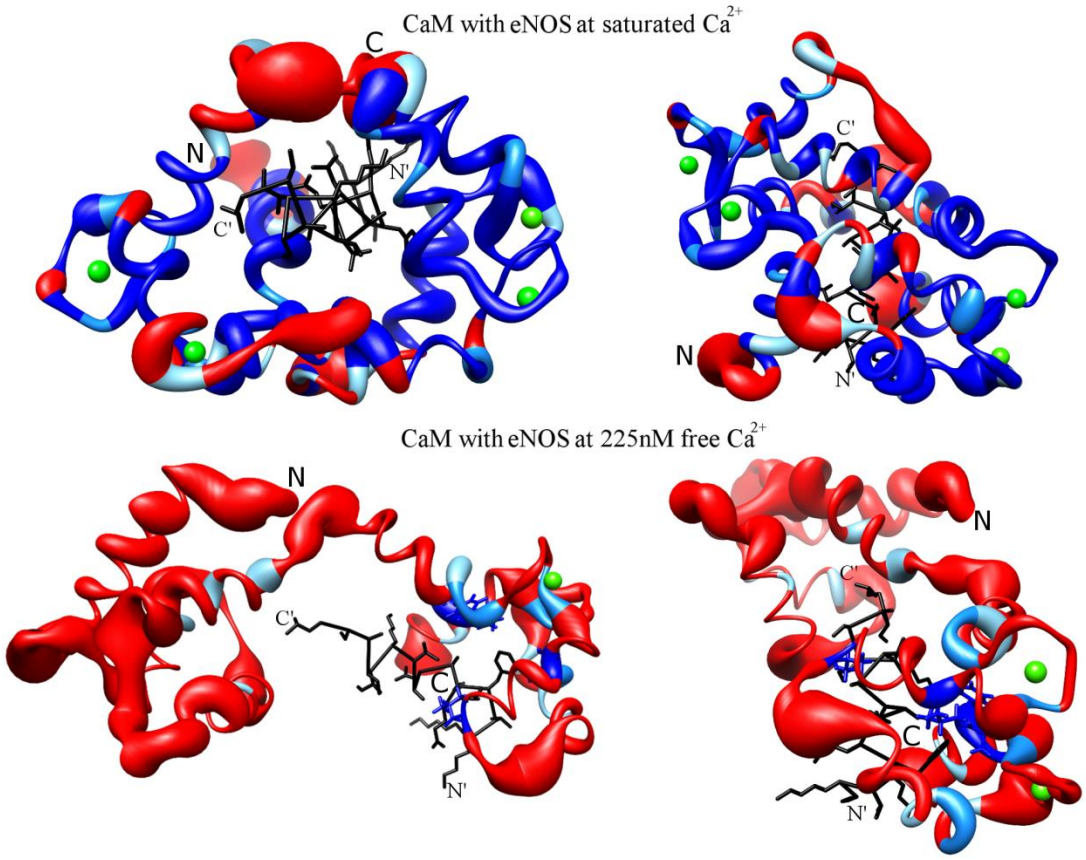

Figure 4.7: Worm models of CaM-eNOS peptide complexes at 225 nM [Ca^{2+}] and saturated [Ca^{2+}] illustrating their internal dynamics and amide H_2O/D_2O exchange data.

The worm models were prepared using UCSF Chimera with the render by attribute function. The worm radius ranges from 0.25, corresponding to a S^2 value of 1, to 4, corresponding to a S^2 value of 0.4. The color of the residue represents its amide H_2O/D_2O exchange data. Residues that display fast D_2O exchange rates are colored red on the ribbon structure. Residues that display intermediate D_2O exchange rates are colored light blue on the ribbon structure. Residues that display slow D_2O exchange rates are colored blue on the ribbon structure with their side chain atoms shown. Worm models and amide H_2O/D_2O exchange data for CaM-eNOS complex at 10 mM $CaCl_2$ projected onto previously determined solution structure of Ca^{2+}-replete CaM-eNOS (PDB 2LL7). Worm models and amide H_2O/D_2O exchange data for CaM-eNOS complex at 225nM free [Ca^{2+}] projected onto a model representative of the NMR data for the CaM-eNOS complex at 225 nM [Ca^{2+}].

4.3.4 Amide Exchange and Internal Protein Dynamics for CaM-iNOS Complexes at Low and Saturating Ca^{2+} Concentrations.

The amide exchange experiments of the CaM-iNOS complex under Ca^{2+} saturated conditions showed very little change over the time period investigated (Figure 4.8), with the same location of residues undergoing H/D exchange as did in the CaM-eNOS complex. This H/D exchange data was projected onto the previously determined solution structure of the Ca^{2+}-replete CaM-iNOS complex using the same color scheme as described earlier (Figure 4.10). However, in contrast to the CaM-eNOS complex at 225nM Ca^{2+} concentration, the C-lobe amides of the CaM-iNOS complex at 225nM Ca^{2+} concentration had faster exchange rates than the N-terminal residues (Figure 4.8). The amides that undergo slow and intermediate exchange correspond to residues that have been found to interact with the 1-5-8-14 anchor residues (L515, V519, V522, and L528) of the iNOS peptide (Figure 4.8, 4.10 and Table 4.1). The iNOS peptide contains hydrophobic residues (V522, L523, Met527, and L528) that interact with hydrophobic residues of the N-lobe of CaM (F16, F19, M36, L39, Met71, Met72, and Met76) (Xia et al., 2009; Piazza et al., 2012). The slower exchange of these N-lobe CaM residues shows they are protected from the D_2O solvent, indicating this is a tight hydrophobic interaction with the iNOS peptide. In contrast to the iNOS peptide, the eNOS peptide contains hydrophilic residues at these locations (with the exception of V503 and L509) that are exposed to the solvent and do not protect the CaM from exchange as shown in the H/D exchange data. The amides of the C-lobe residues of CaM display mostly fast exchange, indicating that there is less protection due to a weaker interaction with the iNOS peptide.

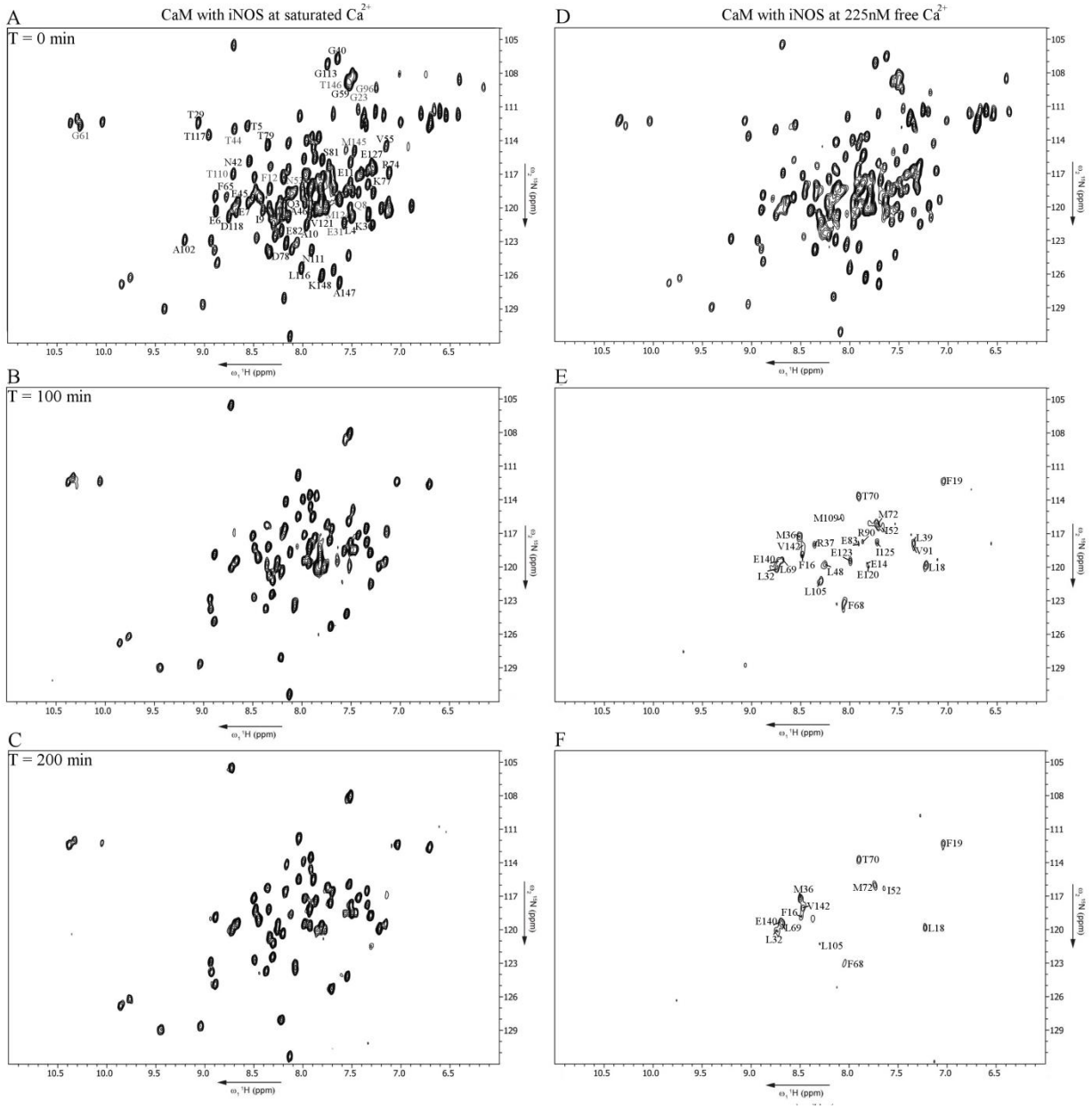

Figure 4.8: Selected spectra from the amide H_2O/D_2O exchange time-course for CaM-iNOS.

(A) ^{1}H-^{15}N HSQC spectrum of CaM-iNOS peptide complex at 10 mM $CaCl_2$ obtained in H_2O. The amide peaks labeled in black indicate amides that have undergone fast exchange with D_2O, amide peaks labeled grey indicate amides that have undergone intermediate exchange. (B,C) Spectra obtained 100 and 200 min after addition of D_2O. (D) ^{1}H-^{15}N HSQC spectrum of CaM-iNOS peptide complex at 225nM free [Ca^{2+}] obtained in H_2O. (E,F) Spectra obtained 100 and 200 min after addition of D_2O.

Analyzing the internal dynamics between the CaM-iNOS complex at 225 nM [Ca^{2+}] and saturating [Ca^{2+}] shows them to agree well with the results found for the H/D exchange experiments. For the CaM-iNOS complex at saturating [Ca^{2+}] low S^2 and high τ_i values were found for the residues of the linker region and also in the loop regions between the EF hand pairs, much like was observed in the CaM-eNOS complex at saturating [Ca^{2+}], which agrees very nicely with the H/D exchange data, (Figure 4.10). S^2 values for the rest of CaM were between 0.8 and 1.0, indicating very little mobility, and agreeing well with the high degree of stability observed from the H/D exchange data.

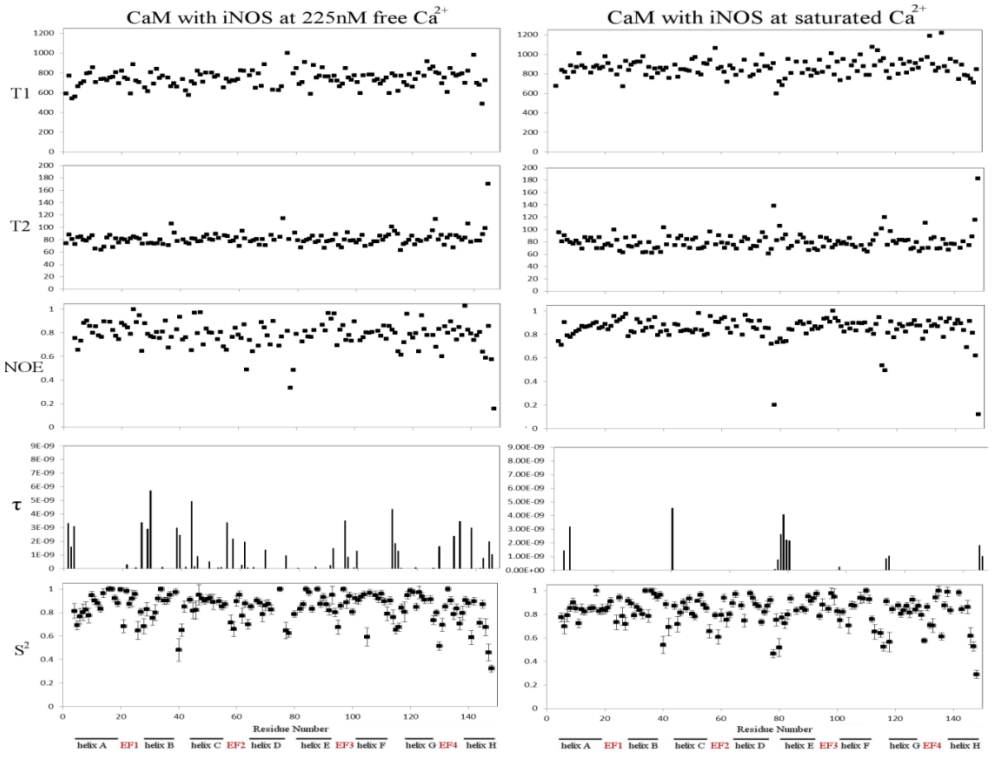

Figure 4.9: ^{15}N Relaxation data and model free order parameters for the CaM-iNOS complex at 225nM Ca^{2+} and saturating Ca^{2+} conditions.

Plots as a function of residue number of the measured T1 and T2 values, the ^{1}H-^{15}N NOE, τ_i, internal correlation times, and the order parameter, S^2, with associated uncertainty are shown. Only residues for which the ^{15}N-^{1}H cross peaks were sufficiently well resolved to permit accurate measurement of its intensity are included.

Table 4.3: Average S^2 order parameter for each structure element of the CaM-iNOS complex.

	S^2														
	A	EF1	B	Loop	C	EF2	D	Link	E	EF3	F	Loop	G	EF4	H
CaM-iNOS 225nM Ca^{2+a}	0.88 ± 0.08	0.84 ± 0.13	0.89 ± 0.08	0.72 ± 0.20	0.89 ± 0.04	0.80 ± 0.11	0.87 ± 0.06	0.68 ± 0.09	0.89 ± 0.07	0.87 ± 0.10	0.89 ± 0.11	0.77 ± 0.09	0.93 ± 0.05	0.79 ± 0.12	0.81 ± 0.14
CaM-iNOS sat Ca^{2+b}	0.83 ± 0.07	0.84 ± 0.08	0.90 ± 0.09	0.75 ± 0.16	0.85 ± 0.07	0.79 ± 0.11	0.87 ± 0.09	0.66 ± 0.20	0.85 ± 0.08	0.87 ± 0.08	0.87 ± 0.10	0.67 ± 0.14	0.84 ± 0.04	0.81 ± 0.14	0.88 ± 0.08

[a]Residues comprising each segment: A 6-14, 16-19; EF1 20-29; B 31-37,39; Loop 40-42, 44; C 45-52, 54-55; EF2 56, 58-64; D 65, 67-72, 75; Link 77-78, 80; E 82-86, 88-92; EF3 93-100; F 101-106, 108-109; Loop 112-118; G 119-125; EF4 127-138; H 139-142, 144.
[b]Residues comprising each segment: A 6-13, 15-19; EF1 20-22, 24-29; B 30-39; Loop 40-42, 44; C 45-55; EF2 56, 58-64; D 65, 67-68, 70-75; Link 76-80; E 81-84, 86, 88-92; EF3 93-95, 97-100; F 101-102, 104-106, 108-111; Loop 112-113, 115-118; G 119, 121-126; EF4 127-138; H 139, 141-143.

When the internal dynamics were analyzed for the CaM-iNOS complex at 225 nM [Ca^{2+}], the same high degree of mobility observed for the linker region and for the loop regions between the EF hands at saturating [Ca^{2+}] is shown (Figures 4.10). The average order parameter values for each structural element of the complex are quite similar at 225 nM and saturating [Ca^{2+}] (Table 4.3), however, the CaM-iNOS complex at 225 nM [Ca^{2+}] displays greater fluctuation in its S^2 values, and also contains a greater number of residues that show an increased τ_i. The observed increase in τ_i for the EF hands and loop regions of CaM indicates that the residues in these regions exhibit faster internal motions at 225 nM [Ca^{2+}] (Figure 4.9). Also Helix H of the CaM-iNOS complex at 225 nM [Ca^{2+}] is found to have an increased internal mobility (lower S^2 values) compared to CaM-iNOS at saturated [Ca^{2+}]. This data indicates that the CaM-iNOS complex has increased internal mobility at lower [Ca^{2+}], with a more dynamic C-lobe than N-lobe, which correlates well with the H/D exchange data.

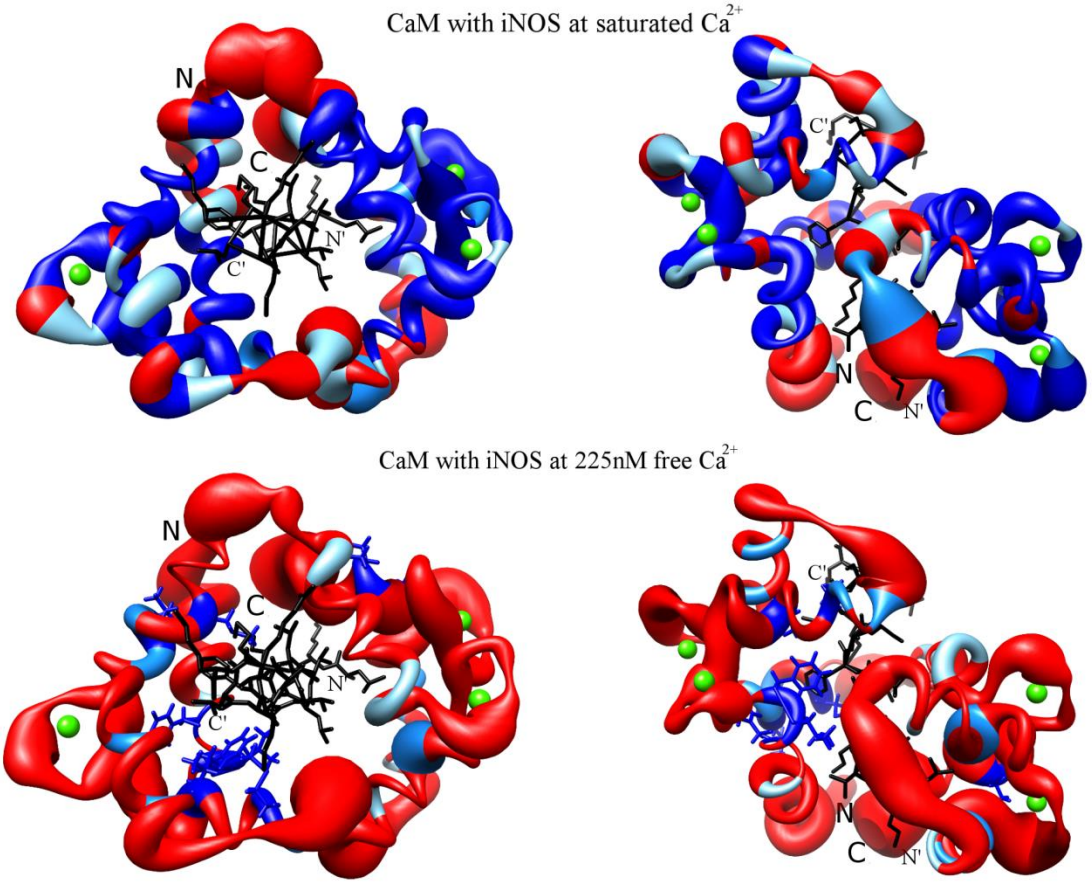

Figure 4.10: Worm models of CaM-iNOS peptide complexes at 225 nM [Ca^{2+}] and saturated [Ca^{2+}] illustrating their internal dynamics and amide H_2O/D_2O exchange data.

The worm models were prepared using UCSF Chimera with the render by attribute function. The worm radius ranges from 0.25, corresponding to a S^2 value of 1, to 4, corresponding to a S^2 value of 0.4. The color of the residue represents its amide H_2O/D_2O exchange data. Residues that display fast D_2O exchange rates are colored red on the ribbon structure. Residues that display intermediate D_2O exchange rates are colored light blue on the ribbon structure. Residues that display slow D_2O exchange rates are colored blue on the ribbon structure with their side chain atoms shown. Worm models and amide H_2O/D_2O exchange data for CaM-iNOS complex at 10mM $CaCl_2$ projected onto previously determined structure of Ca^{2+}-replete CaM-iNOS (PDB 2LL6). Worm models and amide H_2O/D_2O exchange data for CaM-iNOS complex at 225nM free [Ca^{2+}] projected onto previously determined structure of Ca^{2+}-replete CaM-iNOS (PDB 2LL6).

4.4 Discussion

CaM is able to fine-tune the orientation of its domain and residue contacts to accommodate its binding to a variety of target proteins. Mammalian NOS enzymes provide an ideal system for investigating the differences in Ca^{2+} dependent activation of target enzymes. The structures of CaM interacting with target peptides derived from the three enzymes have all been shown to be very similar and to consist of two EF hand pairs lined by a short connector wrapped around a helical peptide target. However, the three NOS enzymes show different Ca^{2+} dependent activation by CaM. The iNOS enzyme is fully active at basal levels of Ca^{2+} (<100 nM) in a cell, eNOS enzymes require 200-300 nM concentrations of free Ca^{2+} to achieve half maximal activity (Sessas et al., 1992; Ruan et al., 1996). Most investigations have focused on the Ca^{2+} dependent activation of NOS enzymes by CaM under non-physiological conditions. Experiments are generally performed in the presence of excess Ca^{2+} or excess Ca^{2+} chelator. In the present study, more physiological relevant free Ca^{2+} conditions were used to investigate the differential CaM Ca^{2+}-dependent binding and activation of iNOS end eNOS enzymes. The dynamics of the binding were monitored using NMR H/D exchange and ^{15}N relaxation experiments under different physiologically relevant free Ca^{2+} concentrations to provide a better understanding of the process. In addition, this approach identified the roles played by the N and C lobes of CaM in the binding and activation of the NOS enzymes. This is important since the binding of Ca^{2+} to CaM is cooperative within each lobe of CaM but not between the lobes, meaning that Ca^{2+}-binding to N- and C-domains is exclusive from one another (Linse et al., 1991; Pedigo and Shea, 1995). On its own, the C-lobe of CaM binds Ca^{2+} with a higher affinity ($K_d = 10^{-6}M$) than the N-lobe ($K_d = 10^{-5}M$).

The Ca^{2+} titration fluorescence experiments provide information about the conformational transitions of CaM during the binding of peptides and Ca^{2+}. In the absence of peptides CaM undergoes a conformational transition from apo to Ca^{2+} bound at Ca^{2+} concentrations above 650 nM. When iNOS peptide is added to the dansyl-CaM a fluorescence maximum is seen at 490nm and no transition is observed during the Ca^{2+} titration, indicating CaM is bound to the iNOS peptide in both the absence and presence of Ca^{2+}. In contrast, the eNOS peptide is not bound to CaM in the absence of Ca^{2+} but binds to CaM when the Ca^{2+} concentration is at least 225 nM, consistent with the results reported for holo eNOS enzymes (Sessas et al., 1992; Ruan et al., 1996).

4.4.1 At Low Ca^{2+} Concentrations CaM's N-Lobe Dissociates From the eNOS Peptide.

At resting intracellular Ca^{2+} concentrations CaM is unable to bind to the eNOS CaM binding domain peptide, whereas it can bind at an elevated free Ca^{2+} concentration of 225 nM. At 225 nM free [Ca^{2+}] NMR data shows the CaM-eNOS complex displays a structure where the C-lobe is bound to the peptide, but the N-lobe is not. In a previous investigation, we used gel mobility shift assays to monitor the binding of the eNOS peptide to different truncated half CaM constructs under Ca^{2+} replete conditions (Spratt et al., 2006). No binding was observed between eNOS and nCaM, and weak binding occurred between the peptide and cCaM. These half CaMs also produced little or no activity of the eNOS enzyme. Our present results showing a closer association between the C-lobe of CaM and the eNOS peptide are consistent with our previous binding studies.

4.4.2 CaM-iNOS Complex Has Similar Conformations at Physiological and Saturating Ca^{2+} Levels.

Most studies analyzing this Ca^{2+}-independent nature of CaM and iNOS use apoCaM, however the cellular environment is not fully deplete of Ca^{2+}, with the basal intracellular Ca^{2+} concentration being on the order of 50-100 nM (Carafoli, 1987; Islam, 2012). In order to characterize the complex under these physiological conditions ^{1}H-^{15}N HSQC experiments of the CaM-iNOS complex were performed at various free Ca^{2+} concentrations ranging from resting intracellular Ca^{2+} levels to elevated Ca^{2+} levels and compared to fully saturated Ca^{2+}-CaM conditions. The current study suggests that CaM has the same structure as observed in Ca^{2+}-replete CaM-iNOS when bound to the iNOS peptide at both resting and elevated intracellular Ca^{2+} levels.

Activity of the iNOS enzyme decreased to less than 25% when co-expressed with a mutant CaM_{1234} used to emulate apoCaM (Spratt et al., 2007a). In a study by Ruan et al (1996), iNOS was found to be maximally active at Ca^{2+} concentrations as low as 0.1 nM in vitro and thus is probably maximally active in vivo at basal intracellular Ca^{2+} levels. This suggests that at the lowest Ca^{2+} level (17 nM) used in this study the CaM-iNOS complex is Ca^{2+} replete, otherwise a decrease in iNOS activity at Ca^{2+} concentrations as low as 0.1 nM would have been seen.

4.4.3 CaM-eNOS and CaM-iNOS Complexes Show Different Dynamic Interactions at Low and Saturating Ca^{2+} Concentrations.

The dynamic properties of these complexes were further investigated by performing amide H/D exchange time-course experiments and NMR ^{15}N relaxation experiments. NH exchange experiments provide detailed information on the degree of protection of specific residues within a protein or protein complex. This information is useful for determining the stability of secondary structural

elements and also identifying residues involved in co-operative binding of a ligand (Williams et al., 2004; Pervushin et al., 2007). The NMR ^{15}N relaxation experiments can be interpreted by the model-free approach to characterize backbone mobility using an order parameter S^2, which may be interpreted as the amplitude of the motion, and a correlation time, τ_i, which is the characteristic time constant of this motion.

At the 225 nM free Ca^{2+} concentration CaM alone does not bind Ca^{2+}, however, the presence of the eNOS peptide enhances the Ca^{2+} affinity of the C-lobe of CaM. The fast exchange of the C-lobe amides corresponding to the residues involved in coordinating the Ca^{2+} ions indicates that this isn't a very stable or strong interaction at the 225 nM free Ca^{2+} concentration, when compared to the strong association at saturating [Ca^{2+}]. The few residues of the N-lobe that exhibit intermediate exchange at low [Ca^{2+}] suggest that even though this lobe is likely Ca^{2+} deplete and not bound to the peptide, based on chemical shift comparison, it still maintains its structural integrity and remains folded. This data correlates well with our previous investigation that showed only full length CaM, and not the half CaMs, is able to fully activate eNOS (Spratt et al., 2006). The internal dynamics for the CaM-eNOS complex at 225 nM [Ca^{2+}] and saturating [Ca^{2+}] also agrees with our H/D exchange data. The lower order parameters observed for the linker region and loop regions between the EF hand pairs at low and saturating [Ca^{2+}] along with the fast exchange observed from the H/D exchange data show these regions have increased internal mobility and less stability. The increased mobility, shown by the lower S^2 and increased τ_i, for the N-lobe of CaM indicates a more dynamic and less rigid structure, which correlates well with the H/D exchange data. The H/D exchange and internal mobility results show that the residues of CaM interacting with eNOS' 1-5-8-14 anchoring residues have a strong interaction at low Ca^{2+} concentrations, which keeps the complex bound, while the rest of the residues of the CaM protein are able to fluctuate or "breathe". More specifically, the residues of

the C-lobe have a lower degree of internal mobility (higher S^2) and higher exchange protection, indicating stronger interaction with the eNOS peptide to hold the complex together, while the N-lobe is more dynamic. At saturating Ca^{2+} concentrations the entire CaM-eNOS complex has become more rigid, or structurally stable, than it is at physiological Ca^{2+} levels.

In contrast, for the CaM-iNOS peptide complex at the 225 nM free Ca^{2+} concentration, the C-lobe shows faster exchange rates than the N-lobe of CaM. This supports our earlier studies using peptides bound to mutant half-CaM proteins indicating that the N-lobe of CaM may not fully dissociated from the iNOS peptide even at very low Ca^{2+} concentrations (Spratt et al., 2006). Notably when compared to Ca^{2+}-replete CaM co-expression, iNOS showed significant 70% activity when co-expressed with only nCaM and only 12% activity when co-expressed with cCaM. These results show that the N-terminal domain of CaM contains important binding and activating elements for iNOS (Spratt et al., 2006, 2011). The internal dynamics for the CaM-iNOS complex also agrees with our H/D exchange data. As seen with the CaM-eNOS complex, the fast amide exchange and faster internal motions observed for the EF hands and loop regions of CaM at the 225 nM [Ca^{2+}] indicates that the co-ordination of Ca^{2+} by these residues isn't a very strong interaction when compared to saturating [Ca^{2+}]. The H/D exchange and internal mobility results show that the residues of CaM interacting with iNOS' 1-5-8-14 anchoring residues have a strong interaction at low [Ca^{2+}], while the rest of the residues of CaM display more dynamics and have less exchange protection. More specifically residues of CaM's N-lobe have a lower degree of internal mobility and higher exchange protection, indicating stronger interaction with the iNOS peptide, compared to the C-lobe. Taken together, this data indicates that the CaM-iNOS complex has increased internal mobility at lower [Ca^{2+}], with a more dynamic C-lobe than N-lobe.

4.4.4 At Low Ca^{2+} Concentrations CaM Has a Different Interaction With the eNOS and iNOS Peptides.

Our H/D exchange and internal dynamics data show the CaM-iNOS and CaM-eNOS complexes exhibit similar dynamic differences between 225 nM and saturated [Ca^{2+}], however, the interaction with the peptide is different with respect to the individual CaM lobes at low [Ca^{2+}]. This is clearly shown by the lower degree of internal mobility (higher S^2 and less residues with τ_i values) and higher exchange protection of the residues of the N-lobe of CaM in the CaM-iNOS complex compared to those of the CaM-eNOS complex, while the residues of the C-lobe of CaM in the CaM-eNOS complex display lower internal mobility (higher S^2 and less residues with τ_i values) and higher exchange protection. Our results provide further evidence of stronger interactions of the N-lobe of CaM with the iNOS peptide compared to the eNOS peptide, contributing to the stronger binding of CaM with iNOS, as seen in previous studies (Venema et al., 1996; Xia et al., 2009; Piazza et al., 2012).

4.5 Conclusions

This is the first study to present NMR structural and dynamics data of the CaM-NOS complexes at free Ca^{2+} concentrations that are in the resting and elevated intracellular Ca^{2+} concentration range. These results demonstrate the importance of performing experiments on CaM-NOS interactions at Ca^{2+} concentrations that correspond to Ca^{2+} levels relevant to the regulation of NOS by CaM *in vivo*. We show that when experiments are performed at Ca^{2+} concentrations that are typically used in the literature, i.e. saturating [Ca^{2+}], the CaM-NOS systems are less dynamic than at Ca^{2+} concentrations corresponding to basal and elevated cellular levels. The studies of the CaM-NOS complexes that were carried out at saturated Ca^{2+} concentrations miss differences in dynamics that are

only detectable at physiological Ca^{2+} levels. Thus, studies involving CaM interactions with NOS at saturating Ca^{2+} concentrations don't allow the investigator to see the contributions of the dynamics present in the CaM-NOS complexes. The structures at saturating Ca^{2+} concentrations don't tell the whole story, one needs to look at the dynamics at the same time to obtain a complete picture of the molecular basis of NOS regulation by CaM. This illustrates the importance of analyzing these complexes at Ca^{2+} concentrations that are within the physiological range in order to fully understand how NOS is regulated by CaM interactions *in vivo*.

Chapter 5

Structure of calmodulin bound to the endothelial nitric oxide synthase calmodulin binding domain peptide at physiological calcium concentration*

5.1 Introduction

CaM consists of two globular domains connected by a flexible central linker region with each globular domain containing two EF hand pairs capable of binding to Ca^{2+}. Upon binding of Ca^{2+} to the EF hands, CaM undergoes a conformational change that exposes hydrophobic patches on each domain that allow CaM to associate with its intracellular target proteins. The binding of Ca^{2+} to CaM is cooperative within each lobe of CaM but not between the lobes, with the C-lobe of CaM able to bind Ca^{2+} with a ten-fold higher affinity than the N-lobe.(Linse et al., 1991; Pedigo and Shea, 1995)

One of CaM's target enzymes is the NOS enzymes, which catalyze the production of nitric oxide (•NO) (Alderton et al., 2001). There are three NOS isoforms in mammals: neuronal NOS (nNOS), endothelial NOS (eNOS), and inducible NOS (iNOS). All are all dimers, with each monomer containing an N-terminal oxygenase domain and a C-terminal reductase domain, connected by a CaM binding domain. The CaM binding domains of NOS contain the classical 1-5-8-14 CaM-binding motif. CaM is found to bind to this binding domain in an antiparallel fashion, with the N-lobe

* *Unless otherwise stated, all of the work reported in this chapter was performed and analyzed by the candidate.*

of CaM binding closer to the C-terminus of this domain, and the C-lobe of CaM binds closer to the N-terminus (Spratt et al., 2007b). CaM's interaction with eNOS and nNOS is Ca^{2+}- dependent, requiring 200-300 nM concentrations of free Ca^{2+} to achieve half maximal activity (Sessas et al., 1992; Ruan et al., 1996), whereas CaM binds to iNOS regardless of intracellular Ca^{2+} concentration and is fully active at basal levels of Ca^{2+} (<100 nM) in the cell (Carafoli, 1987; Busse and Mulsch, 1990; Balligand et al., 1994; Islam, 2012). The oxygenase domain contains binding sites for heme, tetrahydrobiopterin (H_4B), and the substrate L-arginine. The reductase domain contains binding sites for the cofactors FMN, FAD, and NADPH (Alderton et al., 2001; Daff, 2010). Electron flow in the NOS enzymes occurs from the NADPH, through the FAD and FMN cofactors, to the heme oxygenase domain. Recent studies suggest that the NOS enzymes exist in an equilibrium of conformations that alternate between FAD-FMN electron transfer and FMN–heme electron transfer and that CaM binding induces a shift in the conformational equilibrium to allow efficient electron transfer in NOS enzymes (Leferink et al., 2014; Sobolewska-Stawiarz et al., 2014). When CaM is fully bound to NOS, residues of CaM's N-lobe interact with the FMN subdomain of NOS and form a bridge (Tejero et al., 2010). This bridge interaction appears necessary to control the interaction between the FMN and heme, which is what enables CaM to activate NOS.

CaM's interactions with the various NOS isoforms has previously been studied by NMR (Zhang and Vogel, 1994; Zhang et al., 1995b; Matsubara et al., 1997; Piazza et al., 2012, 2014). However, most structural and dynamics studies on CaM-NOS interactions have been performed at non-physiological conditions using either apo (Ca^{2+} free with excess chelators, such as EDTA, present) or Ca^{2+} saturated (greater than 1mM Ca^{2+}) conditions which don't represent the true intracellular Ca^{2+} concentration. In the previous chapter, we determined the minimal free Ca^{2+} concentration needed for CaM to interact with eNOS to be 225 nM (Piazza et al., 2015). Here we

determined the NMR structure of the CaM-eNOS complex at a free Ca^{2+} concentration that represents this elevated intracellular Ca^{2+} concentration of 225 nM, and compared it to the less physiologically relevant high Ca^{2+} concentrations used in previous CaM-eNOS structure calculations. Our study is the first study to determine a solution structure of the CaM-eNOS complex at a free Ca^{2+} concentration that is in the elevated intracellular Ca^{2+} concentration range. In addition, this study identifies the roles played by each individual lobe of CaM in the binding to the eNOS enzyme.

5.2 Methods and experiments

5.2.1 Sample preparation for NMR investigation.

CaM for NMR experiments was expressed in E. coli in 1 L of M9 media (11.03 g/L $Na_2HPO_4 \cdot 7H_2O$, 3.0 g/L KH_2PO_4, 0.5 g/L NaCl, 2 mM $MgSO_4$, 0.1 mM $CaCl_2$, 3 μM $(NH_4)_6(MO_7)_{24}$, 400 μM H_3BO_3, 30 μM $CoCl_2$, 10 μM $CuSO_4$, 80 μM $MnCl_2 \cdot 4H_2O$, 10 μM $ZnCl_2$, 10 mM $FeSO_4$, 100 μg/mL kanamycin) containing 2 g/L ^{13}C-glucose and 1 g/L $^{15}NH_4Cl$. ^{13}C-^{15}N CaM was purified as described in section 2.2.2. Isolation of the CaM protein (148 residues) was confirmed by ESI-MS and purity was judged to be > 95% by SDS-PAGE. The human eNOS (TRKKTFKEVANAVKISASLMGT, 22 residues corresponding to residues 491-512 from the full length eNOS protein) peptide was synthesized and purchased from Sigma.

The 225 nM free [Ca^{2+}] ^{13}C-^{15}N-CaM sample was prepared via a buffer exchange into 30 mM MOPS, 100 mM KCl, 90% H_2O/10% ^2H_2O, pH 7.2, and combination of 10 mM EGTA and 10mM CaEGTA to obtain a final 225 nM concentration of free Ca^{2+} using a YM10 centrifugal filter device (Millipore Corp., Billerica, USA). The sample had a final ^{13}C-^{15}N-CaM concentration of 1 mM in a total volume of 500 μL. The sample was transferred into 5 mm NMR sample tubes and stored at 4^{o}C

until required for NMR experiments. NMR experiments on the complex were conducted on samples titrated with eNOS peptide to saturation in a 1:1 CaM:peptide ratio. Complex formation was monitored after each addition by acquisition of a ^{1}H-^{15}N heteronuclear single-quantum coherence (HSQC) spectrum.

5.2.2 NMR spectroscopy and data analysis.

NMR spectra were recorded at 25^{o}C on Bruker 600 MHz DRX spectrometers equipped with XYZ-gradients triple-resonance HCN probe (Bruker, Billerica, MA, USA). Spectra were analyzed using the program CARA (Keller, 2005). The amide resonances assignments were aided by using the previously obtained amide chemical shifts of Ca^{2+} saturated CaM with eNOS peptide as reference (Piazza et al., 2012). Specific assignments of the backbone resonances were achieved using a combination of three-dimensional triple- resonance experiments, including HNCA, HN(CO)CA, CBCA(CO)NH, and HNCO (Grzesiek and Bax, 1992a, 1992b; Muhandiram and Kay, 1994). Side chain resonances were assigned using the TOCSY-type HC(C)H-TOCSY and (H)CCH- TOCSY experiments (Ikura et al., 1990). Specific assignments of the eNOS peptide were obtained from ^{15}N-double-filtered NOESY experiments (Ikura and Bax, 1992).

5.2.3 Structure calculation of CaM-eNOS peptide at 225 nM [Ca^{2+}].

The ^{1}H, ^{13}C, and ^{15}N resonance assignments were utilized to identify constraints for the structure calculations. Distance constraints for the CaM-eNOS complex were obtained from ^{15}N NOESY-HSQC and ^{13}C NOESY- HSQC, and ^{15}N- double-filtered NOESY spectra acquired on samples containing ^{13}C-^{15}N-CaM and unlabeled peptide (Fesik and Zuiderweg, 1990; Clore and Gronenborn, 1991; Ikura and Bax, 1992). In addition, dihedral angle restraints were derived from chemical shift

analysis with TALOS+. The structure calculation of CaM-eNOS peptide at 225 nM [Ca^{2+}] was performed using CNSsolve version 1.2 (Brunger et al., 1998). The calculation was initiated with an extended conformation file and run through several iterations of a standard simulated annealing protocol to minimize the energies. The final 20 lowest energy structures were selected.

5.2.4 Accession Numbers.

The coordinates and NMR parameters have been deposited in the Protein Data Bank (PDB) and the BioMagResBank (BMRB) and have been assigned PDB entry 2N8J, and BMRB accession number 25852.

5.3 Results and discussion

5.3.1 NMR structure at physiological Ca^{2+} concentrations.

NMR experiments were performed at physiological free Ca^{2+} concentrations to provide further insights into the structural differences of the CaM-eNOS complex at a more relevant Ca^{2+} concentration compared to the less physiological relevant high Ca^{2+} concentrations used in all other CaM-NOS structure calculations. The three-dimensional solution structure of CaM bound to the human eNOS CaM binding domain peptide (CaM−eNOS complex) at 225 nM free Ca^{2+} was determined using multidimensional heteronuclear NMR spectroscopy. The NMR assignment of the CaM-eNOS complex followed a similar procedure as that in sections 1.3.1 and 2.3.2. The NMR analysis of CaM with the eNOS peptide at 225 nM free Ca^{2+} followed routine procedures with the backbone resonance assignment based primarily on 3D triple resonance techniques, using the previously assigned chemical shifts of CaM with wild type eNOS peptide at saturated Ca^{2+} as a starting point. The HNCA experiment was supported by CBCA(CO)NH and HN(CO)CA

experiments. This combination of techniques resulted in complete backbone assignments for CaM, with the exception of the prolines and the first two N-terminal amino acids (Appendix H). Subsequently, sidechain resonances for CaM were assigned using HC(C)H-TOCSY, (H)CCH-TOCSY and H(CCO)NH experiments and for the eNOS peptide using the ^{15}N-double-filtered NOESY experiment. NOEs for structure determination of the eNOS peptide bound to CaM were extracted from ^{15}N-edited NOESY, $^{13}C_{ali}$-NOESY and ^{15}N-double-filtered NOESY experiments. The three dimensional solution structure of CaM bound to the human eNOS CaM binding domain peptide (CaM-eNOS) at 225 nM free Ca^{2+} was determined using the CNSsolve software program. The structure of the complex is based on a large number of experimental constraints and is well-defined. The root-mean-square distance (r.m.s.d.) for ordered residues is 1.9 Å for the backbone atoms and 2.2 Å for all non-hydrogen atoms (Table 5.1).

Table 5.1: Statistics for the structural ensemble of CaM-eNOS peptide at 225 nM Ca^{2+}.

		CaM-eNOS Complex		
NMR-derived distance and dihedral angle restraints				
	Calmodulin	eNOS peptide		CaM-eNOS complex
NOE constraints	2836	86		37
Dihedral angles from TALOS+	280	14		N/A
Total number of restraints		3253		
Structure statistics for the 20 lowest energy structures				
Mean deviation from ideal covalent geometry				
Bond lengths (Å)		0.010		
Bond angles (deg.)		1.2		
Average pairwise RMSD (Å) for all heavy atoms of the 20 lowest energy structures	All Residues	Ordered Residues[a]	C-lobe[b]	N-lobe[c]
Backbone Atoms	2.3	1.9	0.6	0.9
Heavy Atoms	2.6	2.2	1.1	1.4
Ramachandran statistics (%)				
Residues in most favored region		86.3		
Residues in additional allowed regions		13.2		
Residues in generously allowed region		0.4		
Residues in disallowed region		0.0		

[a] Ordered residue ranges: 4A-78A, 81A-134A, 137A-147A, 154B-161B
[b] C-lobe residues: 81A-148A
[c] N-lobe residues: 4A-74A

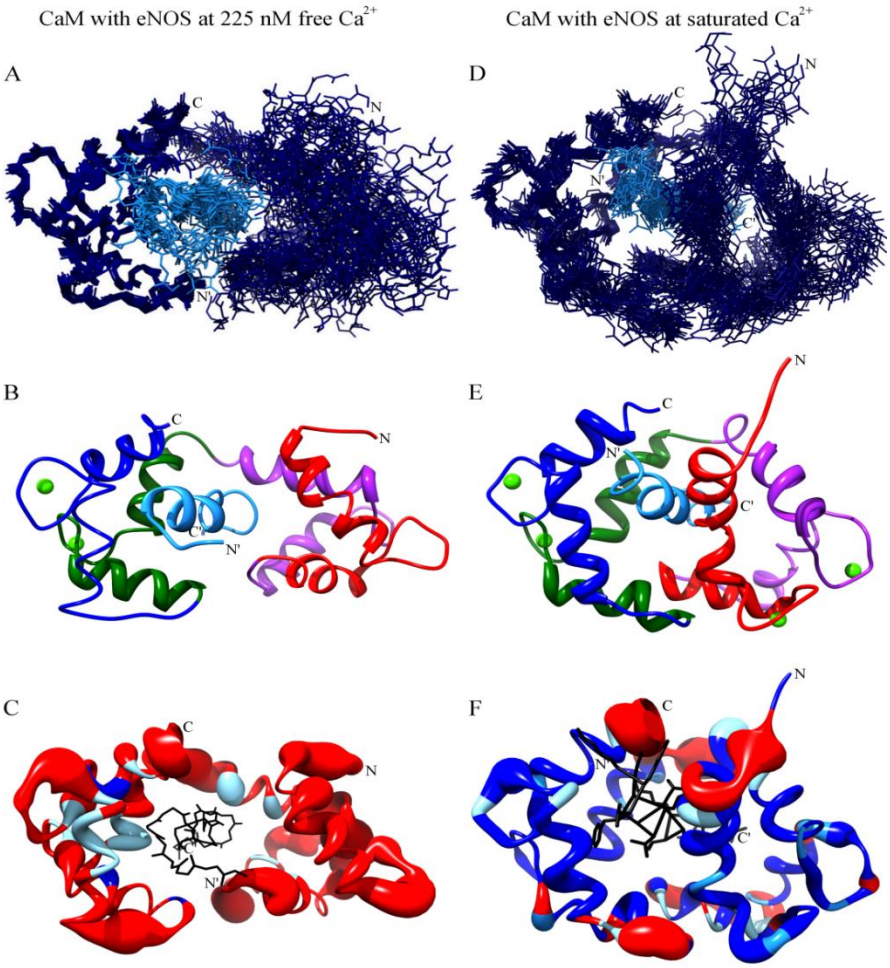

Figure 5.1: Solution structure of CaM-eNOS at 225 nM Ca^{2+}.

Superposition of the ensemble of the 20 lowest-energy calculated NMR solution structures of (A) CaM bound to eNOS peptide at 225 nM Ca^{2+} and (D) the previously determined solution structures of CaM bound to eNOS peptide at saturated Ca^{2+}. The superposition is aligned by the backbone atoms of the C-lobe of CaM. Backbone atom traces of CaM are colored dark blue, and the eNOS peptide colored light blue. Cartoon ribbon view of the average solution structure of the CaM− eNOS complex at (B) 225 nM Ca^{2+} and (E) saturated Ca^{2+}. Residues 1−40 of CaM (EF hand I) are colored red, residues 41−79 (EF hand II) purple, residues 80−114 (EF hand III) green, and residues 115−148 (EF hand IV) blue. The peptide is colored lighter blue. Calcium ions are colored green. Worm models of CaM-eNOS peptide complex at (C) 225 nM Ca^{2+} and (F) saturated Ca^{2+} illustrating their internal dynamics and amide H/D exchange data. The worm models were prepared using UCSF Chimera with the render by attribute function. The worm radius ranges from 0.25 (S^2 value of 1), to 4 (S^2 value of 0.4). Residues that display fast D_2O exchange rates are colored red on the ribbon structure. Residues that display intermediate D_2O exchange rates are colored light blue and residues that display slow D_2O exchange rates are colored blue. The bound peptide is colored black and shown in wire form.

The family of 20 lowest energy structures is shown in Figure 5.1A. When these 20 lowest energy structures are aligned by the C-lobe backbone atoms of CaM, the C-lobes of CaM are shown to superimpose quite well with each other, whereas the N-lobe has a lot of fluctuation in its relative position to the C-lobe, suggesting the N-lobe is less rigid, and more dynamic, than the C-lobe. When a similar comparison is made with the superposition of the backbone of the 20 lowest energy structures for the previously determined Ca^{2+} saturated CaM-eNOS complex (PDB 2LL7, figure 5.1D) superposition via both the C- and N-lobes results in well overlaid structures. This more dynamic N-lobe of CaM in the CaM-eNOS complex structure at 225 nM free Ca^{2+} can also be shown by looking at the r.m.s.d. values for each individual lobe of CaM. The r.m.s.d. for the C-lobe residues is 0.6 Å for the backbone atoms and 1.1 Å for all non-hydrogen atoms, whereas it is 0.9 Å for the backbone atoms and 1.4 Å for all non-hydrogen atoms of the N-lobe.

The CaM-eNOS complex at a physiologically relevant free Ca^{2+} concentration of 225 nM has a Ca^{2+}-replete C-lobe bound to the eNOS peptide and a Ca^{2+} free N-lobe loosely associated to the eNOS peptide as shown in figure 5.1B. Residues 1−4 (corresponding to residues 491−494 of eNOS) at the N-terminus of the eNOS CaM-binding region peptide show a lack of structure because they could not be unambiguously assigned. Comparing to the Ca^{2+} saturated CaM-eNOS complex structure (Figure 5.1E) one can see that the N-lobe at 225 nM free Ca^{2+} has a much looser association to the eNOS peptide.

The dynamic properties of these complexes were previously examined in chapter 4 by amide H/D exchange time-course and NMR ^{15}N relaxation experiments and agree very well with the determined solution structure in this study (Piazza et al., 2015). Amide exchange experiments provide detailed information on the degree of protection of specific residues within a protein complex and are useful for identifying residues involved in co-operative binding of a ligand (Williams et al., 2004;

Pervushin et al., 2007). The NMR ^{15}N relaxation T_1, T_2, and ^{1}H-^{15}N NOE experiments were used to characterize backbone mobility by determining an order parameter, S^2, which may be interpreted to describe internal dynamics on a residue specific level (Lipari and Szabo, 1982b; Kay, 1998; Ishima and Torchia, 2000; Wand, 2001). There are a few residues of the N-lobe that exhibit intermediate exchange, such as M36, M51, M72 and K75. These residues are all found to be part of α-helices and have hydrophobic interactions with L509, one of the anchoring residues of eNOS, in the solution structure of the complex (Figure 5.1C and 5.3C). The amides of the C-lobe residues that show intermediate or slow exchange correspond to CaM residues that also interact with the 1-5-8-14 anchoring residues of the eNOS peptide in the solution structure (Figure 5.3B). The ^{15}N relaxation data also correlates very well with the solution structure of the CaM-eNOS complex at 225 nM Ca^{2+}. The lower overall dynamics of the C-lobe of CaM compared to the N-lobe correspond well with the more rigid C-lobe (and lower r.m.s.d. for the C-lobe) observed in the structure. Whereas the N-lobe of CaM displays increased backbone mobility, indicating increased dynamics, which correlates well with the less rigid N-lobe observed by the increased fluctuations in its overall position relative to the C-lobe (Figure 5.1A) and the N-lobe's higher calculated r.m.s.d. value.

5.3.2 Structure comparison.

When the 225 nM free Ca^{2+} CaM-eNOS complex structure is compared to the previously determined Ca^{2+} saturated CaM−eNOS complex structure (PDB entry 2LL7), one can see that the C-lobes of CaM and peptide orientation are quite similar, however the N-lobe of CaM is structurally different (Figure 5.2A,B). When the two structures are aligned with respect to CaM's C-lobe backbone atoms a r.m.s.d. value of 1.023 Å for the backbone atoms of CaM was found. The C-lobes of CaM and the

eNOS peptide of each structure superimpose quite well on each other, whereas the N-lobes of CaM do not.

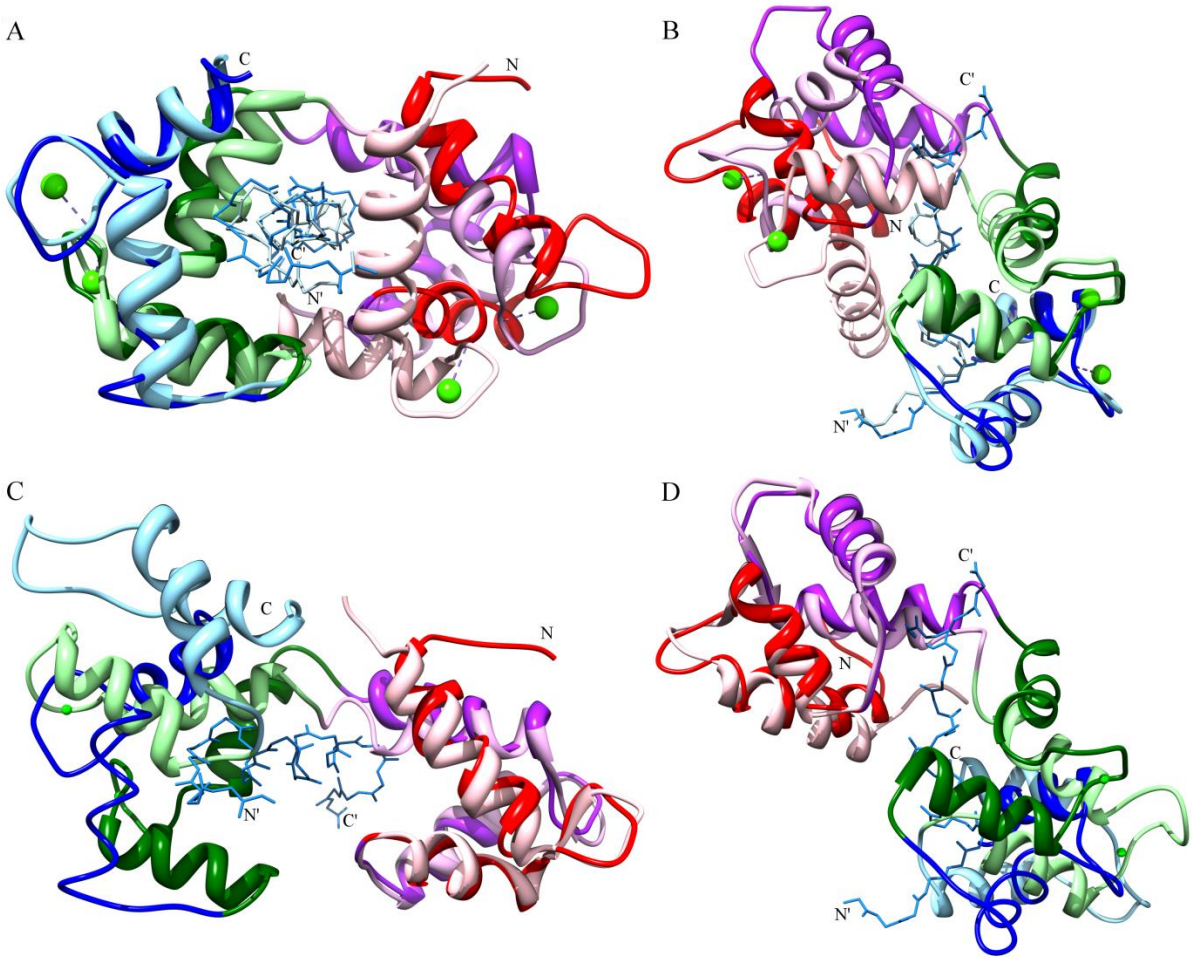

Figure 5.2: Comparison of the solution structure of the CaM-eNOS peptide complex at 225 nM Ca^{2+} with the solution structures of saturated Ca^{2+} CaM-eNOS peptide complex and apoCaM.

The solution structures of the CaM−eNOS peptide at 225 nM Ca^{2+} (dark colors) and at saturated Ca^{2+} (light colors) are aligned by superimposition of the backbone atoms of the C-lobes of CaM (A) viewed along the bound peptide from its N-terminus (N′) to its C-terminus (C′) and (B) rotated around the horizontal axis with the C-terminus of the bound peptide on the top. The solution structures of the CaM−eNOS peptide at 225 nM Ca^{2+} (dark colors) and apoCaM (light colors) are aligned by superimposition of the backbone atoms of the N-lobes of CaM (C) viewed along the bound peptide from its N-terminus (N′) to its C-terminus (C′) and (D) rotated around the horizontal axis with the C-terminus of the bound peptide on the top. The color scheme is the same as that in Figure 5.1.

When the 225 nM free Ca^{2+} CaM-eNOS complex structure is compared to the previously determined apoCaM structure (PDB entry 1CFC), there is structural similarity of the N-lobes of CaM, whereas the C-lobes of CaM show differences (Figure 5.2C,D). When the two structures are aligned with respect to CaM's N-lobe backbone atoms a r.m.s.d. value of 1.042 Å for the backbone atoms of CaM was found. The N-lobes of CaM of each structure superimpose well on each other, whereas the C-lobes of CaM do not.

5.3.3 At low Ca^{2+} concentrations CaM's N-lobe is loosely associated to the eNOS peptide.

At resting intracellular Ca^{2+} concentrations CaM is unable to bind to the eNOS CaM binding domain peptide, whereas it can bind at an elevated free Ca^{2+} concentration of 225 nM. At the 225 nM free Ca^{2+} concentration CaM alone does not bind Ca^{2+} (previously shown by dansyl-CaM fluorescence studies in section 4.3.1), however, the presence of the eNOS peptide enhances the Ca^{2+} affinity of the C-lobe of CaM. At this free Ca^{2+} concentration the CaM-eNOS complex displays a structure with a Ca^{2+}-replete C-lobe bound to the peptide, and a Ca^{2+}-deplete N-lobe that is loosely associated to the peptide via hydrophobic interactions of a few CaM residues to the anchoring residue L509 of eNOS (Figure 5.3A,C). The solution structure shows L509 situated in a hydrophobic pocket of CaM composed of M36, M51, and M72. This interaction is strong enough to allow CaM to bind to eNOS even though this lobe is Ca^{2+}-deplete.

The structure of the CaM-eNOS complex at 225 nM Ca^{2+} shows that the C-lobe of CaM is completely bound to the eNOS peptide in a similar fashion as the holoCaM-eNOS complex. Residues V91, F92, L105, L112, F141 and M144 of the C-lobe of CaM interact via hydrophobic interactions with the anchoring residues F496, A500 and V503 of the eNOS peptide (Figure 5.3A, B). This forms

a tight complex between the eNOS peptide and CaM which allows this region of the eNOS peptide to adopt an α-helical secondary structure. The C-terminus of the eNOS peptide displays a less α-helical secondary structured region due to having a weaker interaction with CaM, which is evidenced by the solution structure and the lower amount of NOE contacts observed in the eNOS peptide NOESY spectrum. This agrees very well with previous studies that show the NOS peptides have no secondary structure when not bound to CaM (Matsubara et al., 1997; Spratt et al., 2007a); and this lack of α-helical secondary structure further supports a looser association of the N-lobe of CaM to the eNOS peptide.

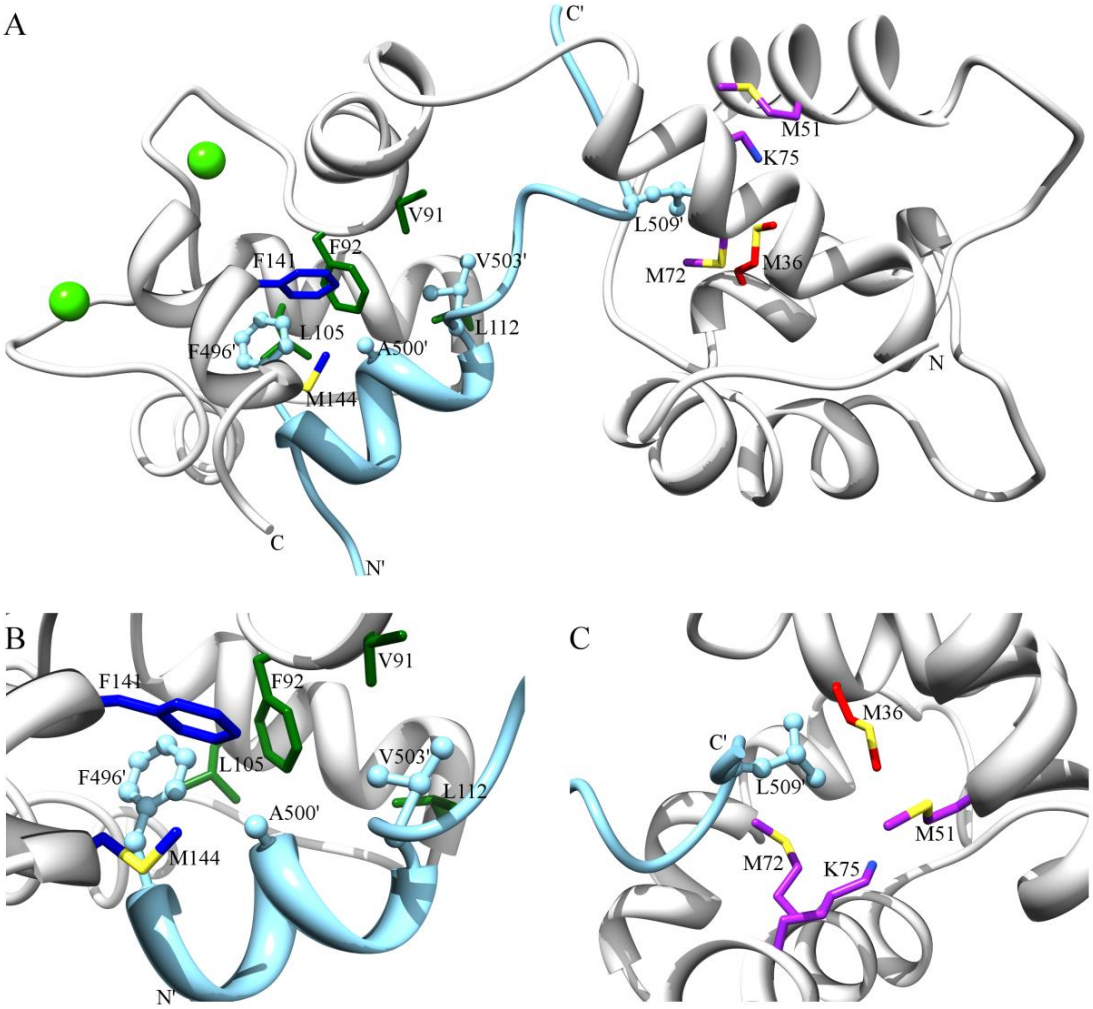

Figure 5.3: Solution structures of CaM bound to the eNOS CaM binding peptide at 225 nM Ca^{2+} showing sidechain residues of CaM interacting with side chains of the anchor residues of the eNOS peptide.

(A) Cartoon ribbon view of the average solution structure of the CaM− eNOS complex at 225 nM Ca^{2+} showing sidechain residues of CaM interacting with side chains of the anchor residues of the eNOS peptide. The side chains are colored by the same color scheme as that in Figure 1. (B) Zoom in of the C-lobe of CaM showing sidechain residues of CaM interacting with side chains of the anchor residues of the eNOS peptide. (C) Zoom in of the N-lobe of CaM showing sidechain residues of CaM interacting with side chains of the anchor residues of the eNOS peptide.

5.4 Conclusions

The solution structure, along with the previous amide exchange and internal mobility results, shows that the residues of CaM interacting with eNOS' 1-5-8-14 anchoring residues have strong interactions at 225 nM free Ca^{2+} concentration, which keeps the complex intact, while the rest of the residues of the CaM protein are able to fluctuate or "breathe". Comparing the two lobes of CaM, the residues of the C-lobe display a more rigid structure (lower r.m.s.d., lower degree of internal mobility from higher S^2, and higher exchange protection), indicating a stronger interaction with the eNOS peptide to hold the complex together, while the N-lobe is more dynamic and loosely associated to the eNOS peptide. This is the first study to determine an NMR structure of the CaM-eNOS complex at a free Ca^{2+} concentration that is within the physiologically relevant elevated intracellular Ca^{2+} concentration range. This structure suggests that the C-lobe of CaM first binds to the N-terminus of eNOS' CaM-binding domain and possibly part of the heme domain, while loosely associating to the C-terminus of eNOS' CaM-binding domain when the intracellular Ca^{2+} concentration is elevated to 225 nM. As the intracellular Ca^{2+} concentration increases the N-lobe then binds Ca^{2+} and becomes tightly bound to the C-terminus of eNOS' CaM-binding domain, allowing for the possibility of a bridge to form between CaM and the FMN domain, which would induce a shift to the FMN-heme electron transfer conformation to allow efficient electron transfer in the NOS enzymes.

Chapter 6

NMR structural studies of Ca^{2+} binding CaM mutants*

6.1 Introduction

CaM consists of two globular domains joined by a flexible central linker region. Each one of these domains contains two EF hand pairs capable of binding to Ca^{2+}. Each EF hand consists of a helix-loop-helix structural element, with the 12 residue long loop being rich in aspartates and glutamates (Figure 1.1). In the absence of Ca^{2+} the helix-loop-helix motif of the EF hands are in a "closed" conformation, with their hydrophobic residues packed into their central core and their charged, hydrophilic residues solvent-exposed (Strynadka and James, 1989). Once a Ca^{2+} ion binds, the helices rearrange into a more "open" conformation, that exposes hydrophobic patches on each domain thereby allowing CaM to associate with its intracellular target proteins (Strynadka and James, 1989). The central linker's flexibility allows it to adapt its conformation to optimally associate with its intracellular targets (Persechini and Kretsinger, 1988). CaM is able to bind to target proteins in the Ca^{2+}-replete and Ca^{2+}-deplete forms. There is considerable interest in obtaining a better understanding of the structural basis for CaM's ability to bind and recognize its numerous target proteins.

NOS enzymes are one of the target proteins bound and regulated by CaM. At elevated Ca^{2+} concentrations, CaM binds to and activates eNOS making it a Ca^{2+}-dependent NOS enzyme. In contrast, iNOS is transcriptionally regulated *in vivo* by cytokines and binds to CaM at basal levels of

* *Unless otherwise stated, all of the work reported in this chapter was performed and analyzed by the candidate.*

Ca^{2+}. The Ca^{2+}-deficient mutant CaM proteins can be used to allow for a specific structural investigation of Ca^{2+}-dependent/independent activation and binding of CaM to iNOS.

To study the Ca^{2+}-dependent/independent properties of binding and activation of target proteins by CaM, numerous studies use a series of CaM mutants These include mutations of glutamate to glutamine residues at position 12 of each EF hand (Maune et al., 1992; Evenäs et al., 1999) or mutation of the conserved aspartate to alanine at position 1 of each EF hand (Geiser et al., 1991; Xia et al., 1998; Xiong et al., 2010). Changing the aspartate residue at position 1 of the EF hand loop of CaM inactivates the EF hand toward Ca^{2+} binding. These CaM proteins are defective in Ca^{2+} binding in either the N-terminal lobe EF hands (CaM_{12}; CaM D20A and D56A mutations), the C-terminal lobe EF hands (CaM_{34}; CaM D93A and D129A), or all four of its Ca^{2+}-binding EF hands (CaM_{1234}; mutations at D20A, D56A, D93A and D129A inclusive), depicted in Figure 6.1.

A recent study by Xiong et al. (2010) has shown that although conversion of D93 and D129 to Ala effectively inhibits Ca^{2+} binding to EF hands III and IV, the mutations may not only cause some structural perturbations in the C-domain but in the N-domain also. This suggests that the Ca^{2+}-deficient CaM mutants may adapt a different structure compared to that of the apo N- and C-domains of CaM. To investigate the effect of mutating Asp at position 1 to Ala in each EF hand we performed NMR structural studies of CaM_{12}, CaM_{34}, and CaM_{1234} in the absence and presence of Ca^{2+}. A low resolution solution structure of CaM_{1234} was determined and the effects of these mutations were compared to the previous solution structure of apoCaM. Previously, Spratt et al. (2007a) performed activity studies on iNOS activity using all three of these mutants and found it was active for both CaM_{34} and CaM_{12} in the presence of Ca^{2+}, with rates of 115% and 75%, respectively, whereas with CaM_{1234} less than 25% activity was found. In the presence of EDTA a substantial decrease in iNOS activity was found for wild type CaM and CaM_{34}, whereas no substantial decrease in iNOS activity

was found for CaM_{12} or CaM_{1234}. In light of these activity studies we determined a high resolution structure of CaM_{34} bound to the iNOS CaM binding domain peptide and compared that to the previously determined holoCaM-iNOS complex to characterize the structural effects this mutation may cause.

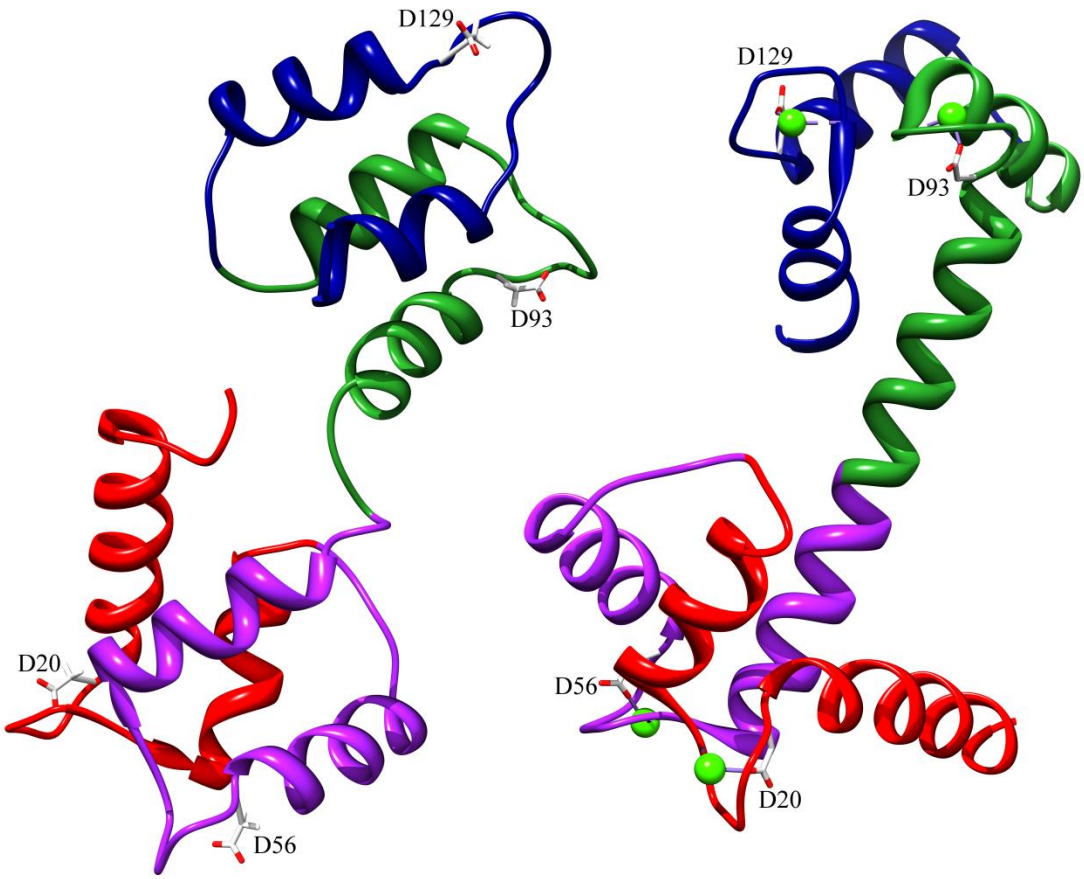

Figure 6.1: Ribbon diagram of apoCaM and Ca^{2+}-saturated CaM displaying Asp residues in position 1 of each EF hand.

Residues 1−40 of CaM (EF hand I) are colored red, residues 41−79 (EF hand II) purple, residues 80−114 (EF hand III) green, and residues 115−148 (EF hand IV) blue. The apoCaM structure was modified from PDB 1CFC (Kuboniwa et al., 1995) and holoCaM from PDB 1CLL (Chattopadhyaya et al., 1992).

6.2 Methods and experiments

6.2.1 Sample preparation for NMR investigation.

CaM_{12}, CaM_{34} and CaM_{1234} for NMR experiments were expressed in E. coli 1 L of M9 media (11.03 g/L $Na_2HPO_4 \cdot 7H_2O$, 3.0 g/L KH_2PO_4, 0.5 g/L NaCl, 2 mM $MgSO_4$, 0.1 mM $CaCl_2$, 3 μM $(NH_4)_6(MO_7)_{24}$, 400 μM H_3BO_3, 30 μM $CoCl_2$, 10 μM $CuSO_4$, 80 μM $MnCl_2 \cdot 4H_2O$, 10 μM $ZnCl_2$, 10 mM $FeSO_4$, 100 μg/mL kanamycin) containing 2 g/L ^{13}C-glucose and 1 g/L $^{15}NH_4Cl$. ^{13}C-^{15}N CaM was purified as described in section 3.2.2. Isolation of the mutant CaM protein (148 residues) was confirmed by ESI-MS and purity was judged to be > 95% by SDS-PAGE. The human iNOS peptide (RREIPLKVLVKAVLFACMLMRK, 22 residues corresponding to residues 510-531 from the full length iNOS protein) was synthesized and purchased from Sigma.

The CaM_{12}-iNOS and CaM_{34}-iNOS samples were prepared for NMR experiments via a buffer exchange into NMR solution (100 mM KCl, 10 mM $CaCl_2$, 0.2 mM NaN_3, 90% H_2O/10% ^2H_2O) at pH 6.0 using a YM10 centrifugal filter device (Millipore Corp., Billerica, USA). The CaM_{1234} sample was prepared for NMR experiments via a buffer exchange into NMR solution (100 mM KCl, 0.2 mM EDTA, 0.2 mM NaN_3, 90% H_2O/10% ^2H_2O) at pH 6.0 using a YM10 centrifugal filter device (Millipore Corp., Billerica, USA). All NMR samples contained at least 1 mM CaM in a total volume of 500 μL. The samples were transferred into 5 mm NMR sample tubes and stored at 4^{o}C until required for NMR experiments. NMR experiments on the CaM_{12}-iNOS and CaM_{34}-iNOS complex were conducted on samples titrated with iNOS peptide to saturation in a 1:1 CaM:peptide ratio. Complex formation was monitored after each addition by acquisition of a ^{1}H-^{15}N heteronuclear single-quantum coherence (HSQC) spectrum.

6.2.2 NMR spectroscopy and data analysis.

NMR spectra were recorded at 25^{o}C on Bruker 600 MHz DRX spectrometers equipped with XYZ-gradients triple-resonance probes (Bruker, Billerica, MA, USA). Spectra were analyzed using the program CARA (Keller, 2005). The amide resonances assignments were aided by using the previously obtained amide chemical shifts of Ca^{2+} saturated CaM with iNOS peptide as reference (Piazza et al., 2012). Specific assignments of the backbone resonances of the CaM_{12}-iNOS and CaM_{34}-iNOS complexes and CaM_{1234} alone were achieved using a combination of three-dimensional triple-resonance experiments, including HNCA, HN(CO)CA, CBCA(CO)NH, and HNCO (Grzesiek and Bax, 1992a, 1992b; Muhandiram and Kay, 1994). Side chain resonances for the CaM_{34}-iNOS complex and CaM_{1234} alone were assigned using the TOCSY-type HC(C)H-TOCSY and (H)CCH-TOCSY experiments (Ikura et al., 1990). Specific assignments of the iNOS peptide in the CaM_{34}-iNOS complex were obtained from ^{15}N-double-filtered NOESY experiments (Ikura and Bax, 1992). ^{15}N T_2 measurements for the CaM_{34}-iNOS complexes were acquired for eight different durations of the T_2 relaxation delay, T= 16.6, 33.2, 49.8, 66.4, 99.6, 116.2, 132.8, and 149.4ms.

6.2.3 Structure calculation of the CaM_{34}-iNOS peptide complex and CaM_{1234} alone.

The ^{1}H, ^{13}C, and ^{15}N resonance assignments were utilized to identify constraints for the structure calculations. Distance constraints for the CaM_{1234} were obtained from a ^{15}N NOESY-HSQC spectrum. Distance constraints for the CaM_{34}-iNOS complex were obtained from ^{15}N NOESY-HSQC and ^{13}C NOESY- HSQC, and ^{15}N- double-filtered NOESY spectra acquired on samples containing ^{13}C-^{15}N-CaM_{34} and unlabeled peptide (Fesik and Zuiderweg, 1990; Clore and Gronenborn, 1991; Ikura and Bax, 1992). In addition, dihedral angle restraints were derived from chemical shift analysis with TALOS+. The structure calculations of CaM_{34}-iNOS peptide complex and of CaM_{1234} alone were

performed using CNSsolve version 1.2 (Brunger et al., 1998). The calculation was initiated with an extended conformation file and run through several iterations of a standard simulated annealing protocol to minimize the energies. The final 20 lowest energy structures were selected.

6.3 Results and discussion

Previously Xiong et al. (2010) showed that the CaM_{34} mutations caused potential structural changes caused by significant changes in amide chemical shifts for apoCaM. They found this mutation also affected chemical shifts in the unmodified N-lobe and altered its Ca^{2+} binding properties. They postulated that this is possibly due to the loss of stabilizing hydrogen bonds between the side chain of Asp93 and backbone amides in apo loop III. We performed NMR studies on the CaM_{12}, CaM_{34} and CaM_{1234} mutant CaM constructs in the presence and absence of Ca^{2+} to investigate the structural perturbations observed by Xiong et al.

6.3.1 NMR structural study of Ca^{2+} saturated CaM_{12} indicates altered N-lobe.

NMR studies were performed on wild type CaM at various free Ca^{2+} concentrations to determine the ^{1}H-^{15}N HSQC spectrum of a C-lobe Ca^{2+}-replete and N-lobe Ca^{2+}-deplete CaM. This spectrum is shown in red in figure 6.2, overlaid with the ^{1}H-^{15}N HSQC spectrum of Ca^{2+}-saturated CaM_{12} in green. CaM_{12} contains mutations in EF hands I and II that make CaM's N-lobe unable to bind Ca^{2+}, thus it should have a Ca^{2+}-replete C-lobe and Ca^{2+}-deplete N-lobe in the presence of Ca^{2+}. This should result in an ^{1}H-^{15}N HSQC spectrum that overlays very well with a C-lobe Ca^{2+}-replete, N-lobe Ca^{2+}-deplete CaM, however, as evidenced by figures 6.2 and 6.3, chemical shift differences are observed throughout the N-lobe, specifically around the loop region of each EF hand. This suggests that the

Asp to Ala mutations not only knock out Ca^{2+}-binding but also cause structural perturbations throughout the whole loop region.

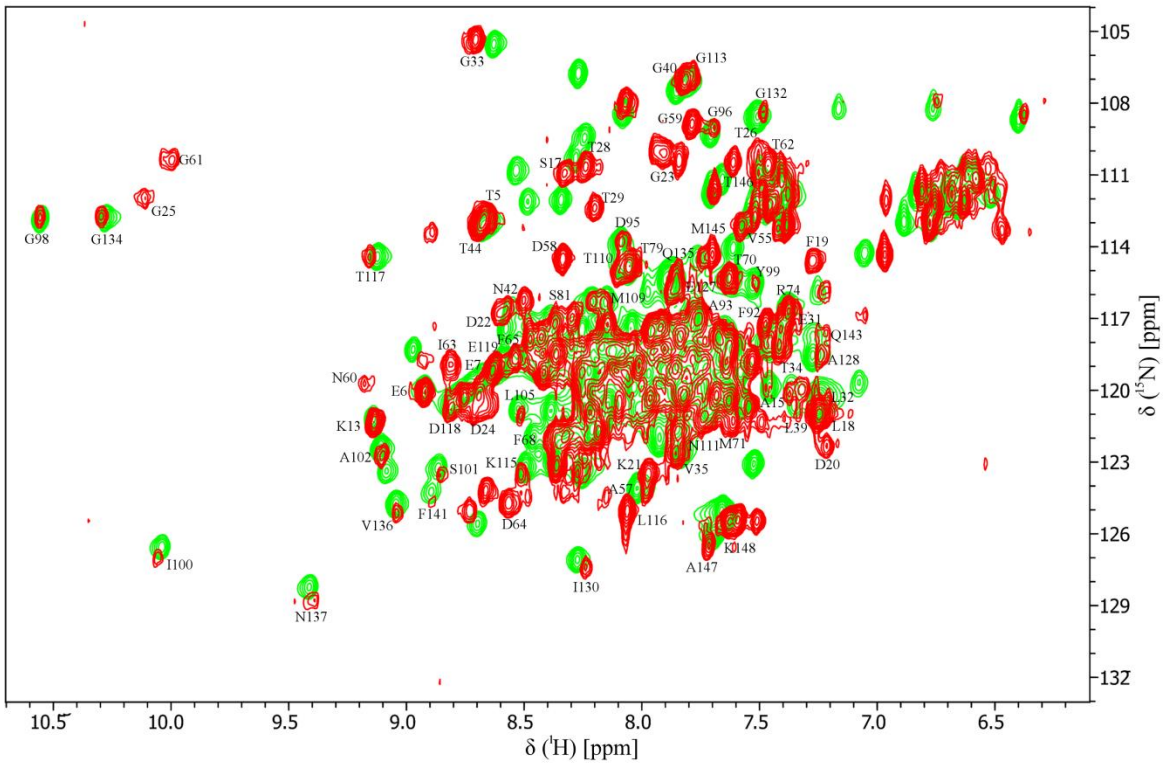

Figure 6.2: Superposition of ^{1}H-^{15}N HSQC spectra of wild type CaM at 1.3 μM free Ca^{2+} (red) and Ca^{2+} saturated CaM_{12} (green).

^{1}H-^{15}N HSQC spectra overlay shows the amide resonances of residues in the N-lobe of CaM_{12} are different from those of wild type CaM at 1.3 μM free Ca^{2+}. The backbone amide resonances of wild type CaM at 1.3 μM free Ca^{2+} are labeled with the amino acid type and position in the sequence.

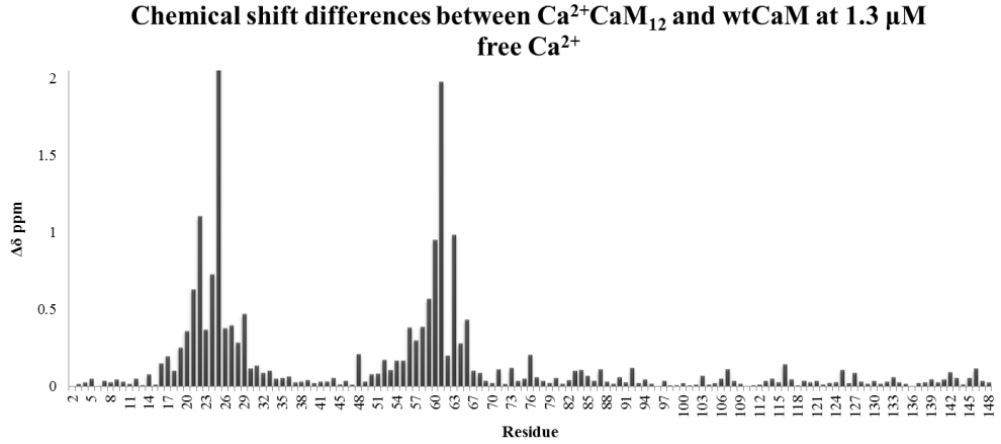

Figure 6.3: Chemical shift differences between CaM at 1.3 µM free Ca^{2+} and Ca^{2+} saturated CaM_{12}.

The contribution of ^{1}HN and ^{15}N chemical shift changes for each residue was calculated as $\Delta\delta = \sqrt{[(\Delta\delta^{1}HN)^2 + (\Delta\delta^{15}N/5)^2]}$, where $\Delta\delta^{1}HN$ and $\Delta\delta^{15}N$ are the differences in ^{1}HN and ^{15}N chemical shifts between the indicated protein. The greatest differences are localized to Ca^{2+} binding loops where each mutation is present.

6.3.2 Structural studies of CaM_{12} and CaM_{34} indicates possible structural perturbations caused by the mutations.

^{1}H-^{15}N HSQC experiments were then performed to determine if potential structural changes occur due to mutations in the CaM_{12} and CaM_{34} EF hands in the absence and presence of Ca^{2+}. The complete backbone assignment of CaM_{12} and CaM_{34} in the absence and presence of Ca^{2+} was completed and previously discussed in chapter 3. These assignments were used to probe the potential structural changes caused by the mutations through an ^{1}H-^{15}N HSQC comparison with apo and holoCaM. Figure 6.4A shows the ^{1}H-^{15}N HSQC spectra overlay of apoCaM, apoCaM_{12} and apoCaM_{34} and figures 6.5A and B shows the chemical shift differences calculated from these spectra. Cross-peaks for amides in the C-lobe of apoCaM_{12} overlap with those of apoCaM, however, amides in the N-lobe, specifically the residues in the loop regions of the EF hands, do not overlap with those of apoCaM. Conversely, cross-peaks for amides in the N-lobe of apoCaM_{34} overlap with those of

apoCaM, however, amides in the C-lobe, specifically the residues in the loop regions of the EF hands, do not overlap with those of apoCaM. This data suggests that the Asp to Ala mutations not only knock out Ca^{2+} binding to the EF hands but also cause potential structural changes. These structural changes appear to only be located to the specific EF hands that contain the mutation and not to the opposite domain in each respective CaM mutant.

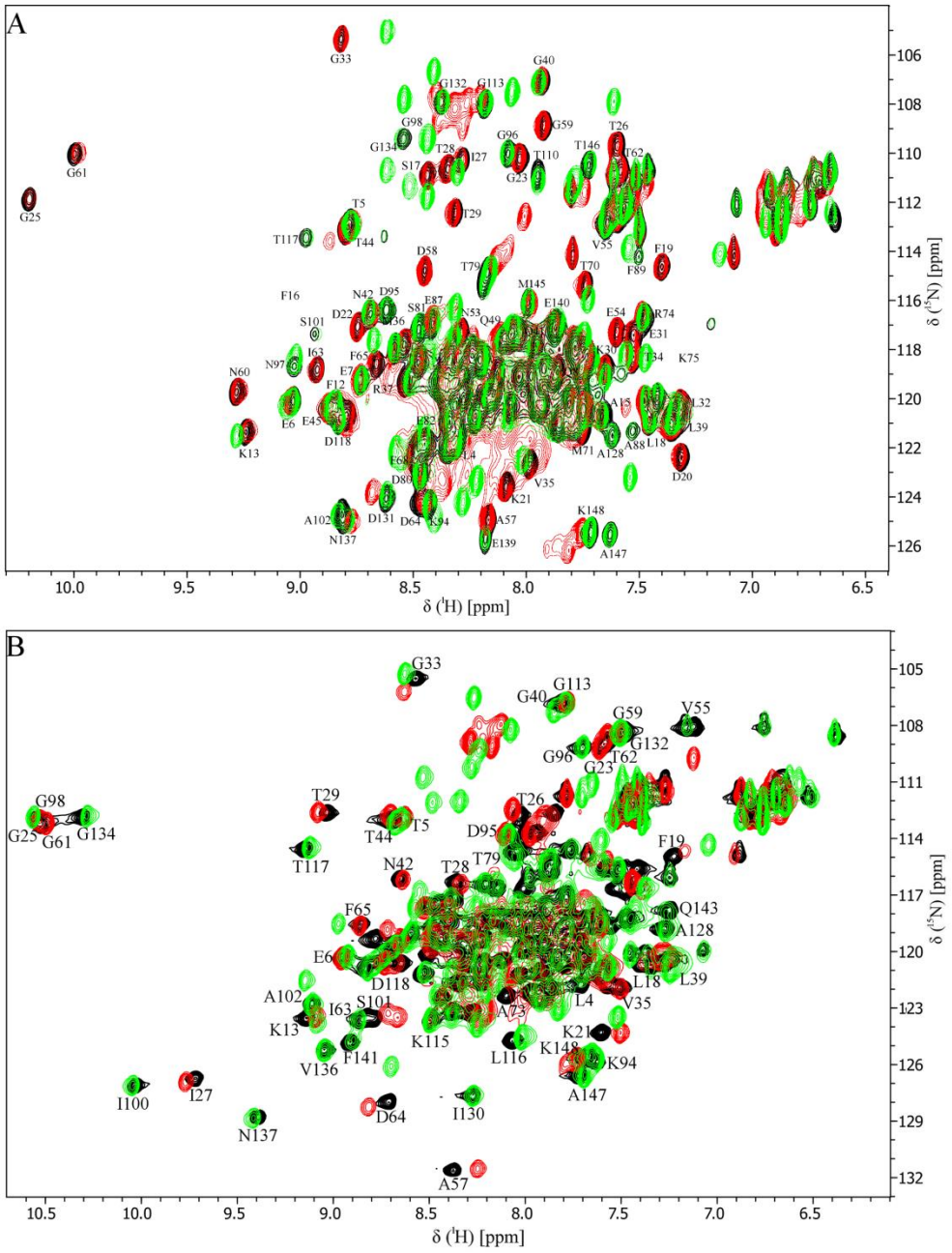

Figure 6.4: Superposition of ^{1}H-^{15}N HSQC spectra of (A) apo and (B) Ca^{2+}-saturated wild type CaM (black), CaM_{12} (green) and CaM_{34} (red).

^{1}H-^{15}N HSQC spectra overlay in (A) shows apoCaM (black), apoCaM_{12} (green) and apoCaM_{34} (red). The backbone amide resonances of apoCaM are labeled. ^{1}H-^{15}N HSQC spectra overlay in (B) shows holoCaM (black), Ca^{2+}-CaM_{12} (green) and Ca^{2+}-CaM_{34} (red). The backbone amide resonances of holoCaM are labeled.

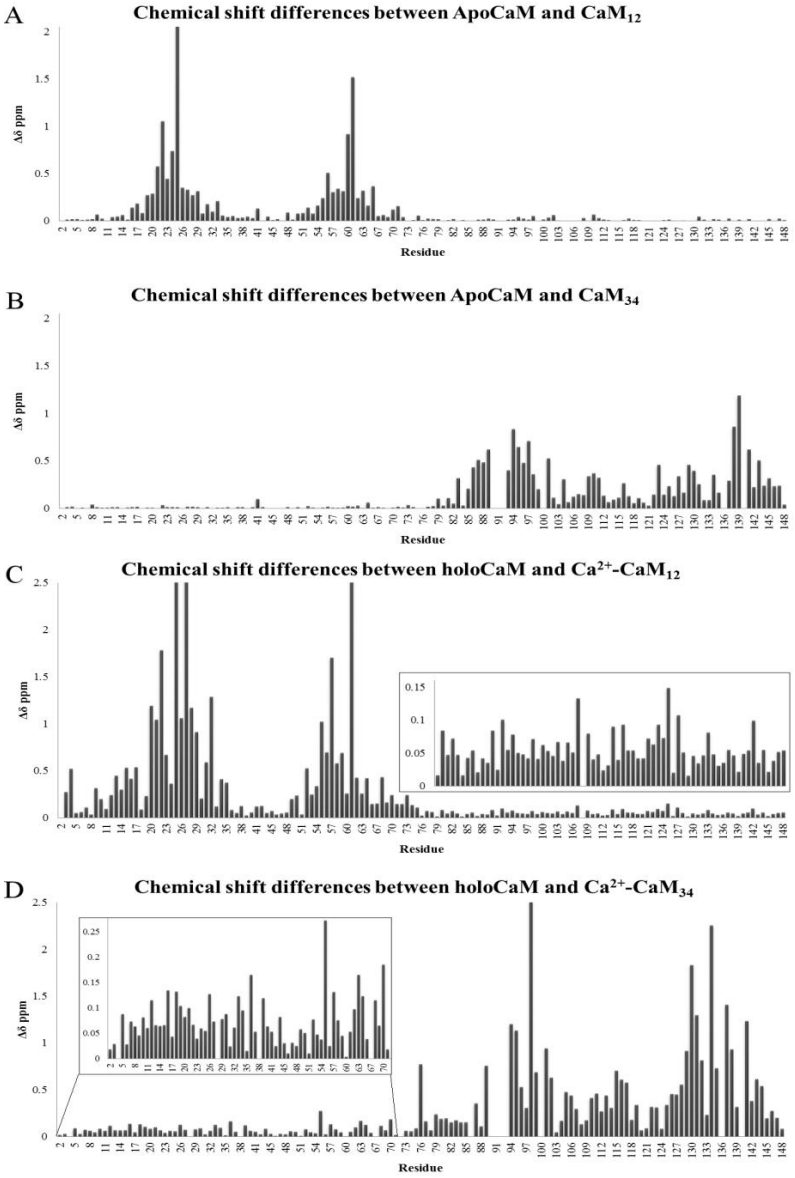

Figure 6.5: Chemical shift differences between apo and Ca^{2+}-replete CaM, CaM_{12} and CaM_{34}.

Chemical shift differences for the amide chemical shifts between (A) apoCaM and $apoCaM_{12}$, (B) apoCaM and $apoCaM_{34}$, (C) holoCaM and Ca^{2+}-CaM_{12}, and (D) holoCaM and Ca^{2+}-CaM_{34} are shown. The insets in C and D show the chemical shift differences of the C-lobe for holoCaM and Ca^{2+}-CaM_{12} and N-lobe for holoCaM and Ca^{2+}-CaM_{34}, respectively. The greatest differences are localized to Ca^{2+} binding loops where each mutation is present. In the presence of Ca^{2+} some chemical shift differences occur for the lobe opposite the mutation sites. The contribution of ^{1}HN and ^{15}N chemical shift changes for each residue was calculated as $\Delta\delta = \sqrt{[(\Delta\delta^{1}HN)^2 + (\Delta\delta^{15}N/5)^2]}$, where $\Delta\delta^{1}HN$ and $\Delta\delta^{15}N$ are the differences in ^{1}HN and ^{15}N chemical shifts between the indicated protein.

Figure 6.4B shows the ^{1}H-^{15}N HSQC spectra overlay of holoCaM, Ca^{2+}-CaM_{12} and Ca^{2+}-CaM_{34} and figures 6.5C and D shows the chemical shift differences calculated from these spectra. As observed for apoCaM_{12}, cross-peaks for the majority of amides in the C-lobe of Ca^{2+}-CaM_{12} overlap with those of holoCaM, and amides in the N-lobe, specifically the residues in the loop regions of the EF hands, do not overlap. However, unlike apoCaM_{12} there are a few residues in the C-lobe that are calculated to have a chemical shift difference greater than 0.1.

Also as observed for apoCaM_{34}, cross-peaks for amides in the C-lobe of Ca^{2+}-CaM_{34} overlap with those of holoCaM, and amides in the N-lobe, specifically the residues in the loop regions of the EF hands, do not. Like Ca^{2+}-CaM_{12}, residues in the opposite lobe appear to be affected by the mutations also. In the Ca^{2+}-CaM_{34} case there are quite a few C-lobe residues, spread throughout the whole domain, that are calculated to have a chemical shift difference greater than 0.1.This data suggests that the Asp to Ala mutations not only knock out Ca^{2+} binding to the EF hands where the mutations occur, but also cause potential structural changes in the opposite lobe. Some of the residues that experience the greatest changes are the hydrophobic residues Phe 12, Phe 16, Leu 18, Phe19 and Met36 in EF hand I and the hydrophobic residues, Val55, Ala57, Ile63 and Phe65 in the Ca^{2+}-coordinating loop of EF hand II. This is similar to what Xiong et al. (2010) had observed in their study. These structural changes appear to not only be located to the specific EF hands that contain the mutation but also to residues of the opposite domain, especially in the case of Ca^{2+}-CaM_{34}.

6.3.3 Solution structure of CaM_{1234}.

To probe these potential conformational changes further the structure determination of apoCaM_{1234} was undertaken. The ^{1}H-^{15}N HSQC spectrum of CaM_{1234} exhibits good resolution and well dispersed signals, indicating a uniform and folded protein structure (Figure 6.2). Comparing this spectrum to

that of apoCaM, chemical shift changes induced by the 4 EF hand mutations appear for the amides throughout all 4 of the Ca^{2+}-binding EF hands (Figures 6.6 and 6.7). The chemical shift differences are a sum of the individual differences observed for the mutated EF hands between apoCaM and CaM_{12}, and apoCaM and CaM_{34}.

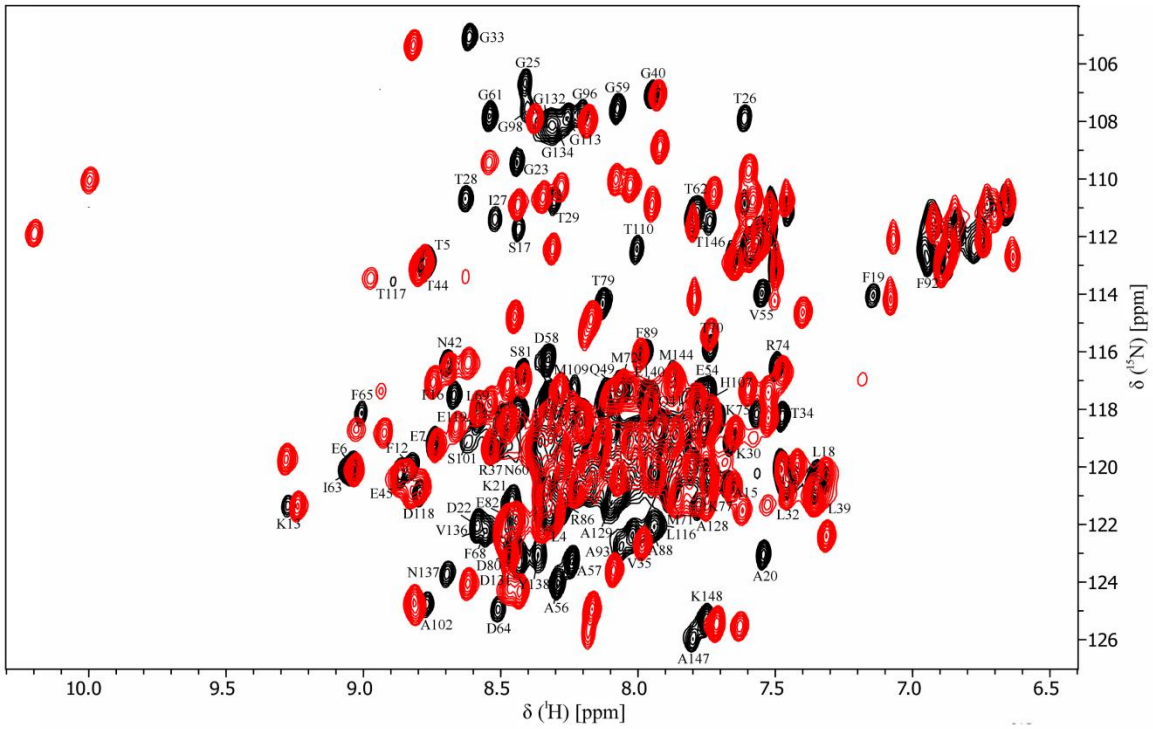

Figure 6.6: Superposition of ^{1}H-^{15}N HSQC spectra of CaM_{1234} (black) and apoCaM (red).
^{1}H-^{15}N HSQC spectra overlay shows the amide resonances of residues in both lobes of CaM_{1234} are different from those of wild type apoCaM. The backbone amide resonances of CaM_{1234} are labeled.

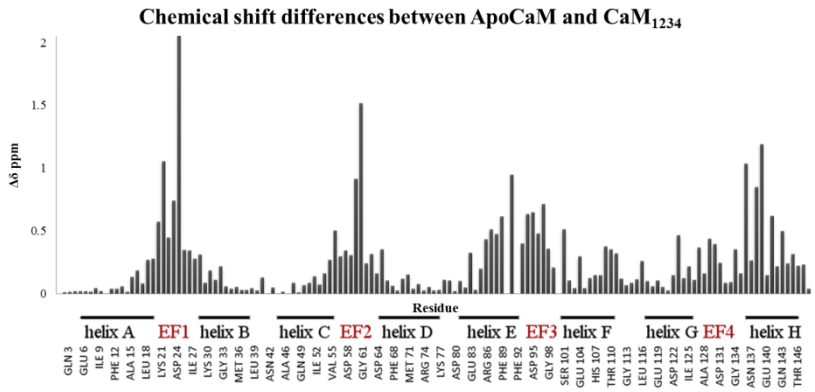

Figure 6.7: Chemical shift differences between CaM_{1234} and apoCaM.

The contribution of ^{1}HN and ^{15}N chemical shift changes for each residue was calculated as $\Delta\delta = \sqrt{[(\Delta\delta^{1}HN)^{2} + (\Delta\delta^{15}N/5)^{2}]}$, where $\Delta\delta^{1}HN$ and $\Delta\delta^{15}N$ are the differences in ^{1}HN and ^{15}N chemical shifts between the indicated protein. The greatest differences are localized to Ca^{2+} binding loops where each mutation is present.

The NMR assignment of CaM_{1234} followed a similar procedure as described in sections 1.3.1 and 2.3.2, with the backbone resonance assignment based primarily on 3D triple resonance techniques using the previously assigned chemical shifts of apoCaM as a starting point. This combination of techniques resulted in complete backbone assignments for CaM_{1234}, with the exception of the two prolines and the first two N-terminal amino acids. Subsequently, sidechain resonances were assigned using TOCSY experiments and NOEs for the structure calculation were extracted from an ^{15}N NOESY-HSQC. The use of only an ^{15}N NOESY-HSQC spectrum for the gathering of structure constraints resulted in a lower resolution structure as shown by the average pairwise r.m.s.d. value of the 20 lowest energy structures (Table 6.1).

The family of 20 lowest energy structures is shown in Figure 6.8A and B. Due to the high degree of flexibility of CaM's central linker it is not possible to superimpose both the C and N-lobes at the same time. Superimposing the ensemble of structures with respect to the N-lobe backbone atoms shows a fairly well overlapped N-lobe of CaM_{1234}, with an r.m.s.d. of 2.2 for the backbone atoms and 2.7 Å for heavy atoms. While superimposing the ensemble with respect to the C-lobe

backbone atoms shows a less well overlapped C-lobe of CaM_{1234}, with an r.m.s.d. of 3.1 for the backbone atoms and 4.0 Å for heavy atoms. This indicates the N-lobe has a more stable structure than the C-lobe, which has previously been reported to have a well-defined hydrophobic core, compared to a C-lobe with a less defined hydrophobic core in the apoCaM structures (Kuboniwa et al., 1995; Zhang et al., 1995a).

Table 6.1: Statistics for the structural ensemble of CaM_{1234}.

		CaM_{1234}		
NMR-derived distance and dihedral angle restraints				
NOE constraints		782		
Dihedral angles from TALOS+		240		
Total number of restraints		1022		
Structure statistics for the 20 lowest energy structures				
Mean deviation from ideal covalent geometry				
Bond lengths (Å)		0.009		
Bond angles (deg.)		0.9		
Average pairwise RMSD (Å) for all heavy atoms of the 20 lowest energy structures	All Residues	Ordered Residues[a]	C-lobe[b]	N-lobe[c]
Backbone Atoms	8.8	7.8	3.1	2.2
Heavy Atoms	9.3	8.3	4.0	2.7
Ramachandran statistics (%)				
Residues in most favored region		93.2		
Residues in additional allowed regions		6.7		
Residues in generously allowed region		0.0		
Residues in disallowed region		0.0		

[a] Ordered residue ranges: 4A-19A,24A-39A,41A-56A,61A-79A,81A-93A,101A-112A,116A-130A,137A-146A
[b] C-lobe residues: 81A-148A
[c] N-lobe residues: 4A-74A

Figure 6.8C shows the structure consists of 8 helices, and the characteristic helix-loop-helix conformation for each EF hand, as observed in other apo and Ca^{2+}-replete structures of CaM (Chattopadhyaya et al., 1992; Kuboniwa et al., 1995; Zhang et al., 1995a). When the ensemble of structures are superimposed with respect to a specific lobe, the linker region is shown to be very flexible, as evidenced by the opposite lobe being distributed in different conformations relative to the

superimposed lobe. Also no long range NOEs observed for the linker residues or observed between the two lobes suggesting CaM_{1234} exists as two independent globular domains.

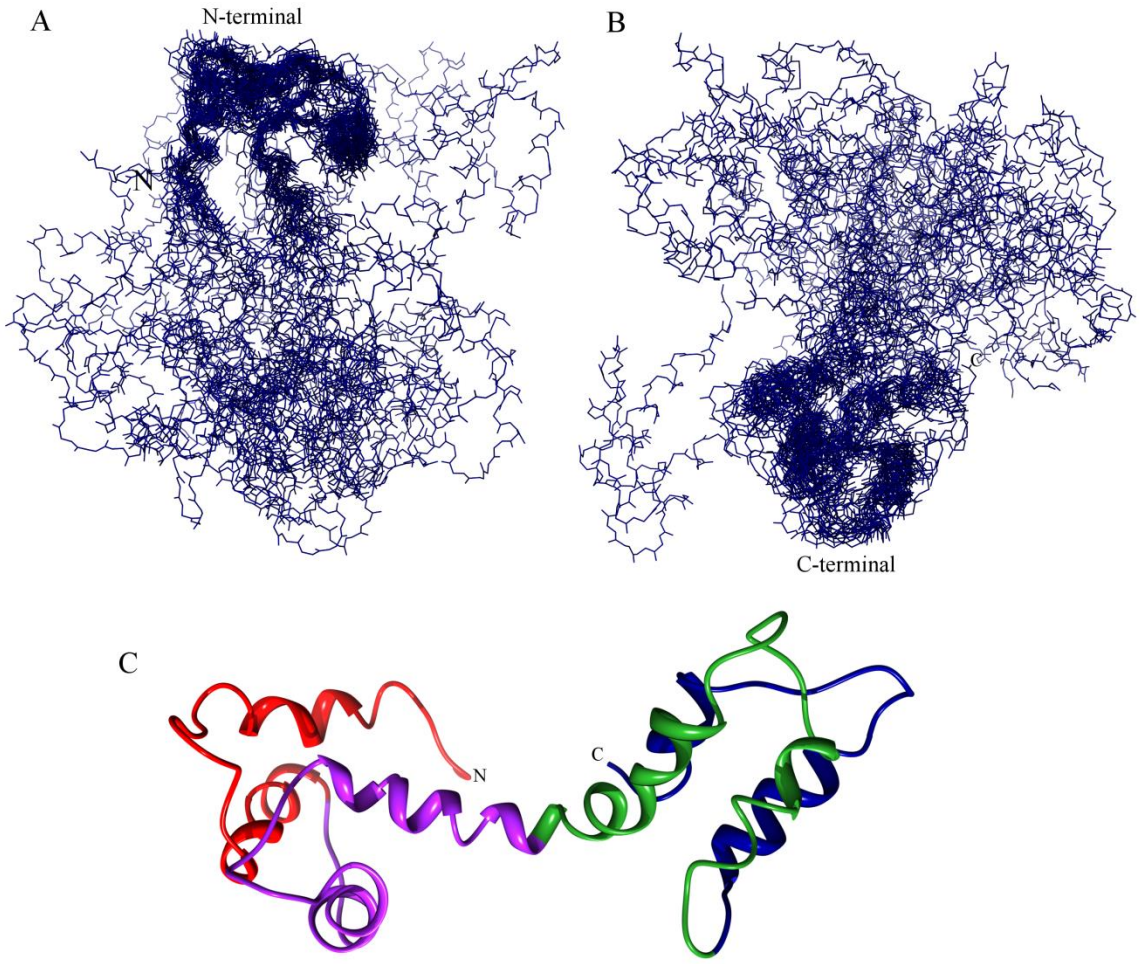

Figure 6.8: Solution structure of CaM1234.

The superposition of the ensemble of the 20 lowest-energy calculated solution structures of CaM_{1234}.(A) The N-terminal domain is superimposed against the energy-minimized average structure. (B) The C-terminal domain is superimposed against the energy-minimized average structure. (C) Cartoon ribbon view of the energy-minimized average solution structure of the CaM_{1234}. Residues are colored following the color-scheme in Figure 6.1.

6.3.3.1 Structure comparison apoCaM.

The CaM_{1234} structure was compared to the previously determined solution structure of apoCaM (PDB entry 1CFC, Kuboniwa et al., 1995), to determine any structural changes incurred by the Asp to Ala mutations in position 1 of the four EF hands. Due to the highly flexible linker region described above, the two lobes of CaM of the two structures were compared separately (Figure 6.9). When the two structures were superimposed with respect to CaM's N-lobe backbone atoms (residues 4-70) a r.m.s.d. value of 2.999 Å was found. Figure 6.9B and C shows the superposition of the N-lobe of CaM_{1234} and apoCaM. In this figure helix C and the loop region between helix B and C overlay quite well in both structures, whereas helix B is shifted down from the Ca^{2+}-binding loop and helix A is tilted away from helix B at the site of the mutation. The biggest structural change observed is in the Ca^{2+}-binding loop region of EF hand I, which had previously been proposed to have the biggest structural change due to the Asp20 to Ala mutation (Xiong et al,. 2010). In the apoCaM structure the side chain of Asp 20 points into the loop and is involved in stabilizing hydrogen. The conversion of Asp to Ala in the CaM_{1234} structure causes the loop to have a less compact structure, unravelling the α-helix at the C-terminal end of helix A and pushing it away from helix B.

The Ca^{2+}-binding loop of EF hand II also displays structural changes, however these aren't as large. In the apoCaM structure the side chain of Asp 56 is exposed to the solvent, thus doesn't have as large of a role in stabilizing the loop structure, which could explain the lower degree of structural change. In the CaM_{1234} structure the substituted Ala 56 side chain points into the loop, this disrupts the α-helix that Asp 56 adopted, unraveling the loop slightly. This explains the similarity in conformation of helix C in both structures. The linker region displays a similar α-helix secondary structure for helices D and E, with a hinge region at residue 80 for both structures.

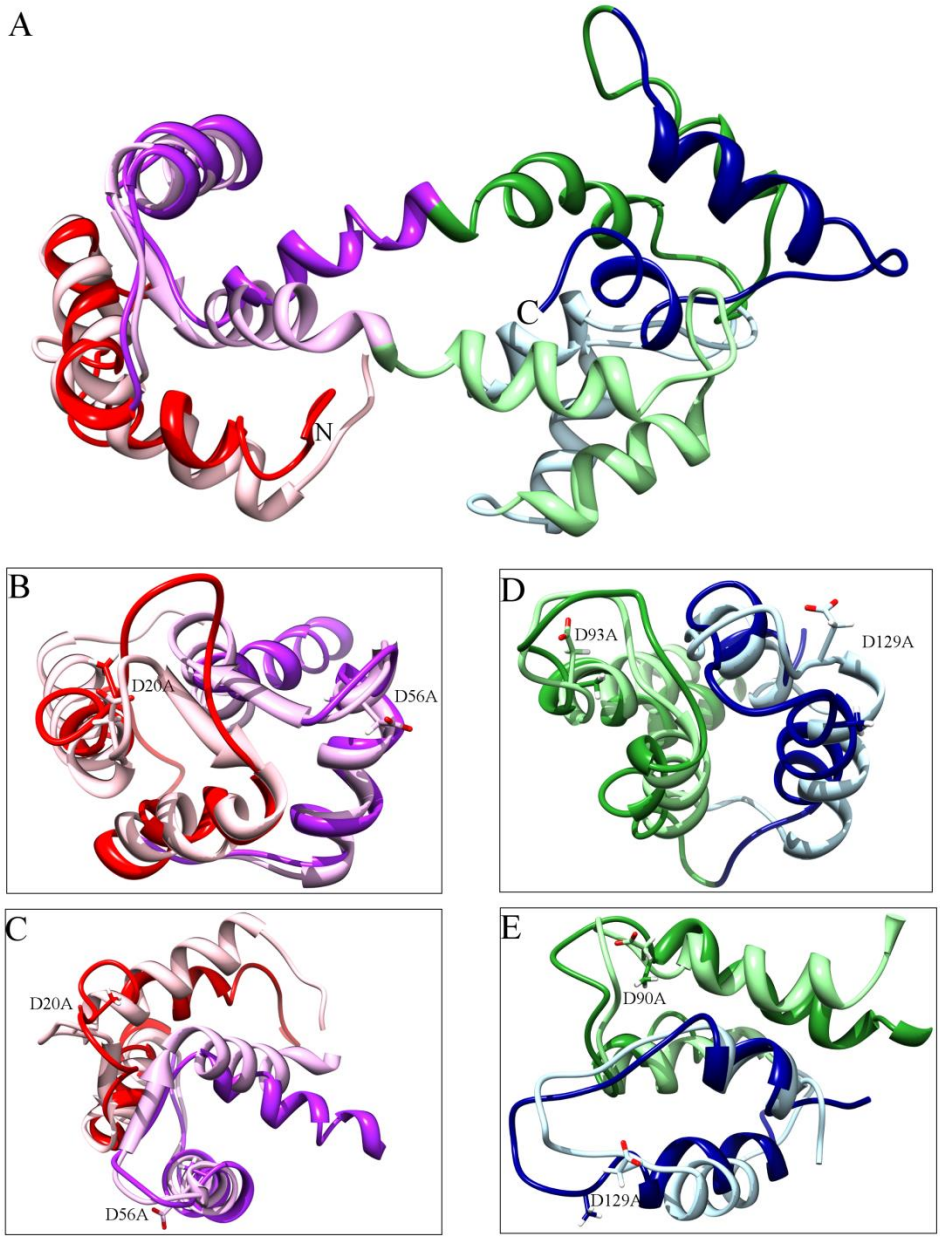

Figure 6.9: Comparison of the solution structure of the CaM_{1234} with the solution structure of apoCaM.

The solution structures of CaM_{1234} (dark colors) and apoCaM (light colors, Structure 14 from PDB 1CFC Kuboniwa et al., 1995)) are aligned by superimposition of the backbone atoms of the N-lobes of CaM in A. For clarity only the N-lobes of CaM_{1234} and apoCaM were superimposed in B and C and the C-lobes superimposed in D and E. The side chains of Asp in apoCaM and Ala in CaM_{1234} are shown and labeled as D20A, D56A, D93A and D129A. The color scheme is the same as figure 6.1.

When the two structures are superimposed with respect to the C-lobe backbone atoms (residues 84-148) a r.m.s.d. value of 3.762 Å was found. Figure 6.9D and E shows the superposition of the C-lobe of CaM_{1234} and apoCaM, which displays less drastic conformational changes compared to the N-lobe, but more subtle changes. Like EF hand I, the side chain of Asp 93 of EF hand III points into the loop, however, the conversion to Ala doesn't cause as large of a structure perturbation as Asp 20 to Ala. The packing of Ala side chain into the loop toward the other hydrophobic side chain groups causes the loop to bulge slightly compared to apoCaM. This causes Ala 102 and Ala103 to lose their α-helical structure, along with helix F to become less helical. The loop region between the two EF hands has a slightly different conformation due to helix G being tilted inward. The Asp 129 to Ala causes the Ca^{2+}-binding loop of EF hand IV to be slightly longer because of this tilt in helix G. Overall the EF hand III and IV mutations cause more overall conformational changes compared to the N-lobe, as evidenced by the higher r.m.s.d. value for the lobe and the aforementioned differences.

These structural changes also correlate well with the chemical shift differences observed between the structures, which shows the N-lobe of CaM_{1234} has larger differences in the Ca^{2+}-binding loops, but less differences in the rest of the N-lobe, whereas the C-lobe shows lower chemical shift difference values in the Ca^{2+}-binding loop but a larger amount of differences throughout the whole lobe.

6.3.4 NMR structure of CaM_{34} and the iNOS CaM binding domain peptide complex.

We then determined the solution structure of CaM_{34} bound to a peptide of a target protein, iNOS. The complex of CaM_{34} with iNOS was chosen because of multiple factors. First off, iNOS is Ca^{2+}-independent, thus binds to CaM in the absence and presence of Ca^{2+}, so a complex will be formed even with the Ca^{2+}-deplete C-lobe. Also this CaM mutant would retain the ability to bind Ca^{2+} in its N

lobe, thus this lobe should interact with the iNOS peptide much like holoCaM does, which has previously been shown to bind tighter to the iNOS peptide than the C-lobe. And lastly, to determine if the EF hand III and IV mutations cause structural changes in the N-lobe as observed from the chemical shift differences between holoCaM and Ca^{2+}-CaM_{34} in figure 6.5D.

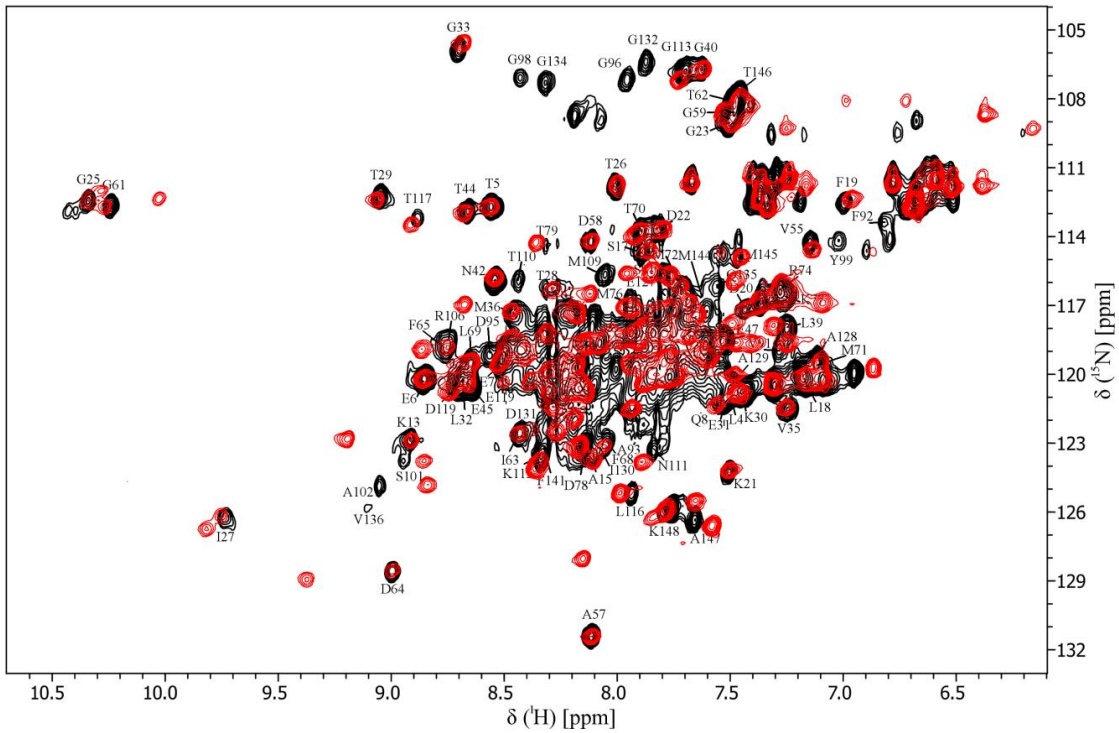

Figure 6.10: Superposition of ^{1}H-^{15}N HSQC spectra of CaM_{34}-iNOS (black) and holoCaM-iNOS (red).

^{1}H-^{15}N HSQC spectra overlay shows the amide resonances of residues in the C-lobe of CaM_{34}-iNOS are different from those of the holoCaM-iNOS complex. The backbone amide resonances of CaM_{34}-iNOS are labeled.

Overall, the ^{1}H- ^{15}N HSQC spectrum of CaM_{34} in complex with the peptide of the iNOS CaM-binding domain exhibits good resolution and well dispersed signals, indicating a uniform and folded protein structure (Figure 6.10). Upon comparison with the ^{1}H- ^{15}N HSQC spectrum of the holoCaM complex chemical shift changes induced by the C-lobe EF hand mutations appear predominately for the amides in the C-domain. Specifically the amides of residues that participate in

coordinating the Ca^{2+} ion in EF hands III and IV, with the greatest differences occurring for the amides in the center of the Ca^{2+}-binding loop (Figure 6.11). The majority of the amide resonances of the N-lobe show little chemical shift differences, suggesting both complexes have a similar structure of the N-lobe bound to iNOS, however, a few meaningful differences are observed.

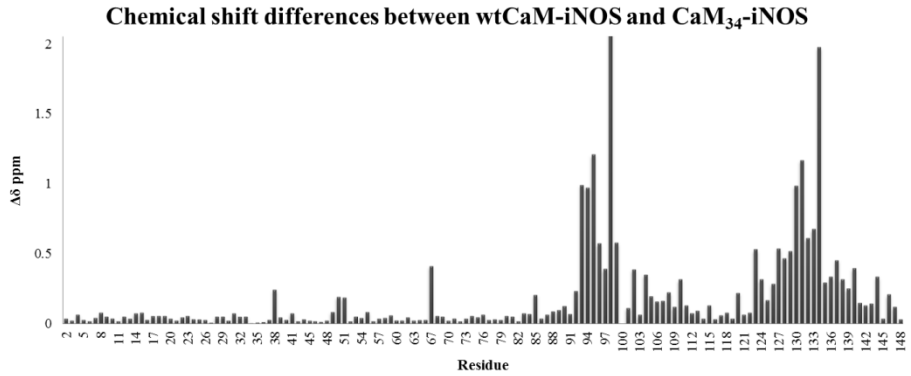

Figure 6.11: Chemical shift differences between CaM_{34}-iNOS and holoCaM-iNOS.
The contribution of ^{1}HN and ^{15}N chemical shift changes for each residue was calculated as $\Delta\delta = \sqrt{[(\Delta\delta^{1}HN)^2 + (\Delta\delta^{15}N/5)^2]}$, where $\Delta\delta^{1}HN$ and $\Delta\delta^{15}N$ are the differences in ^{1}HN and ^{15}N chemical shifts between the indicated protein. The greatest differences are localized to Ca^{2+} binding loops in the C-lobe where each mutation is present.

The three-dimensional solution structure of CaM_{34}-iNOS complex was determined using multidimensional heteronuclear NMR spectroscopy. The NMR assignment of the CaM_{34}-iNOS complex followed the procedure described in sections 1.3.1 and 2.3.2 with the backbone resonance assignment based primarily on 3D triple resonance techniques, using the previously assigned chemical shifts of the holoCaM-iNOS complex as a starting point. This combination of techniques resulted in complete backbone assignments for CaM_{34}, with the exception of the two prolines, the first two N-terminal amino acids and Ile100 (Appendix I). Subsequently, sidechain resonances for CaM_{34} were assigned using HC(C)H-TOCSY, (H)CCH-TOCSY and H(CCO)NH experiments and for the iNOS peptide using the ^{15}N-^{13}C-double-filtered NOESY experiment. NOEs for the structure were extracted from ^{15}N NOESY-HSQC, $^{13}C_{ali}$-NOESY and ^{15}N-^{13}C-double-filtered NOESY experiments.

The structure of the complex is based on a large number of experimental constraints and is well-defined. Residues 1− 12 at the N-terminus of the iNOS peptide (corresponding to residues 503-514 of full length iNOS) show a lack of structure because they could not be unambiguously assigned and were omitted from the structure calculation. The root-mean-square distance (r.m.s.d.) for ordered residues is 1.0 Å for the backbone atoms and 1.4 Å for all non-hydrogen atoms (Table 6.2).

Table 6.2: Statistics for the structural ensemble of the CaM_{34}-iNOS peptide complex.

		CaM_{34}-iNOS Complex		
NMR-derived distance and dihedral angle restraints				
	CaM_{34}	iNOS peptide	CaM_{34}-iNOS complex	
NOE constraints	1718	213	81	
Dihedral angles from TALOS+	262	N/A	N/A	
Total number of restraints		2274		
Structure statistics for the 20 lowest energy structures				
Mean deviation from ideal covalent geometry				
Bond lengths (Å)		0.010		
Bond angles (deg.)		1.2		
Average pairwise RMSD (Å) for all heavy atoms of the 20 lowest energy structures	All Residues	Ordered Residues[a]	C-lobe[b]	N-lobe[c]
Backbone Atoms	1.3	1.0	1.0	0.7
Heavy Atoms	1.7	1.4	1.6	1.2
Ramachandran statistics (%)				
Residues in most favored region		84.4		
Residues in additional allowed regions		14.4		
Residues in generously allowed region		0.5		
Residues in disallowed region		0.7		

[a] Ordered residue ranges: 5A-42A, 44A-92A, 100A-147A, 517B-528B
[b] C-lobe residues: 81A-148A
[c] N-lobe residues: 4A-74A

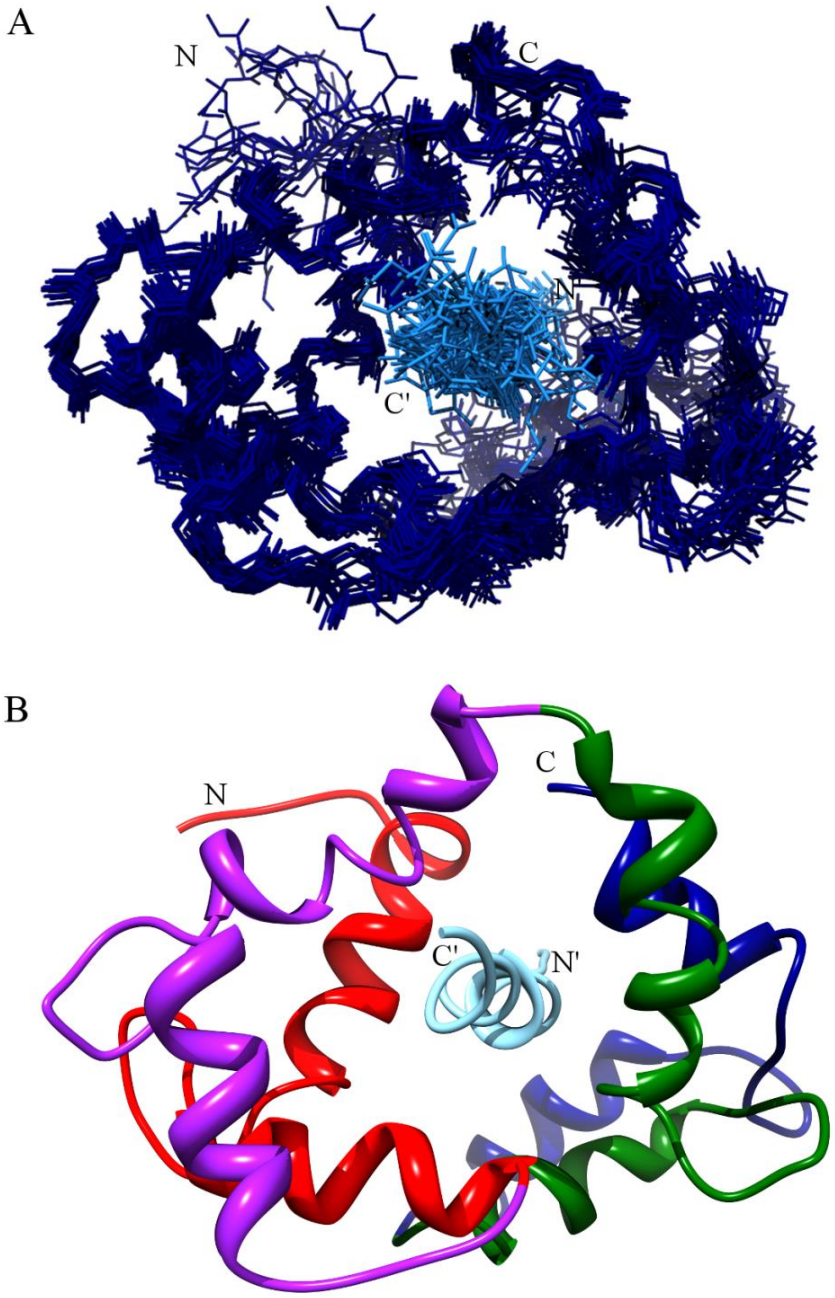

Figure 6.12: Solution structure of the CaM_{34}-iNOS complex.

(A) Superposition of the ensemble of the 20 lowest-energy calculated NMR solution structures of CaM_{34} bound to iNOS peptide Backbone atom traces of CaM are colored dark blue, and the iNOS peptide colored light blue. (B) Cartoon ribbon view of the average solution structure of the CaM_{34}-eNOS complex. CaM has the same color scheme as figure 6.1. The peptide is colored lighter blue.

The family of 20 lowest energy structures is shown in Figure 6.12A. This ensemble of structures shows a more closely overlapped N-lobe of CaM_{34} compared to a C-lobe that displays more fluctuation in the ensemble of structures. This can be further shown by looking at the r.m.s.d. values for each individual lobe of CaM_{34} in complex with the iNOS peptide. The r.m.s.d. for the C-lobe residues is 1.0 Å for the backbone atoms and 1.7 Å for all non-hydrogen atoms, whereas it is 0.7 Å for the backbone atoms and 1.2 Å for all non-hydrogen atoms of the N-lobe. The CaM_{34}-iNOS complex has a Ca^{2+}-replete N-lobe and a Ca^{2+}-deplete C-lobe bound to the iNOS peptide as shown in figure 6.12B. This structure shows CaM is still able to bind to iNOS with both lobes, even when the C-lobe of CaM is Ca^{2+}-deplete due to the Asp to Ala mutations.

6.3.4.1 Structure comparison to the holoCaM-iNOS complex.

When the CaM_{34}-iNOS complex structure is compared to the previously determined solution structure of the holoCaM−iNOS complex (PDB entry 2LL6), the N-lobes of CaM and peptide orientation are quite similar, however the loop regions of EF hands III and IV of the C-lobe of CaM are structurally different (Figure 6.13). When the two structures are aligned with respect to CaM_{34}-iNOS's backbone atoms a r.m.s.d. value of 2.438 Å for the backbone atoms of CaM-iNOS was found. When the two structures are aligned with respect to CaM's N-lobe backbone atoms a r.m.s.d. value of 2.180 Å was found, whereas, an r.m.s.d. value of 3.215 with respect to the C-lobe backbone atoms was found. The N-lobes of CaM and the iNOS peptide of each structure superimpose quite well on each other, whereas the loop regions of EF hands III and IV of the C-lobe of CaM do not. Even though the C-lobe of CaM_{34} is Ca^{2+}-deplete, the α-helices between the EF hand loops still bind to the iNOS peptide in a similar fashion as in the holoCaM-iNOS complex. This is evident from the solution structure and also from the NOESY spectra. The inter-residue NOEs observed for the α-helices between the EF

hand loops of CaM_{34}'s C-lobe are very similar to those observed for the same residues in the holoCaM-iNOS complex.

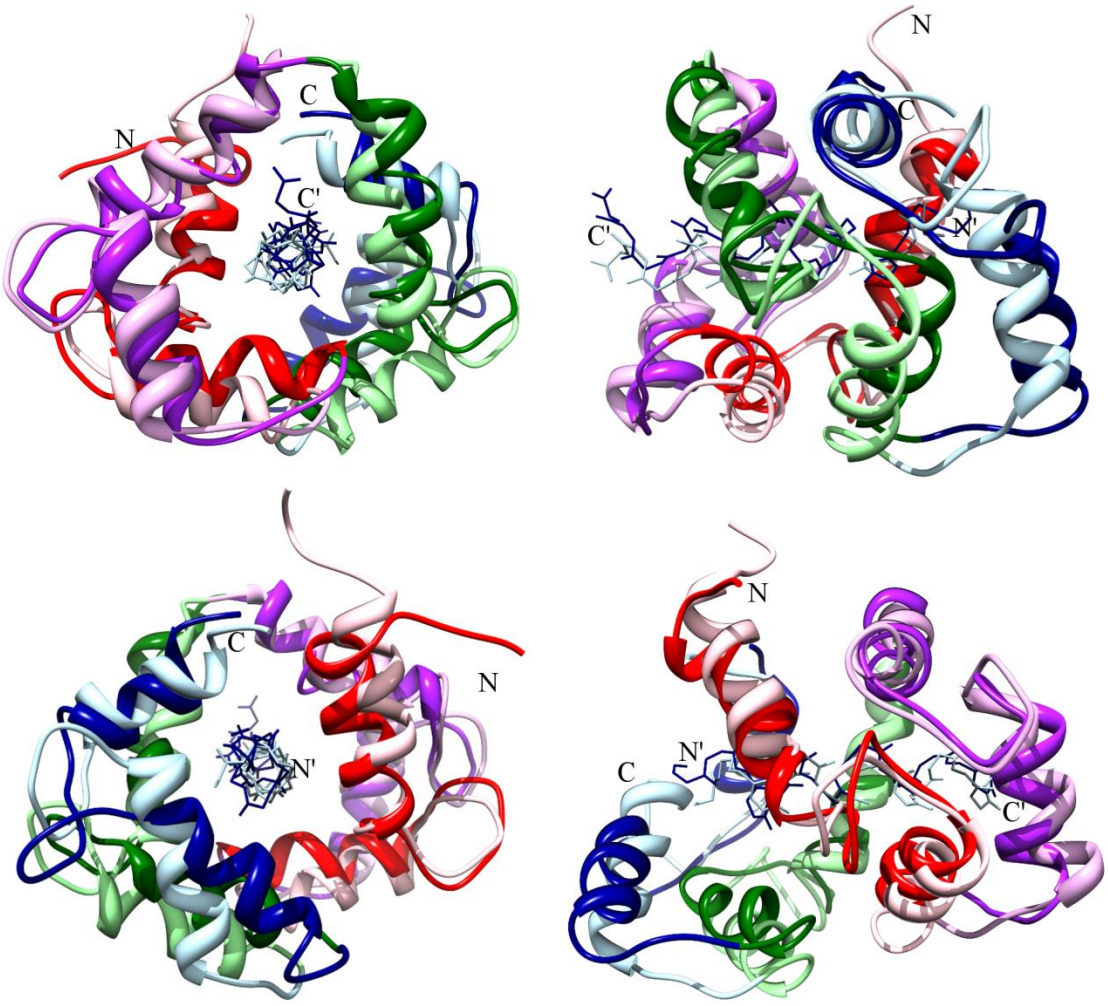

Figure 6.13: Comparison of the solution structure of the CaM_{34}-iNOS peptide complex with the solution structure of wtCaM-iNOS peptide complex.

The solution structures of the CaM_{34}-iNOS peptide (dark colors) and wtCaM-iNOS (light colors) are aligned by superimposition of the backbone atoms of the N-lobes of CaM and the iNOS peptides viewed along the bound peptide from its C-terminus (C′) to its N-terminus (N′) and subsequently rotated 90° around the vertical axis. The color scheme is the same as Figure 6.1.

The loop regions of EF hands III and IV are more compact in the holoCaM-iNOS complex compared to the CaM_{34}-iNOS complex. The mutation of Asp to Ala in position 1 of the loop removes

the oxygen ligand necessary to coordinate a Ca^{2+} ion and causes the loop to adopt a more open conformation. This causes the loop region between EF hands III and IV to move closer to the iNOS peptide. This also causes the loop region between EF hands I and II and helix B (labeling of helices shown in figure 6.7) to be shifted closer to the iNOS peptide. The loop regions between EF hands I and II and between III and IV contain multiple hydrophobic residues that pack close together and interact with the hydrophobic residues of the iNOS peptide. In conclusion the mutation of Asp to Ala causes the Ca^{2+} binding loop regions in the C-lobe EF hands to adopt a more open conformation, which in turn causes local structural changes, as shown in the loop region between EF hands III and IV, and long range structural conformation changes, as shown in the loop region between EF hands I and II and helix B. This may account for the amide chemical shift changes in the N-domain of Ca^{2+}-saturated CaM_{34} observed by Xiong et al.(2010) and in the previous section.

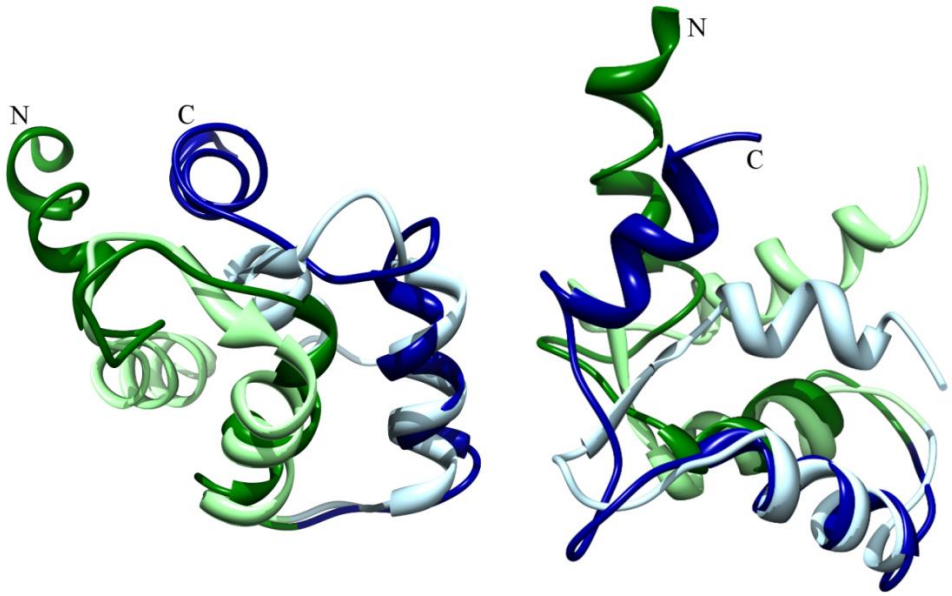

Figure 6.14: : Comparison of the C-terminal residues of the solution structure of the CaM_{34}-iNOS peptide complex with the solution structures of apoCaM.

The solution structures of the CaM_{34}-iNOS peptide (dark colors) and apoCaM (light colors) are aligned by superimposition of the backbone atoms of the C-lobes of CaM. The color scheme is the same as that in Figure 6.1.

When the CaM_{34}-iNOS complex structure is compared to the previously determined apoCaM structure (PDB entry 1CFC, Kuboniwa et al., 1995), there is structural similarity of the loop region of EF hand III of the C-lobes of CaM (Figure 6.14). When the two structures are aligned with respect to CaM's EF hand III loop region backbone atoms (residues 93-104) a r.m.s.d. value of 1.135 Å was found. When the two structures are aligned with respect to CaM's C-lobe backbone atoms (residues 93-140) a r.m.s.d. value of 3.500 Å was found. The structure and r.m.s.d. values suggest the EF hands of the C-lobe adopt a similar Ca^{2+} free conformation for the Ca^{2+}-binding loop region, however the overall conformation of the helix-loop-helix motif is similar to the "open" conformation observed in the Ca^{2+}-replete form, as shown in the right side of figure 6.14.

6.3.4.2 ^{15}N T2 relaxation data indicates CaM_{34}-iNOS' C-lobe residues have higher T2 relaxation times compared to holoCaM-iNOS.

Further to the structure determination of the CaM_{34}-iNOS complex ^{15}N T2 relaxation experiments were acquired. Figure 6.15 compares the results determined in this study to results previously determined for CaM bound to iNOS (Piazza et al., 2012) it is evident that the CaM_{34} mutations have an effect on the T2 relaxation rate of residues in the C-lobe. The N-lobe residues have almost identical T2 relaxation rates, with the exception of a few residues of helix C that have increased rates. These residues also had chemical shift differences when the ^{1}H-^{15}N HSQC spectra were compared. Comparison of the T2 rates for the C-lobe residues shows an increase in rates throughout the whole lobe, with the greatest increases occurring in the loop regions. This could be due to these loop region experiencing a higher degree of flexibility due to the mutations. This data shows that these mutations not only prevent CaM from binding Ca^{2+} in its C-lobe and cause structural perturbations but they also increase the internal dynamics of the C-lobe.

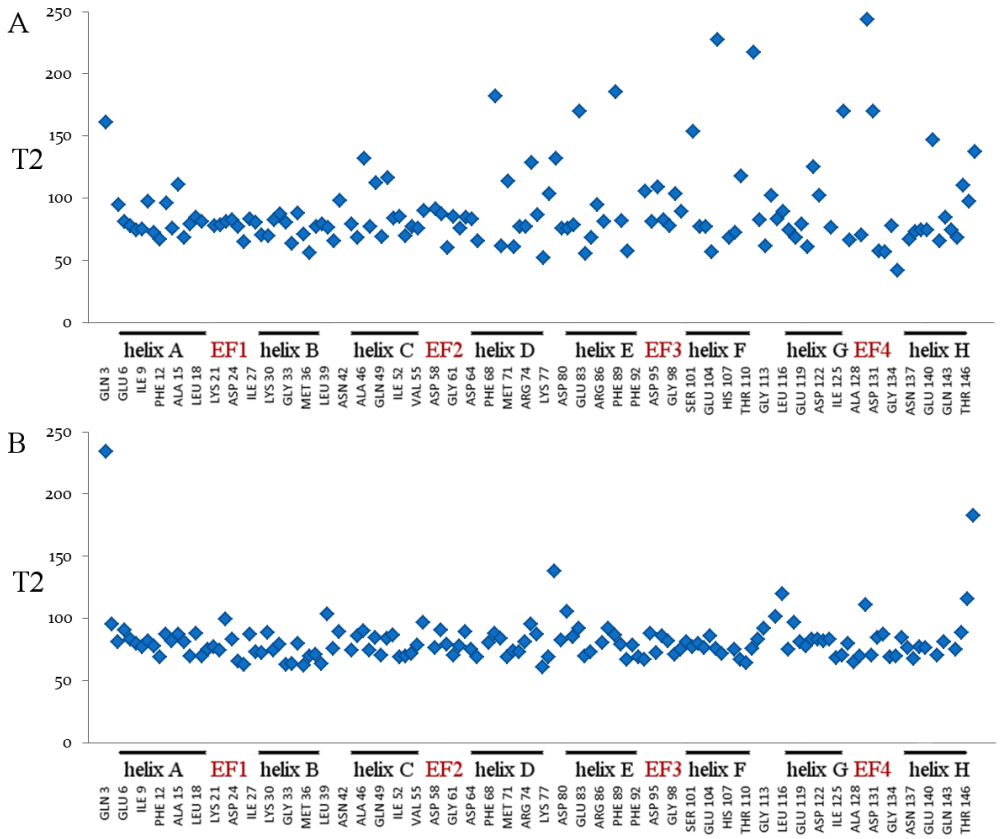

Figure 6.15: ^{15}N T2 Relaxation data for the CaM_{34}-iNOS and holoCaM-iNOS complexes.

Plots as a function of residue number of the measured T2 values for (A) the CaM_{34}-iNOS complex and (B) the holoCaM-iNOS complex. Only residues for which the ^{15}N-^{1}H cross peaks were sufficiently well resolved to permit accurate measurement of its intensity are included.

6.3.4.3 Structural effects on iNOS activation by CaM mutants.

Previously, Spratt et al. (2007a) performed activity studies on iNOS activity using the three CaM mutants. They found that iNOS was active for both CaM_{34} and CaM_{12}, with rates of 115% and 75%, respectively, in the presence of Ca^{2+},whereas CaM_{1234} produced rate of less than 25%. In the presence of EDTA a substantial decrease in iNOS activity was found for wild type CaM and CaM_{34}, whereas no substantial decrease in iNOS activity was found for CaM_{12} or CaM_{1234}. The CaM_{34}-iNOS structure shows that the N-lobe is bound to iNOS in the same conformation as holoCaM. The N-lobe of CaM

alone has previously been shown to activate the iNOS enzyme in the presence of Ca^{2+}, thus its tight association with iNOS, along with the association of the Ca^{2+}-deplete C-lobe may be enough to fully activate iNOS (Spratt et al., 2006, 2007b; Xia et al., 2009). The reduced iNOS activity observed for CaM_{34} in the presence of EDTA could be caused by the rearrangement of EF hands I and II due to the removal of Ca^{2+} from the N-lobe. This conformational change may not allow for the necessary interactions of the N-lobe of CaM to the FMN domain of iNOS required for efficient electron transfer, although CaM may still be bound to the CaM binding domain of the enzyme due to strong hydrophobic interactions. The structural explanation for the reduced activity observed for CaM_{1234} with iNOS can be speculated on by comparing the structure of apoCaM to CaM_{1234}. Although CaM_{1234} is still able to bind to iNOS, binding may only be to the highly hydrophobic CaM-binding domain of iNOS. The structural perturbations induced by the EF hand mutations may affect how CaM_{1234} interacts with the rest of iNOS, specifically CaM's N-lobe interaction with the FMN domain. This may prevent the conformational change required for efficient electron transfer to the heme domain or prevent CaM from stabilizing the FMN to heme electron transfer, "output", state.

6.4 Conclusion

In summary, the use of mutations in the EF hands of CaM to disable Ca^{2+}-binding also cause slight structural perturbations, shown in this study by the use of NMR spectroscopy. The structure determination of CaM_{1234} revealed that the mutation of Asp to Ala causes the EF hand loops to adopt perturbed conformations when compared to apoCaM. The structure also displayed a less stable C-lobe compared to N-lobe as previously observed for apoCaM. To investigate if these mutations also perturb the structure of CaM bound to a target peptide the structure of CaM_{34} bound to the iNOS peptide was determined. The mutation of Asp to Ala causes the Ca^{2+} binding loop regions in the C-

lobe EF hands to adopt a conformation resembling apoCaM, which causes local structural changes, as shown in the loop region between EF hands III and IV, and long range structural conformation changes, as shown in the loop region between EF hands I and II and helix B. This study provides structural evidence of changes that are present in CaM mutants with mutations at Asp in position 1 of the EF hand.

Chapter 7

NMR structural studies of daptomycin*

7.1 Introduction

7.1.1 Overview of daptomycin.

Daptomycin is one of the first approved antibiotic of the cyclic lipopeptides family. The compound was discovered by Eli Lilly and Company in the 1980s and selected for use in clinical trials. Daptomycin is produced as a secondary metabolite by a soil actinomycete, *Streptomyces roseosporus*, as a member of the A21978C lipopeptide family (Figure 7.1). The A21978C lipopeptide family consists of 13 amino acids, 10 of which form a cycle, including 3 D-amino acid residues (D-asparagine, D-alanine, and D-serine) and 3 uncommon amino acids (ornithine, 3-methyl-glutamic acid and kynurenine). The lipopeptide ring is closed by an ester bond that is formed between the C-terminal Kyn13 and the hydroxyl group of Thr4. The difference between the members of this lipopeptide family can be found in the length of the fatty acyl moiety that is attached to the N-terminal Trp1 residue, which ranges from 10-13 carbon atoms. Daptomycin contains a *n*-decanoyl fatty acid chain, which is produced by supplementing decanoic acid to cultures of *S. roseosporus* during fermentation (Huber et al., 1988). It is synthesized by three non-ribosomal peptide synthetases (NRPS) in *S. roseosporus* (Robbel and Marahiel, 2010).

* *Unless otherwise stated, all of the work reported in this chapter was performed and analyzed by the candidate. The bicelles and liposomes for the following work were prepared by Tian Hua Zhang.*

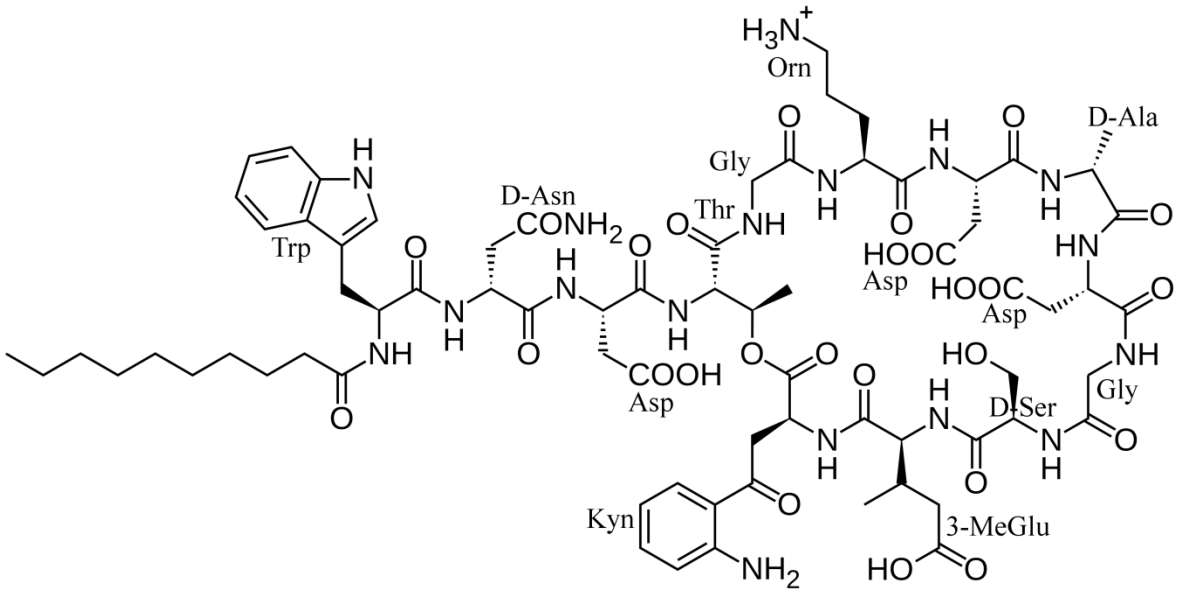

Figure 7.1: Chemical structure of daptomycin.

The clinical trials involved a twice daily dose regimen of daptomycin which produced adverse effects ultimately leading to the termination of the daptomycin trials (Garrison et al., 1990; Rybak et al., 1992). Cubist Pharmaceuticals acquired the rights in 1997 and after successful clinical trials involving a once daily dose regiment daptomycin was approved for treatment in 2003 (Oleson et al., 2000; Sauermann et al., 2008). It has been shown to have a broad spectrum of activity in vitro against Gram-positive bacteria, including methicillin-resistant *Staphylococcus aureus* and vancomycin-resistant enterococci (Eliopoulos et al., 1986; Rybak et al., 1992; Oleson et al., 2000).

7.1.2 Studies of daptomycin structure.

There have been considerably different structures of Ca^{2+}-free daptomycin (apo-daptomycin) and Ca^{2+}-conjugated daptomycin determined by NMR spectroscopy (Ball et al., 2004; Jung et al., 2004; Rotondi and Gierasch, 2005; Scott et al., 2007). These structures were determined in aqueous solution or with DHPC micelles and based on ^{1}H resonances only. Ball et al. (2004) determined the first

solution structure of apo-daptomycin in H_2O shown in figure 7.2. Their study produced a well-defined structure of apo-daptomycin that exhibits an extended conformation with turns at Ala8 and Gly10/Ser11. The side chain groups of the residues of the 10-member ring are solvent exposed with their backbone amide groups pointed inward and the decanoyl chain is flexible, displaying a high degree of conformational freedom. They were unable to produce a structure of Ca^{2+}-conjugated daptomycin due to severely broadened resonances of daptomycin.

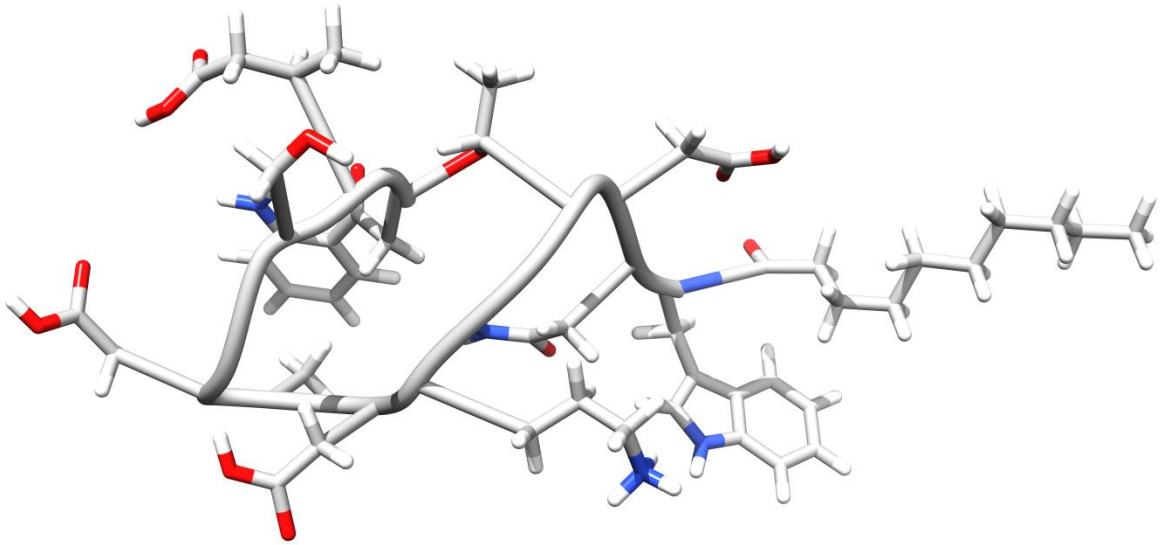

Figure 7.2: NMR structure of apo daptomycin in H_2O.
The apo daptomycin structure was determined in buffer consisting of 0.75 mM daptomycin, in 90% H_2O and 10% D_2O at pH 5.0.This structure was modified from PDB entry 1XT7 (Ball et al., 2004).

Another study by Jung et al. (2004) determined the apo-daptomycin and Ca^{2+}-conjugated daptomycin structures shown in figure 7.3. They found the structure of Ca^{2+}-conjugated daptomycin to be much better defined and more constrained than apo-daptomycin. The apo-daptomycin structure was different than the structure by Ball, here the backbone formed two bends at Asp7 and Asp9 with a highly variable region centered at Gly5. In the Ca^{2+}-conjugated structure the binding of Ca^{2+} caused the ring structure to be drawn inwards, with the side chain of Asp3 to tuck under. A type IV turn was

also formed between Thr 4 and Ala 8. Calcium binding resulted in a reduced total charge of daptomycin and an increase in the amphipathicity and the solvent-exposed hydrophobic surface. This was due to the redistribution of the charged side chains toward the top of the ring structure and the clustering of hydrophobic moieties at the other end.

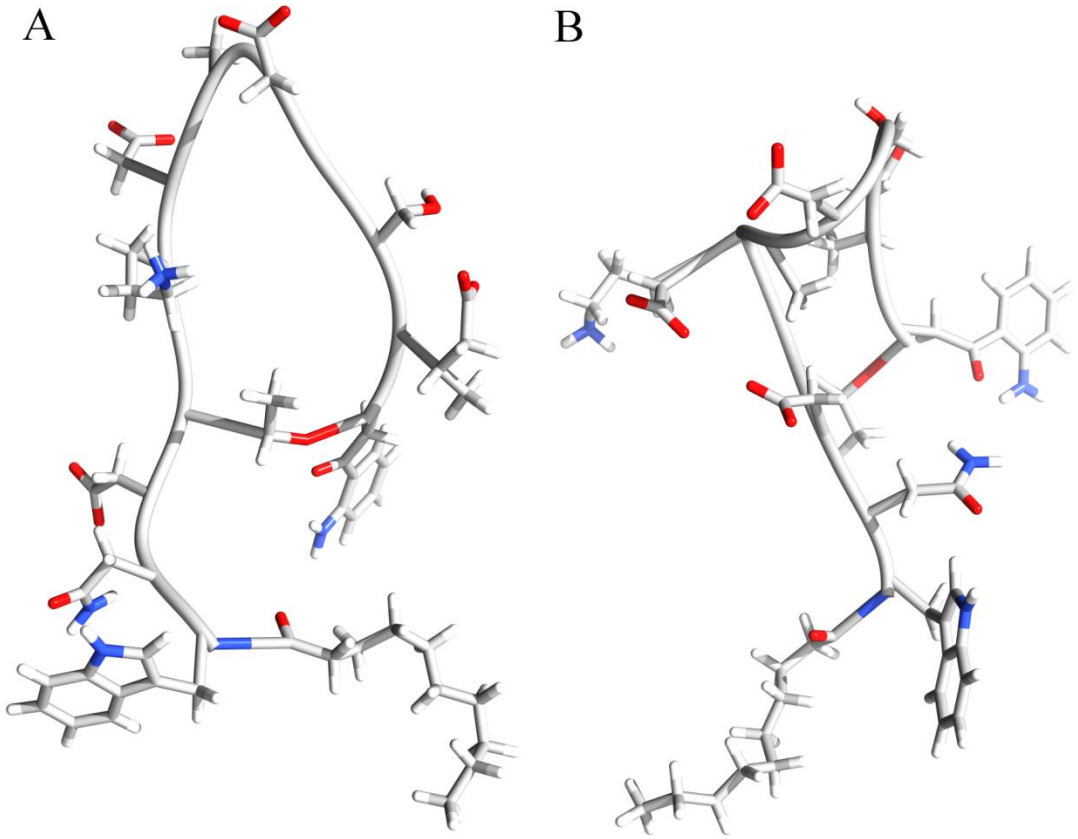

Figure 7.3: NMR structure of apo-daptomycin and Ca^{2+}-bound daptomycin.

(A) The apo daptomycin structure was determined in buffer consisting of 2 mM daptomycin, 100 mM KCl, 0.2 mM EDTA, 1 mM EGTA, and 7 % D_2O, pH 6.6.This structure was modified from PDB entry 1T5M (Jung et al., 2004). (B) The Ca^{2+}-conjugated daptomycin structure was determined in buffer consisting of 2 mM daptomycin, 100 mM KCl, 0.2 mM EDTA, 5 mM $CaCl_2$, and 7 % D_2O, pH 6.7. This structure was modified from PDB entry 1T5N (Jung et al., 2004).

Another NMR study determined the structure of daptomycin in the presence of 1,2-dihexanoyl-sn-glycero-3-phosphocholine (DHPC) micelles (Scott et al., 2007). The calculated

structures were shown to be quite different from the previously reported structures through measurement of backbone Cα RMSDs. In DHPC micelles with Ca^{2+}, daptomycin displays an extended ring structure, most similar to the apo structure determined by the Jung study (Figure 7.4). Scott et al. suggest that apo-daptomycin undergoes a minor conformational rearrangement when interacting with DHPC in the presence of Ca, in contrast to what Jung et al. reported.

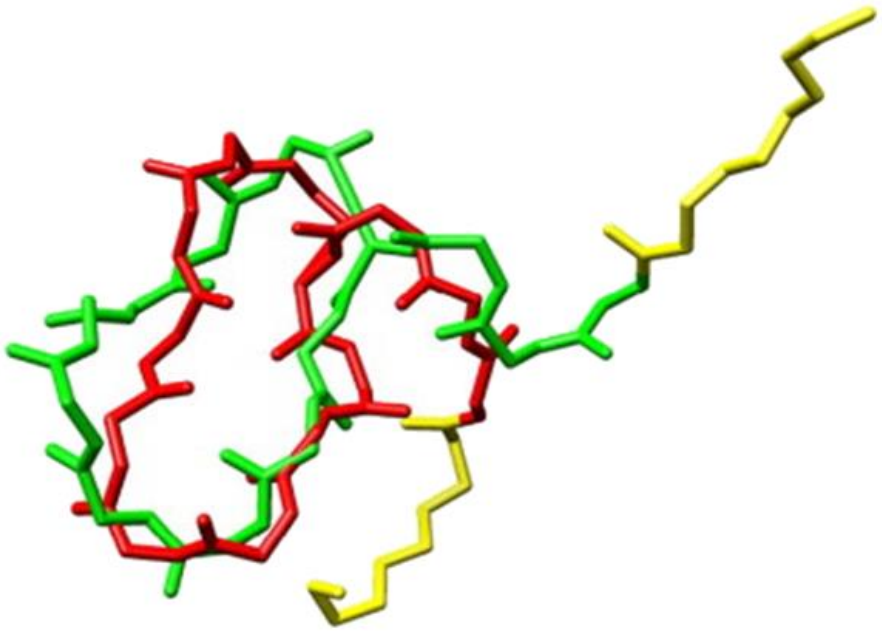

Figure 7.4: NMR structure of daptomycin in DHPC micelles with Ca^{2+}.

Overlay of the structure of daptomycin in DHPC micelles (red) with the apo-daptomycin structure of Jung et al. (green).The daptomycin structure was determined in DHPC micelles with a buffer consisting of 100 mM KCl, 0.2 mM EDTA, 5 mM $CaCl_2$, pH 6.7. The fatty acid chain is shown in yellow. This figure was modified from Scott et al. (2007).

The structural studies described here have been used to try and determine how daptomycin interacts with the bacterial membrane, whether or not oligomerization occurs in the presence of Ca^{2+} and for elucidating the mode of action for daptomycin's activity.

7.1.3 Proposed mode of action by daptomycin.

The proposed mechanism for the mode of action of daptomycin has not been fully elucidated, but most studies agree that daptomycin's activity is calcium-dependent and involves the cell membrane. After the initial cell membrane interaction there are two general schools of thought regarding the mode of action: inhibited synthesis of cell wall macromolecules, specifically peptidoglycan and lipoteichoic acids (Allen et al., 1987; Canepari et al., 1990); and disruption of the cell membrane (Silverman et al., 2003; Ball et al., 2004; Jung et al., 2004; Scott et al., 2007; Zhang et al., 2014b).

The first studies performed by Allen et al. (1987) suggested that daptomycin inhibits the formation of precursor molecules utilized in the biosynthesis of peptidoglycan. Their hypothesis was later revised when they found they could not identify a specific step in cell wall formation that was affected by daptomycin, but that daptomycin associates with the energized membrane, disrupting the membrane potential (Alborn et al., 1991). They proposed that this disruption of membrane potential resulted in the inhibition of the enzymes involved in cell wall synthesis. Other studies by Canepari et al. (Canepari et al., 1990; Boaretti and Canepari, 1995) found that daptomycin binds to the cell membrane irreversibly, thus preventing it from reaching any of the precursor molecules utilized in the biosynthesis of peptidoglycan. They suggested that daptomycin inhibited the synthesis of lipoteichoic acid (LTA) synthesis, but these results were not convincing as they could not identify any specific proteins involved in the synthesis of LTA.

Studies a few years later by Silverman et al. (2003) demonstrated Ca^{2+}-dependent, daptomycin triggered potassium release and showed its bactericidal activity was correlated with the dissipation of the cell membrane potential. They proposed a multistep mechanism of action for daptomycin. The first step of their proposed mechanism involves daptomycin's Ca^{2+}-dependent

insertion into the bacterial cytoplasmic membrane, followed by oligomerization to form possible pores or ion channels. This oligomerization would disrupt the integrity of the membrane, triggering a release of potassium and lead to rapid cell death.

Jung et al. (2004) proposed a two-step model for the interaction of daptomycin with bacterial membranes based on their NMR structural studies and CD spectroscopy experiments. In the initial step Ca^{2+} binds to daptomycin in solution, increasing its amphipathicity and decreasing its charge, thus allowing daptomycin to interact with neutral or acidic membranes. Next, Ca^{2+} bridges the gap between daptomycin and the acidic phospholipids, causing a second structural transition. This allows for a deeper insertion into the membrane bilayer and significant membrane perturbations, including lipid flip-flop. In contrast to Silverman, they found that membrane depolarization may not be the main cause of death as it occurs subsequently, and propose daptomycin's mode of action may involve multiple targets like other antibacterial cationic peptides.

The mode of action proposed by Jung et al. was further revised by Scott et al. (2007). In their mechanism daptomycin first forms a loose micelle that would have a large membrane disruptive potential, which aids in allowing insertion to the bacterial membrane (as previously proposed by Straus and Hancock, 2006). When the Ca^{2+} to daptomycin ratio reaches 1:1, daptomycin oligomerizes to form a 14-16mer (Ho et al., 2008). Their solution structure of daptomycin in DHPC micelles was very similar to the apo-form and showed only a minor conformation change with the addition of Ca^{2+}, indicating daptomycin would not undergo a significant structural change before membrane insertion as proposed by Jung. The next step in the mechanism involves daptomycin dissociation from the micelle and Ca^{2+}-mediated insertion into the bacterial membrane. ^{31}P NMR studies showed that daptomycin was able to perturb acidic membranes by inducing positive curvature strain in a Ca^{2+}-dependent manner (Jung et al., 2008). Next, oligomerization may occur in the membrane followed by

cell death due to membrane depolarization or interference with membrane-associated processes such as synthesis of cell wall components.

The most recent studies by Muraih and Zhang involving daptomycin and 1,2-dimyristoyl-sn-glycero-3-phospho-rac-(1'-glycerol) (DMPG) and 1,2-dimyristoyl-sn-glycero-3-phosphocholine (DMPC) containing liposomes showed daptomycin binds and forms oligomers with 6-7 subunits in the presence of physiological levels of Ca^{2+}. However oligomerization of daptomycin does not occur with PC only liposomes even though daptomycin can bind to these liposomes at much higher Ca^{2+} concentrations (Muraih et al., 2011; Muraih and Palmer, 2012). Zhang confirmed that daptomycin forms discrete pores on PG containing liposomes that are permeable for cations of limited size and suggested a revised mode of action (Zhang et al., 2014b). The first step involves Ca^{2+}-mediated binding of monomeric daptomycin to PG on the outer leaflet of the bacterial membrane. Then a tetramer forms through four bound monomers before being translocated across the membrane to the inner leaflet. Finally, an octameric ion pore forms when two tetramers on the opposite leaflets line up (Zhang et al., 2014a). Cell death would then occur through several factors, including some of the oligomers acting as active pores causing membrane depolarization through the influx of Na^{+}.

All of the suggested modes of action for daptomycin based off of NMR structural studies were performed either free in solution or in the presence of DHPC micelles. The structure of daptomycin in the presence of a PG containing membrane mimetic, which has been shown to be necessary for oligomer formation and activity, has not been previously determined and could be different from the previously determined structures of daptomycin. The following work attempted to determine the solution structure of daptomycin in the presence of Ca^{2+} and a DMPC/DMPG membrane mimetic.

7.2 Materials and methods

7.2.1 Preparing daptomycin samples with SDS micelles.

^{15}N-labeled daptomycin was provided by Cubist Pharmaceuticals. SDS micelles were prepared by dissolving SDS in 400 μL of H2O to a final concentration of 50 mM. ^{15}N-labeled daptomycin was added to this solution and brought up to 450 μL of H2O then 50 μL of D_2O was added. The final sample consisted of 40 mM SDS and 0.5 mM daptomycin in 500 μL of 90:10 H_2O:D_2O.

7.2.2 Preparing daptomycin samples with bicelles.

7.2.2.1 DMPC/DHPC bicelles.

The synthetic lipids DMPC and DHPC (both from Avanti Polar Lipids, Alabaster, AL, USA) were used to prepare the bicelles (Figure 7.5). DMPC was dissolved in 1 mL of chloroform and evaporated under N_2 gas in a round bottom flask, then dried under vacuum for 3 hours. The lipid film was resuspended in 1.5 mL of H_2O and DHPC added to obtain the desired [DMPC]/[DHPC] molar ratios (q). For samples with q = 0.5 and total phospholipid concentration of 15% (w/v) the final sample consisted of 0.5 mM ^{15}N-labeled daptomycin, 189 mM DHPC, 94.5 mM DMPC in 500 μL of 90:10 H_2O:D_2O.

7.2.2.2 DMPC/DMPG/DHPC bicelles.

The synthetic lipid DMPG was also obtained from Avanti Polar Lipids (Alabaster, AL, USA). DMPC and DMPG were dissolved in 1 mL of chloroform and evaporated under N_2 gas in a round bottom flask, then dried under vacuum for 3 hours. The lipid film was resuspended in 1.0 mL of 5.0 mM MOPS pH 6.6 buffer and DHPC added to obtain the desired [DMPC:DMPG]/[DHPC] molar ratios

(q). For samples with q = 0.5 and total phospholipid concentration of 15% (w/v) the final sample consisted of 0.5 mM ^{15}N-labeled daptomycin, 189 mM DHPC, 71.25 mM DMPC, and 71.25 mM DMPG in 500 µL of 5.0 mM MOPS pH 6.6, 90:10 H_2O:D_2O. For samples with q = 0.1 and total phospholipid concentration of 2.0% (w/v) the final sample consisted of 0.5 or 1.0 mM ^{15}N-labeled daptomycin, 40 mM DHPC, 3 mM DMPC and 1 mM DMPG in 500 µL of 5.0 mM MOPS pH 6.6, 90:10 H_2O:D_2O. For samples with q = 0.1 and total phospholipid concentration of 1.0% (w/v) the final sample consisted of 0.5 mM ^{15}N-labeled daptomycin, 20 mM DHPC, 1.5 mM DMPC and 0.5 mM DMPG in 500 µL of 5.0 mM MOPS pH 6.6, 90:10 H_2O:D_2O.

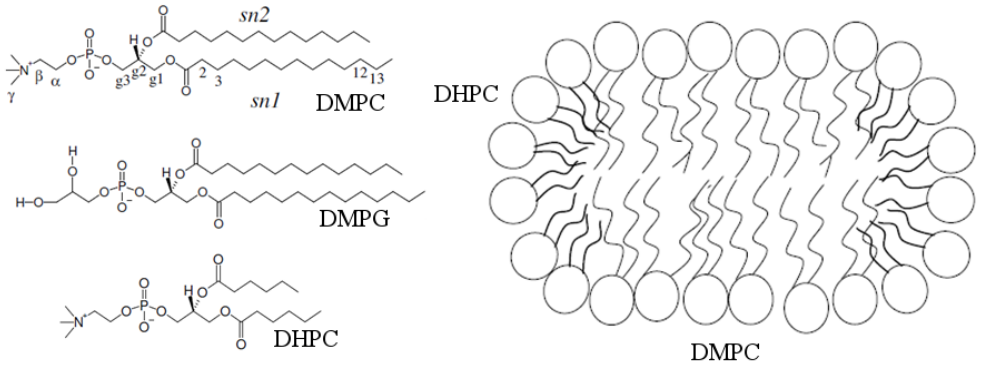

Figure 7.5: Molecular structures of DMPC, DMPG and DHPC, and the schematic representation of a DMPC/DHPC bicelles.

7.2.3 Preparing daptomycin samples with liposomes.

The synthetic lipids 1-palmitoyl-2-oleoyl-*sn*-glycero-3-phosphoethanolamine (POPE) and 1,2-dioleoyl-*sn*-glycero-3-phospho-(1'-*rac*-glycerol) (DOPG) (both from Avanti Polar Lipids, Alabaster, AL, USA) were used to prepare the liposomes (Figure 7.5). POPE and DOPG were dissolved in 1 mL of chloroform in equimolar ratios and evaporated under N_2 gas in a round bottom flask, then dried under vacuum for 3 hours. The lipid film was resuspended in 1.0 mL of 5.0 mM MOPS pH 6.6 buffer. The lipid suspension was extruded through a 100 nm polycarbonate filter 15 times, using a

nitrogen-pressurized extruder to produce the liposomes. The final sample consisted of 0.1 or 0.3 mM ^{15}N-labeled daptomycin, 400 μM POPE/DOPG in 500 μL of 5.0 mM MOPS, 0.5 mM $CaCl_2$, pH 6.6, 90:10 H_2O:D_2O.

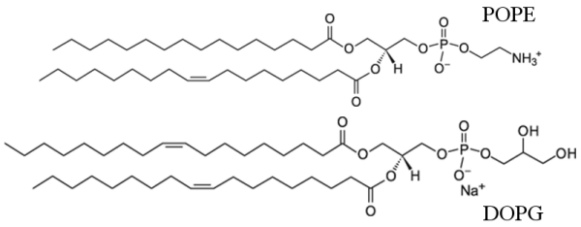

Figure 7.6: Molecular structures of POPE and DOPG.

7.2.4 Preparing ^{19}F modified daptomycin samples with liposomes.

JW2-14, a ^{19}F-modified derivative of daptomycin was provided by the Taylor lab (University of Waterloo). Bicelles were made as described in section 7.2.2.2. Liposomes were made as described in section 7.2.3.1 with either 500 μM DMPC/500 μM DMPG or 400 μM DMPC/500 μM DMPG/100 μM TOCL (lipid tetraoleyl-cardiolipin from Avanti Polar Lipids, Alabaster, AL, USA). The final samples consisted of 0.25 mM JW2-14 in 500 μL of 20 mM HEPES, 150 mM NaCl, pH 7.4, 90:10 H_2O:D_2O with the following: only buffer; DHPC/DMPC/DMPG bicelles; DMPC/DMPG liposomes; or DMPC/DMPG/TOCL liposomes. The samples were examined with no $CaCl_2$ or 0.25 mM $CaCl_2$.

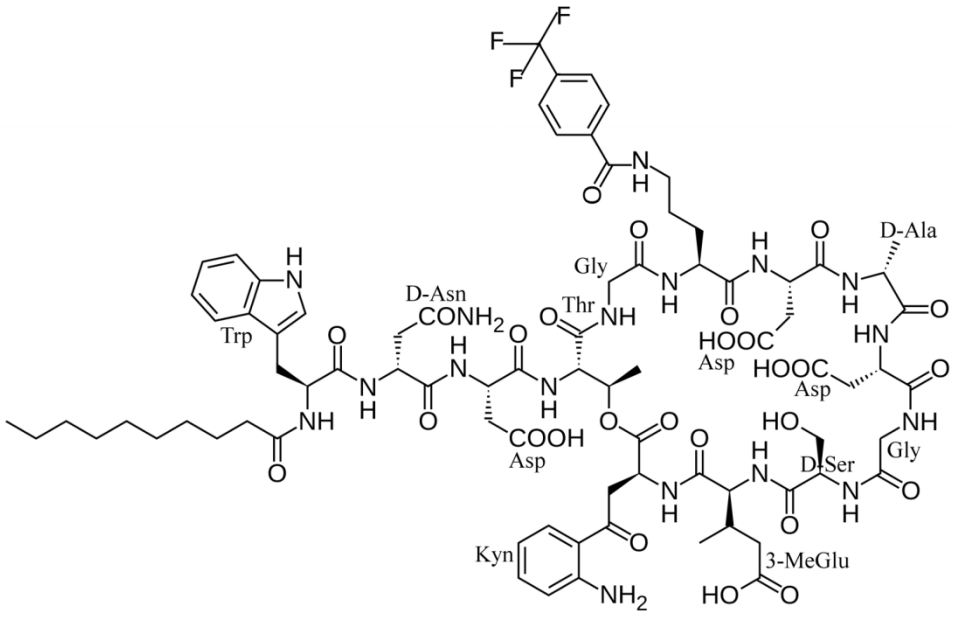

Figure 7.7: Structure of JW2-14, a ^{19}F-modified derivative of daptomycin.
Daptomycin was modified with 4-(Trifluoro-methyl)benzoic acid at the free amino group of Orn6.

7.2.5 In-cell NMR Sample Preparation.

A 10 mL overnight starter culture of *Bacillus subtilis* was grown in LB medium. The culture was centrifuged at 2000 x g for 4 min and the supernatant was discarded. The cell pellet was resuspended in either: 10 mL of fresh LB with 0.1 mM ^{15}N-daptomycin and 1 mM $CaCl_2$; or 10 mL of HBG (HEPES buffered glucose, 20 mM HEPES, 2 g/L glucose, pH 7.1) with 0.1 mM ^{15}N-daptomycin and 1 mM $CaCl_2$. The samples were incubated at 200 RPM, 37°C for 45 min then centrifuged at 2000 x g for 4 min and the supernatant was decanted into a separate tube for further NMR analysis. The cell pellet was resuspended in either 450 µL of fresh LB or HBG, then 50 µL of D_2O was added to each samples. The samples were transferred into 5 mm NMR sample tubes and ^{1}H-^{15}N HSQC and ^{1}H-^{15}N Transverse Relaxation-Optimized Spectroscopy (TROSY) spectra were obtained.

7.2.6 NMR spectroscopy.

^{1}H-^{15}N HSQC, ^{1}H-^{15}N TROSY and 2D HMQC NOESY spectra were recorded at 25^{o}C on Bruker 600 and 700 MHz DRX spectrometers equipped with XYZ-gradients triple-resonance probes (Bruker, Billerica, MA, USA). 1D ^{1}H-decoupled ^{19}F spectra were recorded on Bruker 300 spectrometer equipped with Z-gradient probe (Bruker, Billerica, MA, USA). 2D ^{1}H-^{15}N HMQC-NOESY spectra were acquired with either 50 ms or 120 ms mixing times. Spectra were analyzed using the program CARA (Keller, 2005).

7.3 Results and discussion

The previously determined structures of daptomycin were determined either free in solution or in the presence of DHPC micelles, using only ^{1}H resonance assignments. The structure of daptomycin in the presence of a membrane mimetic that contains PG, which has been shown to be necessary for oligomer formation and activity, has not been previously determined and could be different. In this study solution state NMR experiments were performed with ^{15}N-labelled daptomycin using various membrane mimetic conditions to try and elucidate this structure. The use of ^{15}N-labeled daptomycin will also allow for higher resolution structures to be determined. These experiments were performed with the following membrane mimetics: SDS micelles; DHPC/DMPC bicelles with and without Ca^{2+}; DHPC/DMPC/DMPG bicelles with and without Ca^{2+}; POPE/DOPG liposomes; and on cell experiments with *Bacillus subtilis*.

7.3.1 NMR of Daptomycin with micelles and DHPC/DMPC bicelles.

In order to have bicelles suitable for high resolution solution NMR studies the ratio of long-chain phospholipid (DMPC) relative to short-chain phospholipid (DHPC) must be reduced to obtain a ratio

q, [DMPC/DHPC] < 1. Below this threshold of 1, an isotropic solution of bicelles will be obtained with an estimated diameter of 80-100 Å necessary for solution state NMR (Vold and Prosser, 1996; Vold et al., 1997; Struppe et al., 2000; Whiles et al., 2002; Marcotte and Auger, 2005). For these experiments a total phospholipid concentration of 15% (w/v) is ideal although, total phospholipid concentrations of 1-10% can be used (Struppe and Vold, 1998; Struppe et al., 2000; Whiles et al., 2002). Initially $^{1}H^{15}N$-HSQC experiments were performed on samples consisting of 500 µL of 500 µM ^{15}N labelled daptomycin with SDS micelles and DMPC/DHPC bicelles with a total phospholipid concentration of 15% (w/v) and a q ratio, [DMPC/DHPC] = 0.5 in 5 mM MOPS, pH 6.6, 90:10 H_2O:D_2O with no $CaCl_2$ or 5 mM $CaCl_2$.

Well resolved $^{1}H^{15}N$-HSQC spectra were obtained for daptomycin with SDS and DHPC/DMPC bicelles in the absence of $CaCl_2$ (Figures 7.8A, D and 7.9). Upon comparing the spectra of daptomycin with bicelles to daptomycin with SDS micelles (Figure 7.9) one can see that a couple smaller cross peaks have become visible in the center of the spectrum and that most of the other peaks have experienced a downfield proton shift.

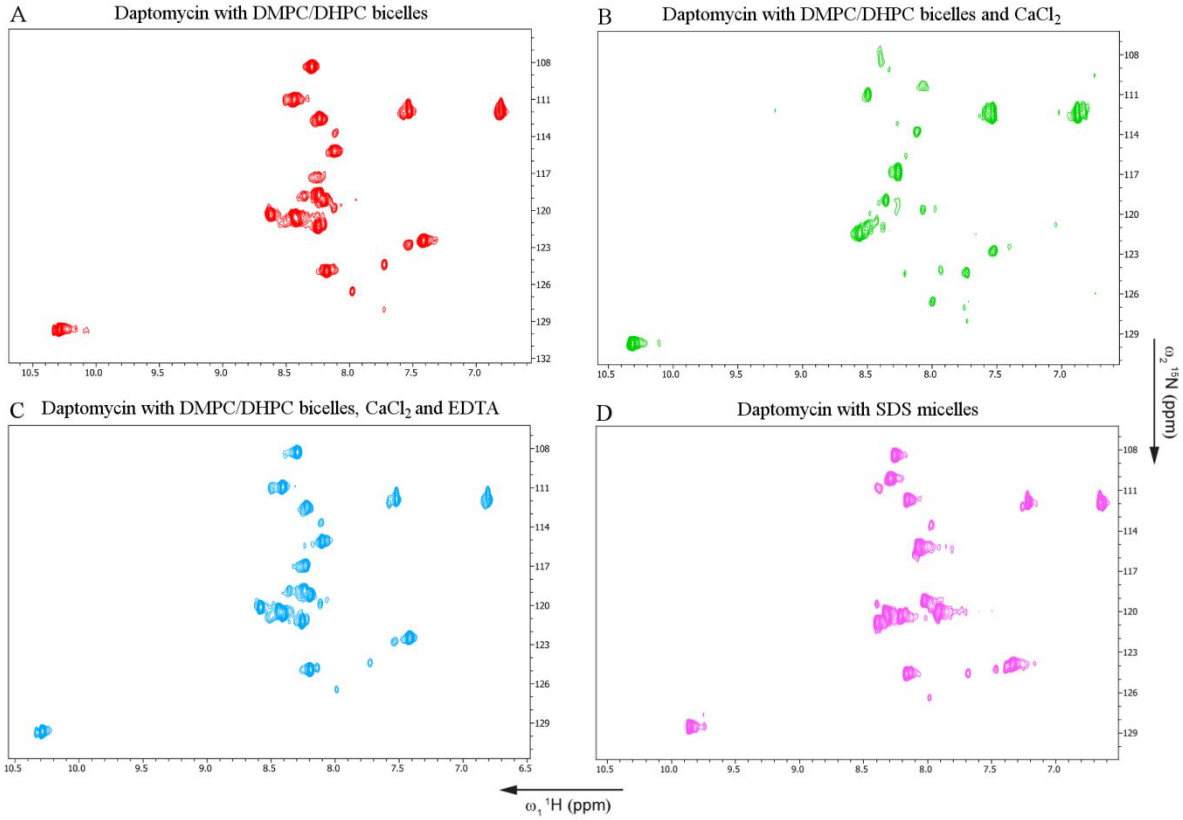

Figure 7.8: ^{1}H-^{15}N HSQC spectra of ^{15}N-labeled Daptomycin with micelles and biecles under various conditions.

^{1}H-^{15}N HSQC spectra of 0.5 mM ^{15}N-labeled daptomycin with 189 mM DMPC/ 94.5 mM DHPC bicelles in 90:10 H_2O:D_2O with (A) no $CaCl_2$, (B) 5 mM $CaCl_2$, and (C) 5 mM $CaCl_2$ and 10 mM EDTA. Total phospholipid w/v = 15% and [DMPC]/[DHPC] = 0.5 was used for all bicelles samples. (D) ^{1}H-^{15}N HSQC spectrum of 0.5 mM ^{15}N-labeled daptomycin with SDS micelles in 90:10 H_2O:D_2O.

When $CaCl_2$ is added to the bicelles sample a few of the strong peaks previously observed have either become weaker or vanished and new smaller cross peaks have arisen (Figure 7.8B and 7.10). This would indicate a change in conformation for daptomycin, which has previously been observed with daptomycin when Ca^{2+} is added in aqueous solution but not observed with the addition of Ca^{2+} in the presence of DHPC micelles (Jung et al., 2004; Scott et al., 2007). This observation

supports the need to perform further NMR experiments with better membrane mimetics to obtain a higher resolution structure of daptomycin.

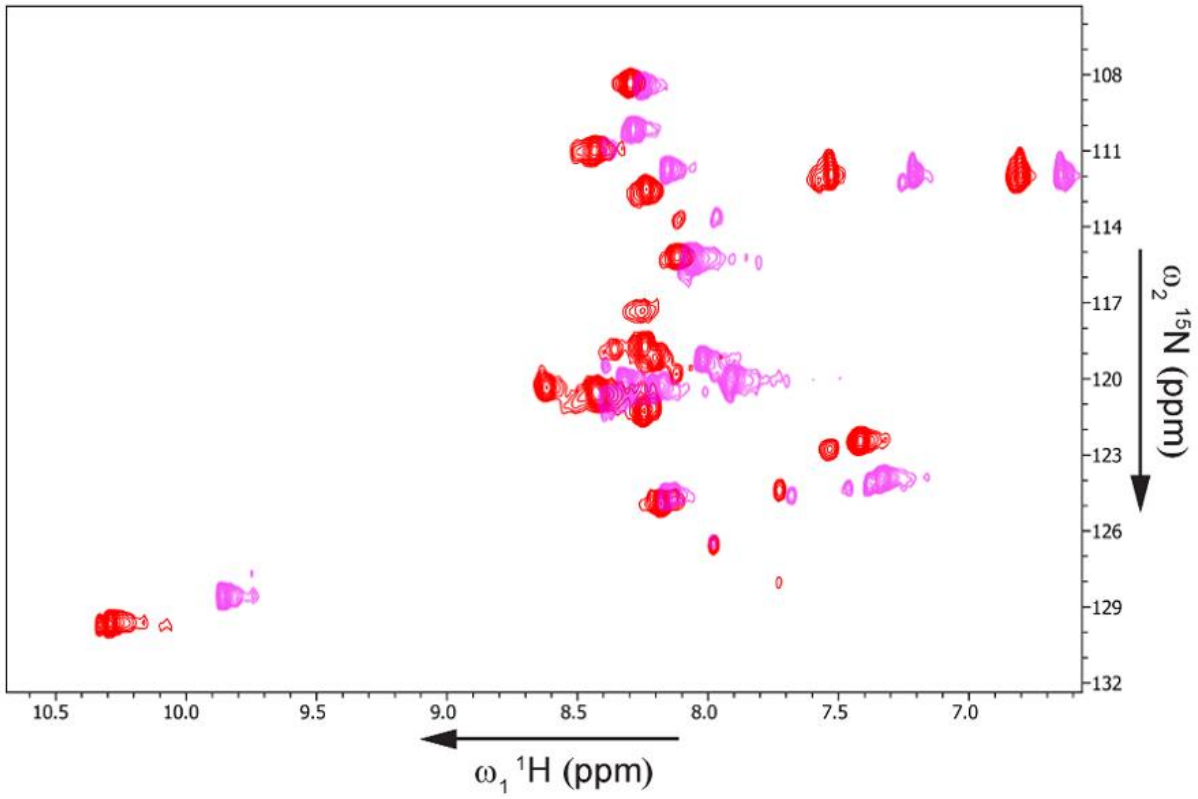

Figure 7.9: Overlay of ^{1}H-^{15}N HSQC spectra of Daptomycin with SDS micelles and DMPC/DHPC bicelles.

^{1}H-^{15}N HSQC spectra of 0.5 mM daptomycin with [DMPC]/[DHPC] = 0.5, total phospholipid w/v = 15% bicelles in 90:10 H_2O:D_2O shown in red and 0.5 mM daptomycin with SDS micelles in 90:10 H_2O:D_2O shown in purple.

The change in spectrum was reversible with the addition of EDTA. When the $^{1}H^{15}N$-HSQC spectra of daptomycin in bicelles with 0.5 mM $CaCl_2$ and with 0.5 mM $CaCl_2$ and 10 mM EDTA were overlaid the cross peaks completely overlap. This suggests that the change in spectrum observed when $CaCl_2$ was added is caused by a conformation change of the residues of daptomycin that interact with the Ca^{2+} ion.

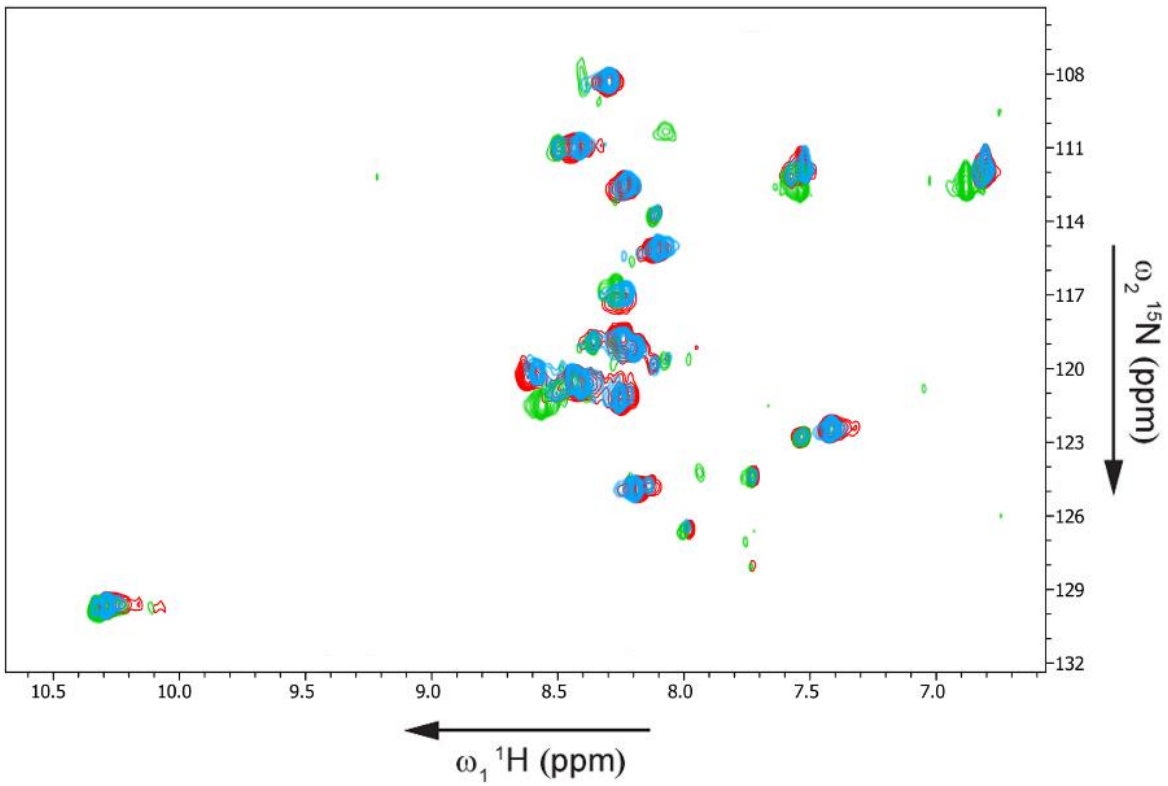

Figure 7.10: Overlay of 1H-15N HSQC spectra of Daptomycin with DMPC/DHPC bicelles under various conditions.

^{1}H-^{15}N HSQC spectra of 0.5 mM daptomycin with [DMPC]/[DHPC] = 0.5, total phospholipid w/v = 15% bicelles in 90:10 H_2O:D_2O shown in red, with 5 mM $CaCl_2$ shown in green and with 5 mM $CaCl_2$ and 10 mM EDTA shown in blue.

7.3.2 ^{31}P NMR of DMPG/DMPC/DHPC bicelles.

These initial experiments prove that NMR studies of daptomycin with bicelles are feasible. The following experiments were performed with bicelles that contain DMPG, which is necessary for daptomycin activity. These bicelles were prepared with DMPC, DMPG and DHPC lipids and had a DMPC to DMPG ratio of 3 to 1 and a DMPG to daptomycin ratio of 1 to 1. The samples were required to have a lower total phospholipid concentration due to only being able to increase the concentration of daptomycin to a maximum of about 1 mM because it was previously shown that a

higher concentration of daptomycin produced broader line widths (Ball et al., 2004) and there is a limited amount of ^{15}N-labeled daptomycin. To ensure bicelles with a lower total phospholipid concentration would be suitable to use for further daptomycin NMR studies ^{31}P NMR experiments were performed.

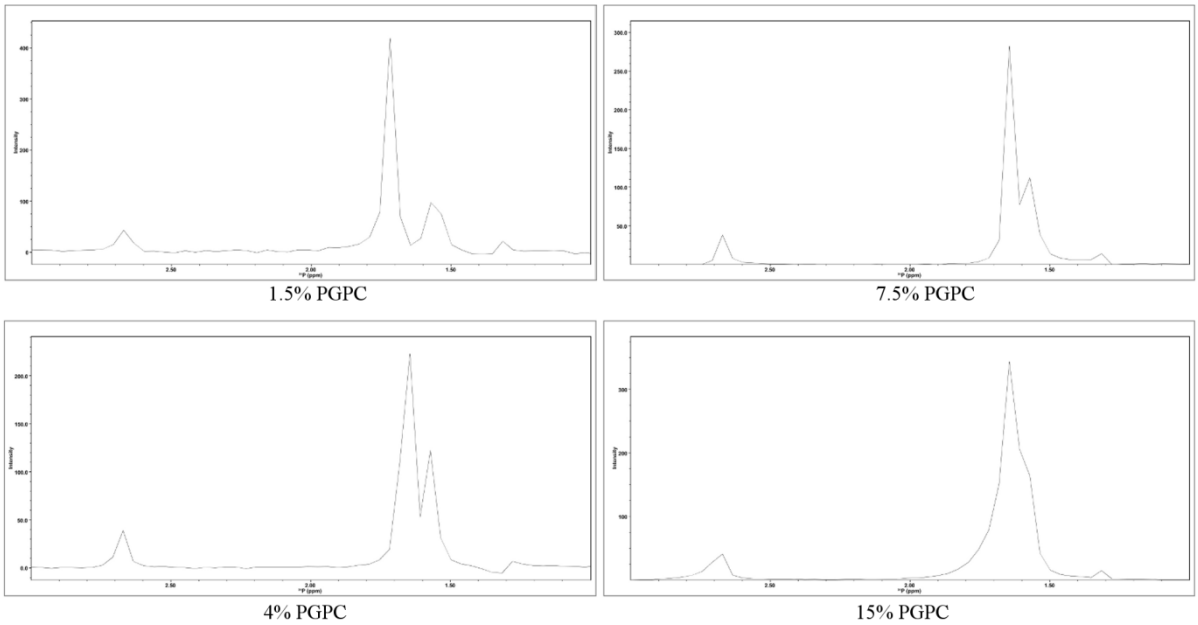

Figure 7.11: ^{31}P NMR spectra of DMPC/DHPC bicelles with q = 0.5 value and varying total phospholipid concentrations.

Bicelles consisted of a total phospholipid w/v of: 1.5 % (19 mM DHPC, 7.125 mM DMPC, 2.375 mM DMPG, q=0.5, [DMPC]:[DMPG] 3:1); 4 % (50.67 mM DHPC, 19 mM DMPC, 6.33 mM DMPG q=0.5, [DMPC]:[DMPG] 3:1); 7.5 % (95 mM DHPC, 33.62 mM DMPC, 11.87 mM DMPG q=0.5, [DMPC]:[DMPG] 3:1); and 15 % (190 mM DHPC, 71.25 mM DMPC, 23.75 mM DMPG q=0.5, [DMPC]:[DMPG] 3:1).

^{31}P spectra were acquired for samples of bicelles with q ratio of 0.5 and varying total phospholipid concentrations (w/v) of 15%, 7.5%, 4% and 1.5%. The spectra show three peaks corresponding to the phosphate from DMPG, DHPC and DMPC. The low intensity downfield peak corresponds to DMPG, which is also present in the lowest concentration in each sample. The largest peak corresponds to DHPC, which is present in the highest concentration in each sample and the peak

upfield of this corresponds to DMPC. These peaks are characteristic for ^{31}P spectra of these lipids in bicelles (Whiles et al., 2002; Triba et al., 2006; Wu et al., 2010). The spectra show little change in the ^{31}P chemical shift observed for DMPG, DHPC and DMPC when the total phospholipid concentration is lowered to concentrations as low as 1.5%, which has been seen by other studies (Struppe and Vold, 1998; Struppe et al., 2000; Whiles et al., 2002). Thus reducing the total phospholipid concentration of the bicelles in future experiments should not be an issue.

7.3.3 NMR of Daptomycin with DMPG/DMPC/DHPC bicelles.

NMR experiments were performed on samples of daptomycin with DMPG/DMPC/DHPC bicelles. As mentioned above the experiments were done with a 1:1 ratio of PG to daptomycin thus a lower concentration of DMPG has to be used. To maintain a high enough total phospholipid concentration required for high resolution NMR studies a higher amount of DHPC was used which resulted in a lower q value for the sample. The samples contained either 0.5 or 1.0 mM ^{15}N-labeled daptomycin with bicelles that have a [DMPC:DMPG/DHPC] q ratio of 0.1 and total phospholipid concentration of 1.0% and 2.0% (w/v). $^{1}H^{15}N$-HSQC experiments were performed on these samples with no $CaCl_2$ present, 0.25 mM $CaCl_2$ (1:2 ratio $CaCl_2$:Dap) and 0.5 mM $CaCl_2$ (1:1 ratio $CaCl_2$:Dap).

A well resolved $^{1}H^{15}N$-HSQC spectrum was obtained in the absence of $CaCl_2$ (Figure 7.12A). When this sample is compared to the Ca^{2+}-free DMPC/DHPC daptomycin sample previously determined, the two spectra overlay extremely well, however, there is a new weak cross peak that is observed at the bottom left of the spectrum (Figure 7.14).

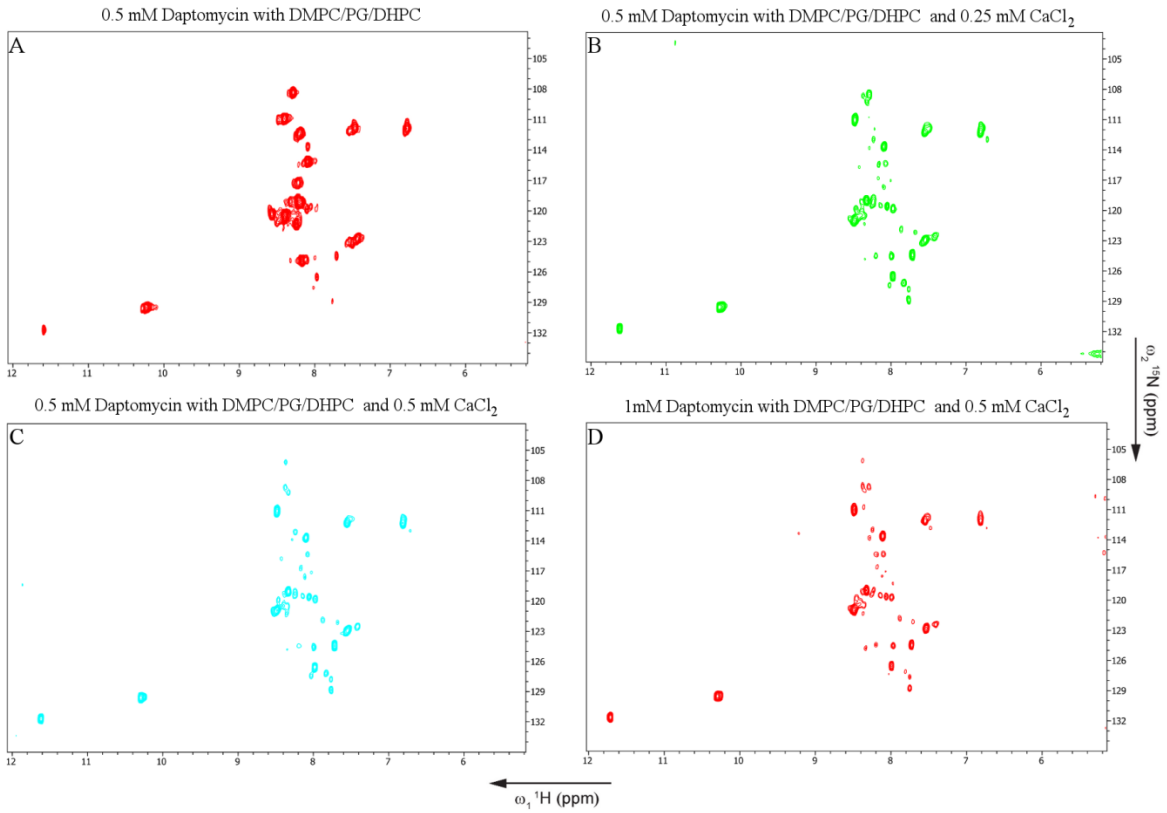

Figure 7.12: ^{1}H-^{15}N HSQC spectra of daptomycin with DMPC/DMPG/DHPC bicelles under various conditions.

^{1}H-^{15}N HSQC spectra of 0.5 mM daptomycin in 20 mM DHPC, 1.5 mM DMPC, 0.5 mM DMPG bicelles with (A) no $CaCl_2$; (B) 0.25 mM $CaCl_2$; (C) and 0.5 mM $CaCl_2$. (D) ^{1}H-^{15}N HSQC spectrum of 1 mM daptomycin with 40 mM DHPC, 3 mM DMPC, 1 mM DMPG bicelles in 90:10 H_2O:D_2O and 0.5 mM $CaCl_2$. Total phospholipid w/v = 1.0% for A-C and 2.0% for D and [DMPC/DMPG]/[DHPC] q value of 0.1 was used for all bicelles samples.

When $CaCl_2$ is added in a 1:2 ratio of $CaCl_2$:Dap a few of the strong peaks previously observed have either become weaker or vanished and new smaller cross peaks have arisen, as was observed with the DMPC/DHPC bicelles, and the peak from the bottom left of the spectrum has increased in intensity (Figure 7.12B and 7.13). In this experiment the signal to noise has become worse and a precipitate had formed in the sample. When this spectrum is compared to that obtained for daptomycin with DMPC/DHPC bicelles (Figure 7.14) there are more cross peaks visible in the PGPC bicelles, however, all the cross peaks visible in the PC bicelles sample overlay very well with

those of the PGPC bicelles. This indicates that daptomycin adopts the same predominate structure in both PGPC bicelles and PC bicelles, and suggests that there are other less predominate conformations present in both samples, possibly those of daptomycin alone, Ca^{2+}-conjugated daptomycin and in the PGPC bicelles a Ca^{2+}-conjugated daptomycin interacting with the PGPC bicelles.

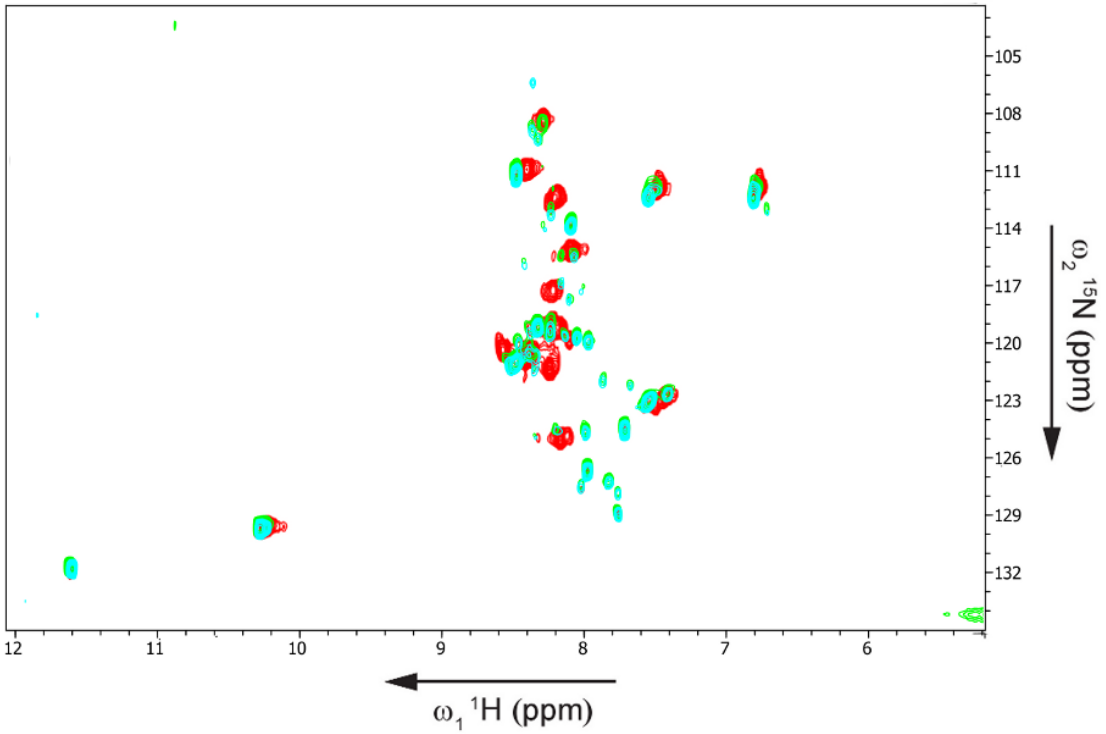

Figure 7.13: Overlay of ^{1}H-^{15}N HSQC spectra of daptomycin with DMPC/DMPG/DHPC bicelles under various conditions.

^{1}H-^{15}N HSQC spectrum of 0.5 mM daptomycin with [DMPC/DMPG]/[DHPC] = 0.1, total phospholipid w/v = 1.0 % bicelles in 90:10 H_2O:D_2O shown in red, with 0.25 mM $CaCl_2$ shown in green and with 0.5 mM $CaCl_2$ shown in blue.

When $CaCl_2$ was added in a 1:1 ratio $CaCl_2$:Dap a precipitate formed before the $^{1}H^{15}N$-HSQC experiment was performed, and a spectrum was obtained that was similar to the 1:2 ratio $CaCl_2$:Dap one (Figures 7.12C and 7.13). The formation of a precipitate makes it difficult to obtain useful NMR data to facilitate a structure calculation and has been observed in other studies (Jung et al., 2004; Scott et al., 2007).

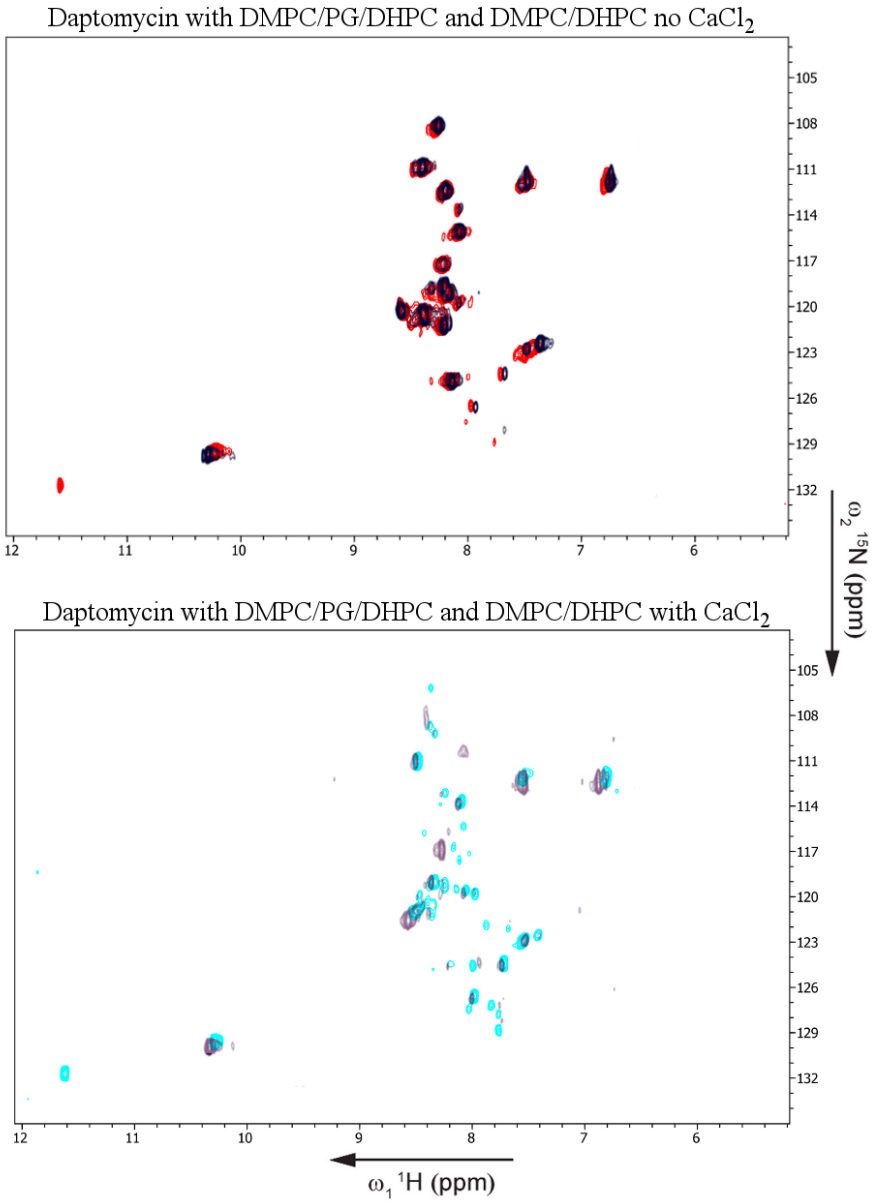

Figure 7.14: Overlay of ^{1}H-^{15}N HSQC spectra of daptomycin with DMPC/DMPG/DHPC bicelles and DMPC/DHPC bicelles under various conditions.

(A) ^{1}H-^{15}N HSQC spectrum of 0.5 mM daptomycin with [DMPC/DMPG]/[DHPC] = 0.1, total phospholipid w/v = 1.0 % bicelles in 90:10 H_2O:D_2O shown in red and 0.5 mM daptomycin with [DMPC]/[DHPC] = 0.5, total phospholipid w/v = 15% bicelles in 90:10 H_2O:D_2O shown in black. (B) ^{1}H-^{15}N HSQC spectrum of 0.5 mM daptomycin with [DMPC/DMPG]/[DHPC] = 0.1, total phospholipid w/v = 1.0 % bicelles in 90:10 H_2O:D_2O, 0.5 mM $CaCl_2$ shown in blue and 0.5 mM daptomycin with [DMPC]/[DHPC] = 0.5, total phospholipid w/v = 15% bicelles in 90:10 H_2O:D_2O 5 mM $CaCl_2$ shown in purple.

In order to obtain NMR data for a structure calculation longer NMR experiments, such as 2D and 3D NOESY and TOCSY, must be acquired. To obtain these various spectra in a reasonable amount of time a more concentrated sample of ^{15}N-labeled daptomycin must be used. An ^{1}H-^{15}N HSQC spectrum of 1 mM daptomycin with 40 mM DHPC, 3 mM DMPC, 1 mM DMPG bicelles in 90:10 H_2O:D_2O and 0.5 mM $CaCl_2$, total phospholipid w/v = 2.0% and [DMPC/DMPG]/[DHPC] q value of 0.1 was acquired. Upon comparison of the spectrum obtained (Figure 7.12D) with the previous daptomycin DMPC/DMPG/DHPC spectrum (Figure 7.12B) it can be seen that they are very similar. This sample was chosen to acquire the future experiments.

2D HMQC NOESY spectra were obtained for samples of 1 mM daptomycin with 40 mM DHPC, 3 mM DMPC, 1 mM DMPG bicelles in 90:10 H_2O:D_2O and 0.5 mM $CaCl_2$. Two NOESY experiments were performed: one with 50 ms mixing time; and one with 120 ms mixing time. The spectra acquired did not produce any useful information as no NOE correlations were observable. Also at the completion of both experiments both samples has sizable precipitates present.

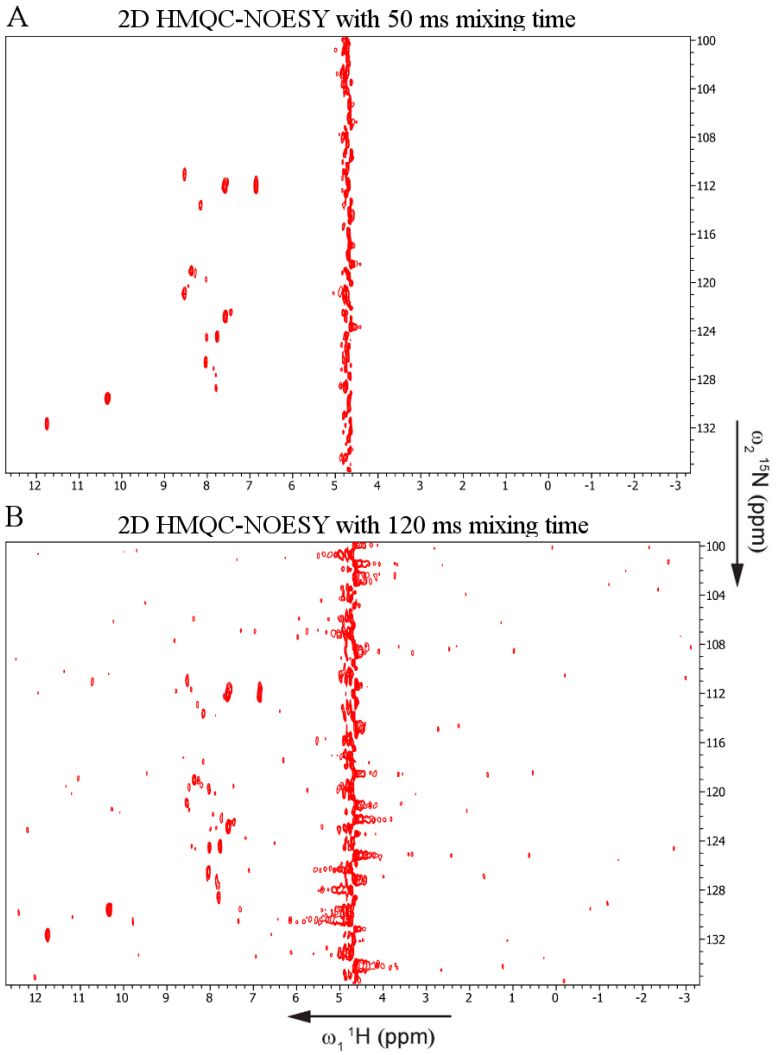

Figure 7.15: 2D ^{1}H-^{15}N HMQC-NOESY spectra of daptomycin with DMPC/DMPG/DHPC bicelles.

^{1}H-^{15}N HMQC-NOESY spectrum of 1 mM daptomycin with 40 mM DHPC, 3 mM DMPC, 1 mM DMPG bicelles in 90:10 H_2O:D_2O and 0.5 mM $CaCl_2$ with (A) 50 ms mixing time and (B) 120 ms mixing time. Total phospholipid w/v = 2.0% and [DMPC/DMPG]/[DHPC] q value of 0.1 was used for all bicelles samples.

7.3.4 NMR of daptomycin with liposomes.

^{1}H^{15}N-HSQC experiments were performed on samples consisting of 500 µL of either 100 or 300 µM

^{15}N labelled daptomycin and 0.5 mM $CaCl_2$ with 400 µM POPE/DOPG liposomes, however, a signal

could not be obtained. The spectra obtained also had poor signal to noise and a large white precipitate was formed by the end of the experiment. The lack of signal is probably due to the large size of the liposomes, which would have a reorientation time that is too long on the NMR timescale (Marcotte and Auger, 2005; Robinson et al., 2012).

7.3.5 NMR of ^{19}F-labeled daptomycin in bicelles and liposomes.

A ^{19}F-labeled daptomycin sample was provided by the Taylor lab (University of Waterloo) which allowed for the acquisition of ^{19}F NMR spectra. ^{19}F NMR spectra were acquired for the modified daptomycin, JW2-14 sample (Figure 7.7) in buffer, DHPC/DMPC bicelles, DMPC/DMPG liposomes and DMPC/DMPG/TOCL liposomes, each with and without Ca^{2+}. TOCL was used in this study because it was found that daptomycin resistant bacteria contain a mutation that enhances cardiolipin synthase activity and its presence could be responsible for preventing membrane translocation of daptomycin oligomers (Palmer et al., 2011; Davlieva et al., 2013; Zhang et al., 2014a)

For every sample in the absence of $CaCl_2$ two ^{19}F signals were observed at 62.8 and 75.7 ppm (Figure 7.14A, C, E and G). Since JW2-14 only contains one F_3 moiety on the modified ornithine residue, these two peaks could be indicative of two distinct conformations of daptomycin. The spectra obtained of JW2-14 with $CaCl_2$ in buffer only and with PGPC bicelles in buffer were very similar to those obtained in the absence of $CaCl_2$ (Figure 7.16A- D). However, the spectra obtained of JW2-14 with $CaCl_2$ in PCPG liposomes and PCPGCL liposomes only had the peak at 75.7 ppm observable (Figure 7.14F and H).

Taking this information together one can see that the addition of Ca^{2+} to samples of JW2-14 in liposomes shifts the equilibrium towards one conformation.

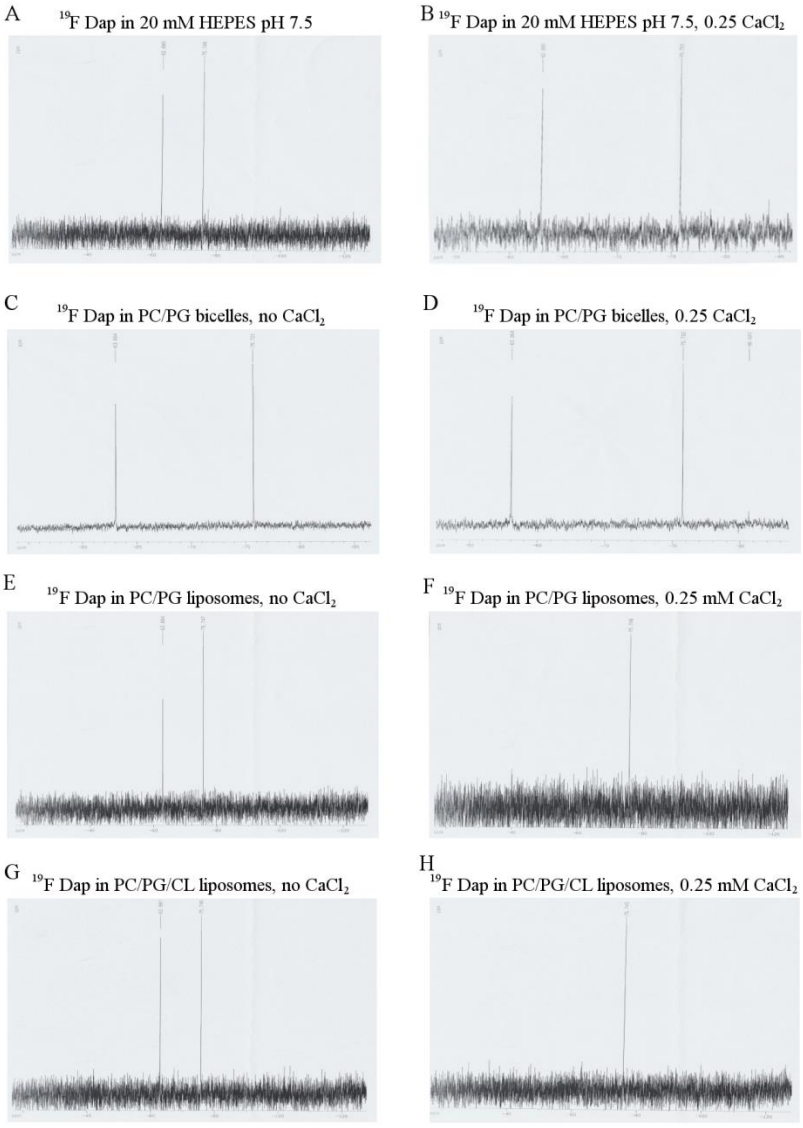

Figure 7.16: ^{19}F spectra of JW2-14 with PC/PG bicelles and liposomes and PC/PG/CL liposomes under various conditions.

All spectra acquired contained 0.25 mM JW2-14 (^{19}F-daptomycin) in 20 mM HEPES, 100 mM NaCl, pH 7.4 buffer with 90:10 H_2O:D_2O with: (A) buffer only; (B) buffer with 0.25 mM $CaCl_2$; (C)) 40 mM DHPC/3 mM DMPC/1 mM DMPG bicelles; (D) 40 mM DHPC/3 mM DMPC/1 mM DMPG bicelles with 0.25 mM $CaCl_2$; (E) 500 μM DMPC and 500 μM DMPG liposomes; (F) 500 μM DMPC and 500 μM DMPG liposomes with 0.25 mM $CaCl_2$; (G) 400 μM DMPC/500 μM DMPG/100 μM TOCL liposomes; and (H) 400 μM DMPC/500 μM DMPG/100 μM TOCL liposomes with 0.25 mM $CaCl_2$. Total phospholipid w/v = 2.0% and [DMPC/DMPG]/[DHPC] q value of 0.1 was used for C and D.

7.3.6 On-cell NMR.

On cell NMR experiments (Reckel et al., 2007; Robinson et al., 2012) with ^{15}N-labelled daptomycin and *Bacillus subtilis* cells were tried also. *Bacillus subtilis* cells were chosen to perform these experiments because it had been previously shown that daptomycin readily forms oligomers on these cells and has high activity (Zhang et al., 2013). ^{1}H^{15}N-HSQC and ^{1}H^{15}N-TROSY experiments were performed on fresh cells with ^{15}N-labelled daptomycin bound that were prepared as described above (7.2.5); however, a signal could not be obtained for either experiment, thus no structural information could be obtained. This could be due to the size of the cell which would be too large for NMR, having a very long rotational correlation time because of slow tumbling, or because daptomycin binds in many different conformations.

^{1}H^{15}N-HSQC and ^{1}H^{15}N-TROSY experiments were performed on the supernatant from the daptomycin incubation to determine if the lack of signal obtained above was due to the daptomycin not associating with the bacterial cells. A weak signal was obtained with the ^{15}N-TROSY experiment (Figure 7.17). Since this signal was so weak it was concluded that most of the daptomycin must be bound to the *Bacillus subtilis* cells, however, because of the size and differences in population of daptomycin per cell no on cell signal could be obtained.

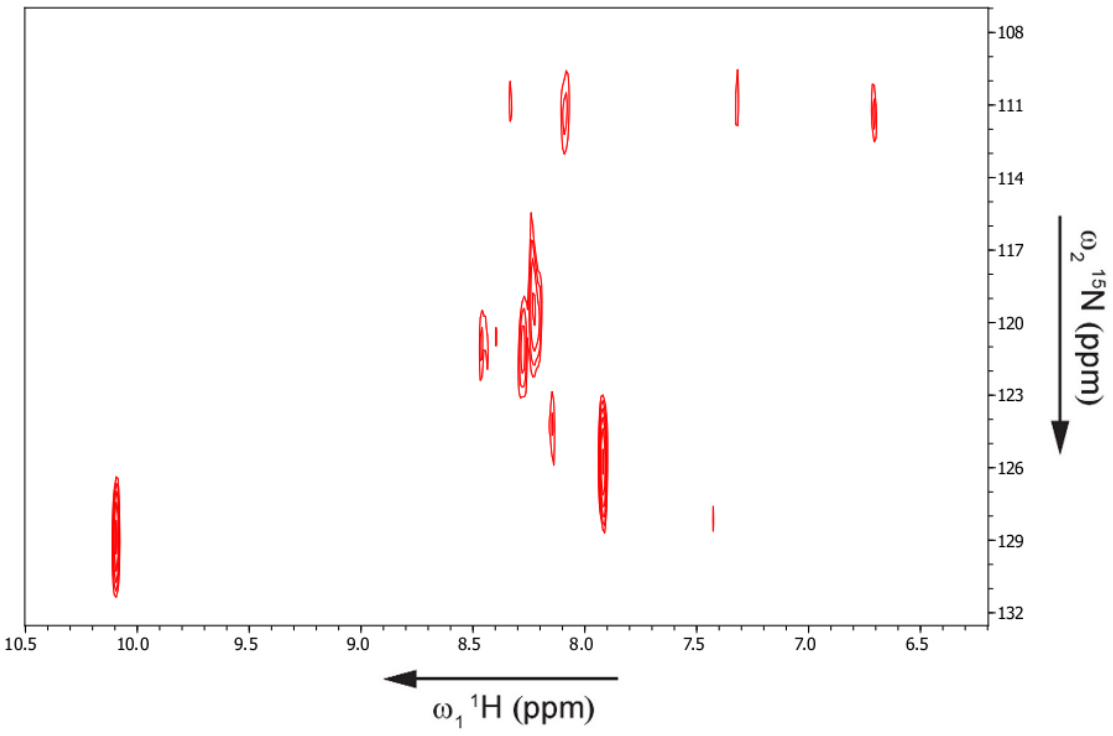

Figure 7.17: ^{1}H-^{15}N TROSY spectrum of the supernatant of daptomycin incubated with *Bacillus subtilis*.

7.4 Conclusion

It is clear from these studies that at this time high resolution solution state NMR studies cannot provide enough information for a full structure determination due to sample aggregation and experimental size limitation. However, the aggregation of daptomycin with PCPG bicelles and liposomes in the presence of Ca^{2+} would not be a problem for solid-state NMR experiments. Preliminary experiments performed at the University of Guelph have produced some promising results and could be an avenue further explored to elucidate a structure. To complete those studies it would be advantageous to obtain a doubly isotopically ^{13}C,^{15}N-labeled daptomycin sample. A high resolution structure of the oligomerization of daptomycin in the presence of Ca^{2+} and PG containing membrane mimetic would be very valuable to better understand the mode of action of daptomycin.

Chapter 8

Summary and future work

8.1 Summary

In chapter 2, the interactions of CaM with the peptides based on the eNOS CaM binding domain or the eNOS CAM binding domain phosphorylated at Thr495 were investigated at various free Ca^{2+} concentrations. We determined through the use of NMR spectroscopy, fluorescence and ITC that this interaction was very similar at saturating Ca^{2+} concentrations. However, at the lower Ca^{2+} concentration of 225nM, near physiological Ca^{2+} levels, no significant binding of CaM to eNOSpThr495 is observed by either method, whereas CaM is binding to nonphosphoryated eNOS. The calcium affinity of the CaM-eNOS peptide complex is reduced due to the Thr495 phosphorylation, and this leads to weaker binding at low physiological calcium concentrations. Our results indicate there is a diminished propensity for the formation of an α-helix by the peptide in combination with electrostatic repulsion that may account for the diminished CaM-dependent activation of the eNOS enzyme under low physiological calcium concentrations.

In chapter 3, we present the complete backbone NMR resonance assignments of C-lobe Ca^{2+}-replete and deplete CaM_{12}, N-lobe Ca^{2+}-replete and deplete CaM_{34}, CaM_{1234} in the absence of Ca^{2+}, and N-lobe Ca^{2+}-replete CaM_{34} with the iNOS peptide. These assignments are necessary to solve the solution structures of these Ca^{2+}-deficient CaM mutants and compare them to known structures of apoCaM or to perform any other NMR studies on these mutants. Furthermore, this method will allow for the quick structural characterization of other CaM or CaM mutants interacting with various NOS

peptides and provides the basis for a detailed study of CaM-NOS interaction dynamics using ^{15}N relaxation methods.

In Chapter 4, the first study to present NMR structural and dynamics data of the CaM-NOS complexes at free Ca^{2+} concentrations that are in the resting and elevated intracellular Ca^{2+} concentration range was shown. These results demonstrate the importance of performing experiments on CaM-NOS interactions at Ca^{2+} concentrations that correspond to Ca^{2+} levels relevant to the regulation of NOS by CaM *in vivo*. We show that when experiments are performed at Ca^{2+} concentrations that are typically used in the literature, i.e. saturating Ca^{2+} concentrations, the CaM-NOS systems are less dynamic than at Ca^{2+} concentrations corresponding to basal and elevated cellular levels. The studies of the CaM-NOS complexes that were carried out at saturated Ca^{2+} concentrations miss differences in dynamics that are only detectable at physiological Ca^{2+} levels. Thus, studies involving CaM interactions with NOS at saturating Ca^{2+} concentrations don't allow the investigator to see the contributions of the dynamics present in the CaM-NOS complexes. This illustrates the importance of analyzing these complexes at Ca^{2+} concentrations that are within the physiological range in order to fully understand how NOS is regulated by CaM interactions *in vivo*.

In chapter 5, the solution structure of the complex of the eNOS peptide with CaM at 225 nM Ca^{2+} concentration was determined, and along with the previous amide exchange and internal mobility results, show that the residues of CaM interacting with eNOS' 1-5-8-14 anchoring residues have a strong interaction at the 225 nM free Ca^{2+} concentration, which keeps the complex intact, while the rest of the residues of the CaM protein are able to fluctuate or "breathe". Comparing the two lobes of CaM, the residues of the C-lobe display a more rigid structure, indicating a stronger interaction with the eNOS peptide to hold the complex together, while the N-lobe is more dynamic and loosely associated to the eNOS peptide. This is the first study to determine an NMR structure of

the CaM-eNOS complex at a free Ca^{2+} concentration that is a physiologically relevant elevated intracellular Ca^{2+} concentration. This structure provides further evidence that the C-lobe of CaM binds first to the N-terminus of eNOS' CaM-binding domain and possibly part of the heme domain, while loosely associating to the C-terminus of eNOS' CaM-binding domain when the intracellular Ca^{2+} concentration is elevated to 225 nM. And possibly as the intracellular Ca^{2+} concentration increases the N-lobe then binds Ca^{2+} and becomes tightly bound to the C-terminus of eNOS' CaM-binding domain, allowing for the possibility of a bridge to form between CaM and the FMN domain, which would induce a shift to the FMN-heme electron transfer conformation to allow efficient electron transfer in the NOS enzymes.

In chapter 6, the use of mutations of Asp in position 1 in the EF hands of CaM to disable Ca^{2+}-binding was shown to cause slight structural perturbations through the use of NMR spectroscopy. The structure determination of CaM_{1234} revealed that the mutation of Asp to Ala causes the EF hand loops to adopt perturbed conformations when compared to apoCaM. The structure also displayed a less stable C-lobe compared to N-lobe as previously observed for apoCaM. To investigate if these mutations also perturb the structure of CaM bound to a target peptide the structure of CaM_{34} bound to the iNOS peptide was determined. The mutation of Asp to Ala causes the Ca^{2+} binding loop regions in the C-lobe EF hands to adopt a conformation resembling apoCaM, which causes local structural changes, affecting the loop region between EF hands III and IV, and long range structural conformation changes, affecting the loop region between EF hands I and II and helix B. This study provides structural evidence of changes that are present in CaM mutants with mutations at Asp in position 1 of the EF hand.

8.2 Future work

8.2.1 Binding kinetics of CaM interacting with the eNOS CaM binding domain at 225 nM free Ca^{2+}.

SPR experiments involving CaM and the eNOS peptide have been undertaken in the lab to compare the binding kinetics at saturating Ca^{2+} and 225 nM free Ca^{2+} concentrations. This work will further complement the solution structure of CaM with eNOS at 225 nM Ca^{2+} to characterize this interaction and determine if there are any differences in binding kinetics upon the increase in Ca^{2+} concentrations.

8.2.2 Higher resolution solution structure of CaM_{1234} and solution structure of CaM_{12} bound to the eNOS CaM binding domain peptide.

To further investigate the possible structural perturbations induced by the 4 EF hand mutations in CaM_{1234} a higher resolution structure could be obtained. This would not require much more work to accomplish and could be facilitated by the addition of $^{13}C_{ali}$ and $^{13}C_{aromatic}$ NOESY experiments to acquire more structure constraints. In chapter 5 a structure of CaM bound to the eNOS CaM binding domain peptide was determined at 225 nM free Ca^{2+}. This structure determined that CaM binds to the eNOS peptide with a Ca^{2+}-replete C-lobe and Ca^{2+}-deplete N-lobe, through interactions predominately in CaM's C-lobe. However, some contacts were observed between the Ca^{2+}-deplete N-lobe and the peptide. The CaM_{12}-eNOS complex structure should be similar to this structure, however, differences may be found due to the N-lobe EF hand mutations. This could provide evidence of whether or not CaM_{12} is a suitable substitute for Ca^{2+}-free N-lobe CaM studies.

8.2.3 NMR structural studies of CaM interacting with nNOS at low free Ca^{2+} concentrations.

The structural and dynamic interaction of CaM with eNOS was performed in this thesis, a similar investigation of CaM with nNOS could be done to see if nNOS has the same characteristics at low Ca^{2+} concentrations.

8.2.4 NMR structural studies of CaM interacting with holo nNOS.

Currently there is no NMR structural data of CaM interacting with the holo-NOS isoforms. Preliminary work in the lab has determined that a large enough quantity of holo-nNOS can be produced to facilitate NMR experiments. However, since the complex of CaM with nNOS is extremely large, conventional ^{1}H-^{15}N HSQC experiments have not been able to produce useful spectra. Preliminary ^{15}N TROSY experiments have shown that structural data is possible with this method, but will require a purer NOS enzyme and possibly higher NMR field strength. This would allow us to determine which residues of CaM interact with regions of the holoNOS enzymes other than the CaM-binding domains though chemical shift changes between the CaM-NOS peptides and CaM-holoNOS spectra. This could lay the ground work for NMR experiments using methionine labeled NOS, which could probe for structural changes in NOS in the absence and presence of CaM and Ca^{2+}.

Appendix A

NMR pulse program information

^{15}N-HSQC:
1 "/opt/xwinnmr/exp/stan/nmr/lists/pp/hsqcetf3gpsi"
;hsqcetf3gpsi
;avance-version (02/07/15)
;HSQC
;2D H-1/X correlation via double inept transfer
; using sensitivity improvement
;phase sensitive using Echo/Antiecho-TPPI gradient selection
;with decoupling during acquisition
;using trim pulses in inept transfer
;using f3 - channel
;A.G. Palmer III, J. Cavanagh, P.E. Wright & M. Rance, J. Magn.
; Reson. 93, 151-170 (1991)
;L.E. Kay, P. Keifer & T. Saarinen, J. Am. Chem. Soc. 114,
; 10663-5 (1992)
;J. Schleucher, M. Schwendinger, M. Sattler, P. Schmidt, O. Schedletzky,
; S.J. Glaser, O.W. Sorensen & C. Griesinger, J. Biomol. NMR 4,
; 301-306 (1994)

HNCA:
1 "/opt/xwinnmr/exp/stan/nmr/lists/pp/hncagp3d"
;hncagp3d
;avance-version (02/05/31)
;HNCA
;3D sequence with
; inverse correlation for triple resonance using multiple
; inept transfer steps
; F1(H) -> F3(N) -> F2(Ca,t1) -> F3(N,t2) -> F1(H,t3)
;on/off resonance Ca and C=O pulses using shaped pulse
;phase sensitive (t1)
;phase sensitive using Echo/Antiecho gradient selection (t2)
;using constant time in t2
;(use parameterset HNCAGP3D)
;S. Grzesiek & A. Bax, J. Magn. Reson. 96, 432 - 440 (1992)
;(J. Schleucher, M. Sattler & C. Griesinger, Angew. Chem. Int. Ed. 32,
; 1489-1491 (1993))
;(L.E. Kay, G.Y. Xu & T. Yamazaki, J. Magn. Reson. A109, 129-133 (1994))
prosol relations=<triple>

HNcoCA:
1 "/opt/xwinnmr/exp/stan/nmr/lists/pp/hncocagp3d"
;hncocagp3d
;avance-version (03/08/05)
;HN(CO)CA
;3D sequence with
; inverse correlation for triple resonance using multiple
; inept transfer steps
; F1(H) -> F3(N) -> F2(C=O) -> F2(Ca,t1)
; -> F2(C=O) -> F3(N,t2) -> F1(H,t3)
;on/off resonance Ca and C=O pulses using shaped pulse
;phase sensitive (t1)
;phase sensitive using Echo/Antiecho gradient selection (t2)
;using constant time in t2
;(use parameterset HNCOCAGP3D)
;S. Grzesiek & A. Bax, J. Magn. Reson. 96, 432 - 440 (1992)
;(L.E. Kay, G.Y. Xu & T. Yamazaki, J. Magn. Reson. A109, 129-133 (1994))
prosol relations=<triple>

CBCAcoNH:
1 "C:/Bruker/XWIN-NMR/exp/stan/nmr/lists/pp/cbcaconhgpwg3d"
;cbcaconhgpwg3d
;avance-version (02/05/31)
;CBCACONH
;3D sequence with
; inverse correlation for triple resonance using inept transfer steps
; F1(H) -> F2(Caliph.,t1 -> Ca) -> F2(C=O) -> F3(N,t2) -> F1(H,t3)
;on/off resonance Ca and C=O pulses using shaped pulse
;phase sensitive (t1)
;phase sensitive (t2)
;using constant time in t1
;using constant time in t2
;water suppression using watergate sequence
;(use parameterset CBCACONHGPWG3D)
;S. Grzesiek & A. Bax, J. Biomol. NMR 3, 185-204 (1993)
;(D.R. Muhandiram & L.E. Kay, J. Magn. Reson. B 103, 203-216 (1994))
prosol relations=<triple>

^{13}C-NOESY HSQC:
#1 "C:/Bruker/XWIN-NMR/exp/stan/nmr/lists/pp/noesyhsqcetgp3d"
;noesyhsqcetgp3d
;avance-version (02/07/15)
;NOESY-HSQC
;3D sequence with
; homonuclear correlation via dipolar coupling
; dipolar coupling may be due to noe or chemical exchange.
; H-1/X correlation via double inept transfer

; using sensitivity improvement
;phase sensitive (t1)
;phase sensitive using Echo/Antiecho-TPPI gradient selection (t2)
;using trim pulses in inept transfer
;with decoupling during acquisition
;using shaped pulses for inversion on f2 - channel
;(use parameterset NOESYHSQCETGP3D)
;A.L. Davis, J. Keeler, E.D. Laue & D. Moskau, J. Magn. Reson. 98,
; 207-216 (1992)
;A.G. Palmer III, J. Cavanagh, P.E. Wright & M. Rance, J. Magn.
; Reson. 93, 151-170 (1991)
;L.E. Kay, P. Keifer & T. Saarinen, J. Am. Chem. Soc. 114,
; 10663-5 (1992)
;J. Schleucher et al., Angew. Chem. 114(10), 1518 (1993)

^{15}N-NOESY HSQC:
1 "C:/Bruker/XWIN-NMR/exp/stan/nmr/lists/pp/noesyhsqcfpf3gpsi3d"
;noesyhsqcfpf3gpsi3d
;avance-version (03/06/18)
;NOESY-HSQC
;3D sequence with
; homonuclear correlation via dipolar coupling
; dipolar coupling may be due to noe or chemical exchange
; H-1/X correlation via double inept transfer
; using sensitivity improvement
;phase sensitive (t1)
;phase sensitive using Echo/Antiecho-TPPI gradient selection (t2)
;with decoupling during acquisition
;using flip-back pulse
;using f3 - channel
;(use parameterset NOESYHSQCFPF3GPSI3D)
;O. Zhang, L.E. Kay, J.P. Olivier & J.D. Forman-Kay,
; J. Biomol. NMR 4, 845 - 858 (1994)
;A.G. Palmer III, J. Cavanagh, P.E. Wright & M. Rance, J. Magn.
; Reson. 93, 151-170 (1991)
;L.E. Kay, P. Keifer & T. Saarinen, J. Am. Chem. Soc. 114,
; 10663-5 (1992)
;J. Schleucher, M. Schwendinger, M. Sattler, P. Schmidt, O. Schedletzky,
; S.J. Glaser, O.W. Sorensen & C. Griesinger, J. Biomol. NMR 4,
; 301-306 (1994)
prosol relations=<triple>

^{15}N-double-filtered NOESY:
1 "C:/Bruker/XWIN-NMR/exp/stan/nmr/lists/pp/noesygpphwgxf"
;noesygpphwgxf
;avance-version (02/02/07)
;2D homonuclear correlation via dipolar coupling
;dipolar coupling may be due to noe or chemical exchange
;phase sensitive
;selecting C-12 or N-14 bound protons in F1 and F2
;water suppression using watergate sequence
;
;M. Ikura & A. Bax, J. Am. Chem. Soc. 114, 2433-2440 (1992)
;M. Piotto, V. Saudek & V. Sklenar, J. Biomol. NMR 2, 661 - 666 (1992)
;V. Sklenar, M. Piotto, R. Leppik $ V. Saudek, J. Magn. Reson.,
; Series A 102, 241 -245 (1993)

HC(C)H-TOCSY:
1 "C:/Bruker/XWIN-NMR/exp/stan/nmr/lists/pp/hcchdigp3d"
;hcchdigp3d
;avance-version (03/01/17)
;HCCH-TOCSY
;3D sequence with
; inverse correlation using multiple inept transfer and
; C-C DIPSI3 spinlock
; F1(H,t1) -> F2(C,t2) -> F2(C') -> F1(H',t3)
;off resonance C=O pulse using shaped pulse
;phase sensitive (t1)
;phase sensitive (t2)
;spinlock during z-filter
;(use parameterset HCCHDIGP3D)
;(L.E. Kay, G.Y. Xu, A.U. Singer, D.R. Muhandiram & J. D. Forman-Kay
; J. Magn. Reson. B 101, 333 - 337 (1993))
prosol relations=<triple>

(H)CCH-TOCSY:
1 "C:/Bruker/XWIN-NMR/exp/stan/nmr/lists/pp/hcchdigp3d2"
;hcchdigp3d2
;avance-version (02/07/16)
;HCCH-TOCSY
;3D sequence with
; inverse correlation using multiple inept transfer and
; C-C DIPSI3 spinlock
; F1(H) -> F2(C,t1) -> F2(C',t2) -> F1(H',t3)
;off resonance C=O pulse using shaped pulse
;phase sensitive (t1)
;phase sensitive (t2)
;spinlock during z-filter
;(use parameterset HCCHDIGP3D2)
;(L.E. Kay, G.Y. Xu, A.U. Singer, D.R. Muhandiram & J. D. Forman-Kay
; J. Magn. Reson. B 101, 333 - 337 (1993))

Appendix B

CaM-eNOSpThr495 Peptide Assigned Chemical Shifts

_Residue_seq_code
_Residue_label
_Atom_name
_Atom_type
_Chem_shift_value
2ASP CA C 51.96
2ASP H H 8.506
2ASP HA H 4.585
2ASP N N 120.378
3GLN CA C 52.735
3GLN CB C 31.074
3GLN CG C 35.178
3GLN H H 8.208
3GLN HA H 4.212
3GLN HB2 H 2.209
3GLN HB3 H 2.209
3GLN N N 119.707
4LEU CA C 51.658
4LEU CB C 39.624
4LEU CG C 23.322
4LEU CD1 C 20.016
4LEU H H 8.181
4LEU HA H 4.14
4LEU HB2 H 1.725
4LEU HB3 H 1.725
4LEU HG H 0.625
4LEU HD1 H 0.537
4LEU HD2 H 0.537
4LEU N N 123.069
5THR CA C 57.687
5THR CB C 68.58
5THR CG2 C 18.99
5THR H H 8.607
5THR HA H 4.322
5THR HB H 4.601
5THR HG2 H 1.169
5THR N N 112.909
6GLU CA C 57.247
6GLU CB C 29.136
6GLU CG C 33.696
6GLU H H 8.877
6GLU HA H 3.825
6GLU HB2 H 1.88
6GLU HB3 H 1.88
6GLU HG2 H 2.219
6GLU HG3 H 2.219
6GLU N N 120.224
7GLU CA C 57.198
7GLU CB C 26.274
7GLU CG C 33.696
7GLU H H 8.524
7GLU HA H 3.917
7GLU HB2 H 1.908
7GLU HB3 H 1.908
7GLU HG2 H 2.201
7GLU HG3 H 2.201
7GLU N N 119.35
8GLN CA C 55.976
8GLN CB C 26.4
8GLN CG C 33.582
8GLN H H 7.603
8GLN HA H 3.903
8GLN HB2 H 1.908
8GLN HB3 H 1.908
8GLN HG2 H 2.201
8GLN HG3 H 2.201
8GLN N N 119.917
9ILE CA C 63.796
9ILE CB C 35.178
9ILE CG1 C 27.54
9ILE CG2 C 14.772
9ILE CD1 C 10.44
9ILE H H 8.26
9ILE HA H 3.639
9ILE HB H 1.801
9ILE HG12 H 0.943
9ILE HG13 H 0.943
9ILE HD1 H 0.708
9ILE N N 119.503
10ALA CA C 52.702
10ALA CB C 15.114
10ALA H H 7.84
10ALA HA H 3.961
10ALA HB H 1.365
10ALA N N 121.044
11GLU CA C 56.563
11GLU CB C 26.4
11GLU CG C 33.468
11GLU H H 7.635
11GLU HA H 3.908
11GLU HB2 H 1.899
11GLU HB3 H 1.899
11GLU HG2 H 2.213
11GLU HG3 H 2.213
11GLU N N 119.113
12PHE CA C 56.954
12PHE CB C 35.064
12PHE H H 8.441
12PHE HA H 4.786
12PHE HB2 H 3.311
12PHE N N 119.574
13LYS CA C 57.296
13LYS CB C 29.592
13LYS CG C 25.83
13LYS CD C 33.696
13LYS H H 9.103
13LYS HA H 3.903
13LYS HB2 H 1.727
13LYS HB3 H 1.727
13LYS HG2 H 1.919
13LYS HG3 H 1.919
13LYS N N 123.454
14GLU CA C 56.465
14GLU CB C 26.502
14GLU CG C 33.584
14GLU H H 7.667
14GLU HA H 3.911
14GLU HB2 H 1.908
14GLU HB3 H 1.908
14GLU HG2 H 2.186
14GLU HG3 H 2.186
14GLU N N 119.525
15ALA CA C 52.751
15ALA CB C 15.228
15ALA H H 7.816
15ALA HA H 3.961
15ALA HB H 1.366
15ALA N N 121.983
16PHE CA C 59.544
16PHE CB C 36.774
16PHE H H 8.764
16PHE HA H 3.095
16PHE HB2 H 2.771
16PHE HB3 H 2.771
16PHE HD1 H 6.477
16PHE HD2 H 6.477
16PHE HE1 H 6.903
16PHE HE2 H 6.903
16PHE HZ H 7.035
16PHE N N 118.874
17SER CA C 58.567
17SER CB C 60.6
17SER H H 7.825
17SER HA H 3.979
17SER HB2 H 3.883
17SER HB3 H 3.883
17SER N N 111.578
18LEU CA C 54.608
18LEU CB C 39.638
18LEU CG C 26.388
18LEU CD1 C 21.819
18LEU H H 7.24
18LEU HA H 3.947
18LEU HB2 H 1.931
18LEU HB3 H 1.931
18LEU HG H 1.679
18LEU HD1 H 0.683
18LEU HD2 H 1.103
18LEU N N 121.167
19PHE CA C 57.247
19PHE CB C 33.81
19PHE H H 7.09
19PHE HA H 3.911
19PHE HB2 H 2.218
19PHE HB3 H 2.218
19PHE HD1 H 6.977
19PHE HD2 H 6.977
19PHE N N 114.405
20ASP CA C 49.476
20ASP CB C 36.782
20ASP H H 7.662
20ASP HA H 4.476
20ASP HB2 H 2.509
20ASP HB3 H 2.509
20ASP N N 115.823
21LYS CA C 56.025
21LYS CB C 29.7
21LYS CG C 21.476
21LYS CD C 25.702
21LYS H H 7.539
21LYS HA H 3.786
21LYS HB2 H 1.688
21LYS HB3 H 1.688
21LYS HG2 H 1.369
21LYS HG3 H 1.283
21LYS HD2 H 1.56
21LYS HD3 H 1.56
21LYS HE2 H 2.881
21LYS HE3 H 2.881
21LYS N N 124.906
22ASP CA C 49.965
22ASP CB C 36.774
22ASP H H 7.965
22ASP HA H 4.431
22ASP HB2 H 2.495
22ASP HB3 H 2.943
22ASP N N 113.55
23GLY CA C 44.442
23GLY H H 7.606
23GLY HA2 H 3.712
23GLY HA3 H 3.712
23GLY N N 109.354
24ASP CA C 51.04
24ASP CB C 37.686
24ASP H H 8.266
24ASP HA H 4.355
24ASP HB2 H 2.905
24ASP HB3 H 2.905
24ASP N N 120.643
25GLY CA C 42.683
25GLY H H 10.545
25GLY HA2 H 3.551

25GLY HA3 H 3.551
25GLY N N 113.205
26THR CA C 56.954
26THR CB C 69.948
26THR CG2 C 18.99
26THR H H 8.02
26THR HA H 5.17
26THR HB H 3.688
26THR HG2 H 0.876
26THR N N 112.852
27ILE CA C 57.931
27ILE CB C 37.23
27ILE CG1 C 24.12
27ILE CG2 C 15.342
27ILE CD1 C 12.948
27ILE H H 9.689
27ILE HA H 3.827
27ILE HB H 1.883
27ILE HG12 H 0.707
27ILE HG13 H 0.707
27ILE HD1 H 0.558
27ILE N N 127.005
28THR CA C 56.612
28THR CB C 69.606
28THR CG2 C 19.56
28THR H H 8.275
28THR HA H 4.642
28THR HB H 4.654
28THR HG2 H 1.175
28THR N N 116.439
29THR CA C 63.845
29THR CB C 65.616
29THR CG2 C 20.472
29THR H H 9.054
29THR HA H 3.635
29THR HB H 4.049
29THR HG2 H 1.115
29THR N N 113.287
30LYS CA C 56.465
30LYS CB C 29.7
30LYS CG C 21.705
30LYS CD C 25.931
30LYS H H 7.578
30LYS HA H 3.903
30LYS HB2 H 1.702
30LYS HB3 H 1.702
30LYS HG2 H 1.35
30LYS HG3 H 1.35
30LYS HD2 H 1.922
30LYS HD3 H 1.922
30LYS N N 121.23
31GLU CA C 57.149
31GLU CB C 26.058
31GLU CG C 33.696
31GLU H H 7.712
31GLU HA H 3.863
31GLU HB2 H 1.92
31GLU HB3 H 1.92
31GLU HG2 H 2.175
31GLU HG3 H 2.175
31GLU N N 122.002
32LEU CA C 55.529
32LEU CB C 39.981
32LEU CG C 23.418
32LEU CD1 C 21.133
32LEU H H 8.509
32LEU HA H 3.925
32LEU HB2 H 1.937
32LEU HB3 H 1.937
32LEU HG H 1.643
32LEU HD1 H 0.659
32LEU HD2 H 1.101
32LEU N N 119.13
33GLY CA C 45.664
33GLY H H 8.388
33GLY HA2 H 3.844
33GLY HA3 H 3.433
33GLY N N 103.747
34THR CA C 64.285
34THR CB C 66.186
34THR CG2 C 18.648
34THR H H 7.935
34THR HA H 3.795
34THR HB H 4.167
34THR HG2 H 1.124
34THR N N 117.487
35VAL H H 7.089
35VAL N N 120.287
36MET CA C 57.101
36MET CB C 29.929
36MET H H 8.318
36MET HA H 3.911
36MET HB2 H 1.715
36MET HB3 H 1.715
36MET HG2 H 1.883
36MET HG3 H 1.883
36MET N N 117.816
37ARG CA C 56.172
37ARG CB C 27.084
37ARG CG C 25.488
37ARG CD C 40.878
37ARG H H 8.233
37ARG HA H 4.698
37ARG HB2 H 1.776
37ARG HB3 H 1.776
37ARG HG2 H 1.846
37ARG HG3 H 1.846
37ARG N N 117.706
38SER CA C 59.251
38SER CB C 67.782
38SER H H 7.874
38SER HA H 4.187
38SER HB2 H 4.072
38SER HB3 H 4.072
38SER N N 118.974
39LEU CA C 51.333
39LEU CB C 39.638
39LEU CG C 23.19
39LEU CD1 C 20.791
39LEU H H 7.248
39LEU HA H 4.139
39LEU HB2 H 1.746
39LEU HB3 H 1.746
39LEU HG H 1.658
39LEU HD1 H 0.517
39LEU HD2 H 0.529
39LEU N N 118.835
40GLY CA C 42.878
40GLY H H 7.471
40GLY HA2 H 4.093
40GLY HA3 H 4.093
40GLY N N 104.99
41GLN CA C 51.187
41GLN CB C 30.618
41GLN CG C 37.116
41GLN H H 7.86
41GLN HA H 4.37
41GLN HB2 H 2.507
41GLN HB3 H 2.507
41GLN HG2 H 2.935
41GLN HG3 H 2.935
41GLN N N 118.032
42ASN CA C 48.694
42ASN CB C 36.554
42ASN H H 8.561
42ASN HA H 5.094
42ASN HB2 H 2.348
42ASN HB3 H 2.348
42ASN N N 115.671
43PRO HA H 4.711
43PRO HD2 H 3.448
44THR CA C 57.638
44THR CB C 68.466
44THR CG2 C 18.99
44THR H H 8.882
44THR HA H 4.321
44THR HB H 4.595
44THR HG2 H 1.162
44THR N N 113.509
45GLU CA C 57.101
45GLU CB C 26.274
45GLU CG C 33.696
45GLU H H 8.662
45GLU HA H 3.88
45GLU HB2 H 1.893
45GLU HB3 H 1.893
45GLU HG2 H 2.175
45GLU HG3 H 2.175
45GLU N N 120.506
46ALA CA C 52.311
46ALA CB C 15.08
46ALA H H 8.139
46ALA HA H 3.925
46ALA HB H 1.26
46ALA N N 120.586
47GLU CA C 56.27
47GLU CB C 26.286
47GLU CG C 33.468
47GLU H H 7.597
47GLU HA H 3.876
47GLU HB2 H 1.908
47GLU HB3 H 1.908
47GLU HG2 H 2.189
47GLU HG3 H 2.189
47GLU N N 118.171
48LEU CA C 55.048
48LEU CB C 39.981
48LEU CG C 23.532
48LEU CD1 C 20.562
48LEU H H 7.848
48LEU HA H 3.927
48LEU HB2 H 1.937
48LEU HB3 H 1.937
48LEU HG H 1.629
48LEU HD1 H 0.763
48LEU HD2 H 1.086
48LEU N N 120.228
49GLN CA C 55.732
49GLN CB C 27.882
49GLN CG C 33.354
49GLN H H 8.037
49GLN HA H 3.901
49GLN HB2 H 1.978
49GLN HB3 H 1.978
49GLN HG2 H 2.219
49GLN HG3 H 2.219
49GLN N N 117.91
50ASP CA C 54.706
50ASP CB C 37.572
50ASP H H 8.01
50ASP HA H 4.157
50ASP HB2 H 2.517
50ASP HB3 H 2.517
50ASP N N 119.284
51MET CA C 56.563
51MET CB C 29.478
51MET H H 7.614
51MET HA H 3.923
51MET HB2 H 1.728
51MET HB3 H 1.728
51MET N N 119.245
52ILE CA C 61.89
52ILE CB C 34.494
52ILE CG1 C 26.058
52ILE CG2 C 13.518
52ILE CD1 C 9.984
52ILE H H 7.514
52ILE HA H 3.328
52ILE HB H 1.786
52ILE HG12 H 0.905
52ILE HG13 H 0.905
52ILE HG2 H 0.557
52ILE HD1 H 0.554
52ILE N N 117.584
53ASN CA C 53.093
53ASN CB C 35.292
53ASN H H 8.418
53ASN HA H 4.222
53ASN HB2 H 2.832
53ASN HB3 H 2.832
53ASN N N 117.126
54GLU CA C 56.123
54GLU CB C 26.4
54GLU CG C 33.582
54GLU H H 7.466
54GLU HA H 3.903
54GLU HB2 H 1.908
54GLU HB3 H 1.908

54GLU HG2 H 2.216
54GLU HG3 H 2.216
54GLU N N 116.38
55VAL CA C 58.176
55VAL CB C 30.162
55VAL CG1 C 18.99
55VAL CG2 C 16.824
55VAL H H 7.044
55VAL HA H 4.314
55VAL HB H 2.216
55VAL HG1 H 1.159
55VAL HG2 H 0.778
55VAL N N 108.622
56ASP CA C 50.991
56ASP CB C 36.896
56ASP H H 7.561
56ASP HA H 4.39
56ASP HB2 H 2.943
56ASP HB3 H 2.503
56ASP N N 121.43
57ALA CA C 51.48
57ALA CB C 16.793
57ALA H H 8.357
57ALA HA H 4.053
57ALA HB H 1.369
57ALA N N 131.84
58ASP CA C 49.916
58ASP CB C 36.774
58ASP H H 7.985
58ASP HA H 4.49
58ASP HB2 H 2.921
58ASP HB3 H 2.517
58ASP N N 113.565
59GLY CA C 44.491
59GLY H H 7.424
59GLY HA2 H 3.727
59GLY HA3 H 3.727
59GLY N N 108.187
60ASN CA C 49.769
60ASN CB C 36.554
60ASN H H 7.919
60ASN HA H 4.446
60ASN HB2 H 2.517
60ASN HB3 H 2.517
60ASN N N 118.065
61GLY CA C 42.878
61GLY H H 10.485
61GLY HA2 H 4.02
61GLY HA3 H 4.02
61GLY N N 113.247
62THR CA C 56.661
62THR H H 7.511
62THR HA H 4.58
62THR HB H 3.788
62THR HG2 H 0.948
62THR N N 108.699
63ILE CA C 57.101
63ILE CB C 37.344
63ILE CG1 C 24.462
63ILE CG2 C 15.684
63ILE CD1 C 10.554
63ILE H H 8.741
63ILE HA H 5.054
63ILE HB H 1.893
63ILE HG12 H 0.631
63ILE HG13 H 0.631
63ILE HG2 H 1.071
63ILE HD1 H 0.705
63ILE N N 122.834
64ASP CA C 49.378
64ASP CB C 36.782
64ASP H H 8.702
64ASP HA H 5.238
64ASP HB2 H 2.626
64ASP HB3 H 2.945
64ASP N N 127.818
65PHE CA C 60.717
65PHE CB C 33.126
65PHE H H 8.847
65PHE HA H 3.861
65PHE HB2 H 2.216
65PHE HB3 H 2.216
65PHE HD1 H 6.59
65PHE HD2 H 6.59
65PHE HZ H 7.035
65PHE N N 118.653
67GLU CA C 56.337
67GLU CB C 26.045
67GLU CG C 33.47
67GLU H H 7.94
67GLU HA H 3.903
67GLU HB2 H 1.908
67GLU HB3 H 1.908
67GLU HG2 H 2.216
67GLU HG3 H 2.216
67GLU N N 117.631
68PHE CA C 58.727
68PHE CB C 37.572
68PHE H H 8.757
68PHE HA H 3.84
68PHE HB2 H 3.081
68PHE HB3 H 3.081
68PHE HD1 H 6.844
68PHE HD2 H 6.844
68PHE HE1 H 6.502
68PHE HE2 H 6.502
68PHE HZ H 7.001
68PHE N N 123.289
69LEU CA C 55.158
69LEU CB C 38.256
69LEU CG C 22.752
69LEU CD1 C 21.27
69LEU CD2 C 22.752
69LEU H H 8.403
69LEU HA H 3.245
69LEU HB2 H 1.361
69LEU HB3 H 1.361
69LEU HG H 0.881
69LEU HD1 H 0.514
69LEU N N 118.867
70THR CA C 63.843
70THR CB C 65.502
70THR CG2 C 19.192
70THR H H 7.54
70THR HA H 3.624
70THR HB H 4.168
70THR HG2 H 1.068
70THR N N 116.302
71MET CA C 56.303
71MET CB C 29.706
71MET H H 7.723
71MET HA H 3.903
71MET HB2 H 1.707
71MET HB3 H 1.707
71MET HG2 H 2.197
71MET HG3 H 2.197
71MET N N 121.71
72MET CA C 53.307
72MET CB C 28.787
72MET CG C 28.787
72MET CE C 15.194
72MET H H 7.982
72MET HA H 3.773
72MET HB2 H 1.291
72MET HB3 H 1.291
72MET HG2 H 1.732
72MET HG3 H 1.732
72MET N N 116.535
73ALA CA C 52.095
73ALA CB C 15.342
73ALA H H 8.074
73ALA HA H 3.88
73ALA HB H 1.252
73ALA N N 121.584
74ARG CA C 55.731
74ARG CB C 27.987
74ARG H H 7.358
74ARG HA H 3.903
74ARG HB2 H 1.805
74ARG HB3 H 1.805
74ARG HG2 H 2.201
74ARG HG3 H 2.201
74ARG HD2 H 3.067
74ARG HD3 H 3.067
74ARG N N 115.784
75LYS CA C 53.947
75LYS CB C 26.4
75LYS CG C 22.068
75LYS CD C 30.96
75LYS CE C 39.738
75LYS H H 7.64
75LYS HA H 3.949
75LYS HB2 H 2.23
75LYS HB3 H 2.23
75LYS HG2 H 1.335
75LYS HG3 H 1.335
75LYS HD2 H 1.658
75LYS HD3 H 1.658
75LYS HE2 H 2.832
75LYS HE3 H 2.832
75LYS N N 117.245
76MET CA C 53.947
76MET CB C 29.478
76MET CG C 29.815
76MET H H 7.794
76MET HA H 4.242
76MET HB2 H 2.027
76MET HB3 H 2.027
76MET HG2 H 2.591
76MET HG3 H 2.591
76MET N N 117.971
77LYS CA C 54.283
77LYS CB C 29.478
77LYS CG C 26.4
77LYS H H 7.622
77LYS HA H 4.152
77LYS HB2 H 2.538
77LYS HB3 H 2.538
77LYS HG2 H 2.025
77LYS HG3 H 2.025
77LYS HD2 H 1.693
77LYS HD3 H 1.693
77LYS N N 119.902
78ASP CA C 52.061
78ASP H H 7.991
78ASP HA H 4.243
78ASP HB2 H 1.864
78ASP HB3 H 1.864
78ASP N N 119.146
79THR CA C 59.03
79THR CB C 67.668
79THR CG2 C 18.534
79THR H H 7.587
79THR HA H 4.17
79THR HB H 4.096
79THR HG2 H 1.08
79THR N N 112.75
80ASP CA C 50.85
80ASP CB C 37.353
80ASP H H 8.354
80ASP HA H 4.371
80ASP HB2 H 2.512
80ASP HB3 H 2.512
80ASP N N 122.888
81SER CA C 57.717
81SER CB C 60.884
81SER H H 8.232
81SER HA H 4.115
81SER HB2 H 3.796
81SER HB3 H 3.796
81SER N N 117.571
82GLU CA C 56.707
82GLU CB C 29.592
82GLU CG C 33.468
82GLU H H 8.364
82GLU HA H 3.883
82GLU HB2 H 1.965
82GLU HG2 H 2.175
82GLU N N 121.86
83GLU CA C 56.606
83GLU CB C 29.364
83GLU CG C 33.582
83GLU H H 8.032
83GLU HA H 3.883
83GLU HB2 H 1.956
83GLU HB3 H 1.956
83GLU HG2 H 2.219
83GLU HG3 H 2.219

83GLU N N 119.398
84GLU CA C 56.606
84GLU CB C 25.817
84GLU CG C 33.47
84GLU H H 8.153
84GLU HA H 3.871
84GLU HB2 H 1.917
84GLU HB3 H 1.917
84GLU HG2 H 2.226
84GLU HG3 H 2.226
84GLU N N 118.279
85ILE CA C 63.439
85ILE CB C 34.608
85ILE CG1 C 27.654
85ILE CG2 C 15.912
85ILE CD1 C 10.212
85ILE H H 7.927
85ILE HA H 3.612
85ILE HB H 1.778
85ILE HG12 H 0.919
85ILE HG13 H 0.919
85ILE HG2 H 1.261
85ILE HD1 H 0.707
85ILE N N 120.97
86ARG CA C 57.515
86ARG CB C 26.856
86ARG CG C 24.69
86ARG CD C 40.536
86ARG H H 8.233
86ARG HA H 4.008
86ARG HB2 H 1.899
86ARG HB3 H 1.899
86ARG HG2 H 1.496
86ARG HG3 H 1.496
86ARG HD2 H 2.81
86ARG HD3 H 2.81
86ARG N N 121.766
87GLU CA C 56.606
87GLU CB C 25.817
87GLU CG C 33.698
87GLU H H 8.156
87GLU HA H 3.902
87GLU HB2 H 1.89
87GLU HB3 H 1.89
87GLU HG2 H 2.175
87GLU HG3 H 2.175
87GLU N N 118.369
88ALA CA C 52.263
88ALA CB C 15.08
88ALA H H 7.877
88ALA HA H 3.949
88ALA HB H 1.368
88ALA N N 120.337
89PHE CA C 59.703
89PHE CB C 36.774
89PHE H H 8.459
89PHE HA H 3.115
89PHE HB2 H 2.731
89PHE HB3 H 2.731
89PHE HD1 H 6.478
89PHE HD2 H 6.478
89PHE HE1 H 7.054
89PHE HE2 H 7.054
89PHE N N 118.191
90ARG CA C 56.168
90ARG CB C 27.654
90ARG CG C 25.716
90ARG CD C 40.764
90ARG H H 7.764
90ARG HA H 3.905
90ARG HB2 H 1.803
90ARG HB3 H 1.803
90ARG HG2 H 2.135
90ARG HG3 H 2.135
90ARG HD2 H 3.073
90ARG HD3 H 3.073
90ARG N N 115.953
91VAL CA C 63.357
91VAL CB C 28.444
91VAL CG1 C 18.164
91VAL CG2 C 19.877
91VAL H H 7.229
91VAL HA H 3.285
91VAL HB H 1.901
91VAL HG1 H 0.388
91VAL HG2 H 0.856
91VAL N N 118.202
92PHE CA C 58.029
92PHE CB C 38.838
92PHE H H 6.699
92PHE HA H 3.945
92PHE HB2 H 2.561
92PHE HB3 H 2.561
92PHE HD1 H 6.373
92PHE HD2 H 6.373
92PHE N N 112.447
93ASP CA C 49.525
93ASP CB C 35.183
93ASP H H 7.881
93ASP HA H 4.476
93ASP HB2 H 2.517
93ASP HB3 H 2.517
93ASP N N 116.461
94LYS CA C 55.976
94LYS CB C 31.414
94LYS CG C 25.246
94LYS CD C 27.644
94LYS CE C 40.764
94LYS H H 7.596
94LYS HA H 3.668
94LYS HB2 H 2.198
94LYS HB3 H 2.198
94LYS HG2 H 1.517
94LYS HG3 H 1.283
94LYS HD2 H 1.794
94LYS HD3 H 1.794
94LYS N N 125.494
95ASP CA C 50.307
95ASP CB C 36.774
95ASP H H 8.097
95ASP HA H 4.415
95ASP HB2 H 2.924
95ASP HB3 H 2.498
95ASP N N 114.015
96GLY CA C 44.344
96GLY H H 7.677
96GLY HA2 H 3.711
96GLY HA3 H 3.711
96GLY N N 109.147
97ASN CA C 49.916
97ASN CB C 35.183
97ASN H H 8.252
97ASN HA H 4.5
97ASN HB2 H 3.271
97ASN HB3 H 3.271
97ASN N N 119.575
98GLY CA C 42.292
98GLY H H 10.462
98GLY HA2 H 3.986
98GLY HA3 H 3.986
98GLY N N 112.465
99TYR CA C 53.582
99TYR CB C 39.981
99TYR H H 7.557
99TYR HA H 4.882
99TYR HB2 H 2.412
99TYR HB3 H 2.412
99TYR HD1 H 6.736
99TYR HD2 H 6.736
99TYR N N 116.256
100ILE CA C 58.616
100ILE CB C 36.432
100ILE CG1 C 24.234
100ILE CG2 C 14.316
100ILE CD1 C 13.632
100ILE H H 9.972
100ILE HA H 4.457
100ILE HB H 1.731
100ILE HG2 H 0.751
100ILE HD1 H 0.771
100ILE N N 126.957
101SER CA C 52.897
101SER CB C 64.134
101SER H H 8.844
101SER HA H 4.711
101SER HB2 H 3.818
101SER HB3 H 3.818
101SER N N 123.739
102ALA CA C 53.093
102ALA CB C 15.114
102ALA H H 9.178
102ALA HA H 3.711
102ALA HB H 1.325
102ALA N N 123.028
103ALA CA C 52.409
103ALA CB C 15.456
103ALA H H 8.132
103ALA HA H 3.861
103ALA HB H 1.262
103ALA N N 118.443
104GLU CA C 56.563
104GLU CB C 26.4
104GLU CG C 33.582
104GLU H H 7.786
104GLU HA H 3.839
104GLU HB2 H 1.917
104GLU HB3 H 1.917
104GLU HG2 H 2.26
104GLU HG3 H 2.26
104GLU N N 120.139
105LEU CA C 55.732
105LEU CB C 40.209
105LEU CG C 23.532
105LEU CD1 C 20.791
105LEU H H 8.24
105LEU HA H 3.902
105LEU HB2 H 1.623
105LEU HB3 H 1.623
105LEU HG H 1.645
105LEU HD1 H 0.643
105LEU HD2 H 1.036
105LEU N N 121.545
106ARG CA C 57.345
106ARG CB C 30.39
106ARG CG C 25.944
106ARG CD C 39.054
106ARG H H 8.761
106ARG HA H 3.839
106ARG HB2 H 1.73
106ARG HB3 H 1.73
106ARG HG2 H 1.922
106ARG HG3 H 1.922
106ARG HD2 H 1.069
106ARG N N 118.625
107HIS CA C 56.807
107HIS CB C 27.198
107HIS H H 7.946
107HIS HA H 3.902
107HIS HB2 H 1.794
107HIS HB3 H 1.794
107HIS N N 119.052
108VAL CA C 64.285
108VAL CB C 28.908
108VAL CG1 C 8.078
108VAL CG2 C 20.7
108VAL H H 7.736
108VAL HA H 3.442
108VAL HB H 2.027
108VAL HG1 H 0.466
108VAL HG2 H 0.861
108VAL N N 119.16
109MET CA C 54.686
109MET CB C 29.706
109MET H H 8.074
109MET HA H 4.139
109MET HB2 H 1.709
109MET HB3 H 1.709
109MET HG2 H 2.038
109MET HG3 H 2.038
109MET N N 15.333
110THR CA C 63.845
110THR CB C 66.072
110THR CG2 C 18.876
110THR H H 8.515
110THR HA H 3.935
110THR HB H 4.168
110THR HG2 H 1.08
110THR N N 116.714

111ASN CA C 53.093
111ASN CB C 35.292
111ASN H H 7.89
111ASN HA H 4.242
111ASN HB2 H 2.689
111ASN HB3 H 2.859
111ASN N N 123.784
112LEU CA C 52.653
112LEU CB C 39.738
112LEU CG C 23.094
112LEU CD1 C 0.244
112LEU H H 7.621
112LEU HA H 4.115
112LEU HB2 H 1.75
112LEU HB3 H 1.75
112LEU HG H 1.643
112LEU HD1 H 0.621
112LEU HD2 H 0.621
112LEU N N 118.227
113GLY CA C 42.536
113GLY H H 7.701
113GLY HA2 H 4.094
113GLY HA3 H 4.094
113GLY N N 106.787
114GLU CA C 52.067
114GLU CB C 26.616
114GLU CG C 31.071
114GLU H H 7.864
114GLU HA H 4.242
114GLU HB2 H 1.518
114GLU HB3 H 1.518
114GLU HG2 H 1.803
114GLU HG3 H 1.803
114GLU N N 120.288
115LYS CA C 52.848
115LYS CB C 30.957
115LYS CG C 26.502
115LYS CD C 21.933
115LYS H H 8.491
115LYS HA H 4.223
115LYS HB2 H 1.773
115LYS HB3 H 1.773
115LYS HG2 H 1.198
115LYS HG3 H 1.198
115LYS HD2 H 1.496
115LYS HD3 H 1.496
115LYS N N 124.987
116LEU CA C 51.089
116LEU CB C 42.588
116LEU CG C 24.804
116LEU CD1 C 21.384
116LEU CD2 C 16.482
116LEU H H 7.978
116LEU HA H 4.712
116LEU HB2 H 1.473
116LEU HB3 H 1.473
116LEU HG H 1.433
116LEU HD1 H 0.663
116LEU N N 124.912
117THR CA C 57.834
117THR CB C 68.58
117THR CG2 C 18.99
117THR H H 9.093
117THR HA H 4.302
117THR HB H 4.647
117THR HG2 H 1.153
117THR N N 114.22
118ASP CA C 55.243
118ASP CB C 37.002
118ASP H H 8.764
118ASP HA H 4.058
118ASP HB2 H 2.488
118ASP HB3 H 2.488
118ASP N N 120.925
119GLU CA C 57.149
119GLU CB C 25.931
119GLU CG C 33.812
119GLU H H 8.509
119GLU HA H 3.927
119GLU HB2 H 1.887
119GLU HB3 H 1.887
119GLU HG2 H 2.203
119GLU HG3 H 2.203
119GLU N N 119.395
120GLU CA C 56.319
120GLU CB C 25.83
120GLU CG C 33.696
120GLU H H 7.585
120GLU HA H 3.896
120GLU HB2 H 1.901
120GLU HB3 H 1.901
120GLU HG2 H 2.209
120GLU HG3 H 2.209
120GLU N N 119.909
121VAL CA C 64.09
121VAL CB C 28.68
121VAL CG1 C 20.7
121VAL CG2 C 18.078
121VAL H H 7.849
121VAL HA H 3.442
121VAL HB H 2.048
121VAL HG1 H 0.772
121VAL HG2 H 0.199
121VAL N N 122.092
122ASP CA C 54.901
122ASP CB C 37.572
122ASP H H 7.912
122ASP HA H 4.157
122ASP HB2 H 2.503
122ASP HB3 H 2.623
122ASP N N 120.167
123GLU CA C 56.612
123GLU CB C 26.172
123GLU CG C 33.468
123GLU H H 7.839
123GLU HA H 3.896
123GLU HB2 H 1.901
123GLU HB3 H 1.901
123GLU HG2 H 2.209
123GLU HG3 H 2.209
123GLU N N 119.087
124MET CA C 56.905
124MET CB C 29.25
124MET H H 7.433
124MET HA H 3.867
124MET HB2 H 1.755
124MET HB3 H 1.755
124MET HG2 H 2.195
124MET HG3 H 2.195
124MET N N 118.897
125ILE CA C 60.131
125ILE CB C 33.24
125ILE CG1 C 13.595
125ILE CG2 C 24.789
125ILE CD1 C 6.906
125ILE H H 7.658
125ILE HA H 3.38
125ILE HB H 2.086
125ILE HG12 H 0.554
125ILE HG13 H 0.554
125ILE HG2 H 1.241
125ILE HD1 H 0.434
125ILE N N 118.001
126ARG CA C 56.673
126ARG CB C 29.478
126ARG CG C 26.058
126ARG CD C 40.992
126ARG H H 7.974
126ARG HA H 3.883
126ARG HB2 H 1.725
126ARG HB3 H 1.725
126ARG N N 117.72
127GLU CA C 56.319
127GLU CB C 26.286
127GLU CG C 33.696
127GLU H H 7.635
127GLU HA H 3.967
127GLU HB2 H 1.916
127GLU HB3 H 1.916
127GLU HG2 H 2.253
127GLU HG3 H 2.253
127GLU N N 117.05
128ALA CA C 48.205
128ALA CB C 20.105
128ALA H H 7.155
128ALA HA H 4.5
128ALA HB H 1.329
128ALA N N 116.966
129ASP CA C 51.822
129ASP CB C 37.686
129ASP H H 7.806
129ASP HA H 4.351
129ASP HB2 H 2.517
129ASP HB3 H 2.517
129ASP N N 118.033
130ILE CA C 60.522
130ILE CB C 36.09
130ILE CG1 C 25.032
130ILE CG2 C 14.43
130ILE CD1 C 9.756
130ILE H H 8.115
130ILE HA H 3.797
130ILE HB H 1.837
130ILE HG12 H 1.549
130ILE HG13 H 1.549
130ILE HG2 H 0.772
130ILE HD1 H 0.708
130ILE N N 127.927
131ASP CA C 51.187
131ASP CB C 37.468
131ASP H H 8.202
131ASP HA H 4.343
131ASP HB2 H 2.9
131ASP HB3 H 2.9
131ASP N N 116.634
132GLY CA C 44.638
132GLY H H 7.535
132GLY HA2 H 3.706
132GLY HA3 H 3.706
132GLY N N 108.586
133ASP CA C 50.942
133ASP CB C 37.458
133ASP H H 8.215
133ASP HA H 4.351
133ASP HB2 H 2.327
133ASP HB3 H 2.899
133ASP N N 120.377
134GLY CA C 43.122
134GLY H H 9.971
134GLY HA2 H 3.295
134GLY HA3 H 3.295
134GLY N N 112.226
135GLN CA C 50.454
135GLN CB C 30.614
135GLN CG C 30.614
135GLN H H 7.835
135GLN HA H 4.131
135GLN HB2 H 1.617
135GLN HB3 H 1.617
135GLN HG2 H 1.711
135GLN HG3 H 1.711
135GLN N N 115.229
136VAL CA C 58.713
136VAL CB C 31.416
136VAL CG1 C 20.358
136VAL CG2 C 19.104
136VAL H H 8.958
136VAL HA H 5.096
136VAL HB H 2.195
136VAL HG1 H 0.948
136VAL HG2 H 1.153
136VAL N N 125.238
137ASN CA C 48.352
137ASN CB C 35.64
137ASN H H 9.435
137ASN HA H 5.226
137ASN HB2 H 2.964
137ASN HB3 H 2.964
137ASN N N 129.058
138TYR CA C 59.669
138TYR CB C 37.572
138TYR H H 8.146
138TYR HA H 3.192
138TYR HB2 H 1.916
138TYR HB3 H 1.916
138TYR HD1 H 6.865
138TYR HD2 H 6.865
138TYR N N 118.627

139GLU CA C 57.54
139GLU CB C 26.274
139GLU CG C 33.812
139GLU H H 7.974
139GLU HA H 3.511
139GLU HB2 H 1.96
139GLU HB3 H 1.96
139GLU HG2 H 2.18
139GLU HG3 H 2.18
139GLU N N 118.701
140GLU CA C 56.025
140GLU CB C 26.274
140GLU CG C 33.24
140GLU H H 8.676
140GLU HA H 3.911
140GLU HB2 H 1.901
140GLU HB3 H 1.901
140GLU HG2 H 2.197
140GLU HG3 H 2.197
140GLU N N 119.774
141PHE CA C 59.447
141PHE CB C 37.686
141PHE H H 8.507
141PHE HA H 3.647
141PHE HB2 H 3.178
141PHE HB3 H 3.178
141PHE HD1 H 6.63
141PHE HD2 H 6.63
141PHE HE1 H 6.99
141PHE HE2 H 6.99
141PHE HZ H 6.39
141PHE N N 124.074
142VAL CA C 64.432
142VAL CB C 28.908
142VAL CG1 C 18.762
142VAL CG2 C 20.586
142VAL H H 8.639
142VAL HA H 2.958
142VAL HB H 1.622
142VAL HG1 H 0.576
142VAL HG2 H 0.291
142VAL N N 119.203
143GLN CA C 56.514
143GLN CB C 25.246
143GLN CG C 31.414
143GLN H H 7.818
143GLN HA H 3.671
143GLN HB2 H 1.912
143GLN HB3 H 1.912
143GLN HG2 H 2.219
143GLN HG3 H 2.219
143GLN N N 120.173
144MET CA C 55.683
144MET CB C 28.11
144MET H H 7.403
144MET HA H 3.882
144MET HB2 H 1.781
144MET HB3 H 1.781
144MET HG2 H 1.781
144MET HG3 H 1.781
144MET HE H 3.09
144MET N N 118.573
145MET CA C 53.63
145MET CB C 29.592
145MET H H 7.534
145MET HA H 3.94
145MET HB2 H 1.725
145MET HB3 H 1.725
145MET HG2 H 1.672
145MET HG3 H 1.672
145MET N N 114.053
146THR CA C 59.251
146THR CB C 67.896
146THR CG2 C 18.534
146THR H H 7.554
146THR HA H 4.175
146THR HB H 4.087
146THR HG2 H 0.977
146THR N N 109.275
147ALA CA C 50.307
147ALA CB C 16.336
147ALA H H 7.406
147ALA HA H 4.117
147ALA HB H 1.256
147ALA N N 126.913
148LYS CA C 54.803
148LYS CB C 30.843
148LYS CG C 21.933
148LYS CD C 26.388
148LYS CE C 39.852
148LYS H H 7.834
148LYS HA H 3.955
148LYS HB2 H 1.652
148LYS HB3 H 1.652
148LYS HG2 H 1.22
148LYS HG3 H 1.22
148LYS HD2 H 1.916
148LYS HD3 H 1.916
148LYS N N 126.268
eNOSpThr495
153THR H H 8.298
153THR HA H 4.078
153THR HB H 3.963
153THR HG2 H 0.91
154PHE H H 8.432
154PHE HA H 4.526
154PHE HB2 H 4.241
154PHE HB3 H 4.241
155LYS H H 8.314
155LYS HA H 3.989
155LYS HB2 H 1.993
155LYS HB3 H 1.993
155LYS HG2 H 0.904
155LYS HG3 H 0.904
155LYS HD2 H 1.402
155LYS HD3 H 1.402
156GLU H H 7.797
156GLU HA H 4.447
156GLU HB2 H 1.402
156GLU HB3 H 1.402
156GLU HG2 H 1.509
156GLU HG3 H 1.509
157VAL H H 7.387
157VAL HA H 3.945
157VAL HB H 1.833
157VAL HG1 H 0.613
157VAL HG2 H 0.733
158ALA H H 7.191
158ALA HA H 4.167
158ALA HB H 1.521
159ASN H H 7.709
159ASN HA H 4.087
159ASN HB2 H 2.885
159ASN HB3 H 2.885
160ALA H H 6.782
160ALA HB H 1.114
161VAL H H 6.561
161VAL HA H 4.393
161VAL HB H 1.313
161VAL HG1 H 0.476
161VAL HG2 H 0.476
162LYS H H 7.348
162LYS HA H 4.393
162LYS HB2 H 2.205
162LYS HB3 H 2.205
162LYS HG2 H 1.03
162LYS HG3 H 1.03
163ILE H H 9.267
163ILE HA H 4.279
163ILE HB H 2.197
163ILE HG12 H 1.318
163ILE HG13 H 1.318
163ILE HD1 H 1.023
164SER H H 8.802
164SER HA H 4.418
164SER HB2 H 2.89
164SER HB3 H 2.89
165ALA H H 7.784
165ALA HA H 4.136
165ALA HB H 1.504
166SER H H 8.539
166SER HA H 4.31
166SER HB2 H 3.497
166SER HB3 H 3.497
167LEU H H 8.648
167LEU HA H 3.857
167LEU HB2 H 2.253
167LEU HB3 H 2.253
167LEU HG H 1.758
167LEU HD1 H 1.226
167LEU HD2 H 0.899
168MET H H 8.451
168MET HB2 H 1.793
168MET HB3 H 1.793
168MET HG2 H 1.993
168MET HG3 H 1.993

Appendix C

CaM Y99E-eNOS Peptide Assigned Chemical Shift

_Residue_seq_code
_Residue_label
_Atom_name
_Atom_type
_Chem_shift_value
2ASP H H 8.493
2ASP N N 120.229
3GLN H H 8.207
3GLN N N 119.571
4LEU H H 8.177
4LEU N N 122.97
5THR H H 8.611
5THR N N 112.923
6GLU H H 8.875
6GLU N N 120.083
7GLU H H 8.532
7GLU N N 119.246
8GLN H H 7.586
8GLN N N 119.77
9ILE H H 8.271
9ILE N N 119.252
10ALA H H 7.84
10ALA N N 120.938
11GLU H H 7.637
11GLU N N 118.88
12PHE H H 8.449
12PHE N N 119.525
13LYS H H 9.106
13LYS N N 123.495
14GLU H H 7.653
14GLU N N 119.053
15ALA H H 7.789
15ALA N N 121.934
16PHE H H 8.766
16PHE N N 118.861
17SER H H 7.826
17SER N N 111.507
18LEU H H 7.237
18LEU N N 121.142
19PHE H H 7.071
19PHE N N 114.305
20ASP H H 7.664
20ASP N N 115.786
21LYS H H 7.55
21LYS N N 124.882
22ASP H H 7.962
22ASP N N 113.582
23GLY H H 7.599
23GLY N N 109.251
24ASP H H 8.254
24ASP N N 120.421
25GLY H H 10.56
25GLY N N 113.19
26THR H H 8.021
26THR N N 112.893
27ILE H H 9.682
27ILE N N 127.001
28THR H H 8.264
28THR N N 116.659
29THR H H 9.056
29THR N N 113.245
30LYS H H 7.575
30LYS N N 121.098
31GLU H H 7.71
31GLU N N 122.001
33GLY H H 8.383
33GLY N N 103.65
34THR H H 7.928
34THR N N 117.566
35VAL H H 7.091
35VAL N N 120.234
36MET H H 8.323
36MET N N 117.714
37ARG H H 8.23
37ARG N N 117.626
38SER H H 7.879
38SER N N 118.88
39LEU H H 7.258
39LEU N N 118.681
40GLY H H 7.46
40GLY N N 104.808
41GLN H H 7.869
41GLN N N 117.938
42ASN H H 8.557
42ASN N N 115.663
44THR H H 8.894
44THR N N 113.567
45GLU H H 8.654
45GLU N N 120.295
46ALA H H 8.137
46ALA N N 120.487
47GLU H H 7.591
47GLU N N 118.007
48LEU H H 7.853
48LEU N N 120.152
49GLN H H 8.028
49GLN N N 117.871
50ASP H H 8.011
50ASP N N 119.212
51MET H H 7.616
51MET N N 119.106
52ILE H H 7.511
52ILE N N 117.539
53ASN H H 8.415
53ASN N N 117.128
54GLU H H 7.465
54GLU N N 116.411
55VAL H H 7.039
55VAL N N 108.519
56ASP H H 7.557
56ASP N N 121.284
57ALA H H 8.359
57ALA N N 131.832
58ASP H H 7.988
58ASP N N 113.582
59GLY H H 7.424
59GLY N N 108.085
60ASN H H 7.918
60ASN N N 117.926
61GLY H H 10.485
61GLY N N 113.23
62THR H H 7.507
62THR N N 108.615
63ILE H H 8.73
63ILE N N 122.672
64ASP H H 8.706
64ASP N N 127.837
65PHE H H 8.845
65PHE N N 118.569
67GLU H H 7.952
67GLU N N 117.588
68PHE H H 8.765
68PHE N N 123.283
69LEU H H 8.405
69LEU N N 118.741
70THR H H 7.542
70THR N N 116.411
71MET H H 7.72
71MET N N 121.576
72MET H H 7.977
72MET N N 116.517
73ALA H H 8.061
73ALA N N 121.465
74ARG H H 7.354
74ARG N N 115.794
75LYS H H 7.636
75LYS N N 117.245
76MET H H 7.792
76MET N N 117.911
77LYS H H 7.627
77LYS N N 119.836
78ASP H H 8.009
78ASP N N 119.273
79THR H H 7.597
79THR N N 112.709
80ASP H H 8.341
80ASP N N 122.718
81SER H H 8.233
81SER N N 117.456
82GLU H H 8.375
82GLU N N 121.788
83GLU H H 8.044
83GLU N N 119.225
84GLU H H 8.159
84GLU N N 118.203
85ILE H H 7.937
85ILE N N 120.792
86ARG H H 8.231
86ARG N N 121.538
87GLU H H 8.161
87GLU N N 118.379
88ALA H H 7.882
88ALA N N 120.239
89PHE H H 8.449
89PHE N N 118.117
90ARG H H 7.775
90ARG N N 116.079
91VAL H H 7.23
91VAL N N 118.183
92PHE H H 6.688
92PHE N N 113.127
93ASP H H 7.819
93ASP N N 116.503
94LYS H H 7.602
94LYS N N 125.373
95ASP H H 8.07
95ASP N N 114.036
96GLY H H 7.613
96GLY N N 108.687
97ASN H H 8.172
97ASN N N 119.358
98GLY H H 10.54
98GLY N N 113.216
100ILE H H 9.928
100ILE N N 127.731
101SER H H 8.782
101SER N N 123.256
102ALA H H 9.162
102ALA N N 122.818
103ALA H H 8.117
103ALA N N 118.189
104GLU H H 7.787
104GLU N N 120.128
105LEU H H 8.231
105LEU N N 121.366
106ARG H H 8.787
106ARG N N 118.502
107HIS H H 7.957
107HIS N N 118.774
108VAL H H 7.685
108VAL N N 119.066
109MET H H 8.11
109MET N N 115.413
110THR H H 8.529
110THR N N 116.879
111ASN H H 7.87
111ASN N N 123.846
112LEU H H 7.667
112LEU N N 118.323
113GLY H H 7.699

113GLY N N 106.76
114GLU H H 7.864
114GLU N N 119.971
115LYS H H 8.49
115LYS N N 124.969
116LEU H H 7.985
116LEU N N 124.895
117THR H H 9.119
117THR N N 114.373
118ASP H H 8.763
118ASP N N 120.773
119GLU H H 8.514
119GLU N N 119.166
120GLU H H 7.568
120GLU N N 119.969
121VAL H H 7.858
121VAL N N 122.014
122ASP H H 7.879
122ASP N N 120.064
123GLU H H 7.809
123GLU N N 119.053
124MET H H 7.427
124MET N N 118.974
125ILE H H 7.707
125ILE N N 118.137
126ARG H H 7.962
126ARG N N 117.749
127GLU H H 7.593
127GLU N N 117.582
128ALA H H 7.167
128ALA N N 116.6
130ILE H H 8.162
130ILE N N 128.314
131ASP H H 8.3
131ASP N N 118.314
132GLY H H 7.555
132GLY N N 108.507
133ASP H H 8.072
133ASP N N 120.492
134GLY H H 9.977
134GLY N N 112.41
135GLN H H 7.715
135GLN N N 115.893
136VAL H H 8.887
136VAL N N 124.77
137ASN H H 9.267
137ASN N N 128.023
138TYR H H 8.12
138TYR N N 118.376
139GLU H H 8.002
139GLU N N 118.503
141PHE H H 8.654
141PHE N N 124.119
142VAL H H 8.677
142VAL N N 119.14
143GLN H H 7.793
143GLN N N 120.24
144MET H H 7.391
144MET N N 118.549
145MET H H 7.544
145MET N N 114.271
146THR H H 7.591
146THR N N 109.129
147ALA H H 7.371
147ALA N N 126.868
148LYS H H 7.855
148LYS N N 126.436

Appendix D

CaM Y99E N111D-iNOS Peptide Assigned Chemical Shift

_Residue_seq_code
_Residue_label
_Atom_name
_Atom_type
_Chem_shift_value
2ASP H H 8.596
2ASP HA H 4.685
2ASP N N 120.326
3GLN H H 8.279
3GLN HA H 4.345
3GLN N N 119.614
4LEU H H 7.598
4LEU HA H 4.666
4LEU N N 120.715
5THR H H 8.647
5THR HA H 4.403
5THR HB H 4.607
5THR HG2 H 1.282
5THR N N 112.651
6GLU H H 8.97
6GLU HA H 3.897
6GLU HB2 H 1.993
6GLU HB3 H 1.993
6GLU HG2 H 2.316
6GLU HG3 H 2.316
6GLU N N 120.228
7GLU H H 8.628
7GLU HA H 4.046
7GLU HB2 H 1.964
7GLU HB3 H 1.964
7GLU HG2 H 2.316
7GLU HG3 H 2.316
7GLU N N 119.446
8GLN H H 7.587
8GLN HA H 3.961
8GLN HB2 H 1.901
8GLN HB3 H 1.901
8GLN HG2 H 2.286
8GLN HG3 H 2.286
8GLN N N 119.987
9ILE H H 8.495
9ILE HA H 3.791
9ILE HB H 1.889
9ILE HG2 H 1.024
9ILE HD1 H 0.783
9ILE N N 120.186
10ALA H H 8.052
10ALA HA H 4.046
10ALA HB H 1.465
10ALA N N 121.495
11GLU H H 7.784
11GLU HA H 4.017
11GLU HB2 H 1.985
11GLU HB3 H 1.985
11GLU HG2 H 2.514
11GLU HG3 H 2.514
11GLU N N 118.214
12PHE H H 8.299
12PHE HA H 4.562
12PHE HB2 H 3.46
12PHE HB3 H 3.46
12PHE N N 117.041
13LYS H H 9.023
13LYS HA H 3.642
13LYS HB2 H 1.759
13LYS HB3 H 1.759
13LYS HG2 H 1.524
13LYS HG3 H 1.524
13LYS N N 122.853
14GLU H H 7.906
14GLU HA H 4.041
14GLU HB2 H 2.155
14GLU HB3 H 2.155
14GLU HG2 H 2.346
14GLU HG3 H 2.346
14GLU N N 120.28
15ALA H H 8.206
15ALA HA H 3.959
15ALA HB H 1.759
15ALA N N 123.678
16PHE H H 8.544
16PHE HA H 3.301
16PHE HB2 H 2.653
16PHE HB3 H 2.287
16PHE N N 118.838
17SER H H 7.965
17SER HA H 4.024
17SER HB2 H 4.024
17SER HB3 H 4.024
17SER N N 114.532
18LEU H H 7.289
18LEU HA H 3.897
18LEU HB2 H 1.649
18LEU HB3 H 1.649
18LEU HG H 1.24
18LEU HD1 H 0.687
18LEU HD2 H 0.687
18LEU N N 120.169
19PHE H H 7.093
19PHE HA H 4.125
19PHE HB2 H 2.683
19PHE HB3 H 2.683
19PHE N N 112.443
20ASP H H 7.547
20ASP HA H 4.498
20ASP HB2 H 2.274
20ASP HB3 H 2.274
20ASP N N 117.116
21LYS H H 7.617
21LYS HA H 3.944
21LYS HB2 H 1.803
21LYS HB3 H 1.803
21LYS HG2 H 1.45
21LYS HG3 H 1.45
21LYS N N 124.017
22ASP H H 7.93
22ASP HA H 4.536
22ASP HB2 H 2.585
22ASP HB3 H 3.023
22ASP N N 113.68
23GLY H H 7.598
23GLY HA2 H 3.833
23GLY HA3 H 3.833
23GLY N N 108.614
24ASP H H 8.417
24ASP HA H 4.472
24ASP HB2 H 2.995
24ASP HB3 H 2.995
24ASP N N 120.703
25GLY H H 10.444
25GLY HA2 H 3.666
25GLY HA3 H 4.302
25GLY N N 112.393
26THR H H 8.12
26THR HA H 5.452
26THR HG2 H 0.98
26THR N N 111.768
27ILE H H 9.846
27ILE HA H 4.792
27ILE HB H 1.7
27ILE N N 126.142
28THR H H 8.412
28THR HA H 4.813
28THR HB H 4.693
28THR HG2 H 1.23
28THR N N 116.292
29THR H H 9.163
29THR HA H 3.736
29THR HB H 4.155
29THR HG2 H 1.239
29THR N N 112.316
30LYS H H 7.575
30LYS HA H 4.089
30LYS HB2 H 1.805
30LYS HB3 H 1.805
30LYS HG2 H 1.324
30LYS HG3 H 1.324
30LYS N N 120.699
31GLU H H 7.653
31GLU HA H 4.046
31GLU HB2 H 1.788
31GLU HB3 H 1.788
31GLU HG2 H 2.345
31GLU HG3 H 2.345
31GLU N N 121.23
32LEU H H 8.793
32LEU HA H 4.238
32LEU HB2 H 1.964
32LEU HB3 H 1.964
32LEU HG H 1.436
32LEU N N 120.113
33GLY H H 8.797
33GLY HA2 H 4.004
33GLY HA3 H 3.514
33GLY N N 105.542
34THR H H 7.861
34THR HA H 3.897
34THR HB H 4.257
34THR HG2 H 1.252
34THR N N 117.079
35VAL H H 7.338
35VAL HA H 3.557
35VAL HB H 1.973
35VAL HG1 H 0.711
35VAL HG2 H 0.423
35VAL N N 121.328
36MET H H 8.572
36MET HA H 3.974
36MET HB2 H 1.685
36MET HB3 H 1.685
36MET HG2 H 2.067
36MET HG3 H 2.067
36MET N N 117.074
37ARG H H 8.369
37ARG HA H 4.792
37ARG HB2 H 1.847
37ARG HB3 H 1.847
37ARG HG2 H 2.008
37ARG HG3 H 2.008
37ARG N N 118.19
38SER H H 7.923
38SER HA H 4.209
38SER HB2 H 4.089
38SER HB3 H 4.089
38SER N N 117.968
39LEU H H 7.414
39LEU HA H 4.196
39LEU HB2 H 1.745
39LEU HB3 H 1.745
39LEU HG H 1.673
39LEU HD1 H 0.627
39LEU HD2 H 0.627
39LEU N N 117.716
40GLY H H 7.706
40GLY HA2 H 3.727
40GLY HA3 H 3.727
40GLY N N 106.394
41GLN H H 7.887
41GLN HA H 4.389
41GLN HB2 H 1.589
41GLN HB3 H 1.589
41GLN HG2 H 2.118
41GLN HG3 H 2.118
41GLN N N 118.053

42ASN H H 8.64
42ASN HA H 5.133
42ASN HB2 H 2.419
42ASN HB3 H 2.741
42ASN N N 115.831
44THR H H 8.77
44THR HA H 4.36
44THR HB H 4.726
44THR HG2 H 1.282
44THR N N 112.903
45GLU H H 8.769
45GLU HA H 3.961
45GLU HB2 H 2.008
45GLU HB3 H 2.008
45GLU HG2 H 2.301
45GLU HG3 H 2.301
45GLU N N 120.256
46ALA H H 8.231
46ALA HA H 4.089
46ALA HB H 1.336
46ALA N N 120.661
47GLU H H 7.648
47GLU HA H 3.969
47GLU HB2 H 1.889
47GLU HB3 H 1.889
47GLU HG2 H 2.31
47GLU HG3 H 2.31
47GLU N N 118.577
48LEU H H 8.347
48LEU HA H 4.196
48LEU HB2 H 1.613
48LEU HB3 H 1.613
48LEU HG H 1.673
48LEU HD1 H 1.18
48LEU HD2 H 0.819
48LEU N N 120.102
49GLN H H 7.993
49GLN HA H 3.983
49GLN N N 118.06
50ASP H H 7.87
50ASP HA H 4.209
50ASP HB2 H 2.695
50ASP HB3 H 2.695
50ASP N N 119.027
51MET H H 7.906
51MET HA H 4.046
51MET HB2 H 1.769
51MET HB3 H 1.769
51MET HG2 H 1.432
51MET HG3 H 1.432
51MET N N 120.127
52ILE H H 7.809
52ILE HA H 3.488
52ILE HB H 2.009
52ILE HG12H 0.771
52ILE HG13H 0.771
52ILE HG2 H 1.228
52ILE HD1 H 0.675
52ILE N N 116.828
53ASN H H 8.303
53ASN HA H 4.6
53ASN HB2 H 2.903
53ASN HB3 H 2.903
53ASN N N 117.324
54GLU H H 7.495
54GLU HA H 4.005
54GLU HB2 H 2.058
54GLU HB3 H 2.058
54GLU HG2 H 2.322
54GLU HG3 H 2.322
54GLU N N 116.85
55VAL H H 7.266
55VAL HA H 4.089
55VAL HB H 2.021
55VAL HG1 H 1.024
55VAL HG2 H 1.024
55VAL N N 114.505
56ASP H H 8.017
56ASP HA H 4.472
56ASP HB2 H 2.683
56ASP HB3 H 2.683
56ASP N N 119.568
57ALA H H 8.225
57ALA HA H 4.209
57ALA HB H 1.465
57ALA N N 131.372
58ASP H H 8.239
58ASP HA H 4.564
58ASP HB2 H 2.976
58ASP HB3 H 2.976
58ASP N N 114.238
59GLY H H 7.615
59GLY HA2 H 3.833
59GLY HA3 H 3.833
59GLY N N 108.616
60ASN H H 8.193
60ASN HA H 4.579
60ASN HB2 H 2.622
60ASN HB3 H 3.26
60ASN N N 118.664
61GLY H H 10.347
61GLY HA2 H 4.259
61GLY HA3 H 4.259
61GLY N N 112.638
62THR H H 7.591
62THR HA H 4.771
62THR HB H 4.693
62THR HG2 H 1.099
62THR N N 108.14
63ILE H H 8.552
63ILE HA H 4.913
63ILE HB H 1.979
63ILE HG2 H 1.128
63ILE HD1 H 0.746
63ILE N N 122.617
64ASP H H 9.118
64ASP HA H 5.426
64ASP HB2 H 2.874
64ASP HB3 H 2.874
64ASP N N 128.589
65PHE H H 8.866
65PHE HA H 3.666
65PHE HB2 H 1.803
65PHE HB3 H 1.803
65PHE N N 118.902
67GLU H H 7.602
67GLU HA H 4.259
67GLU HB2 H 2.033
67GLU HB3 H 2.033
67GLU HG2 H 2.37
67GLU HG3 H 2.37
67GLU N N 118.591
68PHE H H 8.157
68PHE HA H 3.768
68PHE HB2 H 3.372
68PHE HB3 H 3.372
68PHE N N 123.063
69LEU H H 8.746
69LEU HA H 3.131
69LEU N N 119.516
70THR H H 7.992
70THR HA H 3.642
70THR HB H 4.024
70THR HG2 H 1.13
70THR N N 113.666
71MET H H 7.23
71MET HA H 4.046
71MET HB2 H 1.901
71MET HB3 H 1.901
71MET HG2 H 2.118
71MET HG3 H 2.118
71MET N N 119.457
72MET H H 7.834
72MET HA H 3.969
72MET HB2 H 1.877
72MET HB3 H 1.877
72MET HG2 H 2.154
72MET HG3 H 2.154
72MET N N 116.203
73ALA H H 8.421
73ALA HA H 3.919
73ALA HB H 1.24
73ALA N N 119.949
74ARG H H 7.37
74ARG HA H 4.032
74ARG HB2 H 1.865
74ARG HB3 H 1.865
74ARG HG2 H 1.649
74ARG HG3 H 1.649
74ARG N N 116.307
75LYS H H 7.863
75LYS HA H 4.329
75LYS N N 120.043
76MET H H 8.075
76MET HA H 4.302
76MET HB2 H 2.1
76MET HB3 H 2.1
76MET HG2 H 2.788
76MET HG3 H 2.788
76MET N N 116.94
77LYS H H 7.37
77LYS HA H 4.355
77LYS HB2 H 1.469
77LYS HB3 H 1.469
77LYS HG2 H 1.24
77LYS HG3 H 1.24
77LYS N N 116.565
78ASP H H 8.258
78ASP HA H 4.605
78ASP HB2 H 1.656
78ASP HB3 H 1.656
78ASP N N 123.077
79THR H H 8.448
79THR HA H 4.174
79THR HB H 4.663
79THR HG2 H 1.274
79THR N N 114.285
80ASP H H 8.341
80ASP HA H 4.762
80ASP HB2 H 2.731
80ASP HB3 H 2.731
80ASP N N 120.76
81SER H H 7.899
81SER HA H 4.321
81SER HB2 H 4.024
81SER HB3 H 4.024
81SER N N 115.676
82GLU H H 8.306
82GLU HA H 4.047
82GLU HB2 H 2.052
82GLU HB3 H 2.052
82GLU HG2 H 2.272
82GLU HG3 H 2.272
82GLU N N 122.016
83GLU H H 8.02
83GLU HA H 3.919
83GLU N N 118.018
84GLU H H 8.222
84GLU HA H 4.161
84GLU HB2 H 1.396
84GLU HB3 H 1.396
84GLU HG2 H 1.865
84GLU HG3 H 1.865
84GLU N N 118.594
85ILE H H 7.858
85ILE HA H 3.849
85ILE HB H 1.853
85ILE HG12H 1.661
85ILE HG13H 1.661
85ILE HD1 H 0.723
85ILE N N 119.119
86ARG H H 8.295
86ARG HA H 4.053
86ARG HB2 H 1.781
86ARG HB3 H 1.781
86ARG HG2 H 1.396
86ARG HG3 H 1.396
86ARG N N 120.605
87GLU H H 7.899
87GLU HA H 3.909
87GLU HB2 H 2.125
87GLU HB3 H 2.125
87GLU HG2 H 2.301
87GLU HG3 H 2.301
87GLU N N 119.503
88ALA H H 8.356
88ALA HA H 4.165
88ALA HB H 1.729

88ALA N N 122.323
89PHE H H 8.542
89PHE HA H 3.27
89PHE HB2 H 2.668
89PHE HB3 H 2.301
89PHE N N 119.005
90ARG H H 7.91
90ARG HA H 3.74
90ARG HB2 H 1.889
90ARG HB3 H 1.889
90ARG HG2 H 1.685
90ARG HG3 H 1.685
90ARG N N 117.149
91VAL H H 7.33
91VAL HA H 3.356
91VAL HB H 2.154
91VAL HG1 H 0.868
91VAL HG2 H 0.423
91VAL N N 118.456
92PHE H H 6.748
92PHE HA H 3.957
92PHE HB2 H 2.634
92PHE HB3 H 2.634
92PHE N N 112.806
93ASP H H 7.945
93ASP HA H 4.558
93ASP HB2 H 2.115
93ASP HB3 H 2.616
93ASP N N 116.493
94LYS H H 7.769
94LYS HA H 3.856
94LYS HB2 H 1.744
94LYS HB3 H 1.744
94LYS HG2 H 1.348
94LYS HG3 H 1.348
94LYS N N 124.188
95ASP H H 8.133
95ASP HA H 4.508
95ASP HB2 H 3.007
95ASP HB3 H 3.007
95ASP N N 113.847
96GLY H H 7.645
96GLY HA2 H 4.252
96GLY HA3 H 4.252
96GLY N N 108.775
97ASN H H 8.278
97ASN HA H 4.664
97ASN N N 119.457
98GLY H H 10.587
98GLY HA2 H 3.636
98GLY HA3 H 4.259
98GLY N N 112.949
99GLU H H 7.447
99GLU HA H 4.942
99GLU HG3 H 2.118
99GLU HB2 H 1.586
99GLU N N 116.565
100ILE H H 9.856
100ILE HA H 4.558
100ILE HB H 1.773
100ILE HG2 H 0.79
100ILE N N 127.273
101SER H H 8.944
101SER HA H 4.813
101SER HB2 H 3.915
101SER HB3 H 3.915
101SER N N 123.267
102ALA H H 9.278
102ALA HA H 3.897
102ALA HB H 1.436
102ALA N N 122.805
103ALA H H 8.093
103ALA HA H 3.885
103ALA HB H 1.18
103ALA N N 117.991
104GLU H H 7.901
104GLU HA H 3.94
104GLU HB2 H 1.781
104GLU HB3 H 1.781
104GLU HG2 H 2.118
104GLU HG3 H 2.118
104GLU N N 119.736
105LEU H H 8.377
105LEU HA H 4.173
105LEU HB2 H 1.925
105LEU HB3 H 1.925
105LEU HG H 1.408
105LEU HD1 H 0.952
105LEU N N 120.746
106ARG H H 8.914
106ARG HA H 3.724
106ARG HB2 H 1.935
106ARG HB3 H 1.935
106ARG HG2 H 1.45
106ARG N N 118.469
107HIS H H 8.094
107HIS HA H 4.305
107HIS HB2 H 3.404
107HIS HB3 H 3.404
107HIS N N 118.94
108VAL H H 7.776
108VAL HA H 3.38
108VAL HB H 1.481
108VAL HG1 H 0.615
108VAL HG2 H 0.615
108VAL N N 117.624
109MET H H 8.078
109MET HA H 4.196
109MET HB2 H 2.006
109MET HB3 H 2.006
109MET HG2 H 2.491
109MET HG3 H 2.491
109MET N N 115.355
110THR H H 8.646
110THR HA H 3.988
110THR HB H 4.297
110THR HG2 H 1.172
110THR N N 116.934
111ASP H H 8.371
111ASP HA H 4.399
111ASP HB2 H 2.918
111ASP HB3 H 2.918
111ASP N N 126.414
112LEU H H 7.74
112LEU HA H 4.173
112LEU HB2 H 1.877
112LEU HB3 H 1.877
112LEU HG H 1.637
112LEU HD1 H 0.699
112LEU HD2 H 0.699
112LEU N N 118.812
113GLY H H 7.951
113GLY HA2 H 4.217
113GLY HA3 H 4.217
113GLY N N 107.595
114GLU H H 7.997
114GLU HA H 3.776
114GLU HB2 H 1.913
114GLU HB3 H 1.913
114GLU HG2 H 2.07
114GLU HG3 H 2.07
114GLU N N 120.265
115LYS H H 8.464
115LYS HA H 4.366
115LYS HB2 H 1.641
115LYS HB3 H 1.641
115LYS HG2 H 1.26
115LYS HG3 H 1.26
115LYS N N 123.622
116LEU H H 8.092
116LEU HA H 4.751
116LEU HB2 H 1.48
116LEU HB3 H 1.48
116LEU HG H 1.553
116LEU HD1 H 0.776
116LEU HD2 H 0.776
116LEU N N 124.962
117THR H H 8.965
117THR HA H 4.435
117THR HB H 4.726
117THR HG2 H 1.25
117THR N N 113.14
118ASP H H 8.83
118ASP HA H 4.179
118ASP HB2 H 2.595
118ASP HB3 H 2.595
118ASP N N 120.745
119GLU H H 8.604
119GLU HA H 4.068
119GLU HB2 H 1.964
119GLU HB3 H 1.964
119GLU HG2 H 2.316
119GLU HG3 H 2.316
119GLU N N 118.999
121VAL H H 7.961
121VAL HA H 3.62
121VAL HB H 2.178
121VAL HG1 H 0.964
121VAL HG2 H 0.964
121VAL N N 120.225
122ASP H H 7.985
122ASP HA H 4.341
122ASP HB2 H 2.695
122ASP HB3 H 2.695
122ASP N N 119.975
123GLU H H 8.049
123GLU HA H 3.945
123GLU HB2 H 2.021
123GLU HB3 H 2.021
123GLU HG2 H 2.274
123GLU HG3 H 2.274
123GLU N N 119.554
124MET H H 7.725
124MET HA H 3.849
124MET HB2 H 1.901
124MET HB3 H 1.901
124MET HG2 H 2.43
124MET HG3 H 2.43
124MET N N 119.025
125ILE H H 7.776
125ILE HA H 3.407
125ILE HB H 2.058
125ILE HG12H 0.639
125ILE HG13H 0.639
125ILE HG2 H 1.18
125ILE HD1 H 0.603
125ILE N N 117.431
126ARG H H 8.049
126ARG HA H 3.704
126ARG HB2 H 2.045
126ARG HB3 H 2.045
126ARG N N 118.591
127GLU H H 7.412
127GLU HA H 3.915
127GLU HB2 H 1.865
127GLU HB3 H 1.865
127GLU HG2 H 2.142
127GLU HG3 H 2.142
127GLU N N 116.166
128ALA H H 7.168
128ALA HA H 4.558
128ALA HB H 1.336
128ALA N N 116.836
129ASP H H 7.661
129ASP HA H 4.387
129ASP HB2 H 2.31
129ASP HB3 H 2.647
129ASP N N 117.725
130ILE H H 8.314
130ILE HA H 3.871
130ILE HB H 1.935
130ILE HG12H 0.82
130ILE HG13H 0.82
130ILE HG2 H 1.612
130ILE N N 128.275
131ASP H H 8.331
131ASP HA H 4.458
131ASP HB2 H 2.595
131ASP HB3 H 2.595
131ASP N N 116.646
132GLY H H 7.587
132GLY HA2 H 3.842
132GLY HA3 H 3.842
132GLY N N 108.275
133ASP H H 8.331
133ASP HA H 4.426
133ASP HB2 H 2.454
133ASP HB3 H 2.454

133ASP N N 120.427
134GLY H H 10.15
134GLY HA2 H 3.343
134GLY HA3 H 4.005
134GLY N N 112.494
135GLN H H 7.822
135GLN HA H 4.918
135GLN HB2 H 1.773
135GLN HB3 H 1.773
135GLN HG2 H 1.891
135GLN HG3 H 1.891
135GLN N N 116.033
136VAL H H 8.888
136VAL HA H 5.015
136VAL HB H 2.096
136VAL HG1 H 1.113
136VAL HG2 H 0.776
136VAL N N 124.308
137ASN H H 9.381
137ASN HA H 5.324
137ASN HB2 H 3.284
137ASN HB3 H 3.284
137ASN N N 127.502
138TYR H H 8.082
138TYR HA H 4.414
138TYR N N 120.057
139GLU H H 8.029
139GLU HA H 3.812
139GLU HB2 H 2.081
139GLU HB3 H 2.081
139GLU HG2 H 2.331
139GLU HG3 H 2.331
139GLU N N 118.147
140GLU H H 8.739
140GLU HA H 3.855
140GLU HB2 H 2.081
140GLU HB3 H 2.081
140GLU HG2 H 2.345
140GLU HG3 H 2.345
140GLU N N 120.005
141PHE H H 8.582
141PHE HA H 3.812
141PHE HB2 H 3.02
141PHE HB3 H 3.358
141PHE N N 123.762
142VAL H H 8.601
142VAL HA H 3.237
142VAL HB H 1.759
142VAL HG1 H 0.776
142VAL HG2 H 0.512
142VAL N N 118.506
143GLN H H 7.848
143GLN HA H 3.812
143GLN HB2 H 2.07
143GLN HB3 H 2.07
143GLN HG2 H 2.322
143GLN HG3 H 2.322
143GLN N N 119.26
144MET H H 7.444
144MET HA H 4.053
144MET HB2 H 1.565
144MET HB3 H 1.565
144MET HG2 H 1.565
144MET HG3 H 1.565
144MET N N 116.781
145MET H H 7.569
145MET HA H 4.149
145MET HB2 H 1.889
145MET HB3 H 1.889
145MET N N 114.826
146THR H H 7.65
146THR HA H 4.274
146THR HG2 H 1.099
146THR N N 108.642
147ALA H H 7.689
147ALA HA H 4.267
147ALA HB H 1.362
147ALA N N 126.536
148LYS H H 7.884
148LYS HA H 4.077
148LYS HB2 H 1.685
148LYS HB3 H 1.685
148LYS HG2 H 1.333
148LYS HG3 H 1.333
148LYS N N 125.902

Appendix E

CaM_{1234} Assigned Chemical Shifts

_Residue_seq_code
_Residue_label
_Atom_name
_Atom_type
_Chem_shift_value
3GLN CA C 52.566
3GLN CB C 27.393
3GLN H H 8.115
3GLN HA H 4.369
3GLN HB2 H 1.894
3GLN HB3 H 1.894
3GLN N N 118.296
4LEU CA C 51.624
4LEU CB C 40.532
4LEU H H 8.231
4LEU HA H 4.492
4LEU HB2 H 1.665
4LEU HB3 H 1.665
4LEU HG H 1.279
4LEU HD1 H 0.805
4LEU HD2 H 0.805
4LEU N N 121.564
5THR CA C 57.548
5THR CB C 68.371
5THR H H 8.672
5THR HA H 4.439
5THR HB H 4.58
5THR HG2 H 1.139
5THR N N 112.706
6GLU CA C 57.414
6GLU CB C 26.291
6GLU H H 8.952
6GLU HA H 3.913
6GLU HB2 H 1.999
6GLU HB3 H 1.999
6GLU N N 120.025
7GLU CA C 57.38
7GLU CB C 26.055
7GLU H H 8.652
7GLU HA H 3.93
7GLU HB2 H 1.964
7GLU HB3 H 1.964
7GLU N N 119.114
8GLN CA C 55.899
8GLN CB C 26.213
8GLN H H 7.657
8GLN HA H 3.86
8GLN HB2 H 2.139
8GLN HB3 H 2.139
8GLN N N 120.294
9ILE CA C 64.012
9ILE CB C 35.181
9ILE H H 8.18
9ILE HA H 3.386
9ILE HB H 1.736
9ILE HG12 H 0.928
9ILE HG13 H 0.928
9ILE HG2 H 0.787
9ILE HD1 H 0.682
9ILE N N 118.311
10ALA CA C 52.634
10ALA CB C 15.041
10ALA H H 7.85
10ALA HA H 4.141
10ALA HB H 1.455
10ALA N N 120.211
11GLU CA C 56.64
11GLU CB C 26.449
11GLU H H 7.714
11GLU HA H 4.141
11GLU HB2 H 2.016
11GLU HB3 H 2.016
11GLU N N 119.943
12PHE CA C 55.663
12PHE CB C 34.08
12PHE H H 8.736
12PHE HA H 4.738
12PHE HB2 H 3.491
12PHE HB3 H 3.491
12PHE N N 119.942
13LYS CA C 57.144
13LYS CB C 29.281
13LYS H H 9.187
13LYS HA H 3.737
13LYS HB2 H 1.964
13LYS HB3 H 1.964
13LYS HG2 H 1.718
13LYS HG3 H 1.718
13LYS N N 121.35
14GLU CA C 56.774
14GLU CB C 26.37
14GLU H H 7.986
14GLU HA H 4.018
14GLU HB2 H 2.21
14GLU HB3 H 2.21
14GLU N N 120.528
15ALA CA C 52.364
15ALA CB C 16.379
15ALA H H 7.582
15ALA HA H 4.088
15ALA HB H 1.613
15ALA N N 120.583
16PHE CA C 59.4
16PHE CB C 37.935
16PHE H H 8.581
16PHE HA H 3.702
16PHE HB2 H 2.982
16PHE HB3 H 2.982
16PHE N N 117.456
17SER CA C 58.895
17SER CB C 60.309
17SER H H 8.345
17SER HA H 4.018
17SER N N 111.656
18LEU CA C 54.418
18LEU CB C 38.879
18LEU H H 7.261
18LEU HA H 3.913
18LEU HB2 H 1.7
18LEU HB3 H 1.7
18LEU HG H 1.49
18LEU HD1 H 0.752
18LEU HD2 H 0.752
18LEU N N 120.546
19PHE CA C 55.764
19PHE CB C 38.171
19PHE H H 7.056
19PHE HA H 4.123
19PHE HB2 H 2.912
19PHE HB3 H 2.912
19PHE N N 113.968
21LYS CA C 54.485
21LYS CB C 29.91
21LYS H H 8.363
21LYS HA H 4.053
21LYS HB2 H 1.753
21LYS HB3 H 1.753
21LYS N N 121.213
22ASP CA C 52.701
22ASP CB C 38.221
22ASP H H 8.494
22ASP HA H 4.633
22ASP HB2 H 2.561
22ASP HB3 H 2.561
22ASP N N 122.069
23GLY CA C 43.517
23GLY H H 8.351
23GLY HA2 H 3.895
23GLY HA3 H 3.895
23GLY N N 109.345
24ASP CA C 51.624
24ASP CB C 38.596
24ASP H H 7.985
24ASP HA H 4.685
24ASP HB2 H 2.701
24ASP HB3 H 2.701
24ASP N N 119.784
25GLY CA C 43.57
25GLY H H 8.322
25GLY HA2 H 3.983
25GLY HA3 H 3.983
25GLY N N 106.551
26THR CA C 57.043
26THR CB C 70.033
26THR H H 7.523
26THR HA H 5.23
26THR HB H 4.018
26THR HG2 H 0.963
26THR N N 107.782
27ILE CA C 56.808
27ILE CB C 37.847
27ILE H H 8.432
27ILE HA H 4.72
27ILE HB H 1.753
27ILE HG12 H 1.103
27ILE HG13 H 1.103
27ILE HG2 H 0.805
27ILE HD1 H 0.577
27ILE N N 111.325
28THR CA C 57.785
28THR CB C 68.629
28THR H H 8.538
28THR HA H 4.896
28THR HB H 3.948
28THR HG2 H 1.121
28THR N N 110.566
29THR CA C 62.77
29THR CB C 64.887
29THR H H 8.215
29THR HA H 3.72
29THR HB H 4.72
29THR HG2 H 1.209
29THR N N 110.671
30LYS CA C 55.697
30LYS CB C 29.36
30LYS H H 7.571
30LYS HA H 4.123
30LYS HB2 H 1.841
30LYS HB3 H 1.841
30LYS HG2 H 1.542
30LYS HG3 H 1.542
30LYS N N 119.083
31GLU CA C 54.115
31GLU CB C 27.235
31GLU H H 7.478
31GLU HA H 4.018
31GLU HB2 H 1.911
31GLU HB3 H 1.911
31GLU HG2 H 2.157
31GLU HG3 H 2.157
31GLU N N 118.126
32LEU CA C 55.865
32LEU CB C 39.033
32LEU H H 7.37
32LEU HA H 3.807
32LEU HB2 H 1.771
32LEU HB3 H 1.771
32LEU HG H 1.244
32LEU HD1 H 0.735
32LEU N N 120.459
33GLY CA C 45.32
33GLY H H 8.523
33GLY HA2 H 3.737
33GLY HA3 H 3.351
33GLY N N 104.903
34THR CA C 63.608
34THR CB C 65.526
34THR H H 7.385
34THR HA H 3.737
34THR HB H 4.001
34THR HG2 H 1.068
34THR N N 118.195

35VAL CA C 63.709
35VAL CB C 28.415
35VAL H H 7.93
35VAL HA H 3.175
35VAL HB H 1.876
35VAL HG1 H 0.7
35VAL HG2 H 0.471
35VAL N N 122.39
36MET CA C 57.515
36MET CB C 29.045
36MET H H 8.353
36MET HA H 3.913
36MET HB2 H 1.929
36MET HB3 H 1.929
36MET HG2 H 2.052
36MET HG3 H 2.052
36MET N N 118.092
37ARG CA C 56.505
37ARG CB C 27.078
37ARG H H 8.422
37ARG HA H 4.633
37ARG HB2 H 1.823
37ARG HB3 H 1.823
37ARG HG2 H 1.595
37ARG HG3 H 1.595
37ARG N N 119.169
38SER CA C 59.03
38SER CB C 60.208
38SER H H 8.001
38SER HA H 4.176
38SER N N 118.814
39LEU CA C 51.826
39LEU CB C 39.97
39LEU H H 7.261
39LEU HA H 4.65
39LEU HB2 H 1.858
39LEU HB3 H 1.858
39LEU HG H 1.7
39LEU HD1 H 0.928
39LEU N N 120.675
40GLY CA C 42.969
40GLY H H 7.859
40GLY HA2 H 4.334
40GLY HA3 H 3.755
40GLY N N 106.965
41GLN CA C 51.355
41GLN CB C 27.235
41GLN H H 7.673
41GLN HA H 4.334
41GLN HB2 H 1.718
41GLN HB3 H 1.718
41GLN HG2 H 1.981
41GLN HG3 H 1.981
41GLN N N 117.583
42ASN CA C 48.325
42ASN H H 8.605
42ASN HA H 5.107
42ASN HB2 H 2.631
42ASN HB3 H 2.631
42ASN N N 116.352
44THR CA C 57.851
44THR CB C 68.145
44THR H H 8.68
44THR HA H 4.29
44THR HB H 4.613
44THR HG2 H 1.181
44THR N N 112.844
45GLU CA C 57.212
45GLU CB C 26.134
45GLU H H 8.777
45GLU HA H 3.817
45GLU HB2 H 1.977
45GLU HB3 H 1.977
45GLU HG2 H 2.2
45GLU HG3 H 2.2
45GLU N N 120.218
46ALA CA C 52.23
46ALA CB C 15.356
46ALA H H 8.245
46ALA HA H 4.016
46ALA HB H 1.38
46ALA N N 120.747
47GLU CA C 56.168
47GLU CB C 27.078
47GLU H H 7.669
47GLU HA H 3.991
47GLU HB2 H 1.877
47GLU HB3 H 1.877
47GLU HG2 H 2.176
47GLU HG3 H 2.176
47GLU N N 118.663
48LEU CA C 55.394
48LEU CB C 38.958
48LEU H H 8.175
48LEU HA H 3.966
48LEU HB2 H 1.504
48LEU HB3 H 1.504
48LEU HG H 1.628
48LEU HD1 H 0.708
48LEU HD2 H 0.708
48LEU N N 119.754
49GLN CA C 55.899
49GLN CB C 25.269
49GLN H H 7.979
49GLN HA H 3.867
49GLN HB2 H 1.943
49GLN HB3 H 1.943
49GLN HG2 H 2.18
49GLN HG3 H 2.18
49GLN N N 117.263
50ASP CA C 54.721
50ASP CB C 37.62
50ASP H H 7.829
50ASP HA H 4.086
50ASP HB2 H 2.652
50ASP HB3 H 2.652
50ASP N N 118.83
51MET CA C 57.01
51MET CB C 31.09
51MET H H 7.829
51MET HA H 4.002
51MET HB2 H 2.146
51MET HB3 H 2.146
51MET HG2 H 1.91
51MET HG3 H 1.91
51MET N N 118.63
52ILE CA C 62.463
52ILE CB C 35.181
52ILE H H 8.132
52ILE HB H 1.859
52ILE HG2 H 0.813
52ILE HD1 H 0.728
52ILE N N 118.575
53ASN CA C 52.6
53ASN CB C 35.26
53ASN H H 8.23
53ASN HA H 4.356
53ASN HB2 H 2.821
53ASN HB3 H 2.821
53ASN N N 117.456
54GLU CA C 55.63
54GLU CB C 27.235
54GLU H H 7.656
54GLU HA H 4.103
54GLU HB2 H 2.011
54GLU HB3 H 2.011
54GLU HG2 H 2.163
54GLU HG3 H 2.163
54GLU N N 117.344
55VAL CA C 59.905
55VAL CB C 29.989
55VAL H H 7.46
55VAL HA H 4.187
55VAL HB H 2.095
55VAL HG1 H 0.88
55VAL HG2 H 0.745
55VAL N N 113.904
57ALA CA C 51.22
57ALA CB C 16.143
57ALA H H 8.152
57ALA HA H 4.187
57ALA HB H 1.353
57ALA N N 123.284
58ASP CA C 51.258
58ASP CB C 38.097
58ASP H H 8.239
58ASP HA H 4.677
58ASP HB2 H 2.652
58ASP HB3 H 2.652
58ASP N N 116.241
59GLY CA C 43.151
59GLY H H 7.986
59GLY HA2 H 3.901
59GLY HA3 H 3.901
59GLY N N 107.441
60ASN CA C 50.345
60ASN CB C 35.974
60ASN H H 8.341
60ASN HA H 4.677
60ASN HB2 H 2.821
60ASN HB3 H 2.821
60ASN N N 118.036
61GLY CA C 43.099
61GLY H H 8.451
61GLY HA2 H 4.002
61GLY HA3 H 4.002
61GLY N N 107.713
62THR CA C 57.414
62THR CB C 69.599
62THR H H 7.696
62THR HA H 5.115
62THR HB H 4.069
62THR HG2 H 0.998
62THR N N 111.076
63ILE CA C 57.515
63ILE CB C 38.722
63ILE H H 8.978
63ILE HA H 4.575
63ILE HB H 1.791
63ILE HG2 H 1.1
63ILE HD1 H 0.897
63ILE N N 120.045
64ASP CA C 48.998
64ASP CB C 39.102
64ASP H H 8.42
64ASP HA H 5.183
64ASP HB2 H 2.551
64ASP HB3 H 2.551
64ASP N N 124.941
65PHE CA C 60.107
65PHE H H 8.92
65PHE HA H 3.715
65PHE HB2 H 1.876
65PHE HB3 H 1.876
65PHE N N 118.092
67GLU CA C 56.438
67GLU CB C 26.527
67GLU H H 8.027
67GLU HA H 3.868
67GLU HB2 H 1.859
67GLU HB3 H 1.859
67GLU HG2 H 2.276
67GLU HG3 H 2.276
67GLU N N 117.856
68PHE CA C 58.525
68PHE CB C 36.676
68PHE H H 8.464
68PHE HA H 3.976
68PHE HB2 H 2.999
68PHE HB3 H 2.999
68PHE N N 122.207
69LEU CA C 54.99
69LEU CB C 38.171
69LEU H H 8.404
69LEU HA H 3.216
69LEU HB2 H 1.299
69LEU HB3 H 1.299
69LEU HD1 H 0.647
69LEU HD2 H 0.828
69LEU N N 118.368
70THR CA C 63.911
70THR CB C 65.526
70THR H H 7.646
70THR HA H 3.741
70THR HB H 3.994
70THR HG2 H 1.063
70THR N N 115.827
71MET CA C 56.741

71MET CB C 29.596
71MET H H 7.795
71MET HA H 3.994
71MET HB2 H 1.787
71MET HB3 H 1.787
71MET HG2 H 2.058
71MET HG3 H 2.058
71MET N N 120.865
72MET CA C 53.172
72MET CB C 28.551
72MET H H 7.968
72MET HA H 4.049
72MET HB2 H 1.787
72MET HB3 H 1.787
72MET HG2 H 2.312
72MET HG3 H 2.312
72MET N N 117.111
73ALA CA C 52.061
73ALA CB C 15.12
73ALA H H 8.24
73ALA HA H 4.049
73ALA HB H 1.281
73ALA N N 121.186
74ARG CA C 55.798
74ARG CB C 27.235
74ARG H H 7.408
74ARG HA H 3.886
74ARG HB2 H 1.751
74ARG HB3 H 1.751
74ARG HG2 H 1.896
74ARG HG3 H 1.896
74ARG N N 116.472
75LYS CA C 53.947
75LYS CB C 28.966
75LYS H H 7.617
75LYS HA H 4.139
75LYS HB2 H 1.715
75LYS HB3 H 1.715
75LYS N N 118.285
76MET CA C 53.677
76MET CB C 29.91
76MET H H 7.878
76MET HA H 4.157
76MET HB2 H 1.95
76MET HB3 H 1.95
76MET N N 117.498
77LYS CA C 54.216
77LYS CB C 29.989
77LYS H H 7.642
77LYS HA H 4.248
77LYS HB2 H 1.896
77LYS HB3 H 1.896
77LYS N N 120.321
78ASP CA C 52.061
78ASP CB C 38.171
78ASP H H 8.219
78ASP HA H 4.646
78ASP HB2 H 2.692
78ASP HB3 H 2.692
78ASP N N 121.295
79THR CA C 59.77
79THR CB C 66.965
79THR H H 8.039
79THR HA H 4.193
79THR HB H 4.338
79THR HG2 H 1.154
79THR N N 114.252
80ASP CA C 52.061
80ASP CB C 38.327
80ASP H H 8.359
80ASP HA H 4.664
80ASP HB2 H 2.619
80ASP HB3 H 2.619
80ASP N N 122.925
81SER CA C 56.842
81SER CB C 60.907
81SER H H 8.329
81SER HA H 4.302
81SER HB2 H 3.741
81SER HB3 H 3.741
81SER N N 116.628
82GLU CA C 55.529
82GLU CB C 26.921
82GLU H H 8.353
82GLU HA H 4.049
82GLU HB2 H 1.841
82GLU HB3 H 1.841
82GLU HG2 H 2.131
82GLU HG3 H 2.131
82GLU N N 121.876
83GLU CA C 55.773
83GLU CB C 26.527
83GLU H H 8.129
83GLU HA H 3.994
83GLU HB2 H 1.805
83GLU HB3 H 1.805
83GLU HG2 H 2.058
83GLU HG3 H 2.058
83GLU N N 119.886
84GLU CA C 55.865
84GLU CB C 26.921
84GLU H H 7.9
84GLU HA H 3.976
84GLU HB2 H 1.859
84GLU HB3 H 1.859
84GLU N N 118.973
85ILE CA C 60.881
85ILE CB C 36.125
85ILE H H 7.97
85ILE HA H 3.759
85ILE HB H 1.914
85ILE HG2 H 0.919
85ILE HD1 H 0.702
85ILE N N 120.87
86ARG CA C 56.37
86ARG CB C 29.832
86ARG H H 8.179
86ARG HA H 4.03
86ARG N N 121.318
87GLU CA C 55.36
87GLU CB C 26.685
87GLU H H 8.265
87GLU HA H 3.94
87GLU HB2 H 1.823
87GLU HB3 H 1.823
87GLU HG2 H 2.058
87GLU HG3 H 2.058
87GLU N N 119.274
88ALA CA C 51.523
88ALA CB C 15.592
88ALA H H 7.857
88ALA HA H 4.012
88ALA HB H 1.552
88ALA N N 122.158
89PHE CA C 57.097
89PHE H H 7.882
89PHE HA H 2.981
89PHE HB2 H 2.782
89PHE HB3 H 2.782
89PHE N N 115.965
91VAL CA C 62.548
91VAL H H 7.924
91VAL HA H 3.506
91VAL HB H 1.841
91VAL HG1 H 0.846
91VAL HG2 H 0.846
91VAL N N 119.084
92PHE CA C 55.836
92PHE CB C 36.833
92PHE H H 6.854
92PHE HA H 4.266
92PHE HB2 H 2.728
92PHE HB3 H 2.728
92PHE N N 112.485
94LYS CA C 54.855
94LYS CB C 29.832
94LYS H H 7.811
94LYS N N 125.896
95ASP CA C 51.826
95ASP CB C 38.159
95ASP H H 8.266
95ASP HA H 4.664
95ASP HB2 H 2.71
95ASP HB3 H 2.71
95ASP N N 118.967
96GLY CA C 43.047
96GLY H H 8.113
96GLY HA2 H 3.868
96GLY HA3 H 3.868
96GLY N N 107.633
97ASN CA C 50.547
97ASN CB C 36.099
97ASN H H 8.235
97ASN HA H 4.627
97ASN HB2 H 2.782
97ASN HB3 H 2.782
97ASN N N 117.733
98GLY CA C 42.681
98GLY H H 8.312
98GLY HA2 H 3.886
98GLY HA3 H 3.886
98GLY N N 107.446
99TYR CA C 56.909
99TYR H H 7.855
99TYR HA H 4.03
99TYR N N 118.748
101SER CA C 54.923
101SER CB C 62.166
101SER H H 8.529
101SER HA H 3.976
101SER HB2 H 3.669
101SER HB3 H 3.669
101SER N N 119.086
102ALA CA C 52.465
102ALA CB C 15.435
102ALA H H 8.68
102ALA HA H 3.94
102ALA HB H 1.299
102ALA N N 124.831
103ALA CA C 51.927
103ALA CB C 15.513
103ALA H H 8.222
103ALA HA H 3.994
103ALA HB H 1.281
103ALA N N 119.005
104GLU CA C 55.495
104GLU CB C 26.763
104GLU H H 7.735
104GLU HA H 4.012
104GLU N N 118.601
105LEU CA C 54.923
105LEU CB C 38.879
105LEU H H 8.088
105LEU HA H 4.012
105LEU HB2 H 1.769
105LEU HB3 H 1.769
105LEU HG H 1.299
105LEU HD1 H 0.629
105LEU HD2 H 0.629
105LEU N N 120.659
106ARG CA C 56.539
106ARG CB C 27.157
106ARG H H 8.025
106ARG HA H 3.922
106ARG HB2 H 1.751
106ARG HB3 H 1.751
106ARG N N 117.594
107HIS CA C 55.596
107HIS CB C 26.527
107HIS H H 7.68
107HIS HA H 4.229
107HIS HB2 H 1.95
107HIS HB3 H 1.95
107HIS N N 117.689
108VAL CA C 62.497
108VAL CB C 29.202
108VAL H H 7.929
108VAL HA H 3.994
108VAL HB H 2.058
108VAL HG1 H 0.792
108VAL N N 118.922
109MET CA C 54.485
109MET CB C 29.674
109MET H H 8.142
109MET HA H 4.664
109MET HB2 H 1.751
109MET HB3 H 1.751
109MET HG2 H 2.131

109MET HG3 H 2.131
109MET N N 117.291
110THR CA C 61.521
110THR CB C 66.503
110THR H H 7.914
110THR HA H 4.103
110THR HB H 4.229
110THR N N 112.374
111ASN CA C 51.691
111ASN CB C 36.047
111ASN H H 7.906
111ASN HA H 4.682
111ASN HB2 H 2.746
111ASN HB3 H 2.746
111ASN N N 119.669
112LEU CA C 52.768
112LEU CB C 39.72
112LEU H H 7.764
112LEU HA H 4.139
112LEU HB2 H 1.66
112LEU HB3 H 1.66
112LEU HD1 H 0.683
112LEU N N 119.868
113GLY CA C 43.204
113GLY H H 8.168
113GLY HA2 H 3.849
113GLY HA3 H 3.849
113GLY N N 107.803
114GLU CA C 53.711
114GLU CB C 27.157
114GLU H H 8.018
114GLU HA H 4.175
114GLU HB2 H 1.751
114GLU HB3 H 1.751
114GLU HG2 H 1.968
114GLU HG3 H 1.968
114GLU N N 119.894
115LYS CA C 53.812
115LYS CB C 29.674
115LYS H H 8.238
115LYS HA H 4.193
115LYS HB2 H 1.805
115LYS HB3 H 1.805
115LYS N N 120.422
116LEU CA C 51.523
116LEU CB C 41.318
116LEU H H 7.843
116LEU HA H 4.627
116LEU HB2 H 1.516
116LEU HB3 H 1.516
116LEU HD1 H 0.647
116LEU HD2 H 0.647
116LEU N N 122.019
117THR CA C 58.154
117THR CB C 68.224
117THR H H 8.805
117THR HA H 4.447
117THR HB H 4.646
117THR HG2 H 1.19
117THR N N 113.495
118ASP CA C 54.653
118ASP CB C 37.305
118ASP H H 8.706
118ASP HA H 4.193
118ASP HB2 H 2.475
118ASP HB3 H 2.475
118ASP N N 120.936
119GLU CA C 56.741
119GLU CB C 26.449
119GLU H H 8.494
119GLU HA H 4.067
119GLU HB2 H 1.805
119GLU HB3 H 1.805
119GLU N N 118.257
120GLU CA C 56
120GLU CB C 27.471
120GLU H H 7.781
120GLU HA H 4.121
120GLU HB2 H 1.841
120GLU HB3 H 1.841
120GLU N N 120.294
121VAL CA C 63.675
121VAL CB C 27.235
121VAL H H 8.122
121VAL HA H 3.831
121VAL HB H 2.04
121VAL HG1 H 0.883
121VAL N N 120.729
122ASP CA C 54.524
122ASP CB C 42.771
122ASP H H 8.248
122ASP HA H 4.211
122ASP HB2 H 2.619
122ASP HB3 H 2.619
122ASP N N 119.726
123GLU CA C 56.62
123GLU CB C 26.58
123GLU H H 8.222
123GLU HA H 4.049
123GLU HB2 H 1.878
123GLU HB3 H 1.878
123GLU N N 119.915
124MET CA C 56.13
124MET CB C 30.461
124MET H H 7.878
124MET HA H 3.886
124MET HB2 H 2.131
124MET HB3 H 2.131
124MET N N 119.08
125ILE CA C 61.958
125ILE CB C 34.842
125ILE H H 8.169
125ILE HA H 3.795
125ILE HB H 1.733
125ILE HG2 H 0.828
125ILE HD1 H 0.774
125ILE N N 119.157
126ARG CA C 56.202
126ARG CB C 27.629
126ARG H H 7.904
126ARG HA H 4.067
126ARG HB2 H 2.022
126ARG HB3 H 2.022
126ARG N N 119.956
127GLU CA C 54.99
127GLU CB C 26.763
127GLU H H 8.024
127GLU HA H 4.012
127GLU HB2 H 1.932
127GLU HB3 H 1.932
127GLU N N 118.102
128ALA CA C 50.176
128ALA CB C 16.379
128ALA H H 7.689
128ALA HA H 4.175
128ALA HB H 1.353
128ALA N N 121.388
130ILE CA C 58.693
130ILE CB C 35.968
130ILE H H 7.774
130ILE HA H 4.211
130ILE HB H 1.823
130ILE HG12 H 1.208
130ILE HG13 H 1.208
130ILE HD1 H 0.81
130ILE N N 118.856
131ASP CA C 51.388
131ASP CB C 37.384
131ASP H H 8.345
131ASP HA H 4.646
131ASP HB2 H 2.674
131ASP HB3 H 2.674
131ASP N N 123.284
132GLY CA C 43.309
132GLY H H 8.229
132GLY HA2 H 3.813
132GLY HA3 H 3.813
132GLY N N 108.046
133ASP CA C 51.422
133ASP CB C 38.346
133ASP H H 8.19
133ASP HA H 4.682
133ASP HB2 H 2.493
133ASP HB3 H 2.493
133ASP N N 119.587
134GLY CA C 42.89
134GLY H H 8.213
134GLY HA2 H 3.831
134GLY HA3 H 3.831
134GLY N N 108.03
135GLN CA C 52.499
135GLN H H 8.109
135GLN HA H 4.646
135GLN HB2 H 1.769
135GLN HB3 H 1.769
135GLN N N 118.777
136VAL CA C 58.532
136VAL CB C 31.326
136VAL H H 8.476
136VAL HA H 4.609
136VAL HB H 1.878
136VAL HG1 H 1.027
136VAL HG2 H 1.027
136VAL N N 122.094
137ASN CA C 49.537
137ASN CB C 35.889
137ASN H H 8.607
137ASN HA H 4.627
137ASN HB2 H 2.583
137ASN HB3 H 2.583
137ASN N N 123.726
138TYR CA C 58.154
138TYR CB C 35.26
138TYR H H 8.275
138TYR HA H 4.121
138TYR N N 123.091
139GLU CA C 56.606
139GLU CB C 26.501
139GLU H H 8.201
139GLU HA H 3.976
139GLU HB2 H 1.787
139GLU HB3 H 1.787
139GLU HG2 H 2.004
139GLU HG3 H 2.004
139GLU N N 119.717
140GLU CA C 55.899
140GLU CB C 26.921
140GLU H H 7.876
140GLU HA H 4.03
140GLU HB2 H 1.914
140GLU HB3 H 1.914
140GLU N N 117.372
141PHE CA C 57.919
141PHE CB C 36.519
141PHE H H 7.973
141PHE HA H 3.904
141PHE N N 120.644
142VAL CA C 63.237
142VAL CB C 29.26
142VAL H H 8.13
142VAL HA H 3.958
142VAL HB H 1.733
142VAL HG1 H 0.756
142VAL HG2 H 0.756
142VAL N N 118.798
143GLN CA C 55.431
143GLN CB C 29.91
143GLN H H 7.759
143GLN HA H 4.067
143GLN HB2 H 1.914
143GLN HB3 H 1.914
143GLN N N 119.619
144MET CA C 53.543
144MET CB C 28.966
144MET H H 7.784
144MET HA H 4.139
144MET HB2 H 2.022
144MET HB3 H 2.022
144MET N N 116.729
145MET CA C 53.677
145MET CB C 29.674
145MET H H 7.87
145MET HA H 4.229
145MET HB2 H 1.896
145MET HB3 H 1.896
145MET N N 117.399
146THR CA C 59.703
146THR CB C 67.041

146THR H H 7.652
146THR HA H 4.248
146THR HB H 4.067
146THR HG2 H 1.154
146THR N N 111.38
147ALA CA C 49.974
147ALA CB C 16.221
147ALA H H 7.711
147ALA HA H 4.229
147ALA HB H 1.281
147ALA N N 125.991
148LYS CA C 54.889
148LYS H H 7.662
148LYS HA H 4.139
148LYS N N 125.356

Appendix F

CaM_{12} Assigned Chemical Shifts

$ApoCaM_{12}$
_Residue_seq_code
_Residue_label
_Atom_name
_Atom_type
_Chem_shift_value
3GLN H H 8.115
3GLN N N 118.296
4LEU H H 8.231
4LEU N N 121.564
5THR H H 8.672
5THR N N 112.706
6GLU H H 8.944
6GLU N N 119.983
7GLU H H 8.642
7GLU N N 119.1
8GLN H H 7.657
8GLN N N 120.294
9ILE H H 8.183
9ILE N N 118.438
10ALA H H 7.85
10ALA N N 120.211
11GLU H H 7.714
11GLU N N 119.943
12PHE H H 8.748
12PHE N N 119.942
13LYS H H 9.191
13LYS N N 121.35
14GLU H H 7.986
14GLU N N 120.528
15ALA H H 7.576
15ALA N N 120.583
16PHE H H 8.586
16PHE N N 117.484
17SER H H 8.345
17SER N N 111.656
18LEU H H 7.261
18LEU N N 120.546
19PHE H H 7.056
19PHE N N 113.968
20ALA H H 7.452
20ALA N N 123.081
21LYS H H 8.362
21LYS N N 121.199
22ASP H H 8.494
22ASP N N 122.069
23GLY H H 8.347
23GLY N N 109.317
24ASP H H 7.985
24ASP N N 119.784
25GLY H H 8.32
25GLY N N 106.537
26THR H H 7.523
26THR N N 107.782
27ILE H H 8.429
27ILE N N 111.198
28THR H H 8.529
28THR N N 110.566
29THR H H 8.215
29THR N N 110.671
30LYS H H 7.564
30LYS N N 119.055
31GLU H H 7.469
31GLU N N 118.084
32LEU H H 7.362
32LEU N N 120.544
33GLY H H 8.531
33GLY N N 104.903
34THR H H 7.384
34THR N N 118.195
35VAL H H 7.93
35VAL N N 122.39
36MET H H 8.349
36MET N N 118.134
37ARG H H 8.422
37ARG N N 119.169
38SER H H 7.998
38SER N N 118.814
39LEU H H 7.261
39LEU N N 120.675
40GLY H H 7.859
40GLY N N 106.965
41GLN H H 7.673
41GLN N N 117.583
42ASN H H 8.605
42ASN N N 116.352
44THR H H 8.688
44THR N N 112.844
45GLU H H 8.774
45GLU N N 120.218
46ALA H H 8.245
46ALA N N 120.747
47GLU H H 7.669
47GLU N N 118.663
48LEU H H 8.175
48LEU N N 119.754
49GLN H H 7.979
49GLN N N 117.263
50ASP H H 7.837
50ASP N N 118.802
51MET H H 7.844
51MET N N 118.602
52ILE H H 8.132
52ILE N N 118.575
53ASN H H 8.23
53ASN N N 117.456
54GLU H H 7.656
54GLU N N 117.344
55VAL H H 7.458
55VAL N N 113.749
56ALA H H 8.189
56ALA N N 124.057
57ALA H H 8.132
57ALA N N 123.228
58ASP H H 8.223
58ASP N N 116.185
59GLY H H 7.976
59GLY N N 107.385
60ASN H H 8.338
60ASN N N 118.064
61GLY H H 8.451
61GLY N N 107.713
62THR H H 7.696
62THR N N 111.076
63ILE H H 8.967
63ILE N N 120.087
64ASP H H 8.42
64ASP N N 124.941
65PHE H H 8.928
65PHE N N 118.092
67GLU H H 8.02
67GLU N N 117.588
68PHE H H 8.464
68PHE N N 122.207
69LEU H H 8.394
69LEU N N 118.283
70THR H H 7.638
70THR N N 115.827
71MET H H 7.795
71MET N N 120.865
72MET H H 7.968
72MET N N 117.111
73ALA H H 8.211
73ALA N N 120.833
74ARG H H 7.394
74ARG N N 116.554
75LYS H H 7.622
75LYS N N 118.287
76MET H H 7.879
76MET N N 117.661
77LYS H H 7.667
77LYS N N 120.522
78ASP H H 8.248
78ASP N N 121.734
79THR H H 8.072
79THR N N 114.662
80ASP H H 8.381
80ASP N N 122.933
81SER H H 8.385
81SER N N 117.005
82GLU H H 8.362
82GLU N N 121.619
83GLU H H 8.11
83GLU N N 118.269
84GLU H H 7.94
84GLU N N 118.933
85ILE H H 7.857
85ILE N N 120.059
86ARG H H 8.29
86ARG N N 119.229
87GLU H H 8.32
87GLU N N 116.761
88ALA H H 7.442
88ALA N N 121.161
89PHE H H 7.42
89PHE N N 113.977
90ARG H H 8.147
90ARG N N 117.775
91VAL H H 7.09
91VAL N N 116.807
93ASP H H 7.763
93ASP N N 121.119
94LYS H H 8.336
94LYS N N 124.233
95ASP H H 8.53
95ASP N N 116.231
96GLY H H 7.995
96GLY N N 109.905
97ASN H H 8.936
97ASN N N 118.477
98GLY H H 8.368
98GLY N N 109.301
99TYR H H 7.701
99TYR N N 118.033
100ILE H H 8.541
100ILE N N 113.244
101SER H H 8.83
101SER N N 117.204
102ALA H H 8.742
102ALA N N 124.615
103ALA H H 8.194
103ALA N N 118.833
104GLU H H 7.661
104GLU N N 120.033
105LEU H H 8.131
105LEU N N 120.563
106ARG H H 7.971
106ARG N N 117.033
107HIS H H 7.657
107HIS N N 118.426
108VAL H H 8.048
108VAL N N 119.488
109MET H H 8.271
109MET N N 119.06
110THR H H 7.858
110THR N N 110.972

111ASN H H 7.592
111ASN N N 119.492
112LEU H H 7.666
112LEU N N 119.633
113GLY H H 8.091
113GLY N N 107.833
114GLU H H 8.101
114GLU N N 120.033
115LYS H H 8.181
115LYS N N 119.933
116LEU H H 7.695
116LEU N N 120.891
117THR H H 8.875
117THR N N 113.319
118ASP H H 8.74
118ASP N N 120.733
119GLU H H 8.493
119GLU N N 117.747
120GLU H H 7.728
120GLU N N 120.331
121VAL H H 8.142
121VAL N N 120.628
122ASP H H 8.294
122ASP N N 119.034
123GLU H H 7.791
123GLU N N 119.033
124MET H H 7.83
124MET N N 118.533
125ILE H H 8.254
125ILE N N 118.204
126ARG H H 7.867
126ARG N N 119.433
127GLU H H 7.765
127GLU N N 116.802
128ALA H H 7.534
128ALA N N 121.372
129ASP H H 8.281
129ASP N N 119.433
130ILE H H 7.761
130ILE N N 120.833
131ASP H H 8.53
131ASP N N 123.821
132GLY H H 8.281
132GLY N N 107.761
133ASP H H 8.211
133ASP N N 119.133
134GLY H H 8.465
134GLY N N 109.277
135GLN H H 8.228
135GLN N N 119.247
136VAL H H 9.341
136VAL N N 119.233
137ASN H H 8.701
137ASN N N 124.877
138TYR H H 7.441
138TYR N N 122.233
139GLU H H 8.092
139GLU N N 125.599
140GLU H H 7.781
140GLU N N 116.806
141PHE H H 7.488
141PHE N N 118.833
142VAL H H 8.061
142VAL N N 119.833
143GLN H H 7.783
143GLN N N 117.13
144MET H H 7.688
144MET N N 117.833
145MET H H 7.902
145MET N N 115.932
146THR H H 7.632
146THR N N 110.272
147ALA H H 7.54
147ALA N N 125.404
148LYS H H 7.629
148LYS N N 125.305

Ca^{2+}-saturated CaM_{12}

_Residue_seq_code
_Residue_label
_Atom_name
_Atom_type
_Chem_shift_value
3 GLN H H 8.106
3 GLN N N 118.176
4 LEU H H 8.231
4 LEU N N 121.564
5 THR H H 8.672
5 THR N N 112.706
6 GLU H H 8.944
6 GLU N N 119.983
7 GLU H H 8.627
7 GLU N N 119.055
8 GLN H H 7.657
8 GLN N N 120.207
9 ILE H H 8.185
9 ILE N N 118.169
10 ALA H H 7.854
10 ALA N N 120.166
11 GLU H H 7.715
11 GLU N N 120.042
12 PHE H H 8.748
12 PHE N N 119.942
13 LYS H H 9.167
13 LYS N N 121.29
14 GLU H H 7.985
14 GLU N N 120.633
15 ALA H H 7.582
15 ALA N N 120.643
16 PHE H H 8.593
16 PHE N N 117.439
17 SER H H 8.358
17 SER N N 111.805
18 LEU H H 7.261
18 LEU N N 120.546
19 PHE H H 7.062
19 PHE N N 114.117
20 ALA H H 7.536
20 ALA N N 123.26
21 LYS H H 8.403
21 LYS N N 120.975
22 ASP H H 8.481
22 ASP N N 122.174
23 GLY H H 8.259
23 GLY N N 109.143
24 ASP H H 7.992
24 ASP N N 119.59
25 GLY H H 8.284
25 GLY N N 106.363
26 THR H H 7.525
26 THR N N 108.155
27 ILE H H 8.501
27 ILE N N 111.882
28 THR H H 8.548
28 THR N N 110.541
29 THR H H 8.297
29 THR N N 109.975
30 LYS H H 7.593
30 LYS N N 119.266
31 GLU H H 7.462
31 GLU N N 117.972
32 LEU H H 7.36
32 LEU N N 120.668
33 GLY H H 8.646
33 GLY N N 105.027
34 THR H H 7.391
34 THR N N 117.996
35 VAL H H 7.843
35 VAL N N 122.734
36 MET H H 8.321
36 MET N N 118.239
37 ARG H H 8.432
37 ARG N N 119.019
38 SER H H 8.008
38 SER N N 118.829
39 LEU H H 7.261
39 LEU N N 120.675
40 GLY H H 7.862
40 GLY N N 106.965
41 GLN H H 7.673
41 GLN N N 117.782
42 ASN H H 8.57
42 ASN N N 116.561
44 THR H H 8.688
44 THR N N 112.844
45 GLU H H 8.774
45 GLU N N 120.218
46 ALA H H 8.259
46 ALA N N 120.732
47 GLU H H 7.677
47 GLU N N 118.663
48 LEU H H 8.159
48 LEU N N 120.726
49 GLN H H 7.971
49 GLN N N 117.547
50 ASP H H 7.837
50 ASP N N 118.802
51 MET H H 7.844
51 MET N N 118.602
52 ILE H H 8.136
52 ILE N N 118.575
53 ASN H H 8.269
53 ASN N N 117.426
54 GLU H H 7.659
54 GLU N N 117.618
55 VAL H H 7.409
55 VAL N N 113.127
56 ALA H H 8.189
56 ALA N N 123.385
57 ALA H H 8.132
57 ALA N N 123.228
58 ASP H H 8.236
58 ASP N N 116.26
59 GLY H H 7.719
59 GLY N N 111.559
60 ASN H H 8.303
60 ASN N N 118.094
61 GLY H H 8.094
61 GLY N N 108.027
62 THR H H 7.674
62 THR N N 110.952
63 ILE H H 9.103
63 ILE N N 123.58
64 ASP H H 8.716
64 ASP N N 125.893
65 PHE H H 8.992
65 PHE N N 118.301
67 GLU H H 7.992
67 GLU N N 117.962
68 PHE H H 8.463
68 PHE N N 122.072
69 LEU H H 8.398
69 LEU N N 118.283
70 THR H H 7.65
70 THR N N 115.317
71 MET H H 7.722
71 MET N N 120.84
72 MET H H 7.958
72 MET N N 117.305
73 ALA H H 8.174
73 ALA N N 121.237
74 ARG H H 7.394
74 ARG N N 116.455
75 LYS H H 7.624
75 LYS N N 118.287
76 MET H H 7.783
76 MET N N 118.565
77 LYS H H 7.838
77 LYS N N 119.907
78 ASP H H 8.224
78 ASP N N 121.912
79 THR H H 8.057
79 THR N N 114.645
80 ASP H H 8.268
80 ASP N N 123.651
81 SER H H 8.409
81 SER N N 117.061
82 GLU H H 8.415
82 GLU N N 122.075
83 GLU H H 8.252
83 GLU N N 119.834
84 GLU H H 8.025
84 GLU N N 118.582
85 ILE H H 7.956
85 ILE N N 121.955
86 ARG H H 8.343
86 ARG N N 121.407

87 GLU H H 8.002
87 GLU N N 118.379
88 ALA H H 7.929
88 ALA N N 122.314
89 PHE H H 8.49
89 PHE N N 118.562
90 ARG H H 7.619
90 ARG N N 115.235
91 VAL H H 7.477
91 VAL N N 118.088
92 PHE H H 7.515
92 PHE N N 116.283
93 ASP H H 7.798
93 ASP N N 116.769
94 LYS H H 7.648
94 LYS N N 125.517
95 ASP H H 8.106
95 ASP N N 113.638
96 GLY H H 7.718
96 GLY N N 108.939
97 ASN H H 8.239
97 ASN N N 119.2
98 GLY H H 10.581
98 GLY N N 112.653
99 TYR H H 7.537
99 TYR N N 115.477
100 ILE H H 10.065
100 ILE N N 126.889
101 SER H H 8.885
101 SER N N 123.445
102 ALA H H 9.129
102 ALA N N 122.583
103 ALA H H 8.241
103 ALA N N 118.164
104 GLU H H 7.803
104 GLU N N 119.285
105 LEU H H 8.541
105 LEU N N 120.928
106 ARG H H 8.491
106 ARG N N 117.278
107 HIS H H 7.887
107 HIS N N 118.019
108 VAL H H 7.827
108 VAL N N 118.879
109 MET H H 8.17
109 MET N N 116.245
110 THR H H 8.085
110 THR N N 114.782
111 ASN H H 7.879
111 ASN N N 121.72
112 LEU H H 7.803
112 LEU N N 118.518
113 GLY H H 7.81
113 GLY N N 106.619
114 GLU H H 7.833
114 GLU N N 120.2
115 LYS H H 8.513
115 LYS N N 123.469
116 LEU H H 8.035
116 LEU N N 124.335
117 THR H H 9.142
117 THR N N 114.239
118 ASP H H 8.833
118 ASP N N 120.684
119 GLU H H 8.611
119 GLU N N 118.808
120 GLU H H 7.698
120 GLU N N 120.205
121 VAL H H 8.029
121 VAL N N 120.898
122 ASP H H 7.98
122 ASP N N 119.31
123 GLU H H 7.905
123 GLU N N 119.104
124 MET H H 7.792
124 MET N N 118.941
125 ILE H H 7.912
125 ILE N N 117.575
126 ARG H H 8.152
126 ARG N N 118.295
127 GLU H H 7.903
127 GLU N N 115.314
128 ALA H H 7.287
128 ALA N N 118.595
129 ASP H H 7.801
129 ASP N N 117.265
130 ILE H H 8.292
130 ILE N N 127.457
131 ASP H H 8.215
131 ASP N N 116.244
132 GLY H H 7.5
132 GLY N N 108.23
133 ASP H H 8.253
133 ASP N N 120.304
134 GLY H H 10.302
134 GLY N N 112.578
135 GLN H H 7.887
135 GLN N N 115.135
136 VAL H H 9.065
136 VAL N N 125.049
137 ASN H H 9.435
137 ASN N N 128.638
138 TYR H H 8.409
138 TYR N N 118.077
139 GLU H H 8.059
139 GLU N N 118.243
140 GLU H H 8.698
140 GLU N N 119.482
141 PHE H H 8.912
141 PHE N N 124.507
142 VAL H H 8.461
142 VAL N N 118.879
143 GLN H H 7.284
143 GLN N N 117.74
144 MET H H 7.923
144 MET N N 119.454
145 MET H H 7.776
145 MET N N 114.416
146 THR H H 7.516
146 THR N N 111.421
147 ALA H H 7.709
147 ALA N N 126.353
148 LYS H H 7.674
148 LYS N N 125.345

Appendix G

CaM_{34} Assigned Chemical Shift

Apo CaM_{34}
_Residue_seq_code
_Residue_label
_Atom_name
_Atom_type
_Chem_shift_value
3 GLN H H 8.109
3 GLN N N 118.27
4 LEU H H 8.221
4 LEU N N 121.532
5 THR H H 8.691
5 THR N N 112.733
6 GLU H H 8.941
6 GLU N N 119.971
7 GLU H H 8.641
7 GLU N N 119.033
8 GLN H H 7.648
8 GLN N N 120.185
9 ILE H H 8.147
9 ILE N N 118.192
10 ALA H H 7.838
10 ALA N N 120.153
11 GLU H H 7.72
11 GLU N N 119.933
12 PHE H H 8.737
12 PHE N N 120.133
13 LYS H H 9.137
13 LYS N N 121.202
14 GLU H H 7.98
14 GLU N N 120.226
15 ALA H H 7.574
15 ALA N N 120.572
16 PHE H H 8.441
16 PHE N N 117.574
17 SER H H 8.339
17 SER N N 110.792
18 LEU H H 7.278
18 LEU N N 120.947
19 PHE H H 7.308
19 PHE N N 114.477
20 ASP H H 7.228
20 ASP N N 122.233
21 LYS H H 8.001
21 LYS N N 123.433
22 ASP H H 8.653
22 ASP N N 116.965
23 GLY H H 7.939
23 GLY N N 110.063
24 ASP H H 8.696
24 ASP N N 120.533
25 GLY H H 10.101
25 GLY N N 111.703
26 THR H H 7.511
26 THR N N 109.533
27 ILE H H 8.195
27 ILE N N 110.193
28 THR H H 8.258
28 THR N N 110.521
29 THR H H 8.224
29 THR N N 112.262
30 LYS H H 7.561
30 LYS N N 118.659
31 GLU H H 7.44
31 GLU N N 117.284
32 LEU H H 7.27
32 LEU N N 120.701
33 GLY H H 8.723
33 GLY N N 105.223
34 THR H H 7.436
34 THR N N 118.155
35 VAL H H 7.891
35 VAL N N 122.496
36 MET H H 8.386
36 MET N N 118.307
37 ARG H H 8.438
37 ARG N N 119.204
38 SER H H 8.04
38 SER N N 118.782
39 LEU H H 7.263
39 LEU N N 120.896
40 GLY H H 7.841
40 GLY N N 106.903
41 GLN H H 7.691
41 GLN N N 117.431
42 ASN H H 8.592
42 ASN N N 116.392
44 THR H H 8.711
44 THR N N 113.033
45 GLU H H 8.781
45 GLU N N 120.233
46 ALA H H 8.251
46 ALA N N 120.833
47 GLU H H 7.668
47 GLU N N 118.672
48 LEU H H 8.254
48 LEU N N 119.899
49 GLN H H 7.984
49 GLN N N 117.333
50 ASP H H 7.773
50 ASP N N 118.711
51 MET H H 7.891
51 MET N N 118.933
52 ILE H H 8.254
52 ILE N N 118.95
53 ASN H H 8.197
53 ASN N N 117.177
54 GLU H H 7.507
54 GLU N N 117.133
55 VAL H H 7.552
55 VAL N N 112.677
56 ASP H H 8.373
56 ASP N N 121.733
57 ALA H H 8.078
57 ALA N N 124.767
58 ASP H H 8.355
58 ASP N N 114.648
59 GLY H H 7.832
59 GLY N N 108.723
60 ASN H H 9.182
60 ASN N N 119.562
61 GLY H H 9.888
61 GLY N N 109.859
62 THR H H 7.497
62 THR N N 110.65
63 ILE H H 8.832
63 ILE N N 118.662
64 ASP H H 8.354
64 ASP N N 124.049
65 PHE H H 8.577
65 PHE N N 118.448
67 GLU H H 8.021
67 GLU N N 117.392
68 PHE H H 8.401
68 PHE N N 122.199
69 LEU H H 8.393
69 LEU N N 118.488
70 THR H H 7.651
70 THR N N 115.233
71 MET H H 7.668
71 MET N N 121.155
72 MET H H 7.948
72 MET N N 117.24
73 ALA H H 8.179
73 ALA N N 120.928
74 ARG H H 7.394
74 ARG N N 116.495
75 LYS H H 7.641
75 LYS N N 118.033
76 MET H H 7.871
76 MET N N 117.633
77 LYS H H 7.652
77 LYS N N 120.409
78 ASP H H 8.228
78 ASP N N 121.767
79 THR H H 8.039
79 THR N N 114.252
80 ASP H H 8.352
80 ASP N N 122.925
81 SER H H 8.32
81 SER N N 116.613
82 GLU H H 8.353
82 GLU N N 121.876
83 GLU H H 8.125
83 GLU N N 119.864
84 GLU H H 7.9
84 GLU N N 118.973
85 ILE H H 7.977
85 ILE N N 120.899
86 ARG H H 8.179
86 ARG N N 121.318
87 GLU H H 8.265
87 GLU N N 119.274
88 ALA H H 7.866
88 ALA N N 122.173
89 PHE H H 7.883
89 PHE N N 116.002
93 ALA H H 7.973
93 ALA N N 122.815
94 LYS H H 8.068
94 LYS N N 120.302
95 ASP H H 8.266
95 ASP N N 118.968
96 GLY H H 8.113
96 GLY N N 107.633
97 ASN H H 8.232
97 ASN N N 117.894
98 GLY H H 8.304
98 GLY N N 107.446
99 TYR H H 7.843
99 TYR N N 118.763
101 SER H H 8.508
101 SER N N 119.086
102 ALA H H 8.676
102 ALA N N 124.846
103 ALA H H 8.225
103 ALA N N 118.99
104 GLU H H 7.739
104 GLU N N 118.542
105 LEU H H 8.078
105 LEU N N 120.754
106 ARG H H 8.023
106 ARG N N 117.594
107 HIS H H 7.695
107 HIS N N 117.689
108 VAL H H 7.932
108 VAL N N 118.951
109 MET H H 8.14
109 MET N N 117.489
110 THR H H 7.914
110 THR N N 112.447
111 ASN H H 7.906
111 ASN N N 119.669
112 LEU H H 7.773
112 LEU N N 119.89
113 GLY H H 8.168
113 GLY N N 107.803
114 GLU H H 8.014
114 GLU N N 119.894
115 LYS H H 8.238
115 LYS N N 120.422
116 LEU H H 7.854
116 LEU N N 122.019
117 THR H H 8.774
117 THR N N 113.451

118 ASP H H 8.697
118 ASP N N 120.838
119 GLU H H 8.488
119 GLU N N 118.257
120 GLU H H 7.781
120 GLU N N 120.199
121 VAL H H 8.119
121 VAL N N 120.736
122 ASP H H 8.255
122 ASP N N 119.741
123 GLU H H 8.212
123 GLU N N 119.934
124 MET H H 7.853
124 MET N N 119.225
125 ILE H H 8.171
125 ILE N N 119.223
126 ARG H H 7.905
126 ARG N N 120.066
127 GLU H H 8.028
127 GLU N N 117.882
128 ALA H H 7.695
128 ALA N N 121.373
129 ALA H H 7.999
129 ALA N N 121.227
130 ILE H H 7.774
130 ILE N N 118.856
131 ASP H H 8.335
131 ASP N N 123.284
132 GLY H H 8.229
132 GLY N N 108.046
133 ASP H H 8.183
133 ASP N N 119.543
134 GLY H H 8.213
134 GLY N N 108.03
135 GLN H H 8.106
135 GLN N N 118.74
137 ASN H H 8.587
137 ASN N N 123.656
138 TYR H H 8.278
138 TYR N N 123.192
139 GLU H H 8.194
139 GLU N N 119.739
141 PHE H H 7.973
141 PHE N N 120.644
142 VAL H H 8.12
142 VAL N N 118.761
143 GLN H H 7.763
143 GLN N N 119.641
144 MET H H 7.788
144 MET N N 116.758
145 MET H H 7.87
145 MET N N 117.399
146 THR H H 7.649
146 THR N N 111.439
147 ALA H H 7.718
147 ALA N N 126.027
148 LYS H H 7.662
148 LYS N N 125.356

Ca^{2+}-saturated CaM_{34}

_Residue_seq_code
_Residue_label
_Atom_name
_Atom_type
_Chem_shift_value
1ALA H H 8.38
1ALA N N 123.171
2ASP H H 7.998
2ASP N N 117.408
3GLN H H 7.829
3GLN N N 118.016
5THR H H 8.634
5THR N N 112.609
6GLU H H 8.972
6GLU N N 120.15
7GLU H H 8.669
7GLU N N 119.2
8GLN H H 7.675
8GLN N N 119.767
9ILE H H 8.347
9ILE N N 119.371
10ALA H H 7.939
10ALA N N 120.709
11GLU H H 7.716
11GLU N N 119.268
12PHE H H 8.507
12PHE N N 119.555
13LYS H H 9.112
13LYS N N 123.203
14GLU H H 7.69
14GLU N N 119.954
15ALA H H 7.904
15ALA N N 122.354
16PHE H H 8.736
16PHE N N 118.654
17SER H H 7.892
17SER N N 112.667
18LEU H H 7.319
18LEU N N 120.064
19PHE H H 7.186
19PHE N N 114.443
20ASP H H 7.752
20ASP N N 117.819
21LYS H H 7.522
21LYS N N 124.068
22ASP H H 7.943
22ASP N N 113.338
23GLY H H 7.626
23GLY N N 108.959
24ASP H H 8.338
24ASP N N 120.323
25GLY H H 10.546
25GLY N N 112.826
26THR H H 8.084
26THR N N 112.231
27ILE H H 9.788
27ILE N N 126.653
28THR H H 8.362
28THR N N 116.324
29THR H H 9.097
29THR N N 112.41
30LYS H H 7.395
30LYS N N 120.326
31GLU H H 7.593
31GLU N N 120.72
32LEU H H 8.656
32LEU N N 120.383
33GLY H H 8.647
33GLY N N 105.992
34THR H H 7.77
34THR N N 118.049
35VAL H H 7.51
35VAL N N 121.826
36MET H H 8.418
36MET N N 119.254
37ARG H H 8.476
37ARG N N 119.136
38SER H H 7.887
38SER N N 118.704
39LEU H H 7.289
39LEU N N 119.966
40GLY H H 7.799
40GLY N N 106.59
41GLN H H 7.749
41GLN N N 118.152
42ASN H H 8.655
42ASN N N 115.97
44THR H H 8.656
44THR N N 112.731
45GLU H H 8.746
45GLU N N 120.395
46ALA H H 8.214
46ALA N N 120.693
47GLU H H 7.633
47GLU N N 118.445
48LEU H H 8.093
48LEU N N 120.526
49GLN H H 8.183
49GLN N N 118.049
50ASP H H 8.001
50ASP N N 119.95
51MET H H 7.807
51MET N N 118.732
52ILE H H 7.661
52ILE N N 117.69
53ASN H H 8.544
53ASN N N 117.436
54GLU H H 7.46
54GLU N N 116.047
55VAL H H 7.142
55VAL N N 109.529
56ASP H H 7.544
56ASP N N 121.765
57ALA H H 8.267
57ALA N N 131.278
58ASP H H 8.124
58ASP N N 113.547
59GLY H H 7.518
59GLY N N 108.146
60ASN H H 8.051
60ASN N N 118.31
61GLY H H 10.509
61GLY N N 112.999
62THR H H 7.594
62THR N N 108.394
63ILE H H 8.732
63ILE N N 123.051
64ASP H H 8.833
64ASP N N 128.003
65PHE H H 8.879
65PHE N N 118.422
68PHE H H 8.682
68PHE N N 123.255
69LEU H H 8.249
69LEU N N 119.108
70THR H H 7.401
70THR N N 116.545
71MET H H 7.601
71MET N N 121.166
73ALA H H 8.038
73ALA N N 122.383
74ARG H H 7.468
74ARG N N 116.585
75LYS H H 7.614
75LYS N N 118.371
76MET H H 7.931
76MET N N 114.667
77LYS H H 7.669
77LYS N N 120.132
78ASP H H 8.229
78ASP N N 121.253
79THR H H 7.988
79THR N N 113.486
80ASP H H 8.295
80ASP N N 122.305
81SER H H 8.336
81SER N N 116.217
82GLU H H 8.328
82GLU N N 121.891
83GLU H H 8.125
83GLU N N 119.864
84GLU H H 7.901
84GLU N N 118.873
85ILE H H 7.949
85ILE N N 121.398
87GLU H H 8.287
87GLU N N 119.285
88ALA H H 7.897
88ALA N N 122.007
89PHE H H 7.9
89PHE N N 116.274
94LYS H H 8.068
94LYS N N 120.302
95ASP H H 8.253
95ASP N N 119.39
96GLY H H 8.143
96GLY N N 107.709
97ASN H H 8.232
97ASN N N 117.894
98GLY H H 8.259
98GLY N N 107.748
99TYR H H 7.848
99TYR N N 118.619
101SER H H 8.508
101SER N N 119.086
102ALA H H 8.706
102ALA N N 125.209

103ALA H H 8.201
103ALA N N 118.096
104GLU H H 7.757
104GLU N N 118.609
105LEU H H 8.078
105LEU N N 120.754
106ARG H H 8.019
106ARG N N 117.472
107HIS H H 7.679
107HIS N N 117.567
108VAL H H 7.958
108VAL N N 118.951
109MET H H 8.14
109MET N N 117.489
110THR H H 7.927
110THR N N 112.825
111ASN H H 7.906
111ASN N N 119.669
112LEU H H 7.737
112LEU N N 119.89
113GLY H H 8.176
113GLY N N 107.894
114GLU H H 8.019
114GLU N N 119.572
115LYS H H 8.216
115LYS N N 120.422
116LEU H H 7.876
116LEU N N 121.897
117THR H H 8.722
117THR N N 112.559
118ASP H H 8.699
118ASP N N 120.382
119GLU H H 8.419
119GLU N N 117.571
120GLU H H 7.75
120GLU N N 120.199
121VAL H H 8.099
121VAL N N 121.002
122ASP H H 8.296
122ASP N N 119.741
123GLU H H 8.196
123GLU N N 119.994
124MET H H 7.853
124MET N N 119.225
125ILE H H 8.171
125ILE N N 119.223
126ARG H H 7.885
126ARG N N 120.199
127GLU H H 8.05
127GLU N N 117.926
128ALA H H 7.628
128ALA N N 120.98
129ALA H H 8.01
129ALA N N 121.756
130ILE H H 7.788
130ILE N N 118.823
131ASP H H 8.25
131ASP N N 122.876
132GLY H H 8.304
132GLY N N 108.65
133ASP H H 8.169
133ASP N N 119.581
134GLY H H 8.19
134GLY N N 108.876
135GLN H H 8.055
135GLN N N 118.74
137ASN H H 8.507
137ASN N N 123.293
138TYR H H 8.228
138TYR N N 122.875
139GLU H H 8.177
139GLU N N 119.799
141PHE H H 7.957
141PHE N N 120.866
142VAL H H 8.065
142VAL N N 119.038
143GLN H H 7.735
143GLN N N 119.597
144MET H H 7.712
144MET N N 117.192
145MET H H 7.593
145MET N N 114.946
146THR H H 7.734
146THR N N 112.376
147ALA H H 7.809
147ALA N N 125.72
148LYS H H 7.749
148LYS N N 125.508

Appendix H

CaM-eNOS peptide at 225 nM free Ca^{2+} Assigned Chemical Shifts

_Residue_seq_code
_Residue_label
_Atom_name
_Atom_type
_Chem_shift_value

3 GLN CA C 53.5
3 GLN CB C 29.475
3 GLN CG C 33.653
3 GLN H H 8.134
3 GLN HA H 4.688
3 GLN HB2 H 1.877
3 GLN HB3 H 1.877
3 GLN N N 118.12
4 LEU CA C 51.65
4 LEU CB C 40.715
4 LEU CG C 24.216
4 LEU CD1 C 20.665
4 LEU CD2 C 22.383
4 LEU H H 8.202
4 LEU HA H 4.46
4 LEU HB2 H 1.554
4 LEU HB3 H 1.554
4 LEU HG H 1.488
4 LEU HD1 H 0.678
4 LEU HD2 H 0.654
4 LEU N N 121.407
5 THR CA C 59.433
5 THR CB C 67.475
5 THR CG2 C 18.753
5 THR H H 8.691
5 THR HA H 4.265
5 THR HB H 4.091
5 THR HG2 H 1.056
5 THR N N 112.733
6 GLU CA C 56.756
6 GLU CB C 26.508
6 GLU CG C 33.653
6 GLU H H 8.953
6 GLU HA H 3.854
6 GLU HB2 H 1.884
6 GLU HB3 H 1.884
6 GLU HG2 H 2.2
6 GLU HG3 H 2.2
6 GLU N N 119.971
7 GLU CA C 56.756
7 GLU CB C 26.279
7 GLU CG C 33.726
7 GLU H H 8.653
7 GLU HA H 3.898
7 GLU HB2 H 1.899
7 GLU HB3 H 1.899
7 GLU HG2 H 2.222
7 GLU HG3 H 2.222
7 GLU N N 119.133
8 GLN CA C 57.099
8 GLN CB C 26.737
8 GLN CG C 33.612
8 GLN H H 7.645
8 GLN HA H 3.957
8 GLN HB2 H 1.972
8 GLN HB3 H 1.972
8 GLN HG2 H 2.237
8 GLN HG3 H 2.237
8 GLN N N 120.207
9 ILE CA C 62.714
9 ILE CB C 35.216
9 ILE CG1 C 27.654
9 ILE CG2 C 14.936
9 ILE CD1 C 10.811
9 ILE H H 8.153
9 ILE HA H 3.354
9 ILE HB H 1.708
9 ILE HG12 H 0.678
9 ILE HG13 H 0.678
9 ILE HG2 H 0.767
9 ILE HD1 H 0.634
9 ILE N N 118.171
10 ALA CA C 52.746
10 ALA CB C 15.165
10 ALA H H 7.835
10 ALA HA H 3.966
10 ALA HB H 1.34
10 ALA N N 120.124
11 GLU CA C 56.56
11 GLU CB C 27.425
11 GLU CG C 33.841
11 GLU H H 7.706
11 GLU HA H 3.904
11 GLU HB2 H 1.802
11 GLU HB3 H 1.802
11 GLU HG2 H 2.213
11 GLU HG3 H 2.213
11 GLU N N 119.983
12 PHE CA C 55.839
12 PHE CB C 33.955
12 PHE H H 8.728
12 PHE HA H 4.726
12 PHE HB2 H 3.336
12 PHE HB3 H 3.336
12 PHE N N 119.907
13 LYS CA C 57.29
13 LYS CB C 30.174
13 LYS CG C 26.279
13 LYS CD C 33.612
13 LYS H H 9.161
13 LYS HA H 3.904
13 LYS HB2 H 1.681
13 LYS HB3 H 1.681
13 LYS HG2 H 1.886
13 LYS HG3 H 1.886
13 LYS HD2 H 2.213
13 LYS HD3 H 2.213
13 LYS N N 121.208
14 GLU CA C 56.46
14 GLU CB C 26.623
14 GLU CG C 33.497
14 GLU H H 7.98
14 GLU HA H 3.953
14 GLU HB2 H 1.947
14 GLU HB3 H 1.947
14 GLU HG2 H 2.225
14 GLU HG3 H 2.225
14 GLU N N 120.226
15 ALA CA C 52.75
15 ALA CB C 16.425
15 ALA H H 7.563
15 ALA HA H 4.17
15 ALA HB H 1.536
15 ALA N N 120.572
16 PHE CA C 59.54
16 PHE CB C 36.82
16 PHE H H 8.453
16 PHE HA H 3.904
16 PHE HB2 H 2.732
16 PHE HB3 H 2.732
16 PHE N N 117.784
17 SER CA C 58.56
17 SER CB C 60.651
17 SER H H 8.351
17 SER HA H 4.086
17 SER HB2 H 3.892
17 SER HB3 H 3.892
17 SER N N 110.774
18 LEU CA C 55.839
18 LEU CB C 39.111
18 LEU CG C 26.279
18 LEU CD1 C 20.435
18 LEU CD2 C 23.758
18 LEU H H 7.278
18 LEU HA H 3.614
18 LEU HB2 H 1.729
18 LEU HB3 H 1.729
18 LEU HD1 H 0.859
18 LEU HD2 H 0.737
18 LEU N N 120.947
19 PHE CA C 56.87
19 PHE CB C 33.841
19 PHE H H 7.304
19 PHE HA H 3.904
19 PHE HB2 H 2.225
19 PHE HB3 H 2.225
19 PHE N N 114.458
20 ASP CA C 50.454
20 ASP CB C 37.622
20 ASP H H 7.233
20 ASP HA H 4.874
20 ASP HB2 H 2.237
20 ASP HB3 H 2.237
20 ASP N N 122.233
21 LYS CA C 56.025
21 LYS CB C 29.601
21 LYS CG C 21.467
21 LYS CD C 25.82
21 LYS CE C 39.226
21 LYS H H 8.007
21 LYS HA H 3.771
21 LYS HB2 H 1.669
21 LYS HB3 H 1.669
21 LYS HG2 H 1.306
21 LYS HG3 H 1.306
21 LYS HD2 H 1.536
21 LYS HD3 H 1.536
21 LYS HE2 H 2.853
21 LYS HE3 H 2.853
21 LYS N N 123.433
22 ASP CA C 50.683
22 ASP CB C 37.049
22 ASP H H 8.641
22 ASP HA H 4.4
22 ASP HB2 H 2.913
22 ASP HB3 H 2.527
22 ASP N N 116.89
23 GLY CA C 43.745
23 GLY H H 7.938
23 GLY HA2 H 3.76
23 GLY HA3 H 3.76
23 GLY N N 110.068
24 ASP CA C 51.04
24 ASP CB C 37.438
24 ASP H H 8.723
24 ASP HA H 4.367
24 ASP HB2 H 2.927
24 ASP HB3 H 2.542
24 ASP N N 120.219
25 GLY CA C 42.68
25 GLY H H 10.132
25 GLY HA2 H 3.752
25 GLY HA3 H 3.963
25 GLY N N 111.889
26 THR CA C 56.95
26 THR CB C 70.234
26 THR CG2 C 18.832
26 THR H H 7.507
26 THR HA H 5.386
26 THR HB H 3.893
26 THR HG2 H 0.925
26 THR N N 109.844
27 ILE CA C 58.36
27 ILE CB C 35.559
27 ILE CG1 C 27.31
27 ILE CG2 C 14.592
27 ILE CD1 C 10.468
27 ILE H H 8.191
27 ILE HA H 3.891
27 ILE HB H 1.701
27 ILE HG12 H 1.538
27 ILE HG13 H 1.538
27 ILE HG2 H 0.786
27 ILE HD1 H 0.655
27 ILE N N 110.289
28 THR CA C 57.787
28 THR CB C 68.099

28 THR CG2 C 18.831
28 THR H H 8.265
28 THR HA H 4.895
28 THR HB H 4.593
28 THR HG2 H 1.161
28 THR N N 110.507
29 THR CA C 63.84
29 THR CB C 65.807
29 THR CG2 C 18.831
29 THR H H 8.225
29 THR HA H 3.941
29 THR HB H 4.146
29 THR HG2 H 1.065
29 THR N N 112.331
30 LYS CA C 55.839
30 LYS CB C 29.372
30 LYS CG C 21.81
30 LYS CD C 25.935
30 LYS H H 7.559
30 LYS HA H 3.965
30 LYS HB2 H 1.669
30 LYS HB3 H 1.669
30 LYS HG2 H 1.306
30 LYS HG3 H 1.306
30 LYS HD2 H 1.983
30 LYS HD3 H 1.983
30 LYS N N 118.985
31 GLU CA C 57.14
31 GLU CB C 26.393
31 GLU CG C 33.841
31 GLU H H 7.431
31 GLU HA H 3.965
31 GLU HB2 H 1.898
31 GLU HB3 H 1.898
31 GLU HG2 H 2.201
31 GLU HG3 H 2.201
31 GLU N N 117.233
32 LEU CA C 55.52
32 LEU CB C 39.226
32 LEU CG C 24.331
32 LEU CD1 C 21.581
32 LEU CD2 C 20.321
32 LEU H H 7.27
32 LEU HA H 3.88
32 LEU HB2 H 1.584
32 LEU HB3 H 1.584
32 LEU HG H 1.476
32 LEU HD1 H 0.654
32 LEU HD2 H 0.859
32 LEU N N 120.701
33 GLY CA C 45.642
33 GLY H H 8.737
33 GLY HA2 H 3.699
33 GLY HA3 H 3.348
33 GLY N N 105.217
34 THR CA C 63.859
34 THR CB C 65.807
34 THR CG2 C 18.717
34 THR H H 7.446
34 THR HA H 3.916
34 THR HB H 4.157
34 THR HG2 H 1.077
34 THR N N 118.196
35 VAL CA C 64.088
35 VAL CB C 28.799
35 VAL CG1 C 20.55
35 VAL CG2 C 18.029
35 VAL H H 7.889
35 VAL HA H 3.373
35 VAL HB H 2.056
35 VAL HG1 H 0.811
35 VAL HG2 H 0.448
35 VAL N N 122.546
36 MET CA C 56.87
36 MET CB C 26.279
36 MET CG C 33.841
36 MET H H 8.386
36 MET HA H 3.88
36 MET HB2 H 1.778
36 MET HB3 H 1.778
36 MET HG2 H 2.225
36 MET HG3 H 2.225
36 MET N N 118.307
37 ARG CA C 56.17
37 ARG CB C 27.31
37 ARG CG C 25.018
37 ARG CD C 40.715
37 ARG H H 8.451
37 ARG HA H 3.904
37 ARG HB2 H 1.776
37 ARG HB3 H 1.776
37 ARG HG2 H 1.814
37 ARG HG3 H 1.814
37 ARG HD2 H 3.046
37 ARG HD3 H 3.046
37 ARG N N 119.233
38 SER CA C 59.25
38 SER CB C 67.411
38 SER H H 8.04
38 SER HA H 4.176
38 SER HB2 H 4.098
38 SER HB3 H 4.098
38 SER N N 118.72
39 LEU CA C 51.33
39 LEU CB C 40.257
39 LEU CG C 23.987
39 LEU CD1 C 20.894
39 LEU H H 7.263
39 LEU HA H 4.46
39 LEU HB2 H 1.741
39 LEU HB3 H 1.741
39 LEU HG H 1.524
39 LEU HD1 H 0.992
39 LEU N N 120.896
40 GLY CA C 42.88
40 GLY H H 7.841
40 GLY HA2 H 4.122
40 GLY HA3 H 3.687
40 GLY N N 106.917
41 GLN CA C 52.631
41 GLN CB C 30.747
41 GLN CG C 35.33
41 GLN H H 7.687
41 GLN HA H 4.243
41 GLN HB2 H 2.176
41 GLN HB3 H 2.176
41 GLN HG2 H 2.696
41 GLN HG3 H 2.696
41 GLN N N 117.171
42 ASN CA C 48.64
42 ASN CB C 36.591
42 ASN H H 8.601
42 ASN HA H 5.016
42 ASN HB2 H 2.611
42 ASN HB3 H 2.37
42 ASN N N 116.423
44 THR CA C 57.64
44 THR CB C 68.328
44 THR CG2 C 18.831
44 THR H H 8.711
44 THR HA H 4.279
44 THR HB H 4.638
44 THR HG2 H 1.186
44 THR N N 113.033
45 GLU CA C 56.756
45 GLU CB C 26.393
45 GLU CG C 33.726
45 GLU H H 8.781
45 GLU HA H 3.892
45 GLU HB2 H 1.886
45 GLU HB3 H 1.886
45 GLU HG2 H 2.225
45 GLU HG3 H 2.225
45 GLU N N 120.233
46 ALA CA C 52.31
46 ALA CB C 15.394
46 ALA H H 8.251
46 ALA HA H 3.868
46 ALA HB H 1.255
46 ALA N N 120.833
47 GLU CA C 56.641
47 GLU CB C 26.623
47 GLU CG C 33.841
47 GLU H H 7.668
47 GLU HA H 3.965
47 GLU HB2 H 1.923
47 GLU HB3 H 1.923
47 GLU HG2 H 2.225
47 GLU HG3 H 2.225
47 GLU N N 118.672
48 LEU CA C 55.61
48 LEU CB C 39.34
48 LEU CG C 24.216
48 LEU CD1 C 21.696
48 LEU CD2 C 20.665
48 LEU H H 8.244
48 LEU HA H 3.892
48 LEU HB2 H 1.633
48 LEU HB3 H 1.633
48 LEU HG H 1.5
48 LEU HD1 H 0.678
48 LEU HD2 H 0.896
48 LEU N N 119.645
49 GLN CA C 56.756
49 GLN CB C 26.508
49 GLN CG C 33.841
49 GLN H H 7.98
49 GLN HA H 3.892
49 GLN HB2 H 1.911
49 GLN HB3 H 1.911
49 GLN HG2 H 2.225
49 GLN HG3 H 2.225
49 GLN N N 117.446
50 ASP CA C 54.7
50 ASP CB C 37.622
50 ASP H H 7.761
50 ASP HA H 4.267
50 ASP HB2 H 2.611
50 ASP HB3 H 2.611
50 ASP N N 118.733
51 MET CA C 56.56
51 MET CB C 29.601
51 MET H H 7.9
51 MET HA H 3.892
51 MET HB2 H 1.681
51 MET HB3 H 1.681
51 MET N N 118.996
52 ILE CA C 62.484
52 ILE CB C 35.33
52 ILE CG1 C 27.539
52 ILE CG2 C 14.478
52 ILE CD1 C 10.582
52 ILE H H 8.261
52 ILE HA H 3.348
52 ILE HB H 1.705
52 ILE HG12 H 0.763
52 ILE HG13 H 0.666
52 ILE HG2 H 0.763
52 ILE HD1 H 0.642
52 ILE N N 118.833
53 ASN CA C 53.09
53 ASN CB C 35.33
53 ASN H H 8.186
53 ASN HA H 4.243
53 ASN HB2 H 2.684
53 ASN HB3 H 2.684
53 ASN N N 117.296
54 GLU CA C 56.412
54 GLU CB C 26.508
54 GLU CG C 33.612
54 GLU H H 7.501
54 GLU HA H 3.965
54 GLU HB2 H 1.983
54 GLU HB3 H 1.983
54 GLU HG2 H 2.213
54 GLU HG3 H 2.213
54 GLU N N 117.133
55 VAL CA C 59.505
55 VAL CB C 30.174
55 VAL CG1 C 18.717
55 VAL H H 7.575
55 VAL HA H 4.194
55 VAL HB H 2.128
55 VAL HG1 H 0.811
55 VAL HG2 H 0.811
55 VAL N N 112.928
56 ASP CA C 50.99
56 ASP CB C 36.82

56 ASP H H 8.401
56 ASP HA H 4.388
56 ASP HB2 H 2.938
56 ASP HB3 H 2.527
56 ASP N N 121.771
57 ALA CA C 52.402
57 ALA CB C 15.28
57 ALA H H 8.097
57 ALA HA H 4.001
57 ALA HB H 1.343
57 ALA N N 124.771
58 ASP CA C 50.798
58 ASP CB C 36.934
58 ASP H H 8.376
58 ASP HA H 4.4
58 ASP HB2 H 2.926
58 ASP HB3 H 2.515
58 ASP N N 114.518
59 GLY CA C 44.49
59 GLY H H 7.827
59 GLY HA2 H 3.759
59 GLY HA3 H 3.759
59 GLY N N 108.798
60 ASN CA C 51.943
60 ASN CB C 38.424
60 ASN H H 9.253
60 ASN HA H 4.688
60 ASN HB2 H 2.623
60 ASN HB3 H 2.623
60 ASN N N 119.696
61 GLY CA C 42.87
61 GLY H H 10.004
61 GLY HA2 H 4.11
61 GLY HA3 H 3.687
61 GLY N N 110.108
62 THR CA C 59.162
62 THR CB C 67.526
62 THR CG2 C 18.602
62 THR H H 7.481
62 THR HA H 4.629
62 THR HB H 4.098
62 THR HG2 H 1.065
62 THR N N 110.533
63 ILE CA C 60.537
63 ILE CB C 36.018
63 ILE CG1 C 24.904
63 ILE CG2 C 14.478
63 ILE CD1 C 9.78
63 ILE H H 8.82
63 ILE HA H 3.783
63 ILE HB H 1.838
63 ILE HG12 H 1.548
63 ILE HG13 H 1.548
63 ILE HG2 H 0.763
63 ILE HD1 H 0.726
63 ILE N N 118.533
64 ASP CA C 51.027
64 ASP CB C 37.278
64 ASP H H 8.38
64 ASP HA H 4.327
64 ASP HB2 H 2.515
64 ASP HB3 H 2.515
64 ASP N N 122.928
65 PHE CA C 56.87
65 PHE CB C 33.497
65 PHE H H 8.559
65 PHE HA H 3.88
65 PHE HB2 H 2.2
65 PHE HB3 H 2.2
65 PHE N N 118.559
67 GLU CA C 56.87
67 GLU CB C 26.623
67 GLU CG C 33.955
67 GLU H H 7.995
67 GLU HA H 3.904
67 GLU HB2 H 1.902
67 GLU HB3 H 1.902
67 GLU HG2 H 2.213
67 GLU HG3 H 2.213
67 GLU N N 117.546
68 PHE CA C 59.047
68 PHE CB C 36.934
68 PHE H H 8.377
68 PHE HA H 3.904
68 PHE HB2 H 2.95
68 PHE HB3 H 2.95
68 PHE N N 122.032
69 LEU CA C 55.158
69 LEU CB C 38.195
69 LEU CG C 22.727
69 LEU CD1 C 21.238
69 LEU CD2 C 22.727
69 LEU H H 8.393
69 LEU HA H 3.179
69 LEU HB2 H 1.27
69 LEU HB3 H 1.065
69 LEU HG H 0.775
69 LEU HD1 H 0.569
69 LEU N N 118.488
70 THR CA C 63.63
70 THR CB C 65.578
70 THR CG2 C 18.946
70 THR H H 7.658
70 THR HA H 3.638
70 THR HB H 4.122
70 THR HG2 H 1.065
70 THR N N 115.208
71 MET CA C 56.303
71 MET CB C 29.831
71 MET CG C 29.487
71 MET H H 7.653
71 MET HA H 3.892
71 MET HB2 H 1.693
71 MET HB3 H 1.693
71 MET HG2 H 2.249
71 MET HG3 H 2.249
71 MET N N 121.221
72 MET CA C 53.777
72 MET CB C 29.029
72 MET CG C 28.799
72 MET H H 7.956
72 MET HA H 3.892
72 MET HB2 H 1.753
72 MET HB3 H 1.753
72 MET HG2 H 2.056
72 MET HG3 H 2.056
72 MET N N 117.459
73 ALA CA C 52.402
73 ALA CB C 15.28
73 ALA H H 8.23
73 ALA HA H 3.868
73 ALA HB H 1.258
73 ALA N N 120.856
74 ARG CA C 56.297
74 ARG CB C 27.997
74 ARG CG C 25.591
74 ARG CD C 40.83
74 ARG H H 7.409
74 ARG HA H 3.892
74 ARG HB2 H 1.766
74 ARG HB3 H 1.766
74 ARG HG2 H 1.729
74 ARG HG3 H 1.729
74 ARG HD2 H 3.034
74 ARG HD3 H 3.034
74 ARG N N 116.53
75 LYS CA C 55.495
75 LYS CB C 26.279
75 LYS CG C 22.04
75 LYS CD C 30.289
75 LYS CE C 39.455
75 LYS H H 7.657
75 LYS HA H 3.965
75 LYS HB2 H 1.524
75 LYS HB3 H 1.524
75 LYS HG2 H 1.306
75 LYS HG3 H 1.306
75 LYS HD2 H 1.669
75 LYS HD3 H 1.669
75 LYS N N 118.008
76 MET CA C 53.947
76 MET CB C 29.487
76 MET CG C 30.06
76 MET H H 7.883
76 MET HA H 4.146
76 MET HB2 H 2.043
76 MET HB3 H 2.043
76 MET HG2 H 2.478
76 MET HG3 H 2.478
76 MET N N 117.646
77 LYS CA C 56.526
77 LYS CB C 27.425
77 LYS CG C 26.279
77 LYS CD C 33.497
77 LYS CE C 40.83
77 LYS H H 7.658
77 LYS HA H 3.941
77 LYS HB2 H 1.79
77 LYS HB3 H 1.79
77 LYS HG2 H 1.923
77 LYS HG3 H 1.923
77 LYS HD2 H 2.201
77 LYS HD3 H 2.201
77 LYS N N 120.334
78 ASP CA C 52.516
78 ASP CB C 40.028
78 ASP H H 8.212
78 ASP HA H 4.194
78 ASP HB2 H 1.741
78 ASP HB3 H 1.741
78 ASP N N 121.733
79 THR CA C 59.391
79 THR CB C 67.067
79 THR CG2 C 18.717
79 THR H H 8.048
79 THR HA H 4.17
79 THR HB H 4.146
79 THR HG2 H 1.053
79 THR N N 114.651
80 ASP CA C 50.85
80 ASP CB C 36.705
80 ASP H H 8.432
80 ASP HA H 4.363
80 ASP HB2 H 2.515
80 ASP HB3 H 2.515
80 ASP N N 122.484
81 SER CA C 56.87
81 SER CB C 60.884
81 SER H H 8.403
81 SER HA H 4.267
81 SER HB2 H 3.904
81 SER HB3 H 3.904
81 SER N N 117.135
82 GLU CA C 56.707
82 GLU CB C 29.831
82 GLU CG C 33.468
82 GLU H H 8.443
82 GLU HA H 3.883
82 GLU HB2 H 1.85
82 GLU HG2 H 2.213
82 GLU N N 121.723
83 GLU CA C 56.606
83 GLU CB C 29.364
83 GLU CG C 33.582
83 GLU H H 8.118
83 GLU HA H 3.883
83 GLU HB2 H 1.669
83 GLU HB3 H 1.669
83 GLU HG2 H 2.219
83 GLU HG3 H 2.219
83 GLU N N 119.259
84 GLU CA C 56.606
84 GLU CB C 25.817
84 GLU CG C 33.47
84 GLU H H 8.212
84 GLU HA H 3.871
84 GLU HB2 H 1.983
84 GLU HB3 H 1.983
84 GLU HG2 H 2.226
84 GLU HG3 H 2.226
84 GLU N N 118.06
85 ILE CA C 62.484
85 ILE CB C 35.445
85 ILE CG1 C 26.898
85 ILE CG2 C 16.092
85 ILE CD1 C 10.212
85 ILE H H 7.964
85 ILE HA H 3.678

85 ILE HB H 1.705
85 ILE HG12 H 0.654
85 ILE HG13 H 0.654
85 ILE HG2 H 0.992
85 ILE HD1 H 0.642
85 ILE N N 120.736
86 ARG CA C 56.985
86 ARG CB C 26.856
86 ARG CG C 24.69
86 ARG CD C 40.536
86 ARG H H 8.351
86 ARG HA H 3.989
86 ARG HB2 H 1.935
86 ARG HB3 H 1.935
86 ARG HG2 H 1.512
86 ARG HG3 H 1.512
86 ARG HD2 H 2.841
86 ARG HD3 H 2.841
86 ARG N N 121.452
87 GLU CA C 56.606
87 GLU CB C 25.817
87 GLU CG C 33.698
87 GLU H H 8.238
87 GLU HA H 3.861
87 GLU HB2 H 1.89
87 GLU HB3 H 1.89
87 GLU HG2 H 2.213
87 GLU HG3 H 2.213
87 GLU N N 118.288
88 ALA CA C 52.263
88 ALA CB C 15.08
88 ALA H H 7.96
88 ALA HA H 4.013
88 ALA HB H 1.657
88 ALA N N 120.408
89 PHE CA C 59.703
89 PHE CB C 36.774
89 PHE H H 8.498
89 PHE HA H 3.058
89 PHE HB2 H 2.732
89 PHE HB3 H 2.732
89 PHE HD1 H 6.478
89 PHE HD2 H 6.478
89 PHE HE1 H 7.054
89 PHE HE2 H 7.054
89 PHE N N 118.123
90 ARG CA C 56.168
90 ARG CB C 27.654
90 ARG CG C 25.716
90 ARG CD C 40.764
90 ARG H H 7.86
90 ARG HA H 3.892
90 ARG HB2 H 1.79
90 ARG HB3 H 1.79
90 ARG HG2 H 1.995
90 ARG HG3 H 1.995
90 ARG HD2 H 3.046
90 ARG HD3 H 3.046
90 ARG N N 116.002
91 VAL CA C 63.357
91 VAL CB C 28.444
91 VAL CG1 C 18.164
91 VAL CG2 C 19.877
91 VAL H H 7.3
91 VAL HA H 3.243
91 VAL HB H 1.901
91 VAL HG1 H 0.376
91 VAL HG2 H 0.835
91 VAL N N 118.008
92 PHE CA C 57.558
92 PHE CB C 38.838
92 PHE H H 6.805
92 PHE HA H 3.967
92 PHE HB2 H 2.478
92 PHE HB3 H 2.478
92 PHE HD1 H 6.373
92 PHE HD2 H 6.373
92 PHE N N 113.024
93 ASP CA C 49.525
93 ASP CB C 35.788
93 ASP H H 8.018
93 ASP HA H 4.496
93 ASP HB2 H 2.517
93 ASP HB3 H 2.517
93 ASP N N 116.393
94 LYS CA C 56.183
94 LYS CB C 29.945
94 LYS CG C 25.246
94 LYS CD C 27.644
94 LYS CE C 40.944
94 LYS H H 7.721
94 LYS HA H 3.892
94 LYS HB2 H 1.667
94 LYS HB3 H 1.667
94 LYS HG2 H 1.524
94 LYS HG3 H 1.524
94 LYS HD2 H 1.79
94 LYS HD3 H 1.79
94 LYS HE2 H 3.034
94 LYS HE3 H 3.034
94 LYS N N 125.158
95 ASP CA C 50.683
95 ASP CB C 36.774
95 ASP H H 8.156
95 ASP HA H 4.415
95 ASP HB2 H 2.924
95 ASP HB3 H 2.498
95 ASP N N 113.893
96 GLY CA C 44.344
96 GLY H H 7.717
96 GLY HA2 H 3.711
96 GLY HA3 H 3.711
96 GLY N N 108.799
97 ASN CA C 49.916
97 ASN CB C 35.183
97 ASN H H 8.312
97 ASN HA H 4.5
97 ASN HB2 H 2.527
97 ASN HB3 H 2.527
97 ASN N N 119.381
98 GLY CA C 42.434
98 GLY H H 10.555
98 GLY HA2 H 3.339
98 GLY HA3 H 3.972
98 GLY N N 112.33
99 TYR CA C 53.582
99 TYR CB C 39.981
99 TYR H H 7.65
99 TYR HA H 4.871
99 TYR HB2 H 2.474
99 TYR HB3 H 2.474
99 TYR HD1 H 6.736
99 TYR HD2 H 6.736
99 TYR N N 116.075
100 ILE CA C 58.616
100 ILE CB C 35.903
100 ILE CG1 C 24.234
100 ILE CG2 C 14.443
100 ILE CD1 C 10.582
100 ILE H H 10.037
100 ILE HA H 4.493
100 ILE HB H 1.705
100 ILE HG12 H 1.245
100 ILE HG13 H 1.245
100 ILE HG2 H 0.774
100 ILE HD1 H 0.669
100 ILE N N 126.834
101 SER CA C 52.897
101 SER CB C 64.134
101 SER H H 8.904
101 SER HA H 4.738
101 SER HB2 H 3.818
101 SER HB3 H 3.818
101 SER N N 123.486
102 ALA CA C 53.093
102 ALA CB C 15.114
102 ALA H H 9.246
102 ALA HA H 3.747
102 ALA HB H 1.331
102 ALA N N 122.796
103 ALA CA C 52.409
103 ALA CB C 15.456
103 ALA H H 8.214
103 ALA HA H 3.861
103 ALA HB H 1.262
103 ALA N N 118.362
104 GLU CA C 56.563
104 GLU CB C 26.4
104 GLU CG C 33.582
104 GLU H H 7.864
104 GLU HA H 3.904
104 GLU HB2 H 1.917
104 GLU HB3 H 1.917
104 GLU HG2 H 2.225
104 GLU HG3 H 2.225
104 GLU N N 120.187
105 LEU CA C 55.732
105 LEU CB C 39.34
105 LEU CG C 24.102
105 LEU CD1 C 21.696
105 LEU CD2 C 20.321
105 LEU H H 8.341
105 LEU HA H 3.892
105 LEU HB2 H 1.743
105 LEU HB3 H 1.743
105 LEU HG H 1.488
105 LEU HD1 H 0.666
105 LEU HD2 H 0.896
105 LEU N N 121.05
106 ARG CA C 55.724
106 ARG CB C 29.945
106 ARG CG C 25.944
106 ARG CD C 39.054
106 ARG H H 8.852
106 ARG HA H 3.904
106 ARG HB2 H 1.686
106 ARG HB3 H 1.686
106 ARG HG2 H 1.524
106 ARG HG3 H 1.524
106 ARG HD2 H 2.636
106 ARG HD3 H 2.853
106 ARG N N 118.494
107 HIS CA C 56.807
107 HIS CB C 27.198
107 HIS H H 8.045
107 HIS HA H 3.876
107 HIS HB2 H 1.778
107 HIS HB3 H 1.778
107 HIS N N 118.921
108 VAL CA C 64.285
108 VAL CB C 28.908
108 VAL CG1 C 18.078
108 VAL CG2 C 20.7
108 VAL H H 7.766
108 VAL HA H 3.385
108 VAL HB H 2.068
108 VAL HG1 H 0.436
108 VAL HG2 H 0.835
108 VAL N N 118.991
109 MET CA C 54.461
109 MET CB C 29.706
109 MET CG C 29.706
109 MET H H 8.333
109 MET HA H 4.139
109 MET HB2 H 1.681
109 MET HB3 H 1.681
109 MET HG2 H 2.038
109 MET HG3 H 2.038
109 MET N N 115.789
110 THR CA C 63.845
110 THR CB C 66.072
110 THR CG2 C 18.876
110 THR H H 8.603
110 THR HA H 3.935
110 THR HB H 4.168
110 THR HG2 H 1.08
110 THR N N 116.7
111 ASN CA C 53.093
111 ASN CB C 35.292
111 ASN H H 7.991
111 ASN HA H 4.242
111 ASN HB2 H 2.689
111 ASN HB3 H 2.815
111 ASN N N 123.354
112 LEU CA C 52.653
112 LEU CB C 39.738
112 LEU CG C 23.094
112 LEU CD1 C 20.244

112 LEU H H 7.754
112 LEU HA H 4.182
112 LEU HB2 H 1.75
112 LEU HB3 H 1.75
112 LEU HG H 1.669
112 LEU HD1 H 0.666
112 LEU HD2 H 0.666
112 LEU N N 118.291
113 GLY CA C 42.536
113 GLY H H 7.778
113 GLY HA2 H 4.124
113 GLY HA3 H 4.124
113 GLY N N 106.894
114 GLU CA C 52.067
114 GLU CB C 26.616
114 GLU CG C 30.174
114 GLU H H 7.957
114 GLU HA H 4.267
114 GLU HB2 H 1.518
114 GLU HB3 H 1.518
114 GLU HG2 H 2.188
114 GLU HG3 H 2.188
114 GLU N N 119.776
115 LYS CA C 52.848
115 LYS CB C 30.518
115 LYS CG C 26.502
115 LYS CD C 21.933
115 LYS H H 8.591
115 LYS HA H 4.255
115 LYS HB2 H 1.548
115 LYS HB3 H 1.548
115 LYS HG2 H 1.512
115 LYS HD2 H 1.246
115 LYS HD3 H 1.246
115 LYS N N 124.429
116 LEU CA C 51.089
116 LEU CB C 42.588
116 LEU CG C 24.804
116 LEU CD1 C 21.384
116 LEU H H 8.066
116 LEU HA H 4.69
116 LEU HB2 H 1.343
116 LEU HB3 H 1.343
116 LEU HG H 1.512
116 LEU HD1 H 0.663
116 LEU N N 124.724
117 THR CA C 57.834
117 THR CB C 68.58
117 THR CG2 C 18.99
117 THR H H 9.165
117 THR HA H 4.302
117 THR HB H 4.647
117 THR HG2 H 1.153
117 THR N N 113.912
118 ASP CA C 55.243
118 ASP CB C 37.002
118 ASP H H 8.86
118 ASP HA H 4.061
118 ASP HB2 H 2.604
118 ASP HB3 H 2.412
118 ASP N N 120.787
119 GLU CA C 57.149
119 GLU CB C 25.931
119 GLU CG C 33.812
119 GLU H H 8.618
119 GLU HA H 3.892
119 GLU HB2 H 1.886
119 GLU HB3 H 1.886
119 GLU HG2 H 2.203
119 GLU HG3 H 2.203
119 GLU N N 119.091
120 GLU CA C 56.319
120 GLU CB C 25.83
120 GLU CG C 33.696
120 GLU H H 7.659
120 GLU HA H 3.88
120 GLU HB2 H 1.898
120 GLU HB3 H 1.898
120 GLU HG2 H 2.213
120 GLU HG3 H 2.213
120 GLU N N 120.037
121 VAL CA C 64.09
121 VAL CB C 28.68
121 VAL CG1 C 20.7
121 VAL CG2 C 18.078
121 VAL H H 7.887
121 VAL HA H 3.385
121 VAL HB H 2.068
121 VAL HG1 H 0.823
121 VAL HG2 H 0.448
121 VAL N N 122.512
122 ASP CA C 54.901
122 ASP CB C 37.572
122 ASP H H 7.973
122 ASP HA H 4.157
122 ASP HB2 H 2.623
122 ASP HB3 H 2.623
122 ASP N N 119.993
123 GLU CA C 56.612
123 GLU CB C 26.172
123 GLU CG C 33.468
123 GLU H H 7.903
123 GLU HA H 3.88
123 GLU HB2 H 1.978
123 GLU HB3 H 1.978
123 GLU HG2 H 2.213
123 GLU HG3 H 2.213
123 GLU N N 119.521
124 MET CA C 56.905
124 MET CB C 29.25
124 MET H H 7.496
124 MET HA H 3.892
124 MET HB2 H 1.657
124 MET HB3 H 1.657
124 MET HG2 H 2.109
124 MET HG3 H 2.109
124 MET N N 118.961
125 ILE CA C 60.131
125 ILE CB C 33.24
125 ILE CG1 C 13.595
125 ILE CG2 C 24.789
125 ILE CD1 C 6.906
125 ILE H H 7.762
125 ILE HA H 3.409
125 ILE HB H 2.086
125 ILE HG12 H 0.593
125 ILE HG13 H 0.593
125 ILE HG2 H 1.233
125 ILE HD1 H 0.461
125 ILE N N 117.801
126 ARG CA C 56.673
126 ARG CB C 29.478
126 ARG CG C 26.058
126 ARG CD C 40.992
126 ARG H H 8.055
126 ARG HA H 3.883
126 ARG HB2 H 1.681
126 ARG HB3 H 1.681
126 ARG HG2 H 1.983
126 ARG HG3 H 1.983
126 ARG N N 117.729
127 GLU CA C 56.319
127 GLU CB C 26.286
127 GLU CG C 33.696
127 GLU H H 7.7
127 GLU HA H 3.861
127 GLU HB2 H 1.935
127 GLU HB3 H 1.935
127 GLU HG2 H 2.225
127 GLU HG3 H 2.225
127 GLU N N 117.539
128 ALA CA C 48.205
128 ALA CB C 19.633
128 ALA H H 7.223
128 ALA HA H 4.5
128 ALA HB H 1.282
128 ALA N N 116.677
129 ASP CA C 51.485
129 ASP CB C 38.195
129 ASP H H 7.895
129 ASP HA H 4.46
129 ASP HB2 H 2.517
129 ASP HB3 H 2.517
129 ASP N N 118.03
130 ILE CA C 60.522
130 ILE CB C 36.09
130 ILE CG1 C 25.032
130 ILE CG2 C 14.43
130 ILE H H 8.148
130 ILE HA H 3.797
130 ILE HB H 1.837
130 ILE HG12 H 1.548
130 ILE HG13 H 1.548
130 ILE HG2 H 0.751
130 ILE HD1 H 0.708
130 ILE N N 127.693
131 ASP CA C 51.187
131 ASP CB C 37.468
131 ASP H H 8.288
131 ASP HA H 4.376
131 ASP HB2 H 2.517
131 ASP HB3 H 2.9
131 ASP N N 116.409
132 GLY CA C 44.638
132 GLY H H 7.63
132 GLY HA2 H 3.69
132 GLY HA3 H 3.69
132 GLY N N 108.363
133 ASP CA C 50.942
133 ASP CB C 37.458
133 ASP H H 8.298
133 ASP HA H 4.329
133 ASP HB2 H 2.938
133 ASP HB3 H 2.938
133 ASP N N 120.183
134 GLY CA C 43.122
134 GLY H H 10.079
134 GLY HA2 H 3.941
134 GLY HA3 H 3.288
134 GLY N N 112.149
135 GLN CA C 50.454
135 GLN CB C 30.614
135 GLN CG C 30.614
135 GLN H H 7.922
135 GLN HA H 4.844
135 GLN HB2 H 1.617
135 GLN HB3 H 1.617
135 GLN HG2 H 1.862
135 GLN HG3 H 1.862
135 GLN N N 115.069
136 VAL CA C 58.713
136 VAL CB C 31.416
136 VAL CG1 C 20.358
136 VAL CG2 C 19.104
136 VAL H H 9.046
136 VAL HA H 5.096
136 VAL HB H 2.168
136 VAL HG1 H 0.92
136 VAL HG2 H 1.137
136 VAL N N 125.107
137 ASN CA C 48.352
137 ASN CB C 35.64
137 ASN H H 9.458
137 ASN HA H 5.226
137 ASN HB2 H 2.964
137 ASN HB3 H 2.964
137 ASN N N 128.858
138 TYR CA C 59.669
138 TYR CB C 37.572
138 TYR H H 8.235
138 TYR HA H 3.603
138 TYR HB2 H 2.901
138 TYR HB3 H 2.901
138 TYR HD1 H 6.865
138 TYR HD2 H 6.865
138 TYR N N 118.481
139 GLU CA C 57.54
139 GLU CB C 26.274
139 GLU CG C 33.812
139 GLU H H 8.067
139 GLU HA H 3.868
139 GLU HB2 H 1.89
139 GLU HB3 H 1.89
139 GLU HG2 H 2.219
139 GLU HG3 H 2.219
139 GLU N N 118.474
140 GLU CA C 56.025

140 GLU CB C 26.274
140 GLU CG C 33.24
140 GLU H H 8.742
140 GLU HA H 3.88
140 GLU HB2 H 1.846
140 GLU HB3 H 1.846
140 GLU HG2 H 2.197
140 GLU HG3 H 2.197
140 GLU N N 119.279
141 PHE CA C 59.447
141 PHE CB C 37.686
141 PHE H H 8.593
141 PHE HA H 3.602
141 PHE HB2 H 2.945
141 PHE HB3 H 2.945
141 PHE HD1 H 6.63
141 PHE HD2 H 6.63
141 PHE HE1 H 6.99
141 PHE HE2 H 6.99
141 PHE HZ H 6.39
141 PHE N N 124.141
142 VAL CA C 64.432
142 VAL CB C 28.908
142 VAL CG1 C 18.762
142 VAL CG2 C 20.586
142 VAL H H 8.776
142 VAL HA H 2.986
142 VAL HB H 1.633
142 VAL HG1 H 0.576
142 VAL HG2 H 0.291
142 VAL N N 118.383
143 GLN CA C 56.514
143 GLN CB C 25.246
143 GLN CG C 31.414
143 GLN H H 7.787
143 GLN HA H 3.671
143 GLN HB2 H 1.912
143 GLN HB3 H 1.912
143 GLN HG2 H 2.219
143 GLN HG3 H 2.219
143 GLN N N 119.891
144 MET CA C 55.683
144 MET CB C 28.11
144 MET H H 7.45
144 MET HA H 3.892
144 MET HB2 H 1.781
144 MET HB3 H 1.781
144 MET HG2 H 1.781
144 MET HG3 H 1.781
144 MET N N 118.429
145 MET CA C 53.63
145 MET CB C 29.592
145 MET H H 7.724
145 MET HA H 3.905
145 MET HB2 H 1.672
145 MET HB3 H 1.672
145 MET HG2 H 1.672
145 MET HG3 H 1.672
145 MET N N 114.145
146 THR CA C 59.251
146 THR CB C 67.896
146 THR CG2 C 18.534
146 THR H H 7.7
146 THR HA H 4.17
146 THR HB H 4.103
146 THR HG2 H 1.053
146 THR N N 108.482
147 ALA CA C 50.307
147 ALA CB C 16.336
147 ALA H H 7.291
147 ALA HA H 4.095
147 ALA HB H 1.27
147 ALA N N 126.469
148 LYS CA C 54.803
148 LYS CB C 30.843
148 LYS CG C 21.933
148 LYS CD C 26.388
148 LYS CE C 39.852
148 LYS H H 7.993
148 LYS HA H 3.92
148 LYS HB2 H 1.678
148 LYS HB3 H 1.678
148 LYS HG2 H 1.281
148 LYS HG3 H 1.281
148 LYS N N 126.503
eNOSpThr495 peptide
153 THR H H 7.803
153 THR HA H 4.031
153 THR HB H 4.002
153 THR HG2 H 1.225
154 PHE H H 8.13
154 PHE HA H 4.178
154 PHE HB2 H 4.005
154 PHE HB3 H 4.005
155 LYS H H 7.86
155 LYS HA H 3.999
155 LYS HB2 H 2.262
155 LYS HB3 H 2.262
155 LYS HG2 H 0.824
155 LYS HG3 H 0.824
155 LYS HD2 H 1.569
155 LYS HD3 H 1.569
156 GLU H H 7.616
156 GLU HA H 4.152
156 GLU HB2 H 1.549
156 GLU HB3 H 1.549
156 GLU HG2 H 1.844
156 GLU HG3 H 1.844
157 VAL H H 7.338
157 VAL HA H 4.407
157 VAL HB H 1.342
157 VAL HG1 H 0.861
157 VAL HG2 H 1.065
158 ALA H H 7.164
159 ASN H H 7.482
160 ALA H H 6.872
161 VAL H H 6.569
161 VAL HB H 1.331
161 VAL HG1 H 0.872
161 VAL HG2 H 0.872
162 LYS H H 7.256
162 LYS HD2 H 1.383
162 LYS HD3 H 1.383
163 ILE H H 9.23
163 ILE HA H 4.178
163 ILE HB H 2.316
163 ILE HG12 H 1.336
163 ILE HG13 H 1.336
163 ILE HD1 H 1.074
164 SER H H 8.2
164 SER HA H 4.165
164 SER HB2 H 2.266
164 SER HB3 H 2.266
165 ALA H H 7.769
165 ALA HA H 4.172
165 ALA HB H 1.533
166 SER H H 8.067
166 SER HA H 4.158
166 SER HB2 H 2.306
166 SER HB3 H 2.306
167 LEU H H 7.949
167 LEU HA H 4.008
167 LEU HB2 H 2.276
167 LEU HB3 H 2.276
167 LEU HG H 1.558
167 LEU HD1 H 0.935
167 LEU HD2 H 0.853
168 MET H H 7.823
168 MET HA H 4.015
168 MET HB2 H 1.678
168 MET HB3 H 1.678
168 MET HG2 H 1.532
168 MET HG3 H 1.532
169 GLY H H 7.508
170 THR H H 6.83

Appendix I

CaM_{34}-iNOS Peptide Assigned Chemical Shifts

_Residue_seq_code
_Residue_label
_Atom_name
_Atom_type
_Chem_shift_value
2 ASP CA C 51.929
2 ASP CB C 38.505
2 ASP H H 8.499
2 ASP HA H 4.576
2 ASP HB2 H 2.507
2 ASP HB3 H 2.507
2 ASP N N 120.33
3 GLN CA C 52.768
3 GLN CB C 26.518
3 GLN CG C 30.85
3 GLN H H 8.16
3 GLN HA H 4.198
3 GLN HB2 H 1.889
3 GLN HB3 H 1.778
3 GLN HG2 H 2.165
3 GLN HG3 H 2.165
3 GLN N N 119.72
4 LEU CA C 51.584
4 LEU CB C 40.83
4 LEU CG C 23.77
4 LEU CD1 C 20.686
4 LEU H H 7.5
4 LEU HA H 4.448
4 LEU HB2 H 1.528
4 LEU HB3 H 1.353
4 LEU HG H 1.436
4 LEU HD1 H 0.733
4 LEU HD2 H 0.68
4 LEU N N 120.693
5 THR CA C 57.873
5 THR CB C 68.444
5 THR CG2 C 18.858
5 THR H H 8.559
5 THR HA H 4.277
5 THR HB H 4.618
5 THR HG2 H 1.161
5 THR N N 112.728
6 GLU CA C 57.481
6 GLU CB C 26.512
6 GLU CG C 33.586
6 GLU H H 8.854
6 GLU HA H 3.847
6 GLU HB2 H 1.876
6 GLU HB3 H 1.876
6 GLU HG2 H 2.165
6 GLU HG3 H 2.165
6 GLU N N 120.254
7 GLU CA C 57.176
7 GLU CB C 26.054
7 GLU CG C 33.593
7 GLU H H 8.512
7 GLU HA H 3.883
7 GLU HB2 H 1.878
7 GLU HB3 H 1.878
7 GLU HG2 H 2.166
7 GLU HG3 H 2.166
7 GLU N N 119.498
8 GLN CA C 56.411
8 GLN CB C 26.625
8 GLN CG C 33.358
8 GLN H H 7.54
8 GLN HA H 3.87
8 GLN HB2 H 1.778
8 GLN HB3 H 1.887
8 GLN HG2 H 2.165
8 GLN HG3 H 2.165
8 GLN N N 120.119
9 ILE CA C 64.046
9 ILE CB C 34.954
9 ILE CG1 C 27.539
9 ILE CG2 C 14.518
9 ILE CD1 C 10.291
9 ILE H H 8.383
9 ILE HA H 3.634
9 ILE HB H 1.804
9 ILE HG1 H 0.883
9 ILE HG1 H 0.883
9 ILE HG2 H 0.936
9 ILE HD1 H 0.662
9 ILE N N 120.115
10 ALA CA C 52.657
10 ALA CB C 14.975
10 ALA H H 7.935
10 ALA HA H 3.929
10 ALA HB H 1.345
10 ALA N N 121.405
11 GLU CA C 56.673
11 GLU CB C 26.968
11 GLU CG C 33.472
11 GLU H H 7.671
11 GLU HA H 3.89
11 GLU HB2 H 1.778
11 GLU HB3 H 1.883
11 GLU HG2 H 2.165
11 GLU HG3 H 2.165
11 GLU N N 118.499
12 PHE CA C 59.501
12 PHE CB C 35.644
12 PHE H H 8.227
12 PHE HA H 3.152
12 PHE HB2 H 2.173
12 PHE HB3 H 2.173
12 PHE N N 117.342
13 LYS CA C 57.154
13 LYS CB C 26.169
13 LYS CG C 24.455
13 LYS CD C 29.824
13 LYS CE C 39.419
13 LYS H H 8.917
13 LYS HA H 3.923
13 LYS HB2 H 1.883
13 LYS HB3 H 1.883
13 LYS HG2 H 1.527
13 LYS HG3 H 1.527
13 LYS HD2 H 1.761
13 LYS HD3 H 1.761
13 LYS HE2 H 2.517
13 LYS HE3 H 2.517
13 LYS N N 122.871
14 GLU CA C 56.471
14 GLU CB C 26.662
14 GLU CG C 33.479
14 GLU H H 7.78
14 GLU HA H 3.858
14 GLU HB2 H 1.778
14 GLU HB3 H 1.883
14 GLU HG2 H 2.175
14 GLU HG3 H 2.175
14 GLU N N 120.129
15 ALA CA C 52.869
15 ALA CB C 15.232
15 ALA H H 8.102
15 ALA HA H 3.867
15 ALA HB H 1.653
15 ALA N N 123.561
16 PHE CA C 58.983
16 PHE CB C 36.739
16 PHE H H 8.425
16 PHE HA H 3.132
16 PHE HB2 H 2.135
16 PHE HB3 H 2.135
16 PHE N N 118.907
17 SER CA C 58.999
17 SER CB C 60.436
17 SER H H 7.89
17 SER HA H 3.877
17 SER HB2 H 3.923
17 SER HB3 H 3.923
17 SER N N 114.729
18 LEU CA C 54.62
18 LEU CB C 38.374
18 LEU CG C 23.668
18 LEU CD1 C 20.686
18 LEU CD2 C 22.414
18 LEU H H 7.18
18 LEU HA H 3.785
18 LEU HB2 H 1.6
18 LEU HB3 H 1.6
18 LEU HG H 1.528
18 LEU HD1 H 0.472
18 LEU HD2 H 0.611
18 LEU N N 120.066
19 PHE CA C 56.37
19 PHE CB C 39.172
19 PHE H H 6.993
19 PHE HA H 3.949
19 PHE HB2 H 2.801
19 PHE HB3 H 2.801
19 PHE N N 112.537
20 ASP CA C 49.638
20 ASP CB C 37.106
20 ASP H H 7.436
20 ASP HA H 4.447
20 ASP HB2 H 2.489
20 ASP HB3 H 2.489
20 ASP N N 117.217
21 LYS CA C 55.529
21 LYS CB C 29.596
21 LYS CG C 21.714
21 LYS CD C 26.176
21 LYS CE C 39.19
21 LYS H H 7.505
21 LYS HA H 3.811
21 LYS HB2 H 1.699
21 LYS HB3 H 1.699
21 LYS HG2 H 1.331
21 LYS HG3 H 1.233
21 LYS HD2 H 1.491
21 LYS HD3 H 1.491
21 LYS HE2 H 2.816
21 LYS HE3 H 2.816
21 LYS N N 124.296
22 ASP CA C 50.061
22 ASP CB C 36.897
22 ASP H H 7.825
22 ASP HA H 4.421
22 ASP HB2 H 2.485
22 ASP HB3 H 2.88
22 ASP N N 113.736
23 GLY CA C 44.487
23 GLY H H 7.504
23 GLY HA2 H 3.713
23 GLY HA3 H 3.713
23 GLY N N 109.075
24 ASP C C 174.572
24 ASP CA C 50.917
24 ASP CB C 37.683
24 ASP H H 8.304
24 ASP HA H 4.309
24 ASP HB2 H 2.863
24 ASP HB3 H 2.863

24 ASP N N 120.749
25 GLY CA C 42.602
25 GLY H H 10.341
25 GLY HA2 H 3.529
25 GLY HA3 H 3.529
25 GLY N N 112.474
26 THR CA C 56.878
26 THR CB C 70.031
26 THR CG2 C 18.972
26 THR H H 8.01
26 THR HA H 5.299
26 THR HB H 3.666
26 THR HG2 H 0.866
26 THR N N 111.838
27 ILE CA C 58.255
27 ILE CB C 37.133
27 ILE CG1 C 14.89
27 ILE CG2 C 24.348
27 ILE CD1 C 11.352
27 ILE H H 9.735
27 ILE HA H 4.65
27 ILE HB H 1.594
27 ILE HG1 H 0.787
27 ILE HG1 H 0.787
27 ILE HG2 H 0.977
27 ILE HD1 H 0.026
27 ILE N N 126.257
28 THR CA C 56.878
28 THR CB C 70.009
28 THR CG2 C 19.543
28 THR H H 8.315
28 THR HA H 4.651
28 THR HB H 3.838
28 THR HG2 H 0.952
28 THR N N 116.303
29 THR CA C 63.742
29 THR CB C 65.16
29 THR CG2 C 20.586
29 THR H H 9.049
29 THR HA H 3.621
29 THR HB H 4.054
29 THR HG2 H 1.121
29 THR N N 112.277
30 LYS CA C 56.539
30 LYS CB C 29.906
30 LYS CG C 22.171
30 LYS CD C 26.397
30 LYS CE C 39.304
30 LYS H H 7.447
30 LYS HA H 3.949
30 LYS HB2 H 1.692
30 LYS HB3 H 1.692
30 LYS HG2 H 1.256
30 LYS HG3 H 1.331
30 LYS HD3 H 1.502
30 LYS HE2 H 2.827
30 LYS N N 120.776
31 GLU CA C 56.677
31 GLU CB C 27.082
31 GLU CG C 33.593
31 GLU H H 7.521
31 GLU HA H 3.906
31 GLU HB2 H 1.897
31 GLU HB3 H 1.897
31 GLU HG2 H 2.164
31 GLU HG3 H 2.164
31 GLU N N 121.064
32 LEU CA C 55.394
32 LEU CB C 39.852
32 LEU CG C 23.892
32 LEU CD1 C 20.814
32 LEU H H 8.687
32 LEU HA H 4.057
32 LEU HB2 H 1.705
32 LEU HB3 H 1.705
32 LEU HG H 1.53
32 LEU HD1 H 0.702
32 LEU HD2 H 0.702
32 LEU N N 120.376
33 GLY CA C 45.733
33 GLY H H 8.697
33 GLY HA2 H 3.851
33 GLY HA3 H 3.378
33 GLY N N 105.863
34 THR CA C 64.259
34 THR CB C 66.033
34 THR CG2 C 18.515
34 THR H H 7.747
34 THR HA H 3.779
34 THR HB H 4.162
34 THR HG2 H 1.105
34 THR N N 117.298
35 VAL CA C 64.214
35 VAL CB C 28.715
35 VAL CG1 C 17.74
35 VAL CG2 C 20.115
35 VAL H H 7.243
35 VAL HA H 3.405
35 VAL HB H 1.889
35 VAL HG1 H 0.295
35 VAL HG2 H 0.721
35 VAL N N 121.563
36 MET CA C 56.269
36 MET CB C 26.27
36 MET CG C 33.472
36 MET H H 8.458
36 MET HA H 3.901
36 MET HB2 H 1.891
36 MET HB3 H 1.891
36 MET HG2 H 2.16
36 MET HG3 H 2.16
36 MET N N 117.4
37 ARG CA C 56.337
37 ARG CB C 27.317
37 ARG CG C 24.922
37 ARG CD C 40.904
37 ARG H H 8.323
37 ARG HA H 3.89
37 ARG HB2 H 1.759
37 ARG HB3 H 1.759
37 ARG HG2 H 1.515
37 ARG HG3 H 1.515
37 ARG HD2 H 3.017
37 ARG HD3 H 3.017
37 ARG N N 118.303
38 SER CA C 59.635
38 SER CB C 60.376
38 SER H H 7.753
38 SER HA H 3.936
38 SER HB2 H 3.929
38 SER HB3 H 3.929
38 SER N N 119.141
39 LEU CA C 51.438
39 LEU CB C 38.391
39 LEU CG C 24.067
39 LEU CD1 C 23.359
39 LEU CD2 C 20.527
39 LEU H H 7.248
39 LEU HA H 4.112
39 LEU HB2 H 1.575
39 LEU HB3 H 1.575
39 LEU HG H 1.528
39 LEU HD1 H 0.57
39 LEU HD2 H 0.445
39 LEU N N 117.995
40 GLY CA C 42.872
40 GLY H H 7.626
40 GLY HA2 H 4.071
40 GLY HA3 H 4.071
40 GLY N N 106.739
41 GLN CA C 50.853
41 GLN CB C 27.759
41 GLN CG C 30.395
41 GLN H H 7.755
41 GLN HA H 4.269
41 GLN HB2 H 1.742
41 GLN HB3 H 1.742
41 GLN HG2 H 1.989
41 GLN HG3 H 1.989
41 GLN N N 118.046
42 ASN CA C 48.562
42 ASN CB C 36.318
42 ASN H H 8.54
42 ASN HA H 5.013
42 ASN HB2 H 2.606
42 ASN HB3 H 2.329
42 ASN N N 115.94
44 THR CA C 57.851
44 THR CB C 68.317
44 THR CG2 C 18.858
44 THR H H 8.663
44 THR HA H 4.277
44 THR HB H 4.625
44 THR HG2 H 1.154
44 THR N N 112.937
45 GLU CA C 57.245
45 GLU CB C 26.276
45 GLU CG C 33.582
45 GLU H H 8.651
45 GLU HA H 3.896
45 GLU HB2 H 1.876
45 GLU HB3 H 1.876
45 GLU HG2 H 2.165
45 GLU HG3 H 2.165
45 GLU N N 120.439
46 ALA CA C 52.316
46 ALA CB C 15.089
46 ALA H H 8.109
46 ALA HA H 3.923
46 ALA HB H 1.22
46 ALA N N 120.66
47 GLU CA C 56.508
47 GLU CB C 26.632
47 GLU CG C 33.586
47 GLU H H 7.532
47 GLU HA H 3.877
47 GLU HB2 H 1.878
47 GLU HB3 H 1.772
47 GLU HG2 H 2.165
47 GLU HG3 H 2.165
47 GLU N N 118.571
48 LEU CA C 55.327
48 LEU CB C 39.568
48 LEU CG C 29.596
48 LEU CD1 C 23.656
48 LEU CD2 C 21.16
48 LEU H H 8.232
48 LEU HA H 4.059
48 LEU HB2 H 1.699
48 LEU HB3 H 1.699
48 LEU HG H 1.679
48 LEU HD1 H 0.702
48 LEU HD2 H 0.78
48 LEU N N 120.085
49 GLN CA C 55.927
49 GLN CB C 27.145
49 GLN CG C 33.479
49 GLN H H 7.938
49 GLN HA H 3.913
49 GLN HB2 H 1.889
49 GLN HB3 H 1.889
49 GLN HG2 H 2.166
49 GLN HG3 H 2.166
49 GLN N N 118.111
50 ASP CA C 54.953
50 ASP CB C 37.278
50 ASP CG C 33.593
50 ASP H H 7.923
50 ASP HA H 4.021
50 ASP HB2 H 2.48
50 ASP N N 119.876
51 MET CA C 56.976
51 MET CB C 30.374
51 MET CG C 29.831
51 MET H H 7.913
51 MET HA H 3.847
51 MET HB2 H 2.394
51 MET HB3 H 2.65
51 MET HG2 H 1.743
51 MET HG3 H 1.743
51 MET N N 119.513
52 ILE CA C 61.675
52 ILE CB C 33.822
52 ILE CG1 C 13.604
52 ILE CG2 C 26.054
52 ILE CD1 C 8.921
52 ILE H H 7.681
52 ILE HA H 3.348

52 ILE HB H 1.868
52 ILE HG1 H 0.568
52 ILE HG1 H 0.515
52 ILE HG2 H 1.482
52 ILE HD1 H 0.547
52 ILE N N 116.864
53 ASN CA C 52.97
53 ASN CB C 35.078
53 ASN H H 8.202
53 ASN HA H 4.263
53 ASN HB2 H 2.826
53 ASN HB3 H 2.73
53 ASN N N 117.493
54 GLU CA C 55.798
54 GLU CB C 26.857
54 GLU CG C 33.244
54 GLU H H 7.362
54 GLU HA H 3.87
54 GLU HB2 H 1.889
54 GLU HB3 H 1.889
54 GLU HG2 H 2.171
54 GLU HG3 H 2.171
54 GLU N N 116.857
55 VAL CA C 58.727
55 VAL CB C 30.738
55 VAL CG1 C 20.343
55 VAL CG2 C 19.519
55 VAL H H 7.147
55 VAL HA H 3.987
55 VAL HB H 1.91
55 VAL HG1 H 0.93
55 VAL HG2 H 0.891
55 VAL N N 114.264
56 ASP CA C 51.356
56 ASP CB C 38.364
56 ASP H H 7.86
56 ASP HA H 4.435
56 ASP HB2 H 2.506
56 ASP HB3 H 2.368
56 ASP N N 119.756
57 ALA CA C 51.183
57 ALA CB C 16.942
57 ALA H H 8.115
57 ALA HA H 4.08
57 ALA HB H 1.345
57 ALA N N 131.417
58 ASP CA C 50.008
58 ASP CB C 36.897
58 ASP H H 8.12
58 ASP HA H 4.434
58 ASP HB2 H 2.873
58 ASP HB3 H 2.485
58 ASP N N 114.151
59 GLY CA C 44.487
59 GLY H H 7.484
59 GLY HA2 H 3.717
59 GLY HA3 H 3.717
59 GLY N N 108.768
60 ASN C C 174.17
60 ASN CA C 49.974
60 ASN CB C 34.713
60 ASN H H 8.081
60 ASN HA H 4.428
60 ASN HB2 H 2.492
60 ASN HB3 H 2.492
60 ASN N N 118.77
61 GLY CA C 42.905
61 GLY H H 10.243
61 GLY HA2 H 3.327
61 GLY HA3 H 4.067
61 GLY N N 112.712
62 THR CA C 56.774
62 THR CB C 69.688
62 THR CG2 C 19.543
62 THR H H 7.477
62 THR HA H 4.649
62 THR HB H 3.827
62 THR HG2 H 0.947
62 THR N N 108.06
63 ILE CA C 57.75
63 ILE CB C 37.363
63 ILE CG1 C 24.341
63 ILE CG2 C 15.431
63 ILE CD1 C 11.319
63 ILE H H 8.43
63 ILE HA H 4.796
63 ILE HB H 1.855
63 ILE HG2 H 1.096
63 ILE HD1 H 0.787
63 ILE N N 122.617
64 ASP CA C 49.402
64 ASP CB C 39.761
64 ASP H H 8.996
64 ASP HA H 5.333
64 ASP HB2 H 2.814
64 ASP HB3 H 2.814
64 ASP N N 128.615
65 PHE CA C 60.213
65 PHE CB C 32.902
65 PHE H H 8.756
65 PHE HA H 3.542
65 PHE HB2 H 1.673
65 PHE HB3 H 1.673
65 PHE N N 118.892
67 GLU CA C 56.605
67 GLU CB C 26.397
67 GLU CG C 33.25
67 GLU H H 7.814
67 GLU HA H 3.899
67 GLU HB2 H 1.889
67 GLU HB3 H 1.761
67 GLU HG2 H 2.155
67 GLU HG3 H 2.155
67 GLU N N 119.708
68 PHE CA C 58.255
68 PHE CB C 37.591
68 PHE H H 8.048
68 PHE HA H 3.647
68 PHE HB2 H 2.627
68 PHE HB3 H 2.627
68 PHE N N 123.035
69 LEU CA C 54.774
69 LEU CB C 38.577
69 LEU CG C 23.919
69 LEU CD1 C 20.835
69 LEU CD2 C 22.549
69 LEU H H 8.649
69 LEU HA H 3.763
69 LEU HB2 H 1.109
69 LEU HB3 H 1.109
69 LEU HG H 1.529
69 LEU HD1 H 0.478
69 LEU HD2 H 0.603
69 LEU N N 119.481
70 THR CA C 63.861
70 THR CB C 66.045
70 THR CG2 C 18.515
70 THR H H 7.894
70 THR HA H 3.501
70 THR HB H 3.947
70 THR HG2 H 0.997
70 THR N N 113.842
71 MET CA C 56
71 MET CB C 29.595
71 MET CG C 29.481
71 MET H H 7.12
71 MET HA H 3.913
71 MET HB2 H 1.7
71 MET HB3 H 1.7
71 MET HG2 H 2.337
71 MET HG3 H 2.337
71 MET N N 119.518
72 MET CA C 54.99
72 MET CB C 26.617
72 MET CG C 29.595
72 MET H H 7.715
72 MET HA H 3.86
72 MET HB2 H 1.727
72 MET HB3 H 1.727
72 MET HG2 H 2.395
72 MET HG3 H 2.395
72 MET HE H 2.11
72 MET N N 116.386
73 ALA CA C 51.859
73 ALA CB C 15.376
73 ALA H H 8.318
73 ALA HA H 3.832
73 ALA HB H 1.128
73 ALA N N 119.953
74 ARG CA C 55.933
74 ARG CB C 29.14
74 ARG CG C 26.86
74 ARG CD C 40.675
74 ARG H H 7.281
74 ARG HA H 3.86
74 ARG HB2 H 1.664
74 ARG HB3 H 1.664
74 ARG HG2 H 1.762
74 ARG HG3 H 1.762
74 ARG HD2 H 3.039
74 ARG HD3 H 3.039
74 ARG N N 116.354
75 LYS CA C 54.788
75 LYS CB C 26.404
75 LYS CG C 21.714
75 LYS CD C 30.852
75 LYS CE C 39.419
75 LYS H H 7.767
75 LYS HA H 3.948
75 LYS HB2 H 1.494
75 LYS HB3 H 1.494
75 LYS HG2 H 1.223
75 LYS HG3 H 1.223
75 LYS HD2 H 1.626
75 LYS HD3 H 1.626
75 LYS HE2 H 2.805
75 LYS HE3 H 2.805
75 LYS N N 120.084
76 MET CA C 54.552
76 MET CB C 30.052
76 MET CG C 26.204
76 MET CE C 21.978
76 MET H H 7.941
76 MET HA H 3.954
76 MET HB2 H 1.628
76 MET HB3 H 1.628
76 MET HG2 H 1.49
76 MET HG3 H 1.49
76 MET HE H 1.226
76 MET N N 116.881
77 LYS CA C 53.307
77 LYS CB C 27.246
77 LYS CG C 21.828
77 LYS CD C 30.509
77 LYS CE C 39.419
77 LYS H H 7.264
77 LYS HA H 4.221
77 LYS HB2 H 1.495
77 LYS HB3 H 1.495
77 LYS HG2 H 1.229
77 LYS HG3 H 1.346
77 LYS HD2 H 1.644
77 LYS HD3 H 1.793
77 LYS HE2 H 2.805
77 LYS HE3 H 2.805
77 LYS N N 116.614
78 ASP CA C 51.732
78 ASP CB C 39.021
78 ASP H H 8.14
78 ASP HA H 4.426
78 ASP HB2 H 2.312
78 ASP HB3 H 2.312
78 ASP N N 123.089
79 THR CA C 61.15
79 THR CB C 66.147
79 THR CG2 C 18.972
79 THR H H 8.316
79 THR HA H 4.034
79 THR HB H 4.151
79 THR HG2 H 1.128
79 THR N N 114.423
80 ASP CA C 51.759
80 ASP CB C 37.81
80 ASP H H 8.24
80 ASP HA H 4.44
80 ASP HB2 H 2.506
80 ASP HB3 H 2.506
80 ASP N N 120.819

81 SER CA C 57.683
81 SER CB C 60.664
81 SER H H 7.798
81 SER HA H 4.215
81 SER HB2 H 3.801
81 SER HB3 H 3.932
81 SER N N 115.729
82 GLU CA C 56.707
82 GLU CB C 26.625
82 GLU CG C 33.479
82 GLU H H 8.186
82 GLU HA H 3.896
82 GLU HB2 H 1.897
82 GLU HB3 H 1.897
82 GLU HG2 H 2.164
82 GLU HG3 H 2.164
82 GLU N N 122.083
83 GLU CA C 55.928
83 GLU CB C 26.832
83 GLU CG C 33.593
83 GLU H H 7.937
83 GLU HA H 3.873
83 GLU HB2 H 1.761
83 GLU HB3 H 1.889
83 GLU HG2 H 2.166
83 GLU HG3 H 2.166
83 GLU N N 118.04
84 GLU CA C 54.62
84 GLU CB C 26.318
84 GLU CG C 39.34
84 GLU H H 8.08
84 GLU HA H 3.917
84 GLU HB2 H 1.477
84 GLU HB3 H 1.477
84 GLU HG2 H 2.804
84 GLU HG3 H 2.804
84 GLU N N 118.604
85 ILE CA C 63.338
85 ILE CB C 34.688
85 ILE CG1 C 27.45
85 ILE CG2 C 14.324
85 ILE CD1 C 9.984
85 ILE H H 7.863
85 ILE HA H 3.619
85 ILE HB H 1.786
85 ILE HG1 H 0.879
85 ILE HG1 H 0.879
85 ILE HG2 H 0.938
85 ILE HD1 H 0.662
85 ILE N N 120.249
86 ARG CA C 57.346
86 ARG CB C 26.854
86 ARG CG C 24.569
86 ARG CD C 40.715
86 ARG H H 8.177
86 ARG HA H 3.925
86 ARG HB2 H 1.769
86 ARG HB3 H 1.876
86 ARG HG2 H 1.513
86 ARG HG3 H 1.513
86 ARG HD2 H 2.786
86 ARG HD3 H 2.786
86 ARG N N 120.64
87 GLU CA C 56.51
87 GLU CB C 26.401
87 GLU CG C 33.575
87 GLU H H 7.823
87 GLU HA H 3.887
87 GLU HB2 H 1.896
87 GLU HB3 H 1.896
87 GLU HG2 H 2.164
87 GLU HG3 H 2.164
87 GLU N N 119.782
88 ALA CA C 52.566
88 ALA CB C 14.632
88 ALA H H 8.194
88 ALA HA H 4.028
88 ALA HB H 1.609
88 ALA N N 122.318
89 PHE CA C 58.983
89 PHE CB C 36.37
89 PHE H H 8.406
89 PHE HA H 3.133
89 PHE HB2 H 2.183
89 PHE HB3 H 2.607
89 PHE N N 118.832
90 ARG CA C 55.899
90 ARG CB C 27.394
90 ARG CG C 24.993
90 ARG CD C 40.888
90 ARG H H 7.74
90 ARG HA H 3.893
90 ARG HB2 H 1.749
90 ARG HB3 H 1.749
90 ARG HG2 H 1.506
90 ARG HG3 H 1.506
90 ARG HD2 H 3.012
90 ARG HD3 H 3.012
90 ARG N N 116.969
91 VAL CA C 63.333
91 VAL CB C 28.456
91 VAL CG1 C 18.401
91 VAL CG2 C 20.229
91 VAL H H 7.282
91 VAL HA H 3.288
91 VAL HB H 1.848
91 VAL HG1 H 0.296
91 VAL HG2 H 0.75
91 VAL N N 118.958
92 PHE CA C 56.606
92 PHE CB C 39.419
92 PHE H H 6.822
92 PHE HA H 3.954
92 PHE HB2 H 2.798
92 PHE HB3 H 2.798
92 PHE N N 113.384
93 ALA CA C 48.83
93 ALA CB C 16.495
93 ALA H H 7.889
93 ALA HA H 3.921
93 ALA HB H 1.339
93 ALA N N 122.222
94 LYS CA C 54.809
94 LYS CB C 30.71
94 LYS CG C 21.791
94 LYS CD C 26.251
94 LYS CE C 39.63
94 LYS H H 7.836
94 LYS HA H 3.932
94 LYS HB2 H 1.624
94 LYS HB3 H 1.624
94 LYS HG2 H 1.217
94 LYS HG3 H 1.217
94 LYS HD2 H 1.486
94 LYS HD3 H 1.486
94 LYS HE2 H 2.801
94 LYS HE3 H 2.801
94 LYS N N 120.861
95 ASP CA C 52.162
95 ASP CB C 37.8
95 ASP H H 8.567
95 ASP HA H 4.434
95 ASP HB2 H 2.512
95 ASP HB3 H 2.512
95 ASP N N 119.161
96 GLY CA C 43.276
96 GLY H H 7.955
96 GLY HA2 H 3.768
96 GLY N N 107.207
97 ASN CA C 50.244
97 ASN CB C 36.322
97 ASN H H 8.109
97 ASN HA H 4.501
97 ASN HB2 H 2.486
97 ASN HB3 H 2.486
97 ASN N N 117.565
98 GLY CA C 42.636
98 GLY H H 8.429
98 GLY HA2 H 3.768
98 GLY HA3 H 3.768
98 GLY N N 107.108
99 TYR CA C 52.735
99 TYR CB C 37.832
99 TYR H H 7.019
99 TYR HA H 4.437
99 TYR HB2 H 2.502
99 TYR HB3 H 2.502
99 TYR N N 114.221
101 SER CA C 53.879
101 SER CB C 64.091
101 SER H H 8.945
101 SER HA H 4.05
101 SER HB2 H 3.623
101 SER HB3 H 3.623
101 SER N N 123.8
102 ALA CA C 53.24
102 ALA CB C 14.975
102 ALA H H 9.053
102 ALA HA H 3.741
102 ALA HB H 1.342
102 ALA N N 124.809
103 ALA CA C 52.597
103 ALA CB C 15.203
103 ALA H H 8.16
103 ALA HA H 3.874
103 ALA HB H 1.217
103 ALA N N 118.545
104 GLU CA C 56.522
104 GLU CB C 27.395
104 GLU CG C 34.156
104 GLU H H 7.61
104 GLU HA H 3.906
104 GLU HB2 H 1.887
104 GLU HB3 H 1.782
104 GLU HG2 H 2.144
104 GLU N N 118.667
105 LEU CA C 55.764
105 LEU CB C 39.445
105 LEU CG C 23.77
105 LEU CD1 C 21.6
105 LEU H H 8.069
105 LEU HA H 4.116
105 LEU HB2 H 1.769
105 LEU HB3 H 1.769
105 LEU HG H 1.513
105 LEU HD1 H 0.643
105 LEU HD2 H 1.096
105 LEU N N 121.56
106 ARG CA C 57.313
106 ARG CB C 27.084
106 ARG CG C 25.26
106 ARG CD C 40.65
106 ARG H H 8.742
106 ARG HA H 3.939
106 ARG HB2 H 1.765
106 ARG HB3 H 1.882
106 ARG HG2 H 1.48
106 ARG HD2 H 2.795
106 ARG HD3 H 3.005
106 ARG N N 118.436
107 HIS CA C 56.471
107 HIS CB C 26.74
107 HIS H H 7.795
107 HIS HA H 4.241
107 HIS HB2 H 3.178
107 HIS HB3 H 3.178
107 HIS N N 118.439
108 VAL CA C 64.05
108 VAL CB C 29.253
108 VAL CG1 C 20.476
108 VAL CG2 C 18.766
108 VAL H H 7.61
108 VAL HA H 3.413
108 VAL HB H 1.901
108 VAL HG1 H 0.724
108 VAL HG2 H 0.296
108 VAL N N 118.849
109 MET CA C 55.798
109 MET CB C 27.394
109 MET CG C 31.08
109 MET H H 8.054
109 MET HA H 3.899
109 MET HB2 H 1.761
109 MET HB3 H 1.761
109 MET HG2 H 2.166
109 MET HG3 H 2.166
109 MET N N 115.69
110 THR CA C 63.728

110 THR CB C 65.93
110 THR CG2 C 18.818
110 THR H H 8.433
110 THR HA H 3.794
110 THR HB H 4.156
110 THR HG2 H 1.112
110 THR N N 115.945
111 ASN CA C 52.949
111 ASN CB C 34.964
111 ASN H H 7.836
111 ASN HA H 4.267
111 ASN HB2 H 2.827
111 ASN HB3 H 2.827
111 ASN N N 123.336
112 LEU CA C 52.802
112 LEU CB C 39.533
112 LEU CG C 23.541
112 LEU CD1 C 20.248
112 LEU H H 7.643
112 LEU HA H 4.057
112 LEU HB2 H 1.697
112 LEU HB3 H 1.46
112 LEU HG H 1.572
112 LEU HD1 H 0.546
112 LEU N N 119.072
113 GLY CA C 42.636
113 GLY H H 7.698
113 GLY HA2 H 3.597
113 GLY HA3 H 4.077
113 GLY N N 106.862
114 GLU CA C 51.859
114 GLU CB C 27.539
114 GLU CG C 31.651
114 GLU H H 7.841
114 GLU HA H 4.267
114 GLU HB2 H 1.756
114 GLU HB3 H 1.756
114 GLU HG2 H 1.927
114 GLU HG3 H 1.927
114 GLU N N 120.273
115 LYS CA C 53.105
115 LYS CB C 29.481
115 LYS CG C 21.714
115 LYS CD C 26.283
115 LYS CE C 39.304
115 LYS H H 8.336
115 LYS HA H 4.195
115 LYS HB2 H 1.769
115 LYS HB3 H 1.769
115 LYS HG2 H 1.342
115 LYS HG3 H 1.224
115 LYS HD2 H 1.491
115 LYS HD3 H 1.491
115 LYS HE2 H 2.805
115 LYS HE3 H 2.805
115 LYS N N 123.547
116 LEU CA C 51.438
116 LEU CB C 42.168
116 LEU CG C 23.77
116 LEU CD1 C 20.8
116 LEU H H 7.937
116 LEU HA H 4.445
116 LEU HB2 H 1.534
116 LEU HB3 H 1.534
116 LEU HG H 1.513
116 LEU HD1 H 0.632
116 LEU HD2 H 0.632
116 LEU N N 125.24
117 THR CA C 57.851
117 THR CB C 68.352
117 THR CG2 C 18.876
117 THR H H 8.884
117 THR HA H 4.28
117 THR HB H 4.622
117 THR HG2 H 1.164
117 THR N N 113.274
118 ASP CA C 55.259
118 ASP CB C 37.114
118 ASP H H 8.694
118 ASP HA H 4.037
118 ASP HB2 H 2.519
118 ASP HB3 H 2.519
118 ASP N N 120.555
119 GLU CA C 55.091
119 GLU CB C 27.202
119 GLU CG C 33.358
119 GLU H H 8.492
119 GLU HA H 3.927
119 GLU HB2 H 1.759
119 GLU HB3 H 1.876
119 GLU HG2 H 2.157
119 GLU HG3 H 2.157
119 GLU N N 119.03
120 GLU CA C 56.438
120 GLU CB C 27.197
120 GLU CG C 33.358
120 GLU H H 7.769
120 GLU HA H 3.886
120 GLU HB2 H 1.9
120 GLU HB3 H 1.761
120 GLU HG2 H 2.157
120 GLU HG3 H 2.157
120 GLU N N 119.017
121 VAL CA C 63.944
121 VAL CB C 28.567
121 VAL CG1 C 20.343
121 VAL CG2 C 18.744
121 VAL H H 7.927
121 VAL HA H 3.498
121 VAL HB H 2.032
121 VAL HG1 H 0.822
121 VAL HG2 H 0.98
121 VAL N N 120.488
122 ASP CA C 53.776
122 ASP CB C 39.172
122 ASP H H 7.923
122 ASP HA H 3.939
122 ASP HB2 H 1.887
122 ASP HB3 H 2.801
122 ASP N N 120.148
123 GLU CA C 56.746
123 GLU CB C 26.361
123 GLU CG C 33.595
123 GLU H H 8.175
123 GLU HA H 3.877
123 GLU HB2 H 1.896
123 GLU HB3 H 1.896
123 GLU HG2 H 2.164
123 GLU HG3 H 2.164
123 GLU N N 122.029
124 MET CA C 56.438
124 MET CB C 30.973
124 MET CG C 31.446
124 MET H H 7.841
124 MET HA H 3.638
124 MET HB2 H 2.164
124 MET HB3 H 2.164
124 MET HG2 H 2.26
124 MET HG3 H 2.26
124 MET N N 118.2
125 ILE CA C 61.816
125 ILE CB C 34.363
125 ILE CG1 C 26.401
125 ILE CG2 C 14.023
125 ILE CD1 C 9.372
125 ILE H H 7.699
125 ILE HA H 3.36
125 ILE HB H 1.867
125 ILE HG1 H 1.465
125 ILE HG1 H 1.465
125 ILE HG2 H 0.633
125 ILE HD1 H 0.556
125 ILE N N 118.392
126 ARG CA C 56.741
126 ARG CB C 27.426
126 ARG CG C 25.77
126 ARG H H 8.006
126 ARG HA H 3.854
126 ARG HB2 H 2.174
126 ARG HB3 H 2.174
126 ARG HG2 H 1.877
126 ARG HG3 H 1.877
126 ARG N N 119.829
127 GLU CA C 55.529
127 GLU CB C 26.937
127 GLU CG C 33.612
127 GLU H H 7.792
127 GLU HA H 3.937
127 GLU HB2 H 1.692
127 GLU HB3 H 1.692
127 GLU HG2 H 2.174
127 GLU HG3 H 2.174
127 GLU N N 116.582
128 ALA CA C 49.436
128 ALA CB C 18.229
128 ALA H H 7.119
128 ALA HA H 3.917
128 ALA HB H 1.336
128 ALA N N 119.373
129 ALA CA C 49.756
129 ALA CB C 16.625
129 ALA H H 7.502
129 ALA HA H 4.141
129 ALA HB H 1.231
129 ALA N N 120.476
130 ILE CA C 58.238
130 ILE CB C 36.019
130 ILE CG1 C 24.509
130 ILE CG2 C 14.654
130 ILE CD1 C 10.239
130 ILE H H 8.071
130 ILE HA H 3.925
130 ILE HB H 1.676
130 ILE HG1 H 1.274
130 ILE HG1 H 1.274
130 ILE HG2 H 0.681
130 ILE HD1 H 0.662
130 ILE N N 123.246
131 ASP CA C 49.974
131 ASP CB C 37.622
131 ASP H H 8.251
131 ASP HA H 4.411
131 ASP HB2 H 2.482
131 ASP HB3 H 2.482
131 ASP N N 122.43
132 GLY CA C 43.579
132 GLY H H 7.873
132 GLY HA2 H 3.774
132 GLY HA3 H 3.774
132 GLY N N 106.4
133 ASP CA C 50.311
133 ASP CB C 38.143
133 ASP H H 7.603
133 ASP HA H 4.438
133 ASP HB2 H 2.801
133 ASP HB3 H 2.801
133 ASP N N 118.443
134 GLY CA C 43.141
134 GLY H H 8.319
134 GLY HA2 H 3.748
134 GLY HA3 H 3.748
134 GLY N N 107.316
135 GLN CA C 50.951
135 GLN CB C 27.118
135 GLN CG C 30.394
135 GLN H H 7.559
135 GLN HA H 4.684
135 GLN HB2 H 1.679
135 GLN HB3 H 1.679
135 GLN HG2 H 1.879
135 GLN HG3 H 1.879
135 GLN N N 116.214
136 VAL CA C 58.794
136 VAL CB C 29.869
136 VAL CG1 C 19.699
136 VAL CG2 C 18.201
136 VAL H H 9.106
136 VAL HA H 4.628
136 VAL HB H 2.039
136 VAL HG1 H 0.936
136 VAL HG2 H 0.696
136 VAL N N 125.848
137 ASN CA C 48.776
137 ASN CB C 36.428
137 ASN H H 9.112
137 ASN HA H 5.017
137 ASN HB2 H 2.597
137 ASN HB3 H 2.321

137 ASN N N 127.154
138 TYR CA C 59.703
138 TYR CB C 36.335
138 TYR H H 8.347
138 TYR HA H 3.163
138 TYR HB2 H 2.183
138 TYR HB3 H 2.321
138 TYR N N 118.958
139 GLU CA C 57.649
139 GLU CB C 25.94
139 GLU CG C 33.25
139 GLU H H 8.11
139 GLU HA H 3.838
139 GLU HB2 H 1.876
139 GLU HB3 H 1.876
139 GLU HG2 H 2.177
139 GLU HG3 H 2.177
139 GLU N N 118.008
140 GLU C C 173.466
140 GLU CA C 56.101
140 GLU CB C 31.534
140 GLU H H 8.237
140 GLU HA H 3.649
140 GLU HB2 H 2.262
140 GLU HB3 H 2.262
140 GLU N N 119.41
141 PHE CA C 59.097
141 PHE CB C 37.571
141 PHE H H 8.313
141 PHE HA H 3.781
141 PHE HB2 H 2.834
141 PHE HB3 H 2.834
141 PHE N N 123.172
142 VAL CA C 64.214
142 VAL CB C 28.766
142 VAL CG1 C 20.305
142 VAL CG2 C 18.589
142 VAL H H 8.34
142 VAL HA H 3.038
142 VAL HB H 1.644
142 VAL HG1 H 0.349
142 VAL HG2 H 0.592
142 VAL N N 118.252
143 GLN CA C 56.337
143 GLN CB C 25.336
143 GLN CG C 31.511
143 GLN H H 7.634
143 GLN HA H 3.636
143 GLN HB2 H 1.953
143 GLN HB3 H 1.953
143 GLN HG2 H 2.157
143 GLN HG3 H 2.157
143 GLN N N 119.499
144 MET CA C 55.764
144 MET CB C 30.736
144 MET CG C 31.534
144 MET H H 7.605
144 MET HA H 3.662
144 MET HB2 H 2.256
144 MET HB3 H 2.256
144 MET HG2 H 2.288
144 MET HG3 H 2.288
144 MET N N 117.28
145 MET CA C 53.408
145 MET CB C 29.253
145 MET CG C 30.052
145 MET H H 7.467
145 MET HA H 4.004
145 MET HB2 H 2.032
145 MET HB3 H 2.032
145 MET HG2 H 1.907
145 MET HG3 H 1.907
145 MET N N 114.953
146 THR CA C 59.097
146 THR CB C 67.755
146 THR CG2 C 18.401
146 THR H H 7.465
146 THR HA H 4.156
146 THR HB H 4.096
146 THR HG2 H 0.984
146 THR N N 107.746
147 ALA CA C 50.109
147 ALA CB C 16.437
147 ALA H H 7.656
147 ALA HA H 4.123
147 ALA HB H 1.23
147 ALA N N 126.366
148 LYS CA C 54.753
148 LYS CB C 26.283
148 LYS CG C 21.828
148 LYS CD C 30.852
148 LYS CE C 39.419
148 LYS H H 7.758
148 LYS HA H 3.945
148 LYS HB2 H 1.493
148 LYS HB3 H 1.493
148 LYS HG2 H 1.217
148 LYS HG3 H 1.217
148 LYS HD2 H 1.624
148 LYS HD3 H 1.624
148 LYS HE2 H 2.816
148 LYS HE3 H 2.816
148 LYS N N 125.937
iNOS peptide
515 LEU CA C 55.533
515 LEU H H 9.403
515 LEU HA H 3.779
515 LEU HB2 H 1.759
515 LEU HB3 H 1.759
515 LEU HG H 1.333
515 LEU HD1 H 0.717
515 LEU HD2 H 0.717
515 LEU N N 128.585
516 LYS CA C 56.947
516 LYS H H 8.841
516 LYS HA H 3.749
516 LYS HB2 H 1.744
516 LYS HB3 H 1.744
516 LYS HG2 H 1.235
516 LYS HG3 H 1.235
516 LYS N N 115.21
517 VAL CA C 63.221
517 VAL H H 6.876
517 VAL HA H 3.476
517 VAL HB H 1.94
517 VAL HG1 H 0.81
517 VAL HG2 H 0.81
517 VAL N N 117.71
518 LEU CA C 55.392
518 LEU H H 7.67
518 LEU HA H 3.854
518 LEU HB2 H 1.581
518 LEU HB3 H 1.581
518 LEU HG H 1.414
518 LEU HD1 H 0.806
518 LEU N N 120.709
519 VAL CA C 64.212
519 VAL H H 8.606
519 VAL HA H 3.768
519 VAL HB H 1.907
519 VAL HG1 H 0.717
519 VAL HG2 H 0.717
519 VAL N N 111.964
520 LYS CA C 57.786
520 LYS H H 7.112
520 LYS HA H 4.014
520 LYS HB2 H 2.006
520 LYS HB3 H 2.006
520 LYS HG2 H 0.717
520 LYS HG3 H 0.717
520 LYS HD2 H 1.7
520 LYS HD3 H 1.7
520 LYS N N 119.833
521 ALA CA C 53.207
521 ALA H H 7.838
521 ALA HA H 4.161
521 ALA HB H 1.681
521 ALA N N 120.555
522 VAL CA C 64.502
522 VAL H H 8.265
522 VAL HA H 3.557
522 VAL HB H 2.331
522 VAL HG1 H 0.996
522 VAL HG2 H 0.996
522 VAL N N 116.827
523 LEU CA C 56.264
523 LEU H H 8.76
523 LEU HA H 4.003
523 LEU HB2 H 2.036
523 LEU HB3 H 2.036
523 LEU HG H 1.691
523 LEU HD1 H 0.952
523 LEU HD2 H 0.952
523 LEU N N 121.446
524 PHE CA C 58.812
524 PHE H H 7.948
524 PHE HA H 4.184
524 PHE HB2 H 3.428
524 PHE HB3 H 3.428
524 PHE HD1 H 6.773
524 PHE HD2 H 6.773
524 PHE N N 118.793
525 ALA CA C 52.859
525 ALA H H 7.738
525 ALA HA H 3.715
525 ALA HB H 1.578
525 ALA N N 117.951
526 CYS CA C 61.415
526 CYS H H 8.567
526 CYS HA H 4.07
526 CYS HB2 H 3.073
526 CYS HB3 H 2.933
526 CYS N N 115.303
527 MET CA C 56.156
527 MET H H 8.462
527 MET HA H 3.919
527 MET HB2 H 2.046
527 MET HB3 H 2.046
527 MET HG2 H 2.691
527 MET HG3 H 2.691
527 MET N N 120.601
528 LEU CA C 52.975
528 LEU H H 7.196
528 LEU HA H 3.93
528 LEU HB2 H 1.449
528 LEU HB3 H 1.449
528 LEU HG H 1.102
528 LEU HD1 H 0.316
528 LEU HD2 H 0.316
528 LEU N N 118.166
529 MET CA C 54.169
529 MET H H 7.27
529 MET HA H 4.048
529 MET HB2 H 1.963
529 MET HB3 H 1.963
529 MET HG2 H 2.643
529 MET HG3 H 2.643
529 MET N N 117.255
530 ARG CA C 53.31
530 ARG H H 7.981
530 ARG HA H 4.048
530 ARG HB2 H 1.82
530 ARG HB3 H 1.82
530 ARG HG2 H 1.696
530 ARG HG3 H 1.696
530 ARG N N 122.437
531 LYS CA C 54.802
531 LYS H H 7.923
531 LYS HA H 4.184
531 LYS HB2 H 1.601
531 LYS HB3 H 1.601
531 LYS HG2 H 1.276
531 LYS HG3 H 1.276
531 LYS HE2 H 3.104
531 LYS HE3 H 3.104
531 LYS N N 128.142

Appendix J

CaM at 1.3 μM free Ca^{2+} Assigned Chemical Shifts

_Residue_seq_code
_Residue_label
_Atom_name
_Atom_type
_Chem_shift_value
3 GLN H H 8.093
3 GLN N N 118.305
4 LEU H H 8.185
4 LEU N N 121.741
5 THR H H 8.691
5 THR N N 112.733
6 GLU H H 8.919
6 GLU N N 120.077
7 GLU H H 8.634
7 GLU N N 119.231
8 GLN H H 7.629
8 GLN N N 120.437
9 ILE H H 8.115
9 ILE N N 118.313
10 ALA H H 7.835
10 ALA N N 120.124
11 GLU H H 7.684
11 GLU N N 120.059
12 PHE H H 8.691
12 PHE N N 120.241
13 LYS H H 9.138
13 LYS N N 121.341
14 GLU H H 7.966
14 GLU N N 120.352
15 ALA H H 7.545
15 ALA N N 120.716
16 PHE H H 8.428
16 PHE N N 117.813
17 SER H H 8.328
17 SER N N 110.931
18 LEU H H 7.261
18 LEU N N 121.127
19 PHE H H 7.275
19 PHE N N 114.595
20 ASP H H 7.216
20 ASP N N 122.323
21 LYS H H 7.972
21 LYS N N 123.505
22 ASP H H 8.601
22 ASP N N 116.797
23 GLY H H 7.906
23 GLY N N 110.115
24 ASP H H 8.669
24 ASP N N 120.623
25 GLY H H 10.111
25 GLY N N 111.985
26 THR H H 7.504
26 THR N N 110.146
27 ILE H H 8.181
27 ILE N N 110.653
28 THR H H 8.239
28 THR N N 110.721
29 THR H H 8.201
29 THR N N 112.395
30 LYS H H 7.532
30 LYS N N 118.803
31 GLU H H 7.408
31 GLU N N 117.413
32 LEU H H 7.247
32 LEU N N 120.701
33 GLY H H 8.705
33 GLY N N 105.413
34 THR H H 7.415
34 THR N N 118.133
35 VAL H H 7.854
35 VAL N N 122.623
36 MET H H 8.359
36 MET N N 118.307
37 ARG H H 8.416
37 ARG N N 119.233
38 SER H H 8.01
38 SER N N 118.995
39 LEU H H 7.238
39 LEU N N 120.986
40 GLY H H 7.815
40 GLY N N 107.023
41 GLN H H 7.673
41 GLN N N 117.816
42 ASN H H 8.574
42 ASN N N 116.603
44 THR H H 8.711
44 THR N N 113.033
45 GLU H H 8.756
45 GLU N N 120.377
46 ALA H H 8.225
46 ALA N N 121.013
47 GLU H H 7.639
47 GLU N N 118.78
48 LEU H H 8.251
48 LEU N N 119.959
49 GLN H H 7.945
49 GLN N N 117.495
50 ASP H H 7.731
50 ASP N N 118.841
51 MET H H 7.858
51 MET N N 119.059
52 ILE H H 8.257
52 ILE N N 119.121
53 ASN H H 8.146
53 ASN N N 117.304
54 GLU H H 7.48
54 GLU N N 117.349
55 VAL H H 7.52
55 VAL N N 112.777
56 ASP H H 8.357
56 ASP N N 121.841
57 ALA H H 8.061
57 ALA N N 124.805
58 ASP H H 8.335
58 ASP N N 114.525
59 GLY H H 7.787
59 GLY N N 108.859
60 ASN H H 9.179
60 ASN N N 119.705
61 GLY H H 9.997
61 GLY N N 110.402
62 THR H H 7.463
62 THR N N 110.641
63 ILE H H 8.813
63 ILE N N 118.921
64 ASP H H 8.567
64 ASP N N 124.741
65 PHE H H 8.536
65 PHE N N 118.667
67 GLU H H 7.967
67 GLU N N 117.549
68 PHE H H 8.354
68 PHE N N 122.305
69 LEU H H 8.362
69 LEU N N 118.56
70 THR H H 7.629
70 THR N N 115.305
71 MET H H 7.611
71 MET N N 121.295
72 MET H H 7.919
72 MET N N 117.359
73 ALA H H 8.211
73 ALA N N 120.833
74 ARG H H 7.379
74 ARG N N 116.712
75 LYS H H 7.628
75 LYS N N 118.177
76 MET H H 7.837
76 MET N N 117.723
77 LYS H H 7.824
77 LYS N N 120.302
78 ASP H H 8.227
78 ASP N N 121.923
79 THR H H 8.048
79 THR N N 114.681
80 ASP H H 8.274
80 ASP N N 123.52
81 SER H H 8.367
81 SER N N 117.212
82 GLU H H 8.377
82 GLU N N 121.991
83 GLU H H 8.272
83 GLU N N 119.491
84 GLU H H 7.92
84 GLU N N 119.05
85 ILE H H 7.985
85 ILE N N 121.858
86 ARG H H 8.302
86 ARG N N 121.676
87 GLU H H 7.968
87 GLU N N 117.928
88 ALA H H 7.878
88 ALA N N 122.505
89 PHE H H 8.477
89 PHE N N 118.726
90 ARG H H 7.609
90 ARG N N 115.621
91 VAL H H 7.472
91 VAL N N 118.122
92 PHE H H 7.47
92 PHE N N 116.972
93 ASP H H 7.755
93 ASP N N 116.948
94 LYS H H 7.592
94 LYS N N 125.458
95 ASP H H 8.088
95 ASP N N 113.818
96 GLY H H 7.693
96 GLY N N 109.055
97 ASN H H 8.241
97 ASN N N 119.409
98 GLY H H 10.558
98 GLY N N 112.784
99 TYR H H 7.509
99 TYR N N 115.626
100 ILE H H 10.057
100 ILE N N 127.014
101 SER H H 8.855
101 SER N N 123.577
102 ALA H H 9.101
102 ALA N N 122.738
103 ALA H H 8.159
103 ALA N N 118.461
104 GLU H H 7.779
104 GLU N N 119.434
105 LEU H H 8.515
105 LEU N N 121.131
106 ARG H H 8.475
106 ARG N N 117.619
107 HIS H H 7.871
107 HIS N N 118.677
108 VAL H H 7.827
108 VAL N N 118.879
109 MET H H 8.162
109 MET N N 116.356
110 THR H H 8.057
110 THR N N 114.89
111 ASN H H 7.844
111 ASN N N 121.797
112 LEU H H 7.783
112 LEU N N 118.58
113 GLY H H 7.791
113 GLY N N 106.894
114 GLU H H 7.819
114 GLU N N 120.538
115 LYS H H 8.513
115 LYS N N 123.522
116 LEU H H 8.059

116 LEU N N 125.094
117 THR H H 9.146
117 THR N N 114.508
118 ASP H H 8.81
118 ASP N N 120.809
119 GLU H H 8.615
119 GLU N N 119.002
120 GLU H H 7.685
120 GLU N N 120.416
121 VAL H H 8.035
121 VAL N N 120.932
122 ASP H H 7.966
122 ASP N N 119.445
123 GLU H H 7.886
123 GLU N N 119.316
124 MET H H 7.768
124 MET N N 119.181
125 ILE H H 7.852
125 ILE N N 118.182
126 ARG H H 8.132
126 ARG N N 118.295
127 GLU H H 7.858
127 GLU N N 115.842
128 ALA H H 7.239
128 ALA N N 118.592
129 ASP H H 7.774
129 ASP N N 117.274
130 ILE H H 8.238
130 ILE N N 127.45
131 ASP H H 8.205
131 ASP N N 116.317
132 GLY H H 7.489
132 GLY N N 108.454
133 ASP H H 8.231
133 ASP N N 120.693
134 GLY H H 10.297
134 GLY N N 112.745
135 GLN H H 7.854
135 GLN N N 115.315
136 VAL H H 9.04
136 VAL N N 125.163
137 ASN H H 9.389
137 ASN N N 128.788
138 TYR H H 8.389
138 TYR N N 118.049
139 GLU H H 8.077
139 GLU N N 118.303
140 GLU H H 8.68
140 GLU N N 119.706
141 PHE H H 8.912
141 PHE N N 124.776
142 VAL H H 8.421
142 VAL N N 119.43
143 GLN H H 7.219
143 GLN N N 117.644
144 MET H H 7.886
144 MET N N 119.6
145 MET H H 7.7
145 MET N N 114.371
146 THR H H 7.504
146 THR N N 110.949
147 ALA H H 7.713
147 ALA N N 126.535
148 LYS H H 7.625
148 LYS N N 125.506

Permissions

Permission for Figure 1.8A

Mike Piazza

From: PNAS Permissions <PNASPermissions@nas.edu>
Sent: Monday, February 29, 2016 10:50 AM
To: Mike Piazza
Subject: RE: Request for permission

Follow Up Flag: Follow up
Flag Status: Flagged

Permission is granted for your use of the figure as described in your message. Please cite the PNAS article in full when re-using the material. Because this material published after 2008, a copyright note is not needed. There is no charge for this material, either. Let us know if you have any questions.

Best regards,
Kay McLaughlin for
Diane Sullenberger
Executive Editor
PNAS

From: Mike Piazza [mailto:mike_piazza27@hotmail.com]
Sent: Thursday, February 18, 2016 3:18 PM
To: PNAS Permissions
Subject: Request for permission

Hello,
My name is Michael Piazza and I a PhD candidate in the department of Chemistry at the University of Waterloo. 200 University Ave West, Waterloo, On, N2L 3G1, Ontario, Canada, Office ESC 240, 226-808-5504, mpiazza@uwaterloo.ca. I would like permission to reprint Fig. 4. From page E3617 of Campbell, M. G.; Smith, B. C.; Potter, C. S.; Carragher, B.; Marletta, M. a. Molecular Architecture of Mammalian Nitric Oxide Synthases. *Proc. Natl. Acad. Sci. U. S. A.* **2014**, *111* (35), E3614–E3623. Published ahead of print August 14, 2014.

This figure will be modified to be included in my thesis titled: NMR studies of protein and peptide structure and dynamics

I, Michael Piazza, am the sole author of this thesis.

Thanks,

Michael Piazza

PhD Student
GSA Director At-Large
Department of Chemistry
University of Waterloo

Permission for Figure 1.8B

ELSEVIER LICENSE
TERMS AND CONDITIONS

Feb 19, 2016

This is a License Agreement between Michael Piazza ("You") and Elsevier ("Elsevier") provided by Copyright Clearance Center ("CCC"). The license consists of your order details, the terms and conditions provided by Elsevier, and the payment terms and conditions.

All payments must be made in full to CCC. For payment instructions, please see information listed at the bottom of this form.

Supplier	Elsevier Limited The Boulevard,Langford Lane Kidlington,Oxford,OX5 1GB,UK
Registered Company Number	1982084
Customer name	Michael Piazza
Customer address	3 Prouse Dr Brampton, ON L6V 3A3
License number	3812061323962
License date	Feb 18, 2016
Licensed content publisher	Elsevier
Licensed content publication	Journal of Structural Biology
Licensed content title	Holoenzyme structures of endothelial nitric oxide synthase – An allosteric role for calmodulin in pivoting the FMN domain for electron transfer
Licensed content author	Niels Volkmann,Pavel Martásek,Linda J. Roman,Xiao-Ping Xu,Christopher Page,Mark Swift,Dorit Hanein,Bettie Sue Masters
Licensed content date	October 2014
Licensed content volume number	188

Licensed content issue number	1
Number of pages	9
Start Page	46
End Page	54
Type of Use	reuse in a thesis/dissertation
Portion	figures/tables/illustrations
Number of figures/tables/illustrations	1
Format	both print and electronic
Are you the author of this Elsevier article?	No
Will you be translating?	No
Original figure numbers	Fig.3.
Title of your thesis/dissertation	NMR studies of protein and peptide structure and dynamics
Expected completion date	Apr 2016
Estimated size (number of pages)	260
Elsevier VAT number	GB 494 6272 12
Permissions price	0.00 CAD
VAT/Local Sales Tax	0.00 CAD / 0.00 GBP
Total	0.00 CAD

Permission for Figure 1.10

ELSEVIER LICENSE
TERMS AND CONDITIONS

Feb 19, 2016

This is a License Agreement between Michael Piazza ("You") and Elsevier ("Elsevier") provided by Copyright Clearance Center ("CCC"). The license consists of your order details, the terms and conditions provided by Elsevier, and the payment terms and conditions.

All payments must be made in full to CCC. For payment instructions, please see information listed at the bottom of this form.

Supplier	Elsevier Limited The Boulevard,Langford Lane Kidlington,Oxford,OX5 1GB,UK
Registered Company Number	1982084
Customer name	Michael Piazza
Customer address	3 Prouse Dr Brampton, ON L6V 3A3
License number	3812071475414
License date	Feb 18, 2016
Licensed content publisher	Elsevier
Licensed content publication	Nitric Oxide
Licensed content title	NO synthase: Structures and mechanisms
Licensed content author	Simon Daff
Licensed content date	1 August 2010
Licensed content volume number	23
Licensed content issue number	1
Number of pages	11
Start Page	1

End Page	11
Type of Use	reuse in a thesis/dissertation
Intended publisher of new work	other
Portion	figures/tables/illustrations
Number of figures/tables/illustrations	1
Format	both print and electronic
Are you the author of this Elsevier article?	No
Will you be translating?	No
Original figure numbers	Fig. 2.
Title of your thesis/dissertation	NMR studies of protein and peptide structure and dynamics
Expected completion date	Apr 2016
Estimated size (number of pages)	260
Elsevier VAT number	GB 494 6272 12
Permissions price	0.00 USD
VAT/Local Sales Tax	0.00 USD / 0.00 GBP
Total	0.00 USD

Permission for work published in Chapter 2

ACS Publications
Most Trusted. Most Cited. Most Read.

Title: Solution Structure of Calmodulin Bound to the Target Peptide of Endothelial Nitric Oxide Synthase Phosphorylated at Thr495

Author: Michael Piazza, Valentina Taiakina, Simon R. Guillemette, et al

Publication: Biochemistry

Publisher: American Chemical Society

Date: Mar 1, 2014

Logged in as:
Michael Piazza
Account #:
3001001180

LOGOUT

PERMISSION/LICENSE IS GRANTED FOR YOUR ORDER AT NO CHARGE

This type of permission/license, instead of the standard Terms & Conditions, is sent to you because no fee is being charged for your order. Please note the following:

- Permission is granted for your request in both print and electronic formats, and translations.
- If figures and/or tables were requested, they may be adapted or used in part.
- Please print this page for your records and send a copy of it to your publisher/graduate school.
- Appropriate credit for the requested material should be given as follows: "Reprinted (adapted) with permission from (COMPLETE REFERENCE CITATION). Copyright (YEAR) American Chemical Society." Insert appropriate information in place of the capitalized words.
- One-time permission is granted only for the use specified in your request. No additional uses are granted (such as derivative works or other editions). For any other uses, please submit a new request.

BACK CLOSE WINDOW

Permission for work published in Chapter 3

SPRINGER LICENSE
TERMS AND CONDITIONS

Feb 19, 2016

This is a License Agreement between Michael Piazza ("You") and Springer ("Springer") provided by Copyright Clearance Center ("CCC"). The license consists of your order details, the terms and conditions provided by Springer, and the payment terms and conditions.

All payments must be made in full to CCC. For payment instructions, please see information listed at the bottom of this form.

License Number	3812610542226
License date	Feb 19, 2016
Licensed content publisher	Springer
Licensed content publication	Biomolecular NMR Assignments
Licensed content title	Chemical shift assignments of calmodulin constructs with EF hand mutations
Licensed content author	Michael Piazza
Licensed content date	Jan 1, 2016
Type of Use	Thesis/Dissertation
Portion	Full text
Number of copies	1
Author of this Springer article	Yes and you are the sole author of the new work
Order reference number	None
Title of your thesis / dissertation	NMR studies of protein and peptide structure and dynamics
Expected completion date	Apr 2016
Estimated size(pages)	260
Total	0.00 CAD

SPRINGER LICENSE
TERMS AND CONDITIONS

Feb 19, 2016

This is a License Agreement between Michael Piazza ("You") and Springer ("Springer") provided by Copyright Clearance Center ("CCC"). The license consists of your order details, the terms and conditions provided by Springer, and the payment terms and conditions.

All payments must be made in full to CCC. For payment instructions, please see information listed at the bottom of this form.

License Number	3812610678533
License date	Feb 19, 2016
Licensed content publisher	Springer
Licensed content publication	Biomolecular NMR Assignments
Licensed content title	Chemical shift perturbations induced by residue specific mutations of CaM interacting with NOS peptides
Licensed content author	Michael Piazza
Licensed content date	Jan 1, 2015
Volume number	9
Issue number	2
Type of Use	Thesis/Dissertation
Portion	Full text
Number of copies	1
Author of this Springer article	Yes and you are the sole author of the new work
Order reference number	None
Title of your thesis / dissertation	NMR studies of protein and peptide structure and dynamics
Expected completion date	Apr 2016
Estimated size(pages)	260
Total	0.00 CAD

Permission for work published in Chapter 4

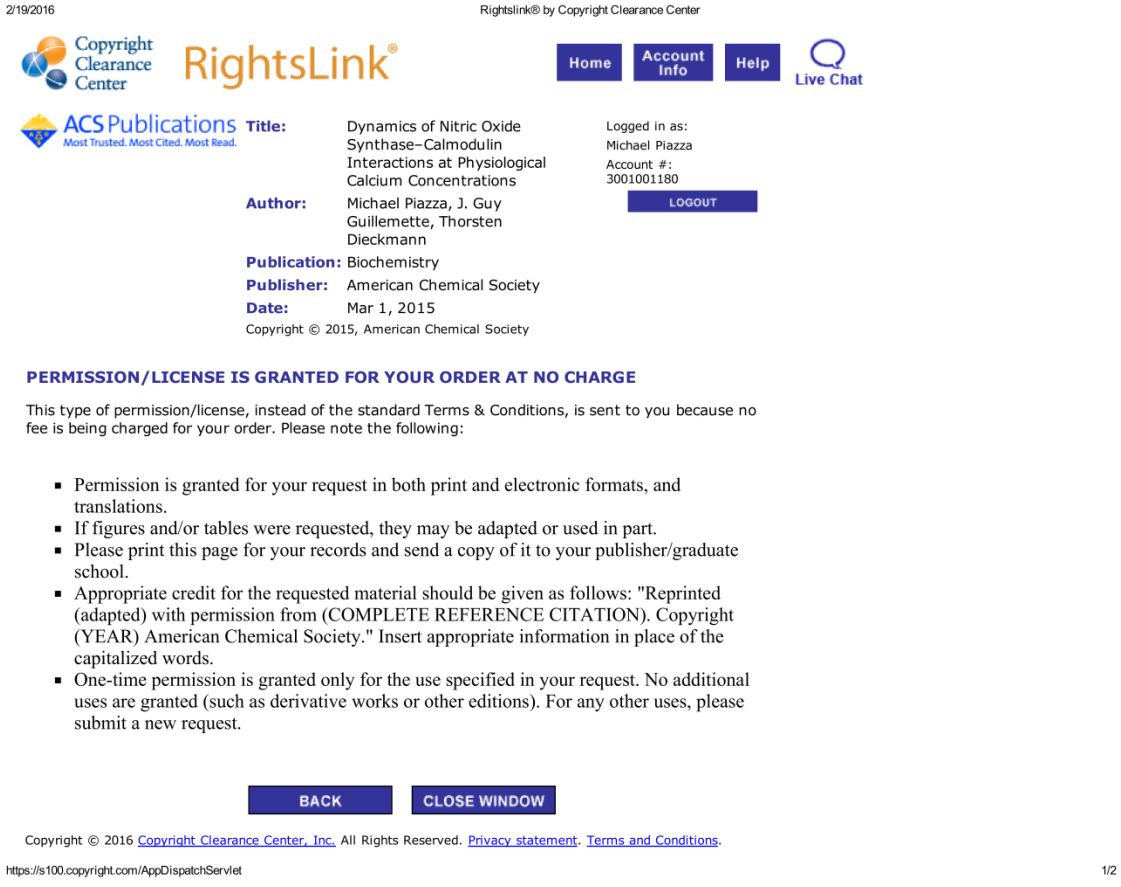

2/19/2016 Rightslink® by Copyright Clearance Center

Copyright Clearance Center RightsLink® Home Account Info Help Live Chat

ACS Publications Most Trusted. Most Cited. Most Read.

Title: Dynamics of Nitric Oxide Synthase–Calmodulin Interactions at Physiological Calcium Concentrations

Author: Michael Piazza, J. Guy Guillemette, Thorsten Dieckmann

Publication: Biochemistry

Publisher: American Chemical Society

Date: Mar 1, 2015

Copyright © 2015, American Chemical Society

Logged in as: Michael Piazza
Account #: 3001001180
LOGOUT

PERMISSION/LICENSE IS GRANTED FOR YOUR ORDER AT NO CHARGE

This type of permission/license, instead of the standard Terms & Conditions, is sent to you because no fee is being charged for your order. Please note the following:

- Permission is granted for your request in both print and electronic formats, and translations.
- If figures and/or tables were requested, they may be adapted or used in part.
- Please print this page for your records and send a copy of it to your publisher/graduate school.
- Appropriate credit for the requested material should be given as follows: "Reprinted (adapted) with permission from (COMPLETE REFERENCE CITATION). Copyright (YEAR) American Chemical Society." Insert appropriate information in place of the capitalized words.
- One-time permission is granted only for the use specified in your request. No additional uses are granted (such as derivative works or other editions). For any other uses, please submit a new request.

BACK CLOSE WINDOW

Copyright © 2016 Copyright Clearance Center, Inc. All Rights Reserved. Privacy statement. Terms and Conditions.

https://s100.copyright.com/AppDispatchServlet 1/2

Bibliography

Afshar, M.; Caves, L. S.; Guimard, L.; Hubbard, R. E.; Calas, B.; Grassy, G.; Haiech, J. Investigating the High Affinity and Low Sequence Specificity of Calmodulin Binding to Its Targets. *Journal of Molecular Biology*. **1994**, pp 554–571.

Alborn, W. E.; Allen, N. E.; Preston, D. a. Daptomycin Disrupts Membrane-Potential in Growing Staphylococcus-Aureus. *Antimicrob. Agents Chemother.* **1991**, *35* (11), 2282–2287.

Alderton, W. K.; Cooper, C. E.; Knowles, R. G. Nitric Oxide Synthases: Structure, Function and Inhibition. *Biochem. J.* **2001**, *357*, 593–615.

Allen, N. E.; Hobbs, J. N.; Alborn, W. E. Inhibition of Peptidoglycan Biosynthesis in Gram-Positive Bacteria by LY146032. *Antimicrob. Agents Chemother.* **1987**, *31* (7), 1093–1099.

Anagli, J.; Hofmann, F.; Quadroni, M.; Vorherr, T.; Carafoli, E. The Calmodulin-Binding Domain of the Inducible (macrophage) Nitric Oxide Synthase. *Eur. J. Biochem.* **1995**, *233* (3), 701–708.

Andrec, M.; Hill, R. B.; Prestegard, J. H. Amide Exchange Rates in Escherichia Coli Acyl Carrier Protein: Correlation with Protein Structure and Dynamics. *Protein Sci.* **1995**, *4* (5), 983–993.

Aoyagi, M.; Arvai, A. S.; Tainer, J. A.; Getzoff, E. D. Structural Basis for Endothelial Nitric Oxide Synthase Binding to Calmodulin. *EMBO J.* **2003**, *22* (4), 766–775.

Babu, Y. S.; Bugg, C. E.; Cook, W. J. Structure of Calmodulin Refined at 2.2 A Resolution. *J. Mol. Biol.* **1988**, *204* (1), 191–204.

Ball, L.-J.; Goult, C. M.; Donarski, J. a; Micklefield, J.; Ramesh, V. NMR Structure Determination and Calcium Binding Effects of Lipopeptide Antibiotic Daptomycin. *Org. Biomol. Chem.* **2004**, *2* (13), 1872–1878.

Balligand, J.-L.; Ungureanu-Longrois, D.; Simmons, W. W.; Pimental, D.; Malinski, T. A.; Kapturczak, M.; Taha, Z.; Lowenstein, C. J.; Davidoff, A. J.; Kelly, R. A.; et al. Cytokine-Inducible Nitric Oxide Synthase (iNOS) Expression in Cardiac Myocytes. Characterization and Regulation of iNOS Expression and Detection of iNOS Activity in Single Cardiac Myocytes in Vitro. *J Biol Chem* **1994**, *269*, 27580–27588.

Bax, A.; Ikura, M. An Efficient 3D NMR Technique for Correlating the Proton and15N Backbone Amide Resonances with the α-Carbon of the Preceding Residue in uniformly15N/13C Enriched Proteins. *J. Biomol. NMR* **1991**, *1* (1), 99–104.

Bax, A.; Clore, M.; Gronenborn, A. M. 1 H- 1 H Correlation via Isotropic Mixing of 13C a New Three-Dimensional Approach for Assigning lH and 13C Spectra of 13C-Enriched Proteins. *J. Magn. Reson.* **1990**, *88*, 425–431.

Benaim, G.; Villalobo, A. Phosphorylation of Calmodulin. Functional Implications. *Eur. J. Biochem.* **2002**, *269* (15), 3619–3631.

Berridge, M. J.; Bootman, M. D.; Lipp, P. Calcium--a Life and Death Signal. *Nature* **1998**, *395* (6703), 645–648.

Boaretti, M.; Canepari, P. Identification of Daptomycin-Binding Proteins in the Membrane of Enterococcus Hirae. *Antimicrob. Agents Chemother.* **1995**, *39* (9), 2068–2072.

Bodenhausen, G.; Ruben, D. J. Natural Abundance Nitrogen-15 NMR by Enhanced Heteronuclear Spectroscopy. *Chem. Phys. Lett.* **1980**, *69* (1), 185–189.

Broncel, M.; Wagner, S. C.; Paul, K.; Hackenberger, C. P. R.; Koksch, B. Towards Understanding Secondary Structure Transitions: Phosphorylation and Metal Coordination in Model Peptides. *Org. Biomol. Chem.* **2010**, *8* (11), 2575–2579.

Brunger, A. T.; Adams, P. D.; Clore, G. M.; Delano, W. L.; Gros, P.; Grosse-kunstleve, R. W.; Jiang, J.; Kuszewski, J.; Nilges, M.; Pannu, N. S.; et al. Crystallography & NMR System : A New Software Suite for Macromolecular Structure Determination. *Acta Cryst.* **1998**, *D54*, 905–921.

Busse, R.; Mulsch, A. Calcium-Dependent Nitric Oxide Synthesis in Endothelial Cytosol Is Mediated by Calmodulin. *FEBS Lett.* **1990**, *265* (1), 133–136.

Campbell, M. G.; Smith, B. C.; Potter, C. S.; Carragher, B.; Marletta, M. a. Molecular Architecture of Mammalian Nitric Oxide Synthases. *Proc. Natl. Acad. Sci. U. S. A.* **2014**, *111* (35), E3614–E3623.

Canepari, P.; Boaretti, M.; Del Mar Lleo, M.; Satta, G. Lipoteichoic Acid as a New Target for Activity of Antibiotics: Mode of Action of Daptomycin (LY146032). *Antimicrob. Agents Chemother.* **1990**, *34* (6), 1220–1226.

Carafoli, E. Intracellular Calcium Homeostasis. *Annu. Rev. Biochem.* **1987**, *56*, 395–433.

Cavanagh, J.; Fairbrother, W. J.; Palmer, A. G. I.; Rance, M.; Skelton, N. J. *Protein NMR Spectroscopy: Principles and Practice*, Second Edi.; Elsevier Academic Press: San Diego, California, **2007**.

Censarek, P.; Beyermann, M.; Koch, K.-W. Target Recognition of Apocalmodulin by Nitric Oxide Synthase I Peptides. *Biochemistry* **2002**, *41* (27), 8598–8604.

Censarek, P.; Beyermann, M.; Koch, K.-W. Thermodynamics of Apocalmodulin and Nitric Oxide Synthase II Peptide Interaction. *FEBS Lett.* **2004**, *577* (3), 465–468.

Chattopadhyaya, R.; Meador, W. E.; Means, A. R.; Quiocho, F. A. Calmodulin Structure Refined at 1.7 Å Resolution. *J. Mol. Biol.* **1992**, *228* (4), 1177–1192.

Chen, R. F. Dansyl Labeled Proteins: Determination of Extinction Coefficient and Number of Bound Residues with Radioactive Dansyl Chloride. *Anal. Biochem.* **1968**, *25*, 412–416.

Chien, Y. H.; Dawid, I. B. Isolation and Characterization of Calmodulin Genes from Xenopus Laevis. *Mol. Cell. Biol.* **1984**, *4* (3), 507–513.

Cho, H. J.; Xie, Q. W.; Calaycay, J.; Mumford, R. a; Swiderek, K. M.; Lee, T. D.; Nathan, C. Calmodulin Is a Subunit of Nitric Oxide Synthase from Macrophages. *J. Exp. Med.* **1992**, *176* (2), 599–604.

Clore, G. M.; Gronenborn, A. M. Applications of Three- and Four-Dimensional Heteronuclear NMR Spectroscopy to Protein Structure Determination. *Prog. Nucl. Magn. Reson. Spectrosc.* **1991**, *23* (1), 43–92.

Corti, C.; Leclerc L'Hostis, E.; Quadroni, M.; Schmid, H.; Durussel, I.; Cox, J.; Dainese Hatt, P.;

James, P.; Carafoli, E. Tyrosine Phosphorylation Modulates the Interaction of Calmodulin with Its Target Proteins. *Eur. J. Biochem.* **1999**, *262* (3), 790–802.

Crivici, A.; Ikura, M. Molecular and Structural Basis of Target Recognition by Calmodulin. *Annu. Rev. Biophys. Biomol. Struct.* **1995**, *24*, 85–116.

Crouch, T. H.; Klee, C. B. Positive Cooperative Binding of Calcium to Bovine Brain Calmodulin. *Biochemistry* **1980**, *19* (16), 3692–3698.

Daff, S. NO Synthase: Structures and Mechanisms. *Nitric Oxide* **2010**, *23* (1), 1–11.

Davlieva, M.; Zhang, W.; Arias, C. A.; Shamoo, Y. Biochemical Characterization of Cardiolipin Synthase Mutations Associated with Daptomycin Resistance in Enterococci. *Antimicrob. Agents Chemother.* **2013**, *57* (1), 289–296.

Dosset, P.; Hus, J. C.; Blackledge, M.; Marion, D. Efficient Analysis of Macromolecular Rotational Diffusion from Heteronuclear Relaxation Data. *J. Biomol. NMR* **2000**, *16*, 23–28.

Drum, C. L.; Yan, S.-Z.; Bard, J.; Shen, Y.-Q.; Lu, D.; Soelaiman, S.; Grabarek, Z.; Bohm, A.; Tang, W.-J. Structural Basis for the Activation of Anthrax Adenylyl Cyclase Exotoxin by Calmodulin. *Nature* **2002**, *415* (6870), 396–402.

Eliopoulos, G. M.; Willey, S.; Reiszner, E.; Spitzer, P. G.; Caputo, G.; Moellering, R. C. In Vitro and in Vivo Activity of LY 146032, a New Cyclic Lipopeptide Antibiotic. *Antimicrob. Agents Chemother.* **1986**, *30* (4), 532–535.

Elshorst, B.; Hennig, M.; Försterling, H.; Diener, a; Maurer, M.; Schulte, P.; Schwalbe, H.; Griesinger, C.; Krebs, J.; Schmid, H.; et al. NMR Solution Structure of a Complex of Calmodulin with a Binding Peptide of the Ca2+ Pump. *Biochemistry* **1999**, *38* (38), 12320–12332.

Englander, S. W.; Mayne, L. Using Hydrogen-Exchange Labeling And Two - Dimensional Nmr. *Annu. Rev. Biophys. Biomol. Struct.* **1992**, *21*, 243–265.

Englander, S.; Kallenbach, N. Hydrogen Exchange and Structural Dynamics of Proteins and Nucleic Acids. *Q Rev Biophys* **1983**, *16*, 521–655.

Ernst, Richard, R.; Bodenhausen, G.; Wokaun, A. *Principles of Nuclear Magnetic Resonance in One and Two Dimensions*; Oxford University Press Inc.: London/New York, **1987**.

Evans, J. N. S. *Biomolecular NMR Spectroscopy*; Oxford University Press Inc.: New York, NY, **1995**.

Evenäs, J.; Malmendal, A.; Forsen, S. Calcium. *Curr. Opin. Chem. Biol.* **1998**, *2*, 293–302.

Evenäs, J.; Forsén, S.; Malmendal, a; Akke, M. Backbone Dynamics and Energetics of a Calmodulin Domain Mutant Exchanging between Closed and Open Conformations. *J. Mol. Biol.* **1999**, *289* (3), 603–617.

Fallon, J.; Quiocho, F. A Closed Compact Structure of Native Ca2+-Calmodulin. *Structure* **2003**, *11* (10), 1303–1307.

Fernando, P.; Abdulle, R.; Mohindra, a; Guillemette, J. G.; Heikkila, J. J. Mutation or Deletion of the

C-Terminal Tail Affects the Function and Structure of Xenopus Laevis Small Heat Shock Protein, hsp30. *Comp. Biochem. Physiol. Part B Biochem. Mol. Biol.* **2002**, *133* (1), 95–103.

Fesik, S. W.; Zuiderweg, E. R. P. Heteronuclear 3-Dimensional Nmr Spectroscopy Of Isotopically Labelled Biological Macromolecules. *Quart. Rev. Biophys* **1990**, *23*, 97–131.

Fischmann, T. O.; Hruza, A.; Niu, X. D.; Fossetta, J. D.; Lunn, C. a; Dolphin, E.; Prongay, a J.; Reichert, P.; Lundell, D. J.; Narula, S. K.; et al. Structural Characterization of Nitric Oxide Synthase Isoforms Reveals Striking Active-Site Conservation. *Nat. Struct. Biol.* **1999**, *6* (3), 233–242.

Fleming, I.; Busse, R. Molecular Mechanisms Involved in the Regulation of the Endothelial Nitric Oxide Synthase. *Am. J. Physiol. Regul. Integr. Comp. Physiol.* **2003**, *284* (1), R1–R12.

Fleming, I.; Bauersachs, J.; Fisslthaler, B.; Busse, R. Ca2+-Independent Activation of the Endothelial Nitric Oxide Synthase in Response to Tyrosine Phosphatase Inhibitors and Fluid Shear Stress. *Circ. Res.* **1998**, *82* (6), 686–695.

Fleming, I.; Fisslthaler, B.; Dimmeler, S.; Kemp, B. E.; Busse, R. Phosphorylation of Thr495 Regulates Ca2+/Calmodulin-Dependent Endothelial Nitric Oxide Synthase Activity. *Circ. Res.* **2001**, *88* (11), e68–e75.

Friedberg, F. Species Comparison of Calmodulin Sequences. *Protein Seq Data Anal* **1990**, *4*, 335–337.

Garcin, E. D.; Bruns, C. M.; Lloyd, S. J.; Hosfield, D. J.; Tiso, M.; Gachhui, R.; Stuehr, D. J.; Tainer, J. a; Getzoff, E. D. Structural Basis for Isozyme-Specific Regulation of Electron Transfer in Nitric-Oxide Synthase. *J. Biol. Chem.* **2004**, *279* (36), 37918–37927.

Garrison, M. W.; Vance-Bryan, K.; Larson, T. A.; Toscano, J. P.; Rotschafer, J. C. Assessments of Effects of Protein Binding on Daptomycin and Vancomycin Killing of Staphylococcus Aureus by Using an in Vitro Pharmacodynamic Model. *Antimicrob. Agents Chemother.* **1990**, *34* (10), 1925–1931.

Geiser, J. R.; van Tuinen, D.; Brockerhoff, S. E.; Neff, M. M.; Davis, T. N. Can Calmodulin Function without Binding Calcium? *Cell* **1991**, *65* (6), 949–959.

Gellman, S. H. On the Role of Methionine Residues in the Sequence-Independent Recognition of Nonpolar Protein Surfaces. *Biochemistry* **1991**, *30* (27), 50–53.

Ghosh, D. K.; Salerno, J. C. Nitric Oxide Synthases: Domain Structure and Alignment in Enzyme Function and Control. *Front. Biosci.* **2003**, No. 8, D193–D209.

Gifford, J. L.; Walsh, M. P.; Vogel, H. J. Structures and Metal-Ion-Binding Properties of the Ca2+-Binding Helix-Loop-Helix EF-Hand Motifs. *Biochem. J.* **2007**, *405* (2), 199–221.

Grzesiek, S.; Bax, A. An Efficient Experiment for Sequential Backbone Assignment of Medium-Sized Isotopically Enriched Proteins. *J. Magn. Reson.* **1992a**, *99* (1), 201–207.

Grzesiek, S.; Bax, A. Correlating Backbone Amide and Side Chain Resonances in Larger Proteins by Multiple Relayed Triple Resonance NMR. *J. Am. Chem. Soc.* **1992b**, *114*, 6291–6293.

Harris, M. B.; Ju, H.; Venema, V. J.; Liang, H.; Zou, R.; Michell, B. J.; Chen, Z. P.; Kemp, B. E.; Venema, R. C. Reciprocal Phosphorylation and Regulation of Endothelial Nitric-Oxide Synthase in Response to Bradykinin Stimulation. *J. Biol. Chem.* **2001**, *276* (19), 16587–16591.

Ho, S. W.; Jung, D.; Calhoun, J. R.; Lear, J. D.; Okon, M.; Scott, W. R. P.; Hancock, R. E. W.; Straus, S. K. Effect of Divalent Cations on the Structure of the Antibiotic Daptomycin. *Eur. Biophys. J.* **2008**, *37* (4), 421–433.

Houdusse, A.; Gaucher, J.-F.; Krementsova, E.; Mui, S.; Trybus, K. M.; Cohen, C. Crystal Structure of Apo-Calmodulin Bound to the First Two IQ Motifs of Myosin V Reveals Essential Recognition Features. *Proc. Natl. Acad. Sci. U. S. A.* **2006**, *103* (51), 19326–19331.

Huber, F. M.; Pieper, R. L.; Tietz, A. J. The Formation of Daptomycin by Supplying Decanoic Acid to Streptomyces Roseosporus Cultures Producing the Antibiotic Complex A21978C. *J. Biotechnol.* **1988**, *7* (4), 283–292.

Ikura, M.; Bax, A. Isotope-Filtered 2D NMR of a Protein-Peptide Complex Study of a Skeletal Muscle MLCK Fragment Bound to Calmodulin. *J. Am. Chem. Soc.* **1992**, No. 114, 2433–2440.

Ikura, M.; Ames, J. B. Genetic Polymorphism and Protein Conformational Plasticity in the Calmodulin Superfamily: Two Ways to Promote Multifunctionality. *Proc. Natl. Acad. Sci. U. S. A.* **2006**, *103* (5), 1159–1164.

Ikura, M.; Kay, L. E.; Bax, A. A Novel Approach for Sequential Assignment of 1H, 13C, and 15N Spectra of Proteins: Heteronuclear Triple-Resonance Three-Dimensional NMR Spectroscopy. Application to Calmodulin. *Biochemistry* **1990**, *29* (19), 4659–4567.

Ikura, M.; Clore, G. Marius; Gronenborn, A. M.; Zhu, G.; Klee, C. B.; Bax, A. Solution Structure of a Calmodulin-Target Peptide Complex by Multidimensional NMR. *Science (80-.).* **1992**, *256* (5057), 632–638.

Ishima, R.; Torchia, D. A. Protein Dynamics from NMR. *Nat. Struct. Biol.* **2000**, *7* (9), 740–743.

Islam, S. *Calcium Signaling*; Spinger, **2012**.

James, T. L.; Oppenheimer, N. K. *Methods in Enzymology. Volume 239. Nuclear Magnetic Resonance Part C.*; Academic Press: San Diego, California, 1994.

Jang, D.-J.; Guo, M.; Wang, D. Proteomic and Biochemical Studies of Calcium- and Phosphorylation-Dependent Calmodulin Complexes in Mammalian Cells. *J. Proteome Res.* **2007**, *6* (9), 3718–3728.

Johnson, J. D.; Wittenauer, L. A. A Fluorescent Calmodulin That Reports the Binding of Hydrophobic Inhibitory Ligands. *Biochem. J.* **1983**, *211*, 473–479.

Jones, R. J.; Smith, S. M. E.; Gao, Y. T.; DeMay, B. S.; Mann, K. J.; Salerno, K. M.; Salerno, J. C. The Function of the Small Insertion in the Hinge Subdomain in the Control of Constitutive Mammalian Nitric-Oxide Synthases. *J. Biol. Chem.* **2004**, *279* (35), 36876–36883.

Jung, D.; Rozek, A.; Okon, M.; Hancock, R. E. W. Structural Transitions as Determinants of the Action of the Calcium-Dependent Antibiotic Daptomycin. *Chem. Biol.* **2004**, *11* (7), 949–957.

Jung, D.; Powers, J. P.; Straus, S. K.; Hancock, R. E. W. Lipid-Specific Binding of the Calcium-Dependent Antibiotic Daptomycin Leads to Changes in Lipid Polymorphism of Model Membranes. *Chem. Phys. Lipids* **2008**, *154* (2), 120–128.

Jurado, L. a; Chockalingam, P. S.; Jarrett, H. W. Apocalmodulin. *Physiol. Rev.* **1999**, *79* (3), 661–682.

Kay, L. E. Protein Dynamics from NMR. *Biochem. Cell Biol.* **1998**, *76*, 145–152.

Kay, L. E. NMR Studies of Protein Structure and Dynamics. *J. Magn. Reson.* **2005**, *173* (2), 193–207.

Kay, L. E. New Views of Functionally Dynamic Proteins by Solution NMR Spectroscopy. *J. Mol. Biol.* **2015**, *428* (2), 323–331.

Kay, L. E.; Frydman, L. A Special "JMR Perspectives" Issue: Foresights in Biomolecular Solution-State NMR Spectroscopy - from Spin Gymnastics to Structure and Dynamics. *J. Magn. Reson.* **2014**, *241* (1), 1–2.

Kay, L. E.; Torchia, D. A.; J, A. B. Backbone Dynamics of Proteins as Studied by 15N Inverse Detected Heteranuckar. *Biochemistry* **1989**, *28*, 8972–8979.

Kay, L. E.; Ikura, M.; Tschudin, R.; Bax, A. Three-Dimensional Triple-Resonance NMR Spectroscopy of Isotopically Enriched Proteins. *J. Magn. Reson.* **1990**, *89* (3), 496–514.

Keller, R. L. J. Optimizing the Process of Nuclear Magnetic Resonance Spectrum Analysis and Computer Aided Resonance Assignment, Swiss Federal Institue of Technology Zurich, **2005**.

Kempf, J. G.; Loria, J. P. Protein Dynamics from Solution NMR: Theory and Applications. *Cell Biochem. Biophys.* **2003**, *37* (3), 187–211.

Kilhoffer, M. C.; Kubina, M.; Travers, F.; Haiech, J. Use of Engineered Proteins with Internal Tryptophan Reporter Groups and Pertubation Techniques to Probe the Mechanism of Ligand-Protein Interactions: Investigation of the Mechanism of Calcium Binding to Calmodulin. *Biochemistry* **1992**, *31* (34), 8098–8106.

Kincaid, R. L.; Vaughan, M.; Osborne, J. C.; Tkachuk, V. A. Ca2+-Dependent Interaction of 5-Dimethylaminonaphthalene-1-Sulfonyl-Calmodulin with Cyclic Nucleotide Phosphodiesterase, Calcineurin, and Troponin I. *J. Biol. Chem.* **1982**, *257* (18), 10638–10643.

Knudsen, G. M.; Nishida, C. R.; Mooney, S. D.; Ortiz de Montellano, P. R. Nitric-Oxide Synthase (NOS) Reductase Domain Models Suggest a New Control Element in Endothelial NOS That Attenuates Calmodulin-Dependent Activity. *J. Biol. Chem.* **2003**, *278* (34), 31814–31824.

Kolluru, G. K.; Siamwala, J. H.; Chatterjee, S. eNOS Phosphorylation in Health and Disease. *Biochimie* **2010**, *92* (9), 1186–1198.

Kortvely, E.; Gulya, K. Calmodulin, and Various Ways to Regulate Its Activity. *Life Sci.* **2004**, *74* (9), 1065–1070.

Kou, R.; Greif, D.; Michel, T. Mechanisms of Signal Transduction : Dephosphorylation of Endothelial Nitric-Oxide Synthase by Vascular Endothelial Growth Factor : Implications for the

Vascular Responses to Cyclosporin A. *J. Biol. Chem.* **2002**, *277*, 29669–29673.

Kuboniwa, H.; Tjandra, N.; Grzesiek, S.; Ren, H.; Klee, C. B.; Bax, A. Solution Structure of Calcium-Free Calmodulin. *Nat. Struct. Biol.* **1995**, *2* (9), 768–776.

Kurokawa, H.; Osawa, M.; Kurihara, H.; Katayama, N.; Tokumitsu, H.; Swindells, M. B.; Kainosho, M.; Ikura, M. Target-Induced Conformational Adaptation of Calmodulin Revealed by the Crystal Structure of a Complex with Nematode Ca(2+)/calmodulin-Dependent Kinase Kinase Peptide. *J. Mol. Biol.* **2001**, *312* (1), 59–68.

Kwan, A. H.; Mobli, M.; Gooley, P. R.; King, G. F.; Mackay, J. P. Macromolecular NMR Spectroscopy for the Non-Spectroscopist. *FEBS J.* **2011**, *278* (5), 687–703.

Lee, W.-S.; Ngo-Anh, T. J.; Bruening-Wright, A.; Maylie, J.; Adelman, J. P. Small Conductance Ca2+-Activated K+ Channels and Calmodulin: Cell Surface Expression and Gating. *J. Biol. Chem.* **2003**, *278* (28), 25940–25946.

Leferink, N. G. H.; Hay, S.; Rigby, S. E. J.; Scrutton, N. S. Towards the Free Energy Landscape for Catalysis in Mammalian Nitric Oxide Synthases. *FEBS J.* **2014**, *282*, 3016–3029.

Li, H.; Raman, C. S.; Marta, P.; Masters, B. S. S.; Poulos, T. L. Crystallographic Studies on Endothelial Nitric Oxide Synthase Complexed with Nitric Oxide and Mechanism-Based Inhibitors. *Biochemistry* **2001**, No. 40, 5399–5406.

Li, H.; Jamal, J.; Plaza, C.; Pineda, S. H.; Chreifi, G.; Jing, Q.; Cinelli, M. a.; Silverman, R. B.; Poulos, T. L. Structures of Human Constitutive Nitric Oxide Synthases. *Acta Crystallogr. Sect. D Biol. Crystallogr.* **2014**, *70* (10), 2667–2674.

Linse, S.; Helmersson, A.; Forsen, S. Calcium Binding to Calmodulin and Its Globular Domains. *J. Biol. Chem.* **1991**, *266* (13), 8050–8054.

Lipari, G.; Szabo, A. Model-Free Approach to the Interpretation of NMR Relaxation in Macromolecules. 2. Analysis of Experimental Results. *J. Am. Chem. Soc.* **1982a**, *104* (17), 4559–4570.

Lipari, G.; Szabo, A. Model-Free Approach to the Interpretation of Nuclear Magnetic Resonance Relaxation in Macromolecules. 1. Theory and Range of Validity. *J. Am. Chem. Soc.* **1982b**, *104*, 4546–4559.

Liu, Y. P.Cheung, W. Y. Cyclic 3':5'-Nucleotide Phosphodiesterase. Ca2+ Confers More Helical Conformation to the Protein Activator. *J. Biol. Chem.* **1976**, *251* (14), 4193–4198.

Ma, B.; Nussinov, R. Polymorphic Triple Beta-Sheet Structures Contribute to Amide Hydrogen/deuterium (H/D) Exchange Protection in the Alzheimer Amyloid beta42 Peptide. *J. Biol. Chem.* **2011**, *286* (39), 34244–34253.

Marcotte, I.; Auger, M. Bicelles as Model Membranes for Solid- and Solution-State NMR Studies of Membrane Peptides and Proteins. *Concepts Magn. Reson. Part A* **2005**, *24A* (1), 17–37.

Martin, S. R.; Andersson Teleman, A.; Bayley, P. M.; Drakenberg, T.; Forsen, S. Kinetics of Calcium Dissociation from Calmodulin and Its Tryptic Fragments. A Stopped-Flow Fluorescence Study Using

Quin 2 Reveals a Two-Domain Structure. *Eur. J. Biochem.* **1985**, *151* (3), 543–550.

Matsubara, M. Regulation of Endothelial Nitric Oxide Synthase by Protein Kinase C. *J. Biochem.* **2003**, *133* (6), 773–781.

Matsubara, M.; Hayashi, N.; Titani, K.; Taniguchi, H. Circular Dichroism and 1H NMR Studies on the Structures of Peptides Derived from the Calmodulin-Binding Domains of Inducible and Endothelial Nitric-Oxide Synthase in Solution and in Complex with Calmodulin. *J. Biol. Chem.* **1997**, *272* (37), 23050–23056.

Matter, H.; Kumar, H. S. A.; Fedorov, R.; Frey, A.; Kotsonis, P.; Hartmann, E.; Fröhlich, L. G.; Reif, A.; Pfleiderer, W.; Scheurer, P.; et al. Structural Analysis of Isoform-Specific Inhibitors Targeting the Tetrahydrobiopterin Binding Site of Human Nitric Oxide Synthases. *J. Med. Chem.* **2005**, *48* (15), 4783–4792.

Maune, J. F.; Klee, C. B.; Beckingham, K. Ca2+ Binding and Conformational Change in Two Series of Point Mutations to the Individual Ca(2+)-Binding Sites of Calmodulin. *J. Biol. Chem.* **1992**, *267* (8), 5286–5295.

Michell, B. J.; Chen Zp; Tiganis, T.; Stapleton, D.; Katsis, F.; Power, D. a; Sim, a T.; Kemp, B. E. Coordinated Control of Endothelial Nitric-Oxide Synthase Phosphorylation by Protein Kinase C and the cAMP-Dependent Protein Kinase. *J. Biol. Chem.* **2001**, *276* (21), 17625–17628.

Michell, B. J.; Brennan Harris, M.; Chen, Z. P.; Ju, H.; Venema, V. J.; Blackstone, M. A.; Huang, W.; Venema, R. C.; Kemp, B. E. Identification of Regulatory Sites of Phosphorylation of the Bovine Endothelial Nitric-Oxide Synthase at Serine 617 and Serine 635. *J. Biol. Chem.* **2002**, *277* (44), 42344–42351.

Mishra, O. P.; Ashraf, Q. M.; Delivoria-Papadopoulos, M. Tyrosine Phosphorylation of Neuronal Nitric Oxide Synthase (nNOS) during Hypoxia in the Cerebral Cortex of Newborn Piglets: The Role of Nitric Oxide. *Neurosci. Lett.* **2009**, *462* (1), 64–67.

Mishra, O. P.; Ashraf, Q. M.; Delivoria-Papadopoulos, M. Mechanism of Increased Tyrosine (Tyr(99)) Phosphorylation of Calmodulin during Hypoxia in the Cerebral Cortex of Newborn Piglets: The Role of nNOS-Derived Nitric Oxide. *Neurochem. Res.* **2010**, *35* (1), 67–75.

Montgomery, H. J.; Romanov, V.; Guillemette, J. G. Removal of a Putative Inhibitory Element Reduces the Calcium-Dependent Calmodulin Activation of Neuronal Nitric-Oxide Synthase. *J. Biol. Chem.* **2000**, *275* (7), 5052–5058.

Mori, M.; Konno, T.; Ozawa, T.; Murata, M.; Imoto, K.; Nagayama, K. Novel Interaction of the Voltage-Dependent Sodium Channel (VDSC) with Calmodulin : Does VDSC Acquire Calmodulin-Mediated Ca2+ -Sensitivity?. *Biochemistry* **2000**, 39, 1316–1323.

Mruk, K.; Farley, B. M.; Ritacco, A. W.; Kobertz, W. R. Calmodulation Meta-Analysis: Predicting Calmodulin Binding via Canonical Motif Clustering. *J. Gen. Physiol.* **2014**, 1–10.

Muhandiram, D. R.; Kay, L. E. Gradient-Enhanced Triple-Resonance 3-Dimensional NMR Experiments with Improved Sensitivity. *J. Magn. Reson.* **1994**, *103*, 203–216.

Muraih, J. K.; Palmer, M. Estimation of the Subunit Stoichiometry of the Membrane-Associated

Daptomycin Oligomer by FRET. *Biochim. Biophys. Acta - Biomembr.* **2012**, *1818* (7), 1642–1647.

Muraih, J. K.; Pearson, A.; Silverman, J.; Palmer, M. Oligomerization of Daptomycin on Membranes. *Biochim. Biophys. Acta - Biomembr.* **2011**, *1808* (4), 1154–1160.

Nahrevanian, H.; Amini, M. Nitric Oxide Functions; an Emphasis on Its Diversity in Infectious Diseases. *Iran J Basic Med Sci* **2009**, *11* (4), 197–204.

Neuhaus, D.; Williamson, M. P. *The Nuclear Overhauser Effect in Structural and Conformational Analysis*, Second.; Wiley: New York, NY, **2000**.

O'Neil, K. T.; DeGrado, W. F. How Calmodulin Binds Its Targets: Sequence Independent Recognition of Amphiphilic Alpha-Helices. *Trends in biochemical sciences*. February **1990**, pp 59–64.

Oleson, J.; Berman, C. L.; Kirkpatrick, J. B.; Regan, K. S.; Lai, J. J.; Tally, F. P. Once-Daily Dosing in Dogs Optimizes Daptomycin Safety. *Antimicrob. Agents Chemother.* **2000**, *44* (11), 2948–2953.

Palfi, A.; Kortvely, E.; Fekete, E.; Kovacs, B.; Varszegi, S.; Gulya, K. Differential Calmodulin Gene Expression in the Rodent Brain. *Life Sci.* **2002**, *70* (24), 2829–2855.

Palmer, K. L.; Daniel, A.; Hardy, C.; Silverman, J.; Gilmore, M. S. Genetic Basis for Daptomycin Resistance in Enterococci. *Antimicrob. Agents Chemother.* **2011**, *55* (7), 3345–3356.

Pedigo, S.; Shea, M. A. Discontinuous Equilibrium Titrations of Cooperative Calcium Binding to Calmodulin Monitored by 1-D 1H-Nuclear Magnetic Resonance Spectroscopy. *Biochemistry* **1995**, *34*, 10676–10689.

Perret, C.; Lomri, N.; Thomasset, M. Evolution of the EF-Hand Calcium-Binding Protein Family: Evidence for Exon Shuffling and Intron Insertion. *J. Mol. Evol.* **1988**, *27* (4), 351–364.

Persechini, A.; Kretsinger, R. H. The Central Helix of Calmodulin Functions as a Flexible Tether. *J. Biol. Chem.* **1988**, *263* (25), 12175–12178.

Pervushin, K.; Vamvaca, K.; Vögeli, B.; Hilvert, D. Structure and Dynamics of a Molten Globular Enzyme. *Nat. Struct. Mol. Biol.* **2007**, *14* (12), 1202–1206.

Pettersen, E. F.; Goddard, T. D.; Huang, C. C.; Couch, G. S.; Greenblatt, D. M.; Meng, E. C.; Ferrin, T. E. UCSF Chimera--A Visualization System for Exploratory Research and Analysis. *J.Comput. Chem.* **2004**, *25* (13), 1605–1612.

Piazza, M.; Futrega, K.; Spratt, D. E.; Dieckmann, T.; Guillemette, J. G. Structure and Dynamics of Calmodulin (CaM) Bound to Nitric Oxide Synthase Peptides: Effects of a Phosphomimetic CaM Mutation. *Biochemistry* **2012**, *51* (17), 3651–3661.

Piazza, M.; Taiakina, V.; Guillemette, S. R.; Guillemette, J. G.; Dieckmann, T. Solution Structure of Calmodulin Bound to the Target Peptide of Endothelial Nitric Oxide Synthase Phosphorylated at thr495. *Biochemistry* **2014**, *53* (8), 1241–1249.

Piazza, M.; Guillemette, J. G.; Dieckmann, T. Dynamics of Nitric Oxide Synthase–Calmodulin Interactions at Physiological Calcium Concentrations. *Biochemistry* **2015**, *54*, 1989–2000.

Piazza, M., Guillemette, J. G., Dieckmann, T., Chemical Shift perturbations induced by residue specific mutations of CaM interacting with NOS peptides, *Biomol NMR Assign*. **2015,** *9*, 299-302.

Piazza, M., Guillemette, J. G., Dieckmann, T., Chemical Shift Assignments of Calmodulin constructs with EF hand mutations, *Biomol NMR Assign.* **2016**, *10*, 193-198.

Pochapsky, T. C.; Kazanis, S.; Dang, M. Conformational Plasticity and Structure/function Relationships in Cytochromes P450. *Antioxid. Redox Signal.* **2010**, *13* (8), 1273–1296.

Polshakov, V. I.; Birdsall, B.; Feeney, J. Effects of Co-Operative Ligand Binding on Protein Amide NH Hydrogen Exchange. *J. Mol. Biol.* **2006**, *356* (4), 886–903.

Quadroni, M.; James, P.; Carafoli, E. Isolation of Phosphorylated Calmodulin from Rat Liver and Identification of the in Vivo Phosphorylation Sites. *J. Biol. Chem.* **1994**, *269* (23), 16116–16122.

Quadroni, M.; L'Hostis, E. L.; Corti, C.; Myagkikh, I.; Durussel, I.; Cox, J.; James, P.; Carafoli, E. Phosphorylation of Calmodulin Alters Its Potency as an Activator of Target Enzymes. *Biochemistry* **1998**, *37* (18), 6523–6532.

Reckel, S.; Hänsel, R.; Löhr, F.; Dötsch, V. In-Cell NMR Spectroscopy. *Prog. Nucl. Magn. Reson. Spectrosc.* **2007**, *51* (2), 91–101.

Rhoads, A. R.; Friedberg, F. Sequence Motifs for Calmodulin Recognition. *FASEB J.* **1997**, *11*, 331–340.

Robbel, L.; Marahiel, M. a. Daptomycin, a Bacterial Lipopeptide Synthesized by a Nonribosomal Machinery. *J. Biol. Chem.* **2010**, *285* (36), 27501–27508.

Robinson, K. E.; Reardon, P. N.; Spicer, L. D. Protein NMR Techniques. **2012**, *831*, 261–277.

Roman, L. J.; Martásek, P.; Masters, B. S. S. Intrinsic and Extrinsic Modulation of Nitric Oxide Synthase Activity. *Chem. Rev.* **2002**, *102* (4), 1179–1190.

Rotondi, K. S.; Gierasch, L. M. A Well-Defined Amphipathic Conformation for the Calcium-Free Cyclic Lipopeptide Antibiotic, Daptomycin, in Aqueous Solution. *Biopolymers* **2005**, *80* (2-3), 374–385.

Ruan, J.; Xie, Q. W.; Hutchinson, N.; Cho, H.; Wolfe, G. C.; Nathan, C. Inducible Nitric Oxide Synthase Requires Both the Canonical Calmodulin-Binding Domain and Additional Sequences in Order to Bind Calmodulin and Produce Nitric Oxide in the Absence of Free Ca2+. *J. Biol. Chem.* **1996**, *271* (37), 22679–22686.

Rybak, M. J.; Bailey, E. M.; Lamp, K. C.; Kaatz, G. W. Pharmacokinetics and Bactericidal Rates of Daptomycin and Vancomycin in Intravenous Drug Abusers Being Treated for Gram-Positive Endocarditis and Bacteremia. *Antimicrob. Agents Chemother.* **1992**, *36* (5), 1109–1114.

Salerno, J. C.; Harris, D. E.; Irizarry, K.; Patel, B.; Morales, a J.; Smith, S. M.; Martasek, P.; Roman, L. J.; Masters, B. S.; Jones, C. L.; et al. An Autoinhibitory Control Element Defines Calcium-Regulated Isoforms of Nitric Oxide Synthase. *J. Biol. Chem.* **1997**, *272* (47), 29769–29777.

Sauermann, R.; Rothenburger, M.; Graninger, W.; Joukhadar, C. Daptomycin: A Review 4 Years after First Approval. *Pharmacology* **2008**, *81* (2), 79–91.

Scott, W. R. P.; Baek, S. B.; Jung, D.; Hancock, R. E. W.; Straus, S. K. NMR Structural Studies of the Antibiotic Lipopeptide Daptomycin in DHPC Micelles. *Biochim. Biophys. Acta* **2007**, *1768* (12), 3116–3126.

Sessas, W. C.; Harrison, J. K.; Barber, C. M.; Zengs, D.; Durieuxn, M. E.; Angelo, D. D. D.; Lynchsll, K. R. Molecular Cloning and Expression of a cDNA Encoding Endothelial Cell Nitric Oxide Synthase. *J. Biol. Chem.* **1992**, *267* (22), 15274–15276.

Shen, X.; Valencia, C. A.; Szostak, J. W.; Szostak, J.; Dong, B.; Liu, R. Scanning the Human Proteome for Calmodulin-Binding Proteins. *Proc. Natl. Acad. Sci. U. S. A.* **2005**, *102* (17), 5969–5974.

Shen, Y.; Delaglio, F.; Cornilescu, G.; Bax, A. TALOS+: A Hybrid Method for Predicting Protein Backbone Torsion Angles from NMR Chemical Shifts. *J. Biomol. NMR* **2009**, *44* (4), 213–223.

Sheta, E. a.; McMillan, K.; Masters, B. S. S. Evidence for a Bidomain Structure of Constitutive Cerebellar Nitric Oxide Synthase. *J. Biol. Chem.* **1994**, *269* (21), 15147–15153.

Sikic, K.; Tomic, S.; Carugo, O. Systematic Comparison of Crystal and NMR Protein Structures Deposited in the Protein Data Bank. *Open Biochem. J.* **2010**, *4*, 83–95.

Silverman, J. A.; Perlmutter, N. G.; Howard, M.; Shapiro, H. M. Correlation of Daptomycin Bactericidal Activity and Membrane Depolarization in Staphylococcus Aureus Correlation of Daptomycin Bactericidal Activity and Membrane Depolarization in Staphylococcus Aureus. *Antimicrob. Agents Chemother.* **2003**, *47* (8), 2538–2544.

Sobolewska-Stawiarz, A.; Leferink, N. G. H.; Fisher, K.; Heyes, D. J.; Hay, S.; Rigby, S. E. J.; Scrutton, N. S. Energy Landscapes and Catalysis in Nitric-Oxide Synthase. *J. Biol. Chem.* **2014**, *289* (17), 11725–11738.

Spratt, D. E.; Newman, E.; Mosher, J.; Ghosh, D. K.; Salerno, J. C.; Guillemette, J. G. Binding and Activation of Nitric Oxide Synthase Isozymes by Calmodulin EF Hand Pairs. *FEBS J.* **2006**, *273* (8), 1759–1771.

Spratt, D. E.; Taiakina, V.; Guillemette, J. G. Calcium-Deficient Calmodulin Binding and Activation of Neuronal and Inducible Nitric Oxide Synthases. *Biochim. Biophys. Acta* **2007a**, *1774* (10), 1351–1358.

Spratt, D. E.; Taiakina, V.; Palmer, M.; Guillemette, J. G. Differential Binding of Calmodulin Domains to Constitutive and Inducible Nitric Oxide Synthase Enzymes. *Biochemistry* **2007b**, *46* (28), 8288–8300.

Spratt, D. E.; Duangkham, Y.; Taiakina, V.; Guillemette, J. G. Mapping the Binding and Calmodulin-Dependent Activation of Nitric Oxide Synthase Isozymes. *Open Nitric Oxide J.* **2011**, *3*, 16–24.

Straus, S. K.; Hancock, R. E. W. Mode of Action of the New Antibiotic for Gram-Positive Pathogens Daptomycin: Comparison with Cationic Antimicrobial Peptides and Lipopeptides. *Biochim. Biophys. Acta* **2006**, *1758* (9), 1215–1223.

Struppe, J.; Vold, R. R. Dilute Bicellar Solutions for Structural NMR Work. *J. Magn. Reson.* **1998**, *135* (2), 541–546.

Struppe, J.; Whiles, J. a; Vold, R. R. Acidic Phospholipid Bicelles: A Versatile Model Membrane System. *Biophys. J.* **2000**, *78* (1), 281–289.

Strynadka, N. C. J.; James, M. N. G. Crystal Structures of the Helix-Loop-Helix Calcium-Binding Proteins. *Annu. Rev. Biochem.* **1989**, *58*, 951–998.

Su, Z.; Blazing, M. ichae. A.; Fan, D.; George, S. E. The Calmodulin-Nitric Oxide Synthase Interaction. Critical Role of the Calmodulin Latch Domain in Enzyme Activation. *J. Biol. Chem.* **1995**, *270* (49), 29117–29122.

Tejero, J.; Haque, M. M.; Durra, D.; Stuehr, D. J. A Bridging Interaction Allows Calmodulin to Activate NO Synthase through a Bi-Modal Mechanism. *J. Biol. Chem.* **2010**, *285* (34), 25941–25949.

Tidow, H.; Nissen, P. Structural Diversity of Calmodulin Binding to Its Target Sites. *FEBS J.* **2013**, *280* (21), 5551–5565.

Tran, Q.-K.; Leonard, J.; Black, D. J.; Persechini, A. Phosphorylation within an Autoinhibitory Domain in Endothelial Nitric Oxide Synthase Reduces the Ca(2+) Concentrations Required for Calmodulin to Bind and Activate the Enzyme. *Biochemistry* **2008**, *47* (28), 7557–7566.

Triba, M. N.; Devaux, P. F.; Warschawski, D. E. Effects of Lipid Chain Length and Unsaturation on Bicelles Stability. A Phosphorus NMR Study. *Biophys. J.* **2006**, *91* (4), 1357–1367.

Tsan, P.; Hus, J. C.; Caffrey, M.; Marion, D.; Blackledge, M. Rotational Diffusion Anisotropy and Local Backbone Dynamics of Carbon Monoxide-Bound Rhodobacter Capsulatus Cytochrome c. *J. Am. Chem. Soc.* **2000**, *122* (12), 5603–5612.

Venema, R. C.; Sayegh, H. S.; Kent, J. D.; Harrison, D. G. Identification, Characterization, and Comparison of the Calmodulin-Binding Domains of the Endothelial and Inducible Nitric Oxide Synthases. *J. Biol. Chem.* **1996**, *271* (11), 6435–6440.

Vetter, S. W.; Leclerc, E. Novel Aspects of Calmodulin Target Recognition and Activation. *Eur. J. Biochem.* **2003**, *270* (3), 404–414.

Vold, R. R.; Prosser, R. S. Magnetically Oriented Phospholipid Bilayered Micelles for Structural Studies of Polypeptides. Does the Ideal Bicelle Exist? *J. Magn. Reson. Ser. B* **1996**, *113* (3), 267–271.

Vold, R. R.; Prosser, R. S.; Deese, a J. Isotropic Solutions of Phospholipid Bicelles: A New Membrane Mimetic for High-Resolution NMR Studies of Polypeptides. *J. Biomol. NMR* **1997**, *9* (3), 329–335.

Volkmann, N.; Martasek, P.; Roman, L. J.; Xu, X. P.; Page, C.; Swift, M.; Hanein, D.; Masters, B. S. Holoenzyme Structures of Endothelial Nitric Oxide Synthase - An Allosteric Role for Calmodulin in Pivoting the FMN Domain for Electron Transfer. *J. Struct. Biol.* **2014**, *188* (1), 46–54.

Vorherr, T.; Knöpfel, L.; Hofmann, F.; Mollner, S.; Pfeuffer, T.; Carafoli, E. The Calmodulin Binding Domain of Nitric Oxide Synthase and Adenylyl Cyclase. *Biochemistry* **1993**, *32* (23), 6081–6088.

Wand, A. J. Dynamic Activation of Protein Function: A View Emerging from NMR Spectroscopy. *Nat. Struct. Biol.* **2001**, *8* (11), 926–931.

Weissman, B. A.; Jones, C. L.; Liu, Q.; Gross, S. S. Activation and Inactivation of Neuronal Nitric Oxide Synthase: Characterization of Ca2+-Dependent [125I]Calmodulin Binding. *Eur. J. Pharmacol.* **2002**, *435* (1), 9–18.

Welland, A.; Daff, S. Conformation-Dependent Hydride Transfer in Neuronal Nitric Oxide Synthase Reductase Domain. *FEBS J.* **2010**, *277* (18), 3833–3843.

Whiles, J. A.; Deems, R.; Vold, R. R.; Dennis, E. A. Bicelles in Structure-Function Studies of Membrane-Associated Proteins. *Bioorg. Chem.* **2002**, *30* (6), 431–442.

Williams, D. H.; Stephens, E.; Zhou, M. Ligand Binding Energy and Catalytic Efficiency from Improved Packing within Receptors and Enzymes. *J. Mol. Biol.* **2003**, *329* (2), 389–399.

Williams, D. H.; Stephens, E.; O'Brien, D. P.; Zhou, M. Understanding Noncovalent Interactions: Ligand Binding Energy and Catalytic Efficiency from Ligand-Induced Reductions in Motion within Receptors and Enzymes. *Angew. Chem. Int. Ed. Engl.* **2004**, *43* (48), 6596–6616.

Wu, G.; Berka, V.; Tsai, A.-L. Binding Kinetics of Calmodulin with Target Peptides of Three Nitric Oxide Synthase Isozymes. *J. Inorg. Biochem.* **2011**, *105* (9), 1226–1237.

Wu, H.; Su, K.; Guan, X.; Sublette, M. E.; Stark, R. E. Assessing the Size, Stability, and Utility of Isotropically Tumbling Bicelle Systems for Structural Biology. *Biochim. Biophys. Acta* **2010**, *1798* (3), 482–488.

Wüthrich, K. *NMR of Proteins and Nucleic Acids*; Wiley: Toronto, On, **1986**.

Xia, C.; Misra, I.; Iyanagi, T.; Kim, J.-J. P. Regulation of Interdomain Interactions by Calmodulin in Inducible Nitric-Oxide Synthase. *J. Biol. Chem.* **2009**, *284* (44), 30708–30717.

Xia, X. M.; Fakler, B.; Rivard, A.; Wayman, G.; Johnson-Pais, T.; Keen, J. E.; Ishii, T.; Hirschberg, B.; Bond, C. T.; Lutsenko, S.; et al. Mechanism of Calcium Gating in Small-Conductance Calcium-Activated Potassium Channels. *Nature* **1998**, *395* (6701), 503–507.

Xiong, L.-W.; Kleerekoper, Q. K.; Wang, X.; Putkey, J. a. Intra- and Interdomain Effects due to Mutation of Calcium-Binding Sites in Calmodulin. *J. Biol. Chem.* **2010**, *285* (11), 8094–8103.

Yamniuk, A. P.; Vogel, H. J. Calmodulin's Flexibility Allows for Promiscuity in Its Interactions with Target Proteins and Peptides. *Mol. Biotechnol.* **2004**, *27* (403), 35–57.

Yamniuk, A. P.; Vogel, H. J. Structural Investigation into the Differential Target Enzyme Regulation Displayed by Plant Calmodulin Isoforms. *Biochemistry* **2005**, *44*, 3101–3111.

Yap, K. L.; Kim, J.; Truong, K.; Sherman, M.; Yuan, T.; Ikura, M. Calmodulin Target Database. *J. Struct. Funct. Genomics* **2000**, *1* (1), 8–14.

Yap, K. L.; Yuan, T.; Mal, T. K.; Vogel, H. J.; Ikura, M. Structural Basis for Simultaneous Binding of Two Carboxy-Terminal Peptides of Plant Glutamate Decarboxylase to Calmodulin. *J. Mol. Biol.* **2003**, *328* (1), 193–204.

Yuan, T.; Vogel, H. J.; Sutherland, C.; Walsh, M. P. Characterization of the Ca2+ -Dependent and -Independent Interactions between Calmodulin and Its Binding Domain of Inducible Nitric Oxide

Synthase. *FEBS Lett.* **1998**, *431* (2), 210–214.

Zhang, J.; Martàsek, P.; Paschke, R.; Shea, T.; Siler Masters, B. S.; Kim, J. J. Crystal Structure of the FAD/NADPH-Binding Domain of Rat Neuronal Nitric-Oxide Synthase. Comparisons with NADPH-Cytochrome P450 Oxidoreductase. *J. Biol. Chem.* **2001**, *276* (40), 37506–37513.

Zhang, M.; Vogel, H. J. Characterization of the Calmodulin-Binding Domain of Rat Cerebellar Nitric Oxide Synthase. *J. Biol. Chem.* **1994**, *269* (2), 981–985.

Zhang, M.; Tanaka, T.; Ikura, M. Calcium-Induced Conformational Transition Revealed by the Solution Structure of Apo Calmodulin. *Nat. Struct. Biol.* **1995a**, *2* (9), 758–767.

Zhang, M.; Yuan, T.; Aramini, J. M.; Vogel, H. J. Interaction of Calmodulin with Its Binding Domain of Rat Cerebellar Nitric Oxide Synthase: A Multinuclear NMR Study. *J. Biol. Chem.* **1995b**, *270* (36), 20901–20907.

Zhang, T. H.; Muraih, J. K.; Tishbi, N.; Herskowitz, J.; Victor, R. L.; Silverman, J.; Uwumarenogie, S.; Taylor, S. D.; Palmer, M.; Mintzer, E. Cardiolipin Prevents Membrane Translocation and Permeabilization by Daptomycin. *J. Biol. Chem.* **2014a**, *289* (17), 11584–11591.

Zhang, T.; Muraih, J. K.; Mintzer, E.; Tishbi, N.; Desert, C.; Silverman, J.; Taylor, S.; Palmer, M. Mutual Inhibition through Hybrid Oligomer Formation of Daptomycin and the Semisynthetic Lipopeptide Antibiotic CB-182,462. *Biochim. Biophys. Acta - Biomembr.* **2013**, *1828* (2), 302–308.

Zhang, T.; Muraih, J. K.; MacCormick, B.; Silverman, J.; Palmer, M. Daptomycin Forms Cation- and Size-Selective Pores in Model Membranes. *Biochim. Biophys. Acta - Biomembr.* **2014b**, *1838* (10), 2425–2430.

Zoche, M.; Bienert, M.; Beyermann, M.; Koch, K. W. Distinct Molecular Recognition of Calmodulin-Binding Sites in the Neuronal and Macrophage Nitric Oxide Synthases: A Surface Plasmon Resonance Study. *Biochemistry* **1996**, *35* (26), 8742–8747.